Abstract

LEE, SANGYUM. Investigation of the Effects of Lime on the Performance of HMA using Advanced Testing and Modeling Techniques. (Under the direction of Dr. Y. Richard Kim.)

The benefits of using hydrated lime as an additive in asphalt concrete are well known. When added to asphalt concrete mixtures, hydrated lime shows the beneficial effects of filler, while also improving resistance to moisture damage. This research presents findings from four studies on the impact of hydrated lime, the impact of the introduction method of the lime on the volumetric optimums, and the performance evaluation of unmodified and lime-modified hot mix asphalt (HMA) mixtures at varying asphalt contents using simple performance tests developed from NCHRP projects 9-19 and 9-29 and viscoelastic continuum damage (VECD) finite element analysis. The performance characteristics evaluated in this study include fatigue cracking and rutting behavior in both dry and moisture-conditioned states. Test methods adopted in this evaluation are: the dynamic modulus (|E*|) test for stiffness characterization; the triaxial repeated load permanent deformation (TRLPD) test for rutting characterization; and the direct tension test for fatigue cracking characterization. From the experimental investigation it is found that the method of lime introduction can have an important effect on the optimum volumetric asphalt content. Regarding the |E*|, it is found that hydrated lime has a minimal impact on the mixtures in this study. However, the findings support conventional understanding of the effects of asphalt content, lime modification, and moisture conditioning on the fatigue cracking and rutting performance of HMA mixtures.

That is, as the asphalt content increases, the resistance to fatigue cracking improves and rutting performance worsens. Another accepted fact is that lime modification reduces the susceptibility for moisture damage in terms of both fatigue cracking and rutting. The contribution of this research, therefore, is to demonstrate advanced test methods and models that can be used in the performance evaluation of various mixtures. With additional validation and calibration, the comprehensive methodology described herein may serve as the foundation for a performance-based HMA mix design and performance-related HMA specifications.

Investigation of the Effects of Lime on the Performance of HMA using Advanced Testing and Modeling Techniques

by

Sangyum Lee

A dissertation submitted to the Graduate Faculty of
North Carolina State University
in partial fulfillment of the
requirements for the degree of
Doctor of Philosophy

Civil Engineering

Raleigh, North Carolina

2007

APPROVED BY:

Dr. Y. Richard Kim Chair of Advisory Committee	Dr. Roy H. Borden Co-Chair of Advisory Committee
Dr. Murthy N. Guddati	Dr. Kimberly S. Weems

Dedication

To my parents, my wife Jae Hee Jin and son Shawn Keonhee Lee

Biography

Sangyum Lee, born in Seoul, Korea and graduated from Kyunghee University, Korea, with an undergraduate degree and master degree in civil engineering. During his master degree program, he specialized in transportation engineering. He went to University of North Carolina State University, joined the Ph.D. program in transportation engineering at the department of Civil Engineering and defended his dissertation in August. 2007.

Acknowledgments

I would like to start by thanking my committee for their time and effort. In particular, I am so grateful that I have Professor Y. Richard Kim as my advisor, and I cannot begin to thank him enough. He is truly a great mentor not only in research but also in everyday life. I would like to thank him for his direction, guidance, time, and endless patience. His efforts and help have meant a tremendous amount to me.

Also I would like to appreciate my committee cochair, Dr. Borden for his unfailing support and guidance during my doctoral program. The members of my dissertation committee, Dr. Guddati, and Dr. Weems, have generously given their time and expertise to better my work. I thank them for their contribution and their good natured support.

There are so many people who helped to make life as a graduate student easier, but I would like to mention a few. To Dr. Jusang Lee: thank you for your ceaseless support and guidance. Shane Underwood: thank you. Without your help, I could not have done much of my research. Also I would like to express my deep gratitude to my fellow members: Jaejun, Taeyoung, Andrew, Fadi, Ardalan, Naresh, Dr. Joon, Dr. Moon, and Dr. Young.

I would like to acknowledge the financial support from The Chemical Lime Company, Southern Transportation Center and, in particular, the assistance of Cheol Min Baek.

Finally, I would like to thank my wonderful family, for always believing in me, even when I did not. I could not have accomplished this without their love and support, especially during

the difficult times. They have kept me focused on what is important in life, no matter what my plans have been.

Table of Contents

List of Tables ..... **x**

List of Figures ..... **xii**

Chapter 1 Introduction **1**

1.1 General Statement 1
1.1.1 Current status of Superpave volumetric mix design 1
1.1.2 Benefits of lime 3
1.2 Research Objectives and Approaches 5

Chapter 2 Literature Review **8**

2.1 Adhesion 8
2.1.1 Physical bonds 8
2.1.1.1 Ionic bonds 8
2.1.1.2 Electrodynamic interactions through the Van der Waals force 9
2.1.2 Chemical bonds 10
2.1.2.1 Interactions through electron pair sharing 10
2.1.2.2 Interactions through contributions of electrons from both entities 10
2.1.2.3 Donor-acceptor interactions 10
2.2 Adhesion in Asphalt Concrete 11
2.2.1 Chemical composition of the asphalt binder 11
2.2.2 Influence of aggregate characteristics on adhesion 15
2.2.3 Mineral fillers 17
2.3 Physical and Chemical Properties of Lime 19
2.3.1 Definition of hydrated lime 19
2.3.2 Physical properties of hydrated lime 20
2.3.3 Chemical properties of hydrated lime 21
2.4 Benefits of Lime in Asphalt Concrete 22
2.4.1 Mechanisms of the lime-asphalt interaction 22
2.4.2 Moisture damage 24
2.4.2.1 Moisture damage due to physico-chemical properties 24
2.4.2.2 Moisture damage with environmental characteristics (heat, heavy rains, freeze/thaw cycles, and traffic) 26
2.4.3 Rutting 28
2.4.4 Cracking from fatigue and low temperatures 29
2.4.4.1 Types and causes of cracking 29
2.4.4.2 Fatigue cracking (load-associated) 30
2.4.4.3 Low temperature cracking (nonload-associated) 30

2.4.4.4 Reflection cracking 31
2.4.4.5 Oxidation and aging that cause brittle pavement 32
2.5 Methods of Introducing Hydrated Lime into Mixes 33
2.5.1 Addition of dry hydrated lime to dry aggregate 33
2.5.2 Addition of dry hydrated lime to wet aggregate 35
2.5.3 Addition of hydrated lime in the form of slurry 35
2.6 Asphalt Concrete Mix Design 38
2.6.1 Historical methods 39
2.6.1.1 Marshall mix design 39
2.6.1.2 Hveem mix design 39
2.6.2 Superpave volumetric mix design 40
2.6.3 Performance-related mix design 42

Chapter 3 Theoretical Background 43

3.1 Linear Viscoelasticity 44
3.2 Viscoelastic Continuum Damage 47
3.2.1 Correspondence principle 47
3.2.2 Viscoelastic continuum damage 49
3.3 VECD-FEP++ Analysis for Pavements 54
3.3.1 Introduction 54
3.3.2 Constitutive model 55
3.3.3 Damage model 57
3.3.4 Finite element implementation 58

Chapter 4 Experimental Program 61

4.1 Materials 62
4.2 Sample Preparation 63
4.2.1 Specimen fabrication for performance tests 63
4.2.2 Target air voids 63
4.3 Testing Setup and Program 64
4.3.1 Testing systems 64
4.3.2 Testing program 67
4.3.2.1 Dynamic modulus testing 67
4.3.2.2 TRLPD tests 72
4.3.2.3 Constant crosshead rate tension tests 76
4.3.2.4 VECD-FEP++ for fatigue damage simulation 77

Chapter 5 Determining the Effects of Hydrated Lime on the Dynamic Modulus of Typical North Carolina Mixtures 80

5.1 Introduction 80
5.2 Experimental Design 81
5.2.1 Mixture selection 81
5.2.2 Mix designs with hydrated lime 85
5.2.3 Dynamic modulus tests 87
5.3 Test Results 88

5.4 Statistical Analysis 95
5.5 Summary and Conclusions 97

Chapter 6 Effects of the Lime Introduction Method on the Performance of the Mixtures 98

6.1 Introduction 98
6.2 Experimental Design 99
6.3 Performance Tests and Analysis of Results 102
6.3.1 Dynamic modulus tests and statistical analysis 104
6.3.2 TRLPD test results 108
6.3.3 Constant crosshead rate monotonic results 112
6.4 VECD-FEP++ Simulation Results 116
6.5 Summary and Conclusions 124

Chapter 7 Evaluation of the Effects of Hydrated Lime on Moisture Damage 125

7.1 Introduction 125
7.2 Experimental Program 127
7.2.1 Sample preparation 127
7.2.2 Moisture conditioning process 128
7.3 Results of Performance Tests and Statistical Analysis 130
7.3.1 Dynamic modulus test 130
7.3.2 TRLPD test results 137
7.3.3 Constant monotonic crosshead strain rate tests and analysis 142
7.3.4 VECD-FEP++ simulation results 145
7.4 Summary and Conclusions 151

Chapter 8 Performance-based Evaluation of Lime-modified Hot Mix Asphalt Mixtures 153

8.1 Introduction 153
8.2 Experimental Program 154
8.3 Results of Performance Tests and Statistical Analysis 154
8.3.1 Dynamic modulus test results 154
8.3.2 TRLPD test Results and Statistical Analysis 160
8.3.3 Constant Crosshead Rate Monotonic Test Results 170
8.4 VECD-FEP++ Simulation Results 175
8.5 Determining optimum asphalt content based on performance 185
8.5.1 Rutting performance indicator 190
8.5.2 Fatigue performance indicator 193
8.5.3 Optimal asphalt content based on performance tests 196
8.6 Summary and Conclusions 201

Chapter 9 Verification Test with Field-Produced Mixture 203

9.1 Field Construction 203
9.2 Field Conditions of the Production Process 205
9.3 Moisture Sensitivity Testing and Results 206

9.4 Asphalt Pavement Analyzer (APA) Rut Test and Results.....210
9.5 Summary and Conclusions 213
Chapter 10 Conclusions and Recommendations.....214
References.....219

List of Tables

Table 2.1 Lime Addition Techniques 37
Table 3.1 Fundamental Elements of the Work Potential Theory 50
Table 4.1 Test Factorial 62
Table 4.2 General Controlled Crosshead Testing Matrix for VEPCD Characterization in Tension 77
Table 5.1 Guidelines for Superpave Mixes in North Carolina 82
Table 5.2 Aggregate Gradations of Selected Mixes for Dynamic Modulus Study 83
Table 5.3 Specifications of Selected Mixes for Dynamic Modulus Study 85
Table 5.4 Mix Design Results for Dynamic Modulus Study 87
Table 5.5 Statistical Analysis of the Impact of Lime on the Dynamic Modulus 96
Table 6.1 Mix Design Results of the Lime Introduction Methods 101
Table 6.2 Gradation Information for the Lime Modification Methods 102
Table 6.3 Statistical Analysis of the Effects of the Lime Introduction Method on the Dynamic Modulus 108
Table 6.4 Statistical Analysis of the Effects of the Lime Introduction Method on the Permanent Deformation Resistance 111
Table 6.5 Statistical Analysis of the Effects of the Lime Introduction Method on Fatigue Resistance 114
Table 6.6 Ranking of Various Lime Introduction Methods 123
Table 7.1 The Level of Saturation for the Moisture Conditioning Process 129
Table 7.2 Results of Statistical Analysis and Dynamic Modulus Ratio (DMR) with the Moisture Damage at Various Reduced Frequencies 134
Table 7.3 Statistical Analysis and Permanent Strain Ratio (PSR) with Moisture Damage at Various Numbers of Load Cycles 141
Table 7.4 Statistical Analysis and Damage Characteristic Ratio (DCR) with the Moisture Damage at Various Damage Levels 144
Table 8.1 Statistical Analysis of the Effect of Asphalt Content on the Permanent Deformation Resistance of the Lime-Modified Mixture 165
Table 8.2 Statistical Analysis of the Effect of Asphalt Content on the Permanent Deformation Resistance of the Unmodified Mixture 165
Table 8.3 Statistical Analysis of the Effects of Asphalt Content on the Resistance to Damage for the Lime-modified Mixture with Varying Asphalt Contents 174
Table 8.4 Statistical Analysis of the Effects of Asphalt Content on the Resistance to Damage for the Unmodified Mixture with Varying Asphalt Contents 174
Table 8.5 Results of the Volumetric Properties of the Lsub Mixture 200
Table 9.1 Field Gradation Information for Lime Modification Study 205
Table 9.2 Comparison of Indirect Tensile Strength Test Results for Lime-modified and Unmodified Mixtures 208

Table 9.3 Comparison of APA Test Results 212

List of Figures

Figure 1.1 Schematic flow of the research approaches 7

Figure 2.1 Molecular fragments of aliphatic carbon, aromatic carbon, and a combination of the two, respectively (Robertson 1991) 11
Figure 2.2 Pyridine and benzothiophene (Robertson 1991) 11
Figure 2.3 Ketones (Robertson 1991) 12
Figure 2.4 (a) Carboxylic acids; (b) sodium and calcium salts (Robertson 1991) 12
Figure 2.5 Carboxylic anhydrides, typically called anhydrides (Robertson 1991) 13
Figure 2.6 (a) Phenols; (b) quinolones; and (c) sulfoxides (Robertson 1991) 13
Figure 2.7 Porphyrins, metals in asphalts (Robertson 1991) 14
Figure 2.8 Classification of aggregates (Mertens et al. 1959) 16
Figure 3.1 (a) Stress–strain behavior for mixtures under LVE cyclic loading; (b) stress-pseudo strain behavior for same data (Daniel 2001) 49
Figure 4.1 LVDT mounting and spacing for: (a) dynamic modulus test; (b) monotonic constant crosshead rate test; and (c) and (d) TRLPD test 66
Figure 4.2 Typical unshifted dynamic modulus in: (a) semi-log space; and (b) log-log space 69
Figure 4.3 Typical dynamic modulus mastercurve in: (a) semi-log space; and (b) log-log space 70
Figure 4.4 Log shift factor function for a typical mixture 70
Figure 4.5 Typical relationship between total cumulative plastic strain and number of load cycles: (a) plotting on arithmetic scale; (b) plotting on log-log scale with regression constants a, b 74
Figure 4.6 Structure of pavement used for the damage simulation 78
Figure 5.1 Gradation chart for selected mixtures 84
Figure 5.2 |E*| comparison between unmodified and lime-modified mixtures (S9.5AF) 89
Figure 5.3 |E*| comparison between unmodified and lime-modified mixtures (S12.5CF) 90
Figure 5.4 |E*| comparison between unmodified and lime-modified mixtures (I19.0BF) 91
Figure 5.5 |E*| comparison between unmodified and lime-modified mixtures (B25.0BF) 92
Figure 5.6 |E*| comparison between unmodified and lime-modified mixtures (S9.5CC) 93
Figure 5.7 Comparison of the |E*| of lime-modified and unmodified measured data in: (a) semi-log; and (b) log-log space 94
Figure 5.8 Rate of rejected null hypothesis with temperature change 97

Figure 6.1 Gradation chart for the lime-modified mixtures 100
Figure 6.2 Effects of the lime introduction method on the |E*| in: (a) semi-log and (b) log-log space 105
Figure 6.3 Effects of the lime introduction method on the phase angle 106
Figure 6.4 Effects of the lime introduction method on the permanent strain accumulation in TRLPD tests 109
Figure 6.5 Damage characteristic relationships for Control, Lsub, Leco, and Lmod mixtures 112
Figure 6.6 Comparison of the Damage Contour Plots at Various Load Cycles for the Different Lime Addition Methods 117
Figure 6.7 Overall comparison of the fatigue performance based on: (a) % Crack area: and (b) Average C 120
Figure 6.8 Discrete comparison of fatigue performance based on (a) % Crack area and (b) Average C at various cycle stages 122
Figure 7.1 Dynamic modulus mastercurves for the Control mixture with conditioning in: (a) semi-log space; (b) log-log space; and (c) the phase angle 131
Figure 7.2 Dynamic modulus mastercurves for the Lsub mixture with conditioning in: (a) semi-log space; (b) log-log space; and (c) the phase angle 132
Figure 7.3 Dynamic modulus ratio (DMR) as a function of reduced frequency 136
Figure 7.4 Permanent strain results with and without moisture conditioning for: (a) Control mixture; and (b) Lsub mixture in arithmetic scale 138
Figure 7.5 Permanent strain results with and without moisture conditioning for: (a) Control mixture; and (b) Lsub mixture in log scale 139
Figure 7.6 Permanent strain ratio between conditioning and unconditioning for the Control mixture and the Lsub mixture 141
Figure 7.7 Effect of the moisture damage on the damage characteristic curves for the (a) Control mixture; and (b) Lsub mixture 143
Figure 7.8 Comparison of the damage contour plots at various load cycles with and without moisture damage 147
Figure 7.9 Discrete comparison of fatigue performance of the Control mixture with and without moisture damage based on: (a) % Crack area; and (b) Average C at various cycle stages 149
Figure 7.10 Discrete comparison of fatigue performance of the Lsub mixture with and without moisture damage based on: (a) % Crack area; and (b) Average C at various cycle stages 150
Figure 8.1 Effect of asphalt content: (a) |E*| in semi-log space; (b) |E*| in log-log space; (c) phase angle (lime-modified mixture) 157
Figure 8.2 Effect of asphalt content: (a) |E*| in semi-log space; (b) |E*| in log-log space; (c) phase angle (unmodified mixture) 158
Figure 8.3 Comparison between Control and Lsub mixtures: (a) |E*| in semi-log space; (b) |E*| in log-log space; (c) phase angle 159
Figure 8.4 Effect of asphalt content on permanent strain accumulation with the lime-modified mixture: (a) arithmetic scale; (b) log-log scale 162

Figure 8.5 Effect of asphalt contents on permanent strain accumulation with the unmodified mixture: (a) arithmetic scale; (b) log-log scale 163
Figure 8.6 Effect of asphalt content on permanent strain accumulation in (a) arithmetic scale; (b) log-log scale 168
Figure 8.7 The relative permanent strain ratio regarding the effect of lime on permanent strain accumulation in (a) arithmetic scale; (b) log-log scale 169
Figure 8.8 Effect of asphalt content on the fatigue resistance of the lime-modified mixture in (a) arithmetic scale; (b) semi-log scale at early stage of damage 172
Figure 8.9 Effect of asphalt content on the fatigue resistance of the unmodified mixture in (a) arithmetic scale; (b) semi-log scale at early stage of damage 173
Figure 8.10 Comparison of the damage contour plots at various load cycles for the lime-modified mixtures 176
Figure 8.11 Comparison of the damage contour plots at various load cycles for the unmodified mixtures 177
Figure 8.12 Discrete comparison of fatigue performance of the lime-modified mixtures with varying asphalt contents based on: (a) % Crack area; and (b) Average C at various cycle stages 178
Figure 8.13 Discrete comparison of fatigue performance of the unmodified mixtures with varying asphalt contents based on: (a) % Crack area; and (b) Average C at various cycle stages 179
Figure 8.14 The overall trends of the % Crack area of mixtures with varying asphalt contents in semi-log scale for the (a) lime-modified mixture; (b) unmodified mixture 182
Figure 8.15 The changes in % Crack area at each cycle as a function of asphalt content: (a) lime-modified mixture; (b) unmodified mixture 184
Figure 8.16 Concept of the performance related mix design methodology in case of (c) volumetric optimum above the optimum candidate range; and (d) no optimum candidate range 188
Figure 8.17 Relationship between the total cumulative plastic strain and the number of load cycles using a regression line in log-log scale 191
Figure 8.18 Rutting indicator *b* as a function of asphalt content for: (a) lime-modified mixture; and (b) unmodified mixture 192
Figure 8.19 Potential fatigue minimum criteria and rutting maximum criteria as a function of asphalt content for (a) lime-modified mixture; and (b) unmodified mixture 195
Figure 8.20 Balanced optimal asphalt contents for (a) lime-modified mixture; and (b) unmodified mixture 198
Figure 8.21 Volumetric propeties of the Lsub and Control mixture 199
Figure 9.2 Loading frame used for measuring indirect tensile strength 207
Figure 9.3 Comparison of loss in tensile strength values for lime-modified and unmodified mixtures (TSR tests for NCSU Lab mix and Field mix were done by DOT and Field lab, respectively.) 208
Figure 9.4 Comparison of loss in tensile strength values for lime-modified and unmodified mixtures (TSR tests for Field mixes were done by DOT and field Lab.) 209
Figure 9.5 Comparison of loss in tensile strength values for lime-modified and unmodified mixtures (TSR tests for NCSU Lab mix and Field mix were done by DOT.) 209

Figure 9.6 Asphalt Pavement Analyzer 211

Chapter 1

Introduction

1.1 General Statement

1.1.1 Current status of Superpave volumetric mix design

In 1987, the Strategic Highway Research Program (SHRP) began developing a new system for specifying asphalt materials. Superior Performing Asphalt Pavements (Superpave) is the final product of the SHRP asphalt research program. Superpave represents an improved system for specifying the asphalt binder and mineral aggregate, developing the asphalt mixture design, and analyzing and establishing pavement performance prediction. The system includes an asphalt binder specification, a hot mix asphalt (HMA) design and analysis system, and computer software that integrates the system's components. The core of the Superpave system is a performance-based specification system that has a direct relationship to field performance. The Superpave design method for HMA consists of three phases: (1) material selection for the asphalt binder and aggregate, (2) aggregate blending, and (3) volumetric analysis of specimens compacted using the Superpave Gyratory Compactor (Witczak et al. 2000).

Although performance information from full-scale test tracks such as WesTrack and MnRoad was used to define the relationships between material properties and pavement performance, results from other experimental construction projects and some accelerated tests questioned whether the Superpave volumetric mixture design procedure alone is sufficient for determining the acceptance or rejection of HMA mixtures under current traffic and climatic conditions. Without additional general strength tests to complement the volumetric mix design method, the more traditional Marshall and Hveem mixture design methods remain the only current means to assess HMA mixture performance. In addition, industry demands necessitate a simple performance-related test that can provide reliable performance data of the HMA mixture during the volumetric mixture design process using the Superpave Gyratory Compactor.

A Simple Performance Test (SPT) is defined as a test method that accurately and reliably measures a mixture response characteristic or parameter that is highly correlated to the occurrence of pavement distress (cracking and rutting) over a diverse range of traffic and climatic conditions. One of the requirements for a SPT is that it can measure a fundamental engineering property that can be linked to the advanced material characterization methods of the detailed distress prediction models, which include the permanent deformation model, the fatigue cracking model, and the thermal cracking model (Witczak et al. 2000).

In order to address the need for a SPT, the Federal Highway Administration (FHWA) has committed funding to identify and evaluate a simple strength test and, further, has authorized the University of Maryland Superpave Models Team to develop all necessary test protocols, criteria, and guidelines for the SPT to support the Superpave volumetric mix

design procedure.

1.1.2 Benefits of lime

Hydrated lime is acknowledged as a superior additive for asphalt concrete and has an extensive track record nationally. The beneficial nature of this material in asphalt concrete is related to both the particular chemistry of the system and the mechanical nature of fine particles in an asphalt binder matrix. Numerous studies over the years detail the benefits of hydrated lime as both (1) a filler and (2) as an agent to reduce moisture-induced stripping (Little et al. 2005, Petersen et al. 1987a, b, Plancher et al. 1976, Collins 1988, Sebaaly et al. 2003, Tunnicliff 1977, Welch et al. 1977).

First, the use of mineral filler (lime is an example) for improving the performance of asphalt concrete mixtures has been repeatedly demonstrated over the years (Little et al. 2005, Anderson 1973, Tayebali et al. 2000). With regard to fatigue performance, properly selected fillers, which have physico-chemical characteristics compatible with the asphalt binder and aggregate particles, act as bond-strengthening and crack-arresting agents (Little et al. 2005, Craus et al. 1978). Similarly, compatible mineral fillers aid in reducing permanent deformation by increasing the viscosity of the mastic, thus improving the plastic and viscoplastic characteristics of mixtures (Petersen et al. 1987b, Craus et al. 1978, Mohammad 2006). The observed benefits of hydrated lime range from very significant as active filler, to less significant but still useful filler, i.e., similar to more standard inert fillers such as baghouse fines (Little et al. 2005).

Moisture-induced stripping occurs when the bond between the asphalt cement and the

aggregate breaks down due to the presence of moisture. Certain types of aggregates are particularly susceptible to stripping. In addition to stripping as a chemical phenomenon, environmental characteristics, such as heat, heavy rains, freeze/thaw (F-T) cycles, and traffic, also play a major role in stripping. When lime is added to HMA, it reacts with the aggregates, strengthening the bond between the bitumen and the aggregate. At the same time that lime treats the aggregate, it also reacts with the asphalt itself. Lime reacts with highly polar molecules that can otherwise react in the mix to form water-soluble soaps that promote stripping. When those molecules react with lime, they form insoluble salts that no longer attract water (Petersen et al. 1987).

In addition, the dispersion of hydrated lime throughout the mix makes the mix stiffer and tougher, thereby reducing the possibility that the bond between the asphalt cement and the aggregate will be broken mechanically, even if there is no water effect.

The benefits of using hydrated lime in asphalt cements can be summarized as follows.

- Hydrated lime improves stiffness and, therefore, reduces rutting.
- Hydrated lime reduces cracking.
- Hydrated lime reduces oxidation and aging.
- Hydrated lime improves resistance to moisture sensitivity.

Even though it has been shown repeatedly that the use of hydrated lime in asphalt concrete mixtures is beneficial, confusion still exists as to the best method for adding lime to asphalt mixtures. Selecting the appropriate method for adding the lime is complicated by the lack of consistent results from the literature. Some researchers suggest that the method used

for lime addition is not an important factor at all (Collins 1988, Gardiner et al. 1987), whereas others clearly demonstrate that differences in material properties are evident when the lime addition method changes (Sebaaly et al. 2003, Button et al. 1983, Kennedy et al. 1983). The conflicting results from the literature indicate that further study is needed on this topic.

1.2 Research Objectives and Approaches

The primary objectives of this study are to investigate the effect of lime modification on the fundamental behavior of asphalt concrete mixtures and to examine ways in which the lime introduction procedure can further influence these behaviors using different volumetric mix designs. In addition, the effect of lime on moisture susceptibility is evaluated by comparing the fundamental behaviors of various asphalt mixtures.

Four separate studies are presented herein. In the first, a single lime addition procedure is applied to multiple mixtures, and the effect on material properties is assessed via the dynamic modulus (|E*|). In the second study, the |E*| test is complemented by additional performance testing to ascertain the effect of the lime introduction technique on material behavior. In the third study, the effect of lime on performance, with the favorable lime introduction method selected among multiple mixtures, is investigated using advanced testing and modeling techniques. Additionally, moisture susceptibility of the selected lime-modified mixture is examined using the same parameters. To evaluate mixture performance, the SPTs recommended by NCHRP 465 are conducted; these tests include |E*| and flow number tests as well as characterization tests for the tensile Viscoelastoplastic Continuum Damage

(VEPCD) model. Further, the finite element program, VECD-FEP++, is used to evaluate the field responses obtained by the cyclic fatigue simulation on the pavement. The research approaches are schematized in Figure 1.1.

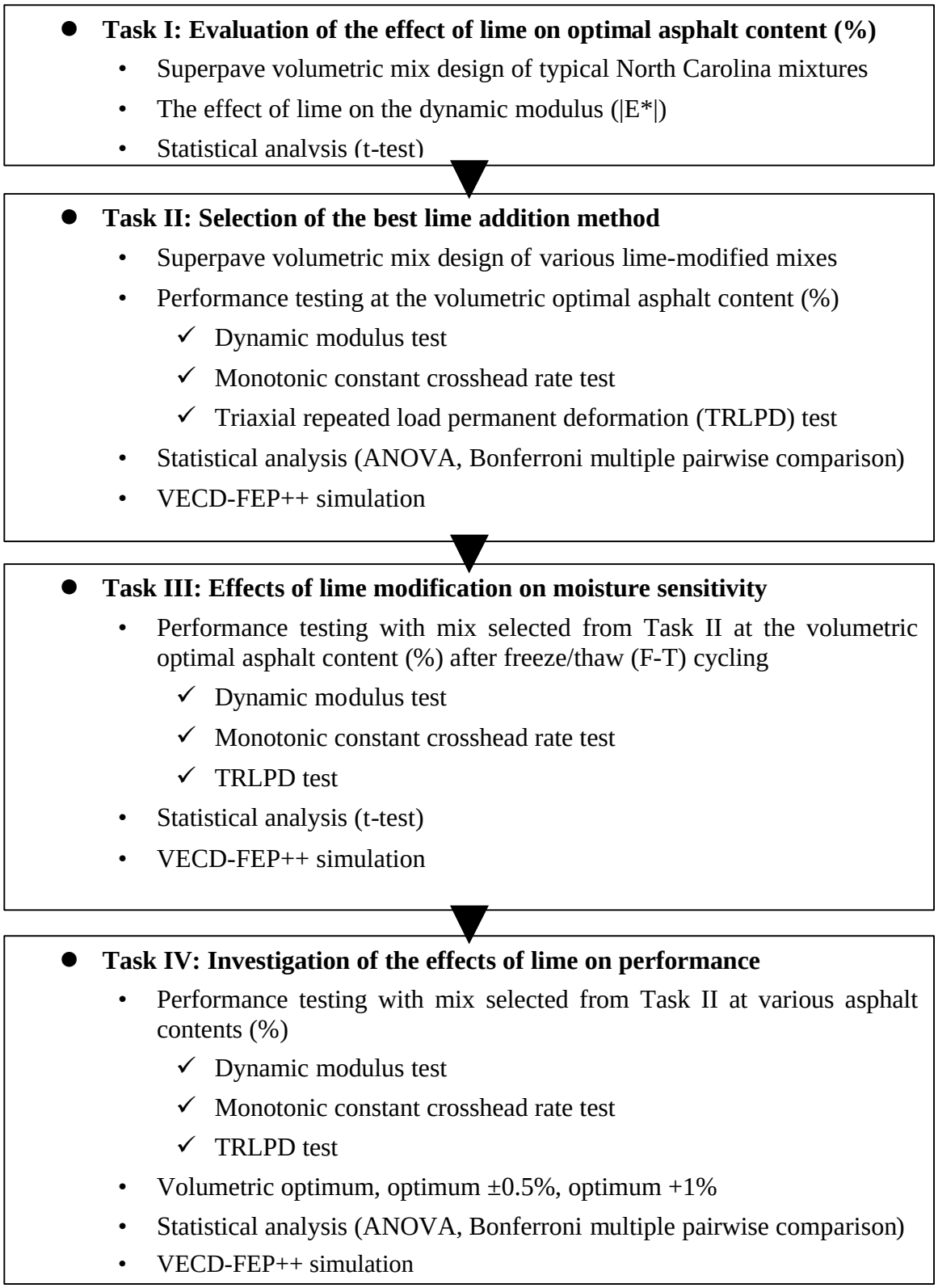

Figure 1.1 Schematic flow of the research approaches

Chapter 2

Literature Review

The literature review includes the following topics:

1) Adhesion;

2) Adhesion in asphalt concrete;

3) Physical and chemical properties of lime;

4) Benefits of lime in asphalt concrete;

5) Methods of introducing hydrated lime into mixes; and

6) Asphalt concrete mix design.

2.1 Adhesion

2.1.1 Physical bonds

2.1.1.1 Ionic bonds

In a discussion of chemical bonding, Companion (1979) states:

> The basis for understanding intermolecular forces is the Coulomb force, which is the electrostatic force between two separated charges. Electrostatic forces play a primary role in the formation of ionic bonds. An ideal ionic bond is formed when a positive

ion (cation) and negative ion (anion), as charged particles, attract each other whereby the ion pair gains classical electrostatic stabilization energy.

2.1.1.2 Electrodynamic interactions through the Van der Waals force

The Van der Waals force is the sum of three interactions that include dipole-dipole interactions, dipole-induced dipole interactions, and induced dipole-induced dipole interactions (Butt et al., 2003).

a) Dipole-dipole interactions. A molecular dipole exists when an atom of high electronegativity at one end of the molecule draws electrons more to that end than the other, resulting in a partial separation of the charge. The magnitude of these virtual charges and the distance separating them characterize a dipole moment. When two dipoles interact, the oppositely charged ends of the dipoles attract, while the other ends naturally repel, which changes their relative spatial orientation.

b) Dipole-induced dipole interactions. In neutral atoms or symmetric molecules, with no dipole moment, the nuclei and electron clouds are attracted in opposite directions when exposed to an electrical field or dipole; i.e., polarization takes place.

c) Induced dipole-induced dipole interactions. For two atoms or molecules with spherical, symmetrical charge distribution, London proposes a type of force that explains the attraction between the non-polar molecules. Based on the finite probability that, at any instant in time, electrons are all on one side of an atom or molecule with a partially unshielded nucleus on the other side, an instantaneous dipole is created. This process induces an instantaneous dipole in another species and results in forces of attraction.

2.1.2 Chemical bonds

2.1.2.1 Interactions through electron pair sharing

Whereas interactions facilitated by weak electrical forces that result from oscillating charges are regarded as physical bonding, a union of two species through the sharing of an electron pair is often referred to as chemical bonding. Chemical interactions take place through the rearrangement of bonding electrons within the interacting entities in order to establish balanced electron distributions among them.

2.1.2.2 Interactions through contributions of electrons from both entities

In this type of interaction, each atom contributes one of the shared electrons to form a new molecule. A bond formed in this way is called a covalent bond. A physical accumulation of electrons that occupy overlapping orbitals in the space between nuclei takes place.

2.1.2.3 Donor-acceptor interactions

Good (1966) describes this type of interaction as acid-base bonding and states that it can also be considered weak-electron-sharing bonding. The Brönsted-Lowery theory defines an acid as a substance capable of giving up a proton, and a base as a substance with a tendency to accept a proton. According to this theory, acids are limited to hydrogen-containing compounds. According to the Lewis theory, an acid is an electron pair acceptor, and a base is an electron pair donor.

2.2 Adhesion in Asphalt Concrete

2.2.1 Chemical composition of the asphalt binder

An explanation of asphalt composition is helpful because the structure of asphalt molecules influences the bonding of the asphalt to the aggregate.

The chemical properties and composition of asphalt are summarized in a SHRP report by Robertson (1991). The proposed bitumen functional groups that influence bonding are shown in Figure 2.1 to Figure 2.7. Asphalt binder is composed of various hydrocarbon molecular fragments, such as aliphatic carbon, aromatic carbon, and a mixture of both aliphatic and aromatic carbon fragments.

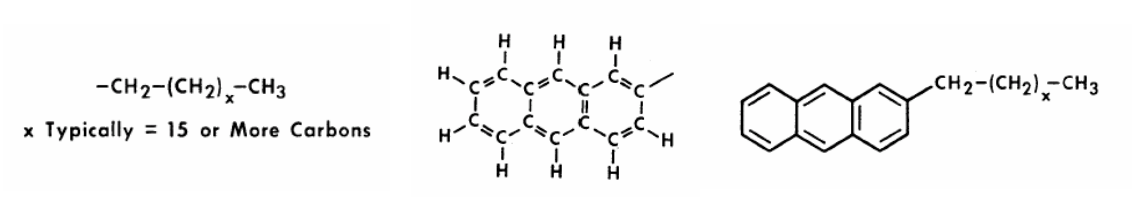

Figure 2.1 Molecular fragments of aliphatic carbon, aromatic carbon, and a combination of the two, respectively (Robertson 1991)

Pyridine is a carbon molecular fragment containing heteroatom nitrogen, and sulfur is a benzothiophene.

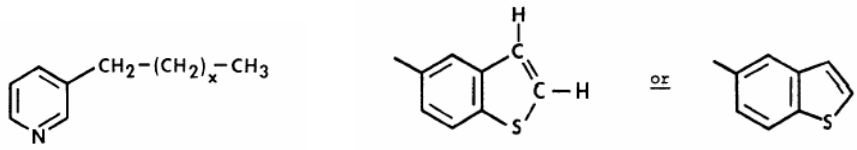

Figure 2.2 Pyridine and benzothiophene (Robertson 1991)

Certain types of carbon in asphalt are susceptible to oxidation. An aliphatic carbon next to an aromatic ring is known as a benzyl carbon and is an example of a readily oxidizable site. Ketones are formed by the oxidation.

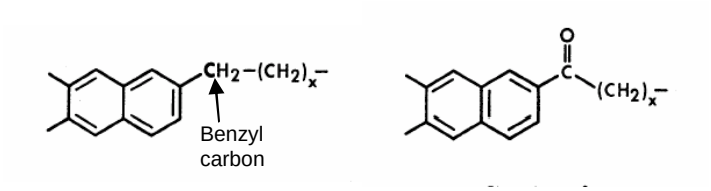

Figure 2.3 Ketones (Robertson 1991)

More severe oxidation can form carboxylic acids. Carboxylic acids, whether present in their original crude form or formed upon oxidation, can be converted to sodium (Na) salts or calcium (Ca) salts by appropriate reaction with sodium or calcium inorganic compounds.

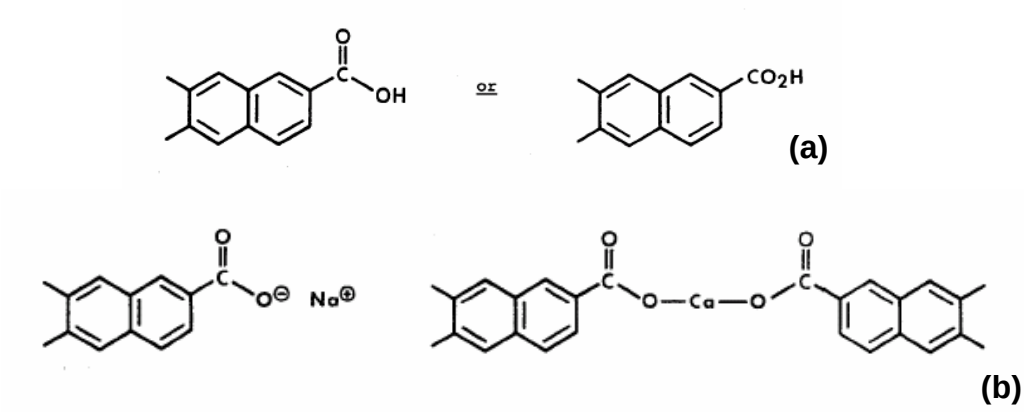

Figure 2.4 (a) Carboxylic acids; (b) sodium and calcium salts (Robertson 1991)

Carboxylic acid anhydrides may be formed upon oxidation when two benzyl carbons are present on adjacent aromatic rings.

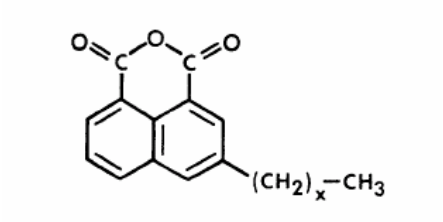

Figure 2.5 Carboxylic anhydrides, typically called anhydrides (Robertson 1991)

Another type of oxygen-containing molecule that may be present in asphalt is a functional group known as phenols, where oxygen is attached directly to an aromatic ring. Another important class of compounds typically found in aged asphalts is quinolones. Many sulfur compounds are also susceptible to oxidation and typically form sulfoxides.

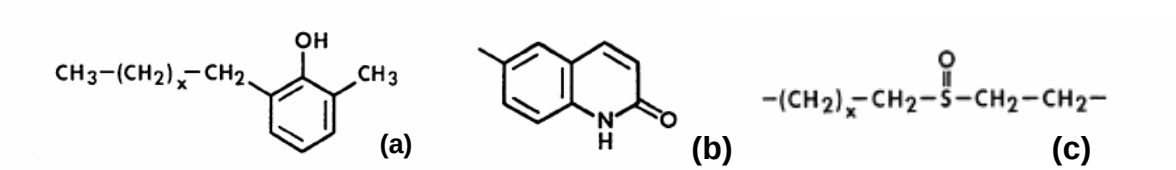

Figure 2.6 (a) Phenols; (b) quinolones; and (c) sulfoxides (Robertson 1991)

Metals are also present in asphalts, again in varying amounts and distributions. The most common metals are vanadium, nickel, and iron, although other metals may also be present. Typically, metals are present as organo-metallic materials, specifically as porphyrins, as shown in Figure 2.7.

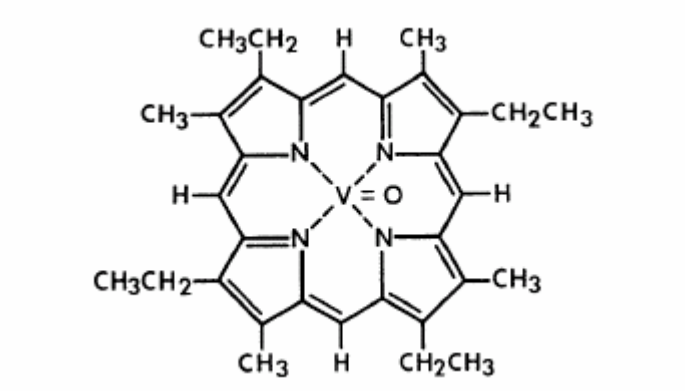

Figure 2.7 Porphyrins, metals in asphalts (Robertson 1991)

All of the naturally occurring heteroatoms, nitrogen, sulfur, oxygen, and metals, contribute to polarity within these molecules. Moreover, oxidation molecules from aging are polar and further contribute to the polarity of the entire system. Polarity, which is the separation of charges within a molecule, has a tendency to cause molecules to organize themselves into preferred orientations, which are related to the intermolecular level. Due to their separated charges, or dipoles, the attraction or repellent among molecules organizes the structure by electrostatic and other short-range forces that are weaker than the covalent chemical bonds. Such functional groups play a major role in the interaction between binder and aggregate surfaces. The interfacial bond strength depends on the relative tendency of the functional groups to adsorb onto aggregate surfaces and to be displaced by water. Earlier studies (Petersen et al. 1974, Plancher et al. 1977, Crutis et al. 1991, Petersen et al. 1998) rank the affinity of bitumen functional groups to adsorb onto and desorb from dry and wet aggregate surfaces. Generally, the most strongly adsorbed polar compounds, such as carboxylic acids and anhydrides, seem to be displaced most easily by water. The highest resistance to water displacement is associated with phenolics, ketones and nitrogen-based pyridinics.

2.2.2 Influence of aggregate characteristics on adhesion

Roberts et al. (1991) state:

> Aggregates typically provide a heterogeneous surface onto which specific bitumen chemical functionalities preferentially adsorb by interacting with aggregate adsorption sites. The forces of interfacial interaction depend on the type and surface activities of the aggregate, which themselves depend on the nature of minerals and metallic ions present. Common minerals in aggregates include silica, feldspars, ferromagnesian, limestone and clay minerals.

Petersen et al. (1998) explain that silica mineral (SiO_2), abundant in quartz, constitutes the bulk of quartzites and granites. Silica is important due to its natural abundance of siliceous surfaces in most aggregates used in practice. Active sites on these surfaces range from surface hydroxyl groups of varying acidities to hydrogen bonding sites of high acidity. Also, Jones et al. (2004) note that feldspar minerals have mobile species within their crystal structures. Limestone is comprised mainly of $CaCO_3$ which, after crushing, exposes calcium ions with electropositive characteristics. The calcium ions are then available for competition between water and bitumen. Cheng et al. (2002) measured the bonding energy using a Universal sorption device. Their results show that the bonding energies per unit mass for the limestone are higher than that for the granite. Little et al. (1991), in their research on stripping, discuss aggregate surfaces rich in metallic elements, such as calcium, that seem to improve stripping resistance. This resistance to stripping is due to the fact that such metals strongly associate with bitumen acids, and thus form hydrophobic salts that are not water soluble. Jamieson et al. (1995) have also pointed out that interfacial bonding is enhanced by relatively large concentrations of iron, calcium, magnesium and aluminum at the aggregate

surface. Yoon et al. (1988) report that some of the aggregate physical properties that influence moisture damage include surface roughness, porosity, shape, friability and the presence and nature of adsorbed coatings. Good bonding is promoted by rough-textured aggregate surfaces. A general, and traditional, classification of aggregates based on surface charge is presented in Figure 2.8.

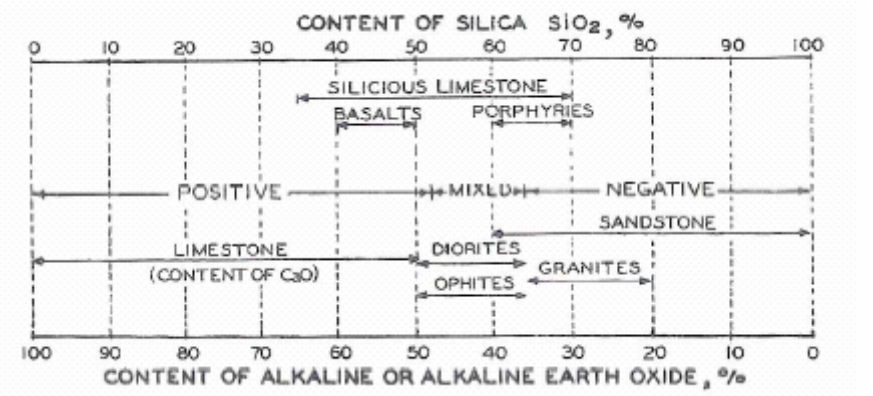

Figure 2.8 Classification of aggregates (Mertens et al. 1959)

2.2.3 Mineral fillers

Mineral fillers have traditionally been used in asphalt mixtures to fill the voids between the larger aggregate particles. Generally, the aggregate material passing the No.200 sieve is referred to as filler. In ASTM D242, mineral filler is defined as consisting of finely divided mineral matter, such as rock dust, slag dust, hydrated lime, hydraulic binder, fly ash, loess, or other suitable mineral matter. Other materials, such as carbon black and sulfur, have been used primarily to modify asphalt binder properties, but they do have a role as filler, also. Typically, an increase in filler lowers the optimal asphalt content, increases the density, and increases the stability (Brown et al. 1989).

Tunnicliff (1967) and Puzinauskas define mineral fillers as the portion of the mineral aggregate generally passing the No. 200 sieve and occupying void spaces between the coarser aggregate particles in order to reduce the size of these voids and provide contact points between larger aggregate particles, thereby strengthening the mixture. Further, when mixed with the asphalt, mineral fillers form a high consistency binder or matrix of colloidal suspension in the asphalt binder and become mastic with a stiffer consistency to hold larger aggregate particles together.

Fillers may be used to:

- fill voids and, hence, reduce the optimum asphalt content;
- meet specifications for aggregate gradation;
- increase stability; and
- improve the bond between asphalt cement and aggregate.

Mineral fillers have been used primarily to fill in the voids between the aggregate particles and to meet specified gradations for HMA. However, it has been documented extensively in the literature that mineral fillers such as baghouse fines do affect the behavior of asphalt binders and HMA mixtures (Kandhal 1981, Anderson 1987). Mineral fillers cause a general stiffening or reinforcing effect in HMA mixtures. However, the extent of the stiffening effect is generally dependent upon the Rigden void content (i.e., voids between the fine particles in a dry compacted state) which, in turn, is affected by mineralogic type, size distribution, particle shape, and surface texture of the mineral fillers (Kandhal 1981). Some baghouse fines, primarily those containing clay, can increase the potential for stripping in HMA mixtures.

All fillers must be fed to the asphalt mixture consistently and in correct proportions; otherwise, the mix properties are adversely affected. Excessive amounts of filler usually reduce the voids in mineral aggregate (VMA) to a point where sufficient asphalt content for a durable mix cannot be added. High filler content also increases the aggregate surface area and, thus, greatly reduces the asphalt film thickness. Further, mineral filler characteristics vary with the gradation of the filler. If the size of the mineral filler particles is smaller than about 10 microns, the filler acts as an extender of the asphalt cement because the thickness of most asphalt films in dense-graded HMA is less than 10 microns. If the mineral filler size is larger than 10 microns, it acts more like an aggregate. If an excessive amount of this larger sized mineral filler is present, the asphalt content may increase because of increased VMA. Therefore, care must be taken to consider not only the amount of mineral filler, but also its

size when evaluating whether an excessive amount of fine material is present in a mix that is being designed or controlled in the field (Roberts et al. 1996).

Some specifications place limits on the dust-to-asphalt cement ratio. A typical specification requires the dust-to-asphalt cement ratio to be between 0.6 and 1.2 by weight. An ideal specification should require that such a ratio based on volume should take into account the Rigden voids (which generally control the stiffening effect). However, stiffer consistency mastic may create brittle mixtures that lead to adverse effects such as cracks in pavements under low temperature conditions. However, based on the study of Chen (1998), the asphalt-mineral filler mastics show an increased tensile strength and tensile failure strain with the addition of mineral fillers; these findings are valid for limited mastic systems, and the moisture effects were not considered. Nonetheless, the effects of active filler, through its chemical interaction with an asphalt-aggregate system, can compensate for the adverse effects of inert filler.

2.3 Physical and Chemical Properties of Lime

2.3.1 Definition of hydrated lime

Quicklime (CaO) is produced by calcining high quality limestone at a temperature (1315°C) that is long and high enough to dissociate the carbonates, thus volatizing the carbon dioxide (CO_2) by half the weight of the limestone. Hydrated lime ($Ca(OH)_2$) is a dry powder obtained by hydrating quicklime with sufficient water to form a hydroxide. Lime may also include magnesium oxide or magnesium hydroxide, designated as dolomitic lime (5% to 35%

magnesium carbonate in the limestone), which is less reactive with soil than high calcium lime (0% to 5% of magnesium carbonate in the limestone).

The following chemical diagrams explain the reaction of high calcium and dolomitic quicklime:

Limestone + Heat ? High Calcium Quicklime + Carbon Dioxide

$CaCO_3$ + (~1315°C) ? CaO + CO_2

Dolomitic Limestone + Heat ? Dolomitic Quicklime + Carbon Dioxide

$CaCO_3 \cdot MgCO_3$+ (~1315°C) ? $CaO \cdot MgO + CO_2$

The hydration process that transforms quicklime to hydrated lime is as follows:

High Calcium Quicklime + Water ? Calcium Hydroxide + Heat

CaO + H_2O ? $Ca(OH)_2$ + Heat

Dolomitic Quicklime + Water ? Hydrated Lime + Heat

$CaO \cdot MgO + H_2O$? $Ca(OH)_2 \cdot MgO$ or $Ca(OH)_2 \cdot Mg(OH)_2$ + Heat

2.3.2 Physical properties of hydrated lime

The substantial physical properties of lime for soil stabilization, as discussed by Boynton (1979), are specific gravity, bulk density, particle size, heat of hydration and solubility of hydrated lime.

The range of specific gravities and bulk-specific gravities for different hydrates are 2.3 to 2.9 and 400 to 640 kg/m^3, respectively. The molecular weight of CaO and $Ca(OH)_2$ are 56.08 and 74.10, respectively, due to the extra H_2O molecule attached. The equal amounts of lime available to react with the soil are provided by the molecular weight ratio. The normal

grades of hydrated lime have 75% to 95% passing the No. 200 sieve. High calcium lime provides more available calcium for stabilization than $Mg(OH)_2$ because $Ca(OH)_2$ is about 100 times more soluble. Also, MgO in dolomitic quicklime may retard the rate of reaction of lime that results in expansion after compaction due to its slow hydration, even though it does not affect the solubility of $Ca(OH)_2$.

2.3.3 Chemical properties of hydrated lime

The destabilizing effect of quicklime and hydrated lime can be influenced by moisture and CO_2 , respectively. Specifically, carbon dioxide results in the reformation of calcium carbonate ($CaCO_3$).

The pH of lime-water solutions gradually rises, and sharply increases with the addition of low concentrations of $Ca(OH)_2$ up to the pH value of 11. Due to its reactivity with soil minerals at high pH levels, which results in a cementitious product, the high pH of solutions is important in stabilization. Also, the rate of lime solubility increases with the higher specific surface areas of hydroxide particles.

A pozzolan is defined by ASTM as:

> A siliceous or siliceous and aluminous material, which by itself possess little or no cementitious value, but will, when in a finely divided form and in the presence of moisture, chemically react with calcium hydroxide at ordinary temperature to form compounds possessing cementitious properties.

The pozzolanic cemented products that help reduce plasticity are calcium-silicate-hydrates (CSH : Ca^{++} + OH^- + Soluble Clay Silica) and calcium-aluminate-hydrates (CAH :

Ca^{++} + OH^{-} + Soluble Clay Alumina). Clay is a possible source of silica and alumina for a pozzolanic reaction.

The addition of lime provides a high pH to dissolve the silica and alumina. Lime also provides the available calcium divalent cation (Ca^{++}) to combine with the silica and alumina supplied by the clay to produce a pozzolanic reaction.

2.4 Benefits of Lime in Asphalt Concrete

2.4.1 Mechanisms of the lime-asphalt interaction

Hydrated lime has the potential to perform as a multifunctional modifier in asphalt. Lime improves the rheological properties of asphalt binders as inert filler. As inert filler, lime imparts a stiffening of the asphalt mixture and an improvement in resistance to permanent deformation. Lime also has an active filler effect, which is the unique ability to reduce age-hardening characteristics of asphalt mixtures by interacting with reactive polar compounds in the binder, thus reducing the carboxyl-type oxidation products formed during aging and reducing the ratio of asphaltenes to oxidation products formed upon oxidation.

Lime is also well known and widely used in asphalt for its ability to substantially reduce the deleterious effects of moisture. Moisture in asphalt promotes loss of strength and loss of aggregate. The mechanism responsible for the ability of hydrated lime to reduce the effects of moisture damage is synergic to the reduction of the age-hardening process and the ability of lime to improve the bond between the binder and the aggregate (Little 1996).

Carboxylic acids contribute to a strong bond formation, although only small amounts are present in bitumen. The WRI (Western Research Institute, located in Wyoming and under

FHWA contract) studied the mechanisms of acid-base complex formation and its effect on mixes; its research focused on the role of carboxylic acids (2003).

Calcium carbonate reacts with weak acids, carboxylic acids, in bitumen (Logaraj 2002). At mixing temperatures, an insoluble salt of carboxylic acid, water, and carbon dioxide is produced.

$CaCO_3 + 2RCOOH \rightarrow (RCOOH^-)_2 + H_2O + CO_2$

When hydrated lime (or calcium hydroxide, Ca(OH)2) is present in the absence of carbonates, water is the only reaction product formed.

$Ca(OH)_2 + 2RCOOH \rightarrow (RCOO^-)_2Ca + 2H_2O$

Logaraj (2002) states that when aggregates are exposed to a direct flame in the HMA plant, temperatures up to 700°C can be encountered, at least for a brief moment. Under these conditions, the calcium carbonate surface can decompose into calcium oxide (CaO, or quicklime) and carbon dioxide. Furthermore, calcium oxide, which is a strong base, reacts instantaneously with the acids in the bitumen, as depicted in the following reaction.

$CaO + 2RCOOH \rightarrow (RCOO^-)_2 + H_2O$

It is well known that hydrated lime, as active filler, changes the physical properties of a mix through its chemical interaction with the bitumen. Little and Jones (2003) report that hydrated lime ties up carboxylic acids and 2-quinolones in the bitumen with the formation of insoluble calcium organic salts; this process prevents these functionalities from reacting with a siliceous surface to form water-sensitive bonds. This phenomenon leaves important active sites on the siliceous surface to form strong water-resistant bonds with nitrogen groups in the bitumen.

Some specific types of HMA pavement distress modes affect pavement performance and are related to the rheological properties of asphalt cement.

2.4.2 Moisture damage

Moisture damage can occur when the bond between asphalt cement and aggregate breaks down due to the presence of moisture on the interface of the asphalt-aggregate system, thus causing the binder to separate from the aggregate surface. This failure causes loss of strength, stiffness and durability in an asphalt mixture. Usually moisture damage is considered as a premature failure, and often occurs within a few years after construction.

Loss of adhesion and moisture damage occur together. While loss of adhesion causes a serious moisture damage problem, a different type of moisture damage may also occur more slowly. In such a case, stripping may not be obvious, but the integrity of the mix performance, which relates to the resistance to fatigue cracking and rutting, is gradually diminished by moisture. The former case is directly related to the physico-chemical properties of the material (i.e., internal factors) and the latter relates to external factors, such as heat, heavy rains, F-T cycles, and traffic-induced premature stripping, that affect the in-place properties of HMA pavements. Most research has focused on the first type of failure, and less attention has been given to the second case.

2.4.2.1 Moisture damage due to physico-chemical properties

Adhesion of asphalt to aggregate is controlled either at the molecular level or at the inter-molecular level. In the SHRP, it has been shown that polarities of the aggregates vary with the environment, such as moisture content, temperature, etc. However, for this discussion, the aggregate is considered to be simply a highly polar surface. Since polarity

promotes the attraction of the polar in the asphalt to the polar in the surface of the aggregate, adhesion occurs.

Based on the observations of Petersen and Plancher (1998), the specific chemical types on the aggregate surface are carboxylic acids and anhydrides, sulfoxides, 2-quinolone types, ketones, phenolics, and nitrogen compounds. At the molecular level of asphalt, it has been observed that basic nitrogen compounds (pyridines) tend to adhere strongly to aggregate surfaces. Carboxylic acid salts tend to be removed from the aggregate more easily, but this tendency varies with the type of salt. Monovalent cation salts, such as sodium or potassium, of acids tend to be removed from aggregate quite easily. Calcium or other divalent salts of acids are much more resistant to the action of water.

Results from a dry benzene extraction experiment indicate that the strongly adsorbed asphalt fractions that are not extracted with benzene exist on the aggregate surface as a single molecule monolayer in thickness (Petersen et al. 1982).

Carboxylic acids and 2-quinolone types are found to be the compound types most strongly adsorbed on an aggregate surface, and also most easily displaced from most aggregates by moisture. Sulfoxides are also adsorbed on the aggregate surface in high concentrations, and usually are sensitive to water displacement.

The selective adsorption of carboxylic acids and related components on siliceous aggregates, and their selective displacement by water, is of particular significance regarding pavement moisture damage. Siliceous aggregate surfaces have high concentrations of hydroxyl groups that have high affinity for both carboxylic acids and water. Thus, adsorption

of carboxylic acid components of the asphalts by the siliceous aggregate creates an asphalt-aggregate interface sensitive to disruption by the action of water (Petersen et al. 1998).

Water is a highly polar material and is transported into the asphalt due to the attraction of polar water molecules to polar asphalt components. In the presence of moisture in the asphalt, moisture affects the mechanical properties of the asphalt, such as softening the asphalt. This occurrence typically results in strength reduction and further permanent deformation or other distresses.

Aged asphalts more tend to incorporate water than virgin asphalts due to their given greater amounts of polar. The probability of moisture presence increases with pavement age. However, aged pavements are also stiffer than their new pavement, thus the effects of moisture and oxidation somewhat counteract each other.

2.4.2.2 Moisture damage with environmental characteristics (heat, heavy rains, freeze/thaw cycles, and traffic)

Inadequate pavement drainage creates water or moisture vapor, which induces stripping. Extensive research has been conducted at the University of Idaho into the mechanisms of asphalt stripping; it is reported that:

> . . . . air voids in asphalt concrete may become saturated with water even from vapor condensation due to water in the subgrade or subbase. A temperature rise after this saturation can cause expansion of the water trapped in the mixture voids resulting in significant void pressure when the voids are saturated.

It has been found that void water pressure may develop to 20 psi under differential thermal expansion of the compacted asphalt mixture and could exceed the adhesive strength of the binder aggregate surface. If the asphalt concrete is permeable, water can flow out of

the void spaces under the pressure developed by the rise in temperature and, in time, relieve that developed pressure. If not, then the tensile stress resulting from the pressure may break the adhesive bonds and the water could then flow around the aggregates, thus causing stripping. Lottman (1971) states in his research on moisture mechanisms:

> The stripping damage due to void water pressure and external cyclic stress (by traffic) mechanism is internal in the specimens, the exterior sides of the specimens do not show stripping damage unless opened up for visual examination.

Majidzadeh and Brovold (1966) state that the pore pressure from traffic-induced stresses can also cause failure of the binder-aggregate bond. Initially, the traffic stresses may further compact the mixture and trap or greatly reduce the internal water drainage. Therefore, the initial water is in frequent motion (cyclic), and considerable pore pressure builds up under the action of the traffic.

Further, other factors that cause premature stripping are: inadequate compaction of HMA; excessive dust and clay coatings on the aggregate, which can inhibit the necessary intimate contact between the asphalt cement and aggregate and can provide a channel for penetrating water; inadequate drying of the aggregate, thus causing a high residual moisture content in the mineral aggregate; weak and friable aggregate under heavy traffic, thus causing the degradation or delamination that exposes new uncoated aggregate surfaces that are susceptible to moisture absorption; and overlay on deteriorated concrete pavement (Kandhal 1992).

When lime is added to HMA, it reacts with the aggregates, strengthening the bond between the bitumen and the aggregate. At the same time that it treats the aggregate, lime

also reacts with the asphalt itself. Lime reacts with highly polar molecules that can otherwise react in the mix to form water-soluble soaps that promote stripping. When those molecules react with lime, they form insoluble salts that no longer attract the water (Petersen et al. 1987). In addition, the dispersion of the tiny hydrated lime particles throughout the mix makes the mix stiffer and tougher, thereby reducing the possibility that the bond between the asphalt cement and the aggregate will be broken mechanically, even if water is not present.

2.4.3 Rutting

Rutting is a permanent deformation of the asphalt, caused when elasticity is exceeded by the progressive movement of materials under repeated loads either in the asphalt pavement layers or the underlying base. This phenomenon can occur either through consolidation or plastic flow (Roberts et al. 1996).

Consolidation is the further compaction of HMA pavements by traffic after construction. When compaction is poor, the traffic provides a repeated kneading action in the wheel track areas and completes the consolidation to the designed air voids. A substantial amount of rutting can occur if very thick asphalt layers are consolidated by the traffic.

Rutting also results from lateral plastic flow (permanent deformation) of the HMA from the wheel tracks. Use of excessive asphalt cement is the most common cause for this phenomenon. Too much asphalt cement in the mix causes the loss of internal friction between aggregate particles and results in the loads being carried by the asphalt cement rather than the aggregate structure. Plastic flow can be minimized by using large-sized

aggregate, angular and rough-textured aggregate, and providing adequate compaction at the time of construction.

The viscosity of asphalt cement plays a relatively small role in the rut resistance of HMA if well-graded, angular and rough-textured aggregates are used. Some increased resistance to rutting can be obtained by using stiffer asphalt cements. However, stiffer asphalt cements are more prone to cracking during winter in cold regions, especially if they are used in the surface courses. Certain mineral fillers (such as baghouse fines) also increase the apparent viscosity of asphalt cement and, thus, make the mix more resistant to rutting. However, use of excessive fines should be avoided.

Hydrated lime significantly improves the performance of asphalt in this respect. Unlike most mineral fillers, lime is chemically active rather than inert. It reacts with the bitumen, removing undesirable components at the same time that its tiny particles disperse throughout the mix, thus making it more resistant to rutting and fatigue cracking (Petersen et al. 1987).

The stiffening that results from the addition of hydrated lime can increase the performance grade (PG) rating of asphalt cement. Moreover, the addition of the lime does not cause the mix to become more brittle at lower temperatures. At low temperatures, the hydrated lime becomes less chemically active and behaves like any other inert filler (Little et al. 2005).

2.4.4 Cracking from fatigue and low temperatures

2.4.4.1 Types and causes of cracking

Pavement cracks can generally be described according to their geometry, such as longitudinal, transverse, polygonal (also alligator and map) and block. Over the years,

engineers have categorized cracking into two phenomenological groups, load-associated and nonload-associated.

Causes associated with cracking in asphalt pavements are varied, depending to some extent on the type of cracking. Probably the most common associations are made with the following factors: structural design, asphalt properties, asphalt concrete mix design, construction procedures, aggregate properties, asphalt and aggregate durability, subgrade support, the condition of the underlying pavement (for overlays), temperature, drainage (or lack of drainage) and traffic (Finn et al. 1976).

2.4.4.2 Fatigue cracking (load-associated)

Load-associated cracking has been described as fatigue cracking, which is fracture under repeated or fluctuating stress having a maximum value less than the tensile strength of the material. It is generally suggested by researchers that any pavement will eventually exhibit fatigue cracking. Exactly when such cracking will occur depends on the fatigue properties of the pavement section. It is pertinent to note that other types of load-associated cracks exist, e.g., those caused by a single excessive load, slippage, lateral movements in fills due to traffic, and excessive strains associated with rutting. Reflection cracking can also be considered at least partially load-associated. Fatigue cracking can be minimized by controlling several variables, such as aggregate gradation, asphalt content with rough-textured aggregate, air voids, and water content.

2.4.4.3 Low temperature cracking (nonload-associated)

Low temperature cracking is the most prevalent distress found in asphalt pavements constructed in cold weather climates. As the temperature drops, the restrained pavement

tends to shrink. The tensile stresses build up to a critical point when a crack is formed and partial stress relief occurs. These cracks can be initiated by traffic, cycles of temperature changes, and then propagated by a large drop in temperature. The most significant effects on crack formation and propagation are aging and moisture. The current Superpave specification attempts to address this issue by specifying a limiting low temperature for the asphalt binder.

2.4.4.4 Reflection cracking

Reflection cracking can be described as the surface replication of the joints and cracks that are located in the underlying layers of the pavement and foundation materials. Reflection cracking includes the cracking of a surface course of the original pavement due to the reflection of a joint or crack originating in a base course or subgrade, as well as cracking of an overlay.

In general, cracking occurs often in stiffer asphalt mixes due to the formation of microcracks; however, the addition of lime improves fatigue characteristics and reduces cracking because these microcracks are intercepted and deflected by very small hydrated lime particles. The stiffening effect of the filler is considerably less at temperatures near the glass transition of the bitumen than at high temperatures. This characteristic causes the binder to relax at low temperatures, thus dissipating energy through deformation instead of fracture. Further, lime reduces cracking more than inactive fillers because of the reaction between the lime and the polar molecules in the asphalt cement, which increases the effective volume of the lime particles by surrounding them with large organic chains (Lesueur et al. 1999). Consequently, the lime particles are better able to intercept and deflect microcracks, thus

preventing the microcracks from growing together into macrocracks that can cause pavement failure.

Little et al. (2005) evaluated the stiffening effect of fillers through a fracture toughness test at low temperatures using the complex modulus (E*) that accounts for the viscoelastic effects. The lower the temperature, the more closely hydrated lime-treated mastic (bitumen + filler) behaves as classical filler in the asphalt binder.

2.4.4.5 Oxidation and aging that cause brittle pavement

Aging is actually considered as a conditioning step that may be beneficial for a soft mixture that has the potential to rut and deform, or it can be detrimental in terms of excessive hardening that has the potential to crack under traffic loading and thermal stress. Oxidative hardening, which increases the amounts of polarities present among asphalt molecules, creates permanent hardening in asphalt, whereas the organizational hardening caused by temperature and molecular orientation is reversible.

Based on the SHRP report by Robertson (1991), the greater polarity and larger amounts of the molecules impart a propensity for the molecules to associate themselves due to stronger attraction. However, the aging process in a pavement is very slow due to the high viscosity of the asphalt; eventually the molecules find the best orientation to reach a thermodynamic equilibrium state, which results in a stiffer material.

The addition of hydrated lime to asphalt cement reduces the rate at which the asphalt oxidizes and ages due to the chemical reactions that occur between the calcium hydroxide and the highly polar molecules in the bitumen.

From their experimental research, Plancher et al. (1976) proposed that lime reduces the formation of oxidation products in asphalt by the removal of polar compounds (carboxyl acids and 2 quinolones) that react with the products of oxidation to form viscosity-building associations (asphaltenes). That is, lime reduces the sensitivity of the asphalts. Further, the more polarized molecules, including quinolones and carboxylic acids, and the higher asphaltene content in bitumen, which indicates high viscosity and aging characteristics, interact more intensively with hydrated lime because of an increase in specific surface, the nature of calcium hydroxide, or a combination of both. The effects of these interactions in the hydrated lime improve low temperature flow properties and aging characteristics (Petersen et al. 1987, Hoffman et al. 1998, Little et al. 2005).

2.5 Methods of Introducing Hydrated Lime into Mixes

Even though it has been shown repeatedly that the use of hydrated lime in asphalt concrete mixtures is beneficial, confusion still exists as to the best method for adding lime to asphalt mixtures. In general, contractors and/or transportation departments have adopted one or more of three popular techniques that incorporate lime into HMA. The three techniques, along with a brief description of each and the major positive and negative features of each, are listed in Table 2.1 (Button et al. 1983).

2.5.1 Addition of dry hydrated lime to dry aggregate

Adding dry hydrated lime to dry aggregates is the simplest method of introducing hydrated lime to asphalt mixes. This method was first adopted by the state of Georgia in the early 1980s. In this method, hydrated lime and mineral filler are added in a drum mixer

immediately after the asphalt is introduced. Hydrated lime thus comes in contact with the aggregates directly, resulting in an improved bond between the aggregate and asphalt. The portion of lime that fails to come in contact with the aggregate gets mixed in with the asphalt. This reaction of the lime with highly polar molecules in the asphalt forms insoluble salts that no longer attract water, thus reducing the stripping and oxidation potential.

2.5.2 Addition of dry hydrated lime to wet aggregate

Adding dry hydrated lime to wet aggregate is the most general method of adding hydrated lime to asphalt mixes. In this method, hydrated lime is metered into aggregate that already has a moisture content of 2% to 3% over its saturated-surface-dry (SSD) condition. After hydrated lime is added to the wet aggregate, the lime-aggregate mix is processed in a pugmill to insure thorough mixing. The advantages of introducing dry hydrated lime to wet aggregate are that the asphalt mixture provides better coverage and allows for proper application as compared to the method that adds dry hydrated lime to dry aggregate. These advantages are possible because moisture ionizes lime and helps distribute it on the surface of the aggregate. The portion of hydrated lime that does not adhere to the aggregate eventually gets mixed with the asphalt, thus contributing to the same improvements that are inherent of the dry method. The main disadvantage of this method is the extra effort and fuel required to dry the aggregates before mix production. When using this method of adding hydrated lime, many states require that the lime-aggregate mix marinate for about 48 hours.

2.5.3 Addition of hydrated lime in the form of slurry

In this method of adding lime, a slurry mixture of lime and water is metered and applied to the aggregate to achieve a superior coverage of the stone surfaces. Lime slurries are made from hydrated lime, but sometimes quicklime is also used. The treated aggregates can be marinated or used directly. The advantages of using this method include: 1) the resistance of HMA to stripping; 2) minimal lime dispersion due to dusting and blowing; and 3) the fact that it provides the best coverage of lime over the aggregate. The disadvantages of

using lime slurries include: 1) fuel consumption during the drying process; and 2) the need to purchase and maintain specialized costly equipment.

Table 2.1 Lime Addition Techniques

Method	Description	Major Positives	Major Negatives
Dry	– Simplest method – Lime and mineral filler introduced immediately after introduction of asphalt	– Least expensive method – Direct contact between aggregates and hydrated lime – Lime and mineral filler introduced immediately after introduction of asphalt	– Dusting and lime loss – Minimal mixing and coating of aggregates
Wet	– Lime metered into aggregate at a moisture content of 2-3% higher than SSD condition – Mixture processed in pugmill to ensure thorough mixing	– Proper coverage and application – Portion not mixing with aggregate will mix with asphalt, thus still aiding as anti-stripping agent	– Expensive due to extra fuel needed to dry aggregates before mix production
	– Aggregates kept in moist condition and marinated for up to 48 hours	– Moisture content slowly reduces over stockpiling period – Stockpiling can be separated from production, thus providing an economic advantage	– Aggregate handling effort is increased – Storage space needed for aggregate stockpiling – Concerns over carbonation of stockpiles with long stockpiling times
Slurry	– Slurry of lime and water applied to aggregates – Marinating optional	– Improved coverage of aggregates – Reduced dispersion and loss of lime – Improved stripping protection	– Increased water and fuel costs – Expensive, specialized equipment requirements

2.6 Asphalt Concrete Mix Design

The objectives of HMA concrete mix designs are to develop an economical blend of aggregates and asphalt that meet design requirements as a function of traffic levels and climate conditions.

An effective HMA mix design must include:

- Sufficient asphalt to ensure a durable pavement;
- Sufficient stability under traffic loads;
- Sufficient air voids (with an upper limit to prevent excessive environmental damage, such as water and aging, and a lower limit to allow room for initial densification due to traffic); and
- Sufficient workability.

Typically, mix design methods consist of three basic steps: aggregate selection, asphalt binder selection, and optimal asphalt binder content determination corresponding to 4% air voids with specific compaction efforts.

It is important to recognize that mix design methods are designed to be constructed in the field with the appropriate asphalt content. It is also important to understand the limitations of the design method. If the service conditions of the designed mixture are different from the conditions for which the design method was developed, then the mixture design may not be adequate for service even though it has been designed according to the method.

To enhance understanding of this idea, three mix design methods are discussed in the following subchapters.

2.6.1 Historical methods

2.6.1.1 Marshall mix design

The earliest version of the Marshall mix design was developed by Bruce Marshall for the Mississippi Highway Department in the late 1930s. The Corps of Engineers Waterway Experiment Station (WES) began a study in 1943 to develop a simple apparatus for airfield pavements with increased wheel loads during World War II. These engineers also evaluated various compaction efforts, such as impact compaction, and produced densities in the laboratory that were similar to those achieved in the field. In addition, they simulated aircraft loadings in order to select the proper, optimal asphalt content. The number of blows and the foot design for the compactor were determined as a standard. Initial criteria were established and upgraded for increased tire pressures and loads. Stability testing (for stability and flow) was also performed to check if the optimal asphalt binder content passed the requirements.

The advantages of the Marshall mix design include that it is easy to use and control and that it uses relatively light, portable and inexpensive equipment. Also, the Marshall mix design pays proper attention to voids, strength, and durability. However, disadvantages include problems that stem from the impact compaction method and the disregard for the shear strength and the axis of compaction perpendicular to the applied load.

2.6.1.2 Hveem mix design

The basic concepts of the Hveem mix design method were originally developed by Francis Hveem when he was a Resident Engineer for the California Division of Highways in

the late 1920s and 1930s. This mix design is still being used in a few west coast states. It addresses similar design considerations as the Marshall mix design. It considers asphalt absorption by the aggregate and uses a kneading compactor to prepare specimens. The shear strength and horizontal deformation of samples under loading along the axis of compaction are measured using the Hveem stabilometer to determine stability. Then, the selected optimum asphalt content corresponding to 4% air voids can be checked as to whether it passes the requirements of stability and cohesion.

The advantages of the Hveem mix design include attention to air voids, strength, and durability as well as the use of the kneading compactor, which simulates field conditions. Also, the Hveem mix design provides a strength parameter, i.e., a direct indication of the internal friction component of shear strength. However, the disadvantages include that it is expensive, employs equipment that is not easily portable, and it does not offer a wide range of stability measurements.

2.6.2 Superpave volumetric mix design

The Superpave mix design method is a direct result of the SHRP. The primary purpose of this program is to develop a rational mix design procedure. The aggregate is selected using gradation specifications, requirements of aggregate angularity, flat and elongated particles, clay content, and aggregate criteria such as durability and soundness. For the asphalt binder specification, Superpave PG systems are selected based on the expected pavement temperature extremes in the area of their intended use. The Superpave Gyratory Compactor

(SGC) was selected as the compactor because it orients the aggregate particles in a way similar to that observed in the field.

The mix design method uses volumetrics to select the optimal asphalt content. Mixtures are compacted in the laboratory to provide a density equal to the estimated density in the field after various levels of traffic. The number of gyrations is varied to simulate anticipated traffic. The air voids at Ninitial, Ndesign, and Nmaximum are measured to evaluate the mixture quality. The mixture should have a certain level of minimum air voids at each gyration number.

In the Superpave mix design process, no accepted standard performance tests are included, so no tests similar or analogous to the Hveem stability and cohesion tests were used. In addition, industry demands necessitate a simple performance-related test that provides reliable performance of the HMA mixture during the volumetric mixture design process using the SGC. For that reason, the FHWA committed funding to identify and evaluate a simple strength test and further authorized the University of Maryland Superpave Models Team to develop all necessary test protocols, criteria, and guidelines for a SPT to support the Superpave volumetric mix design procedure. A SPT is defined as a test method that accurately and reliably measures a mixture response characteristic or parameter that is highly correlated to the occurrence of pavement distress (cracking and rutting) over a diverse range of traffic and climatic conditions. One of the requirements for a SPT is that it can measure a fundamental engineering property that can be linked to the advanced material characterization methods of the detailed distress prediction models, which are the permanent deformation model, the fatigue cracking model, and the thermal cracking model.

2.6.3 Performance-related mix design

The performance-balanced mix design has been studied for a long time by other researchers (C. L. Monismith, J. A. Epps, F. N. Finn, R. Leahy, R. G. Hicks). When rutting problems occurred in the 1980s, reducing rutting became a predominant issue. As a consequence of using coarse gradation, extra filler, and hard-grade asphalt binder, and reducing the asphalt binder content, this problem of rutting has diminished markedly. However, improved rutting resistance has brought about a negative result for fatigue resistance, such as early cracking, insufficient durability with increased air voids, and poor workability with the use of stiffer asphalt concrete mixtures (Brown 2005).

It is important to note that a mix designer does not concentrate on optimizing only one property of a mix at the expense of others. It is comparatively easy to produce a rut-resistant mix by using a hard-grade binder, reducing the binder content and adding extra filler. Such a mix, however, would likely fail through fatigue and would probably be prone to rapid oxidation hardening. For a successful performance-based mix design procedure, a balance should be obtained between the results of the volumetric mix design and of the performance-based mix design by employing SPTs for both rutting deformation and fatigue resistance.

Chapter 3

Theoretical Background

The development of a SPT for assessing fatigue performance has been less successful than the development of such a protocol for permanent deformation performance (Witczak et al. 2000). Further, work at North Carolina State University (NCSU) has led to the development of the Viscoelastoplastic Continuum Damage (VEPCD) model for asphalt concrete behavior. Based on the fundamental, mechanistic basis of this model and the ease with which it can be characterized (i.e., linear viscoelastic (LVE) characterization and constant crosshead rate tests at multiple rates and temperatures), it was decided to utilize the VEPCD model to assess the fatigue performance of the mixtures in this study.

The underlying principles of the VEPCD modeling approach are linear viscoelasticity, continuum damage mechanics and strain-hardening viscoplasticity. For a more rigorous treatment of the subject, refer to previous work (Chehab et al. 2002, 2003; Underwood et al. 2006) and to the work of Schapery (1990, 1999) for linear viscoelasticity and continuum damage mechanics.

The theory of linear viscoelasticity describes the constitutive behavior of time-dependent materials, such as asphalt concrete. Characterization of LVE behavior in the VEPCD model is accomplished using |E*| tests. On the simplest level, continuum damage mechanics considers a damaged body with some stiffness as an undamaged body with a reduced stiffness. Thus, the goal of continuum damage mechanics in the VEPCD model is to quantify the amount of damage that has occurred in the sample and determine the impact of this damage on the material behavior. For quantifying the damage occurring in the material, an internal state variable, S, based on Schapery's work potential theory, is utilized. The relationship between S and material integrity is termed the *damage characteristic curve*, or C vs. S curve, and represents the fundamental resistance of a mixture to damage.

3.1 Linear Viscoelasticity

The theory of viscoelasticity has been successfully applied by many researchers to describe the characteristics of asphalt concrete. As a viscoelastic (VE) material, asphalt concrete is time- and rate-dependent. The response of a VE material depends not only on the current state of input, but also on all past history of input; that is, the material has a memory for all past input. The response of a LVE body to any loading history may be expressed in terms of a convolution integral. To check if the system is linear, the following two conditions should be satisfied:

a) homogeneity: $R\{AI\}=A\{RI\}$ and (3.1)

b) superposition: $R\{I_1+I_2\}=R\{I_1\}+R\{I_2\}$, (3.2)

where I, I_1, I_2 = input histories; R = response; and A = arbitrary constant. The brackets { } indicate that the response is a function of the input history. The homogeneity, or proportionality condition, essentially states that the output is directly proportional to the input; i.e., if the input is doubled, the response doubles as well. The superposition condition states that the response to the sum of two inputs is equivalent to the sum of the responses from the individual inputs.

For LVE materials, the input-response relationship is expressed through the hereditary integral as

$$R = \int_0^t R_H(t,t)\frac{dI}{dt}dt \ , \tag{3.3}$$

where R_H is the unit response function. With a known unit response function, the response to any input history can be calculated. Equation (3.3) is applicable to an aging system in which time zero is the time of fabrication rather than the time of load application. In this research, it is assumed that the asphalt concrete behavior is that of a non-aging system; thus, Equation (3.3) reduces to

$$R = \int_0^t R_H(t-t)\frac{dI}{dt}dt \ . \tag{3.4}$$

For uniaxial loading, the non-aging constitutive relationships for LVE materials are typically expressed in the convolution integral form, as shown in Equations (3.5) and (3.6):

$$s = \int_0^t E(t-t)\frac{de}{dt}dt \quad \text{and} \tag{3.5}$$

$$e = \int_0^t D(t-t)\frac{ds}{dt}dt \ , \tag{3.6}$$

where E(t) and D(t) are the relaxation modulus and creep compliance, respectively. Both E(t)

and D(t) are referred to as LVE response functions that include the complex modulus, E*, which relates the stresses and strains of a LVE material subjected to sinusoidal loading. The E* is composed of the |E*| and the phase angle ? . To calculate the |E*|, Equation (3.7) is used:

$$|E^*| = \frac{|s^*|}{|e^*|}, \tag{3.7}$$

where $|s^*|$ is the stress amplitude and $|e^*|$ is the strain amplitude of sinusoidal loading. The phase angle ($?$) is calculated using Equation (3.8):

$$? = 2pf?t, \tag{3.8}$$

where f is the loading frequency and $?t$ is the time lag between the stress and strain response.

Viscoelastic response functions can be determined through experiments conducted in the LVE range or through interconversion from other known response functions. LVE properties can be obtained from very short times and small amounts of LVE behavior. Thus, the time-dependent modulus values, i.e., the relaxation modulus and the creep compliance, are oftentimes difficult to obtain because of constraints that stem from the experiments themselves. However, the LVE properties can be measured within a wide range of frequency domains without inducing damage in the specimen; such measurements can be obtained from the E* of a material loaded in a steady-state cyclic sinusoidal manner, which approximates loading histories in many engineering applications. It is then possible, through the theory of linear viscoelasticity, to convert this frequency-dependent property, i.e., the E*, to $E(t)$ and $D(t)$.

3.2 Viscoelastic Continuum Damage

3.2.1 Correspondence principle

Schapery proposed the extended elastic-viscoelastic correspondence principle to address the problem of crack propagation; this principle is applicable to both linear and non-LVE materials (Schapery, 1984). He suggests that constitutive equations for certain VE media are identical to constitutive relationships for elastic cases. Depending upon the boundary condition, three corresponding principles (CPs) were developed:

- CP I: Both pseudo stress and strain (general boundary conditions);
- CP II: Physical stress and pseudo strain (as the crack increases, the traction boundary condition grows), and;
- CP III: Pseudo stress and physical strain (as the crack heals, the traction boundary condition reduces).

For a non-LVE material or a VE material with some type of damage, constitutive relationships cannot be expressed in the convolution integral form. Stresses and strains are not necessarily physical quantities in the VE body. Rather, they are pseudo variables in the form of convolution integrals. Pseudo variables take care of all the hereditary effects. Thus, the time-dependent effects from the stress-strain relationship can be separated, even in the case of non-LVE or damaged materials.

In other words, VE problems can be solved with elastic solutions when physical strains are replaced by pseudo strains. According to Schapery, the uniaxial pseudo strain, e^R, is defined as

$$e^R = \frac{1}{E_R}\int_0^t E(t-\tau)\frac{de}{d\tau}d\tau \,, \tag{3.9}$$

where e is the uniaxial strain; E_R is a reference modulus set as an arbitrary constant typically taken as one; E(t) is the uniaxial relaxation modulus; t is the time of interest; and τ is an integration constant.

Using the definition of pseudo strain in Equation (3.9), Equation (3.5) can be rewritten as

$$s = E_R e^R \,. \tag{3.10}$$

A correspondence can be found between Equation (3.10) and a linear elastic stress-strain relationship (Hooke's Law). The power of the pseudo strain can be seen in Figure 3.1. Figure 3.1(a) shows the stress-strain behavior for controlled-stress cyclic loading within the material's LVE range (such as in a E* test). Because the material is being tested in its LVE range, no damage is induced, and the hysteretic behavior and accumulating strain are due only to viscoelasticity. Figure 3.1(b) shows the same stress data plotted against the calculated pseudo strains. All of the cycles collapse to a single line with a slope of 1.0. The use of pseudo strain simplifies the modeling approach significantly by allowing for the separation of VE (time-dependent) behavior from any accumulated damage.

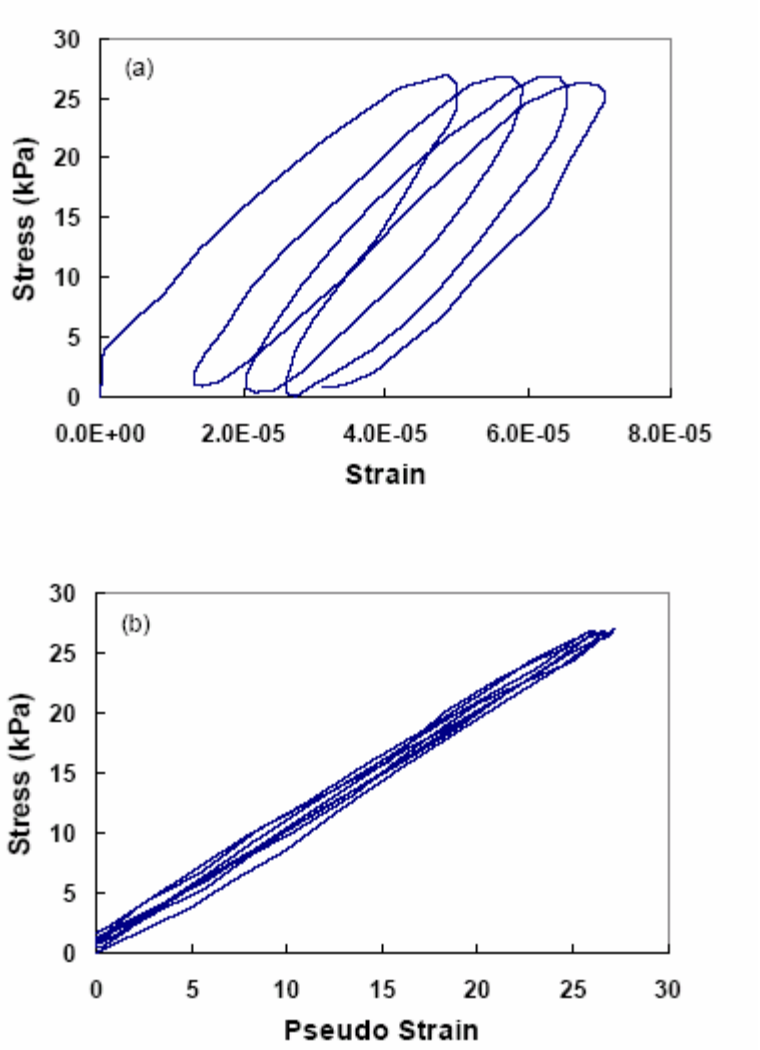

Figure 3.1 (a) Stress–strain behavior for mixtures under LVE cyclic loading; (b) stress-pseudo strain behavior for same data (Daniel 2001)

3.2.2 Viscoelastic continuum damage

The constitutive model was developed by Kim and Lee (Lee 1996, Kim et al. 1997, Lee and Kim 1998a). This model utilizes the elastic-viscoelastic correspondence principle to eliminate the time dependence of the material. The work potential theory (Schapery 1990) is then used to model both the damage growth and healing in the material. The term *damage* is

defined as all structural changes in the constitution of the material, except linear viscoelasticity, that result in the reduction of stiffness or strength as the material undergoes loading. Microdamage healing includes everything except LVE relaxation that contributes to the recovery of stiffness or strength during rest periods, and can include such factors as fracture healing, steric hardening, and non-LVE relaxation.

Schapery (1990) developed a theory using the method of thermodynamics of irreversible processes to describe the mechanical behavior of elastic composite materials with growing damage. Three fundamental elements comprise the work potential theory, as illustrated in Table 3.1.

Table 3.1 Fundamental Elements of the Work Potential Theory

	Elasticity with Damage	Viscoelasticity with Damage
1. Strain energy density function	$W = W(e, S) \quad W = \frac{1}{2} E e^2$	$W^R = W^R(e^R, S)$ $W^R = \frac{1}{2} C(S)(e^R)^2$
2. Constitutive equation (stress-strain relationship)	$s = \frac{\partial W}{\partial e}$	$s = C(S) e^R$ *C(S) : Pseudo secant stiffness*
3. Damage evolution law	$-\frac{\partial W}{\partial S} = \frac{\partial W_S}{\partial S}$ *Energy input = energy required to propagate the crack*	$\dot{S} = \left(-\frac{\partial W^R}{\partial S} \right)^a$

In Table 3.1, the damage parameter, S, represents the internal state variables, and Ws = Ws(S) is the dissipated energy due to structural changes. Using Schapery's elastic-viscoelastic correspondence principle and rate-type damage evolution law (Schapery 1984 and 1990, Park et al. 1996), the physical strains (e) are replaced with pseudo strains (e^R) to include the effects of viscoelasticity. The use of pseudo strain accounts for all the time-

dependent effects of the material through the convolution integral. Thus, the strain energy density function, $W = W(e, S)$, transforms to the pseudo strain energy density function, $W^R = W^R(e^R, S)$.

Schapery's correspondence principle cannot be used to transform the elastic damage evolution law for use with VE materials because both the available force for the growth of Sm and the resistance against the growth of Sm in the damage evolution law are rate-dependent for most VE materials (Park et al. 1996). Simply put, microcracking damage is rate-dependent in asphalt concrete. Therefore, a form similar to power-law crack growth laws is used to describe the damage evolution in a VE material:

$$\dot{S} = \left(-\frac{\partial W^R}{\partial S} \right)^a , \tag{3.11}$$

where $\dot{S}$ is the damage evolution rate, W^R is the pseudo strain energy density function, and a is the material constant.

Lee and Kim (1998b) developed a constitutive model that is independent of mode-of-loading in which the fatigue and microdamage healing of asphalt concrete under uniaxial tensile cyclic loading is described. The slope of the hysteretic stress-pseudo strain loop in damage-inducing testing decreases as loading continues in both controlled stress and controlled strain testing. The decrease in the slope of the loop indicates a reduction in the stiffness of the material as damage accumulates. The stiffness reduction is defined by the pseudo secant modulus (pseudo stiffness). This quantity is typically normalized for specimen-to-specimen variability by the factor, *I*, and denoted as *C*:

$$C = \frac{s}{e^R \times I} . \tag{3.12}$$

Because all the tests conducted in this research for the purpose of VE behavior characterization are in strain control, particularly the constant crosshead-rate tests, if I = 1, the constitutive equations reduce to

$$W_d^R = \frac{1}{2} C(S)(e^R)^2 \text{ and} \tag{3.13}$$

$$s = C(S)e^R, \tag{3.14}$$

where C(S) is a function of the internal state variable, S, that represents the changing stiffness of the material due to microstructure changes, such as accumulating damage or healing. This internal state variable quantifies any microstructural changes that result in the observed stiffness reduction. The relationship between damage (*S)* and the normalized pseudo secant modulus (*C)* is known as the damage characteristic relationship and is a material function independent of loading conditions (Daniel 2001).

To characterize the function C in Equation (3.14), the damage evolution law and experimental data are used. With the ratio of measured stresses to calculated pseudo strains, C values can be determined using Equation (3.11). To find the characteristic relationship between C and S, the values of S must be obtained through Equation (3.15):

$$\frac{dS}{dt} = \left(-\frac{\partial W_d^R}{\partial S} \right)^a . \tag{3.15}$$

Substituting Equation (7) into (5) and simplifying, Equation (3.16) is derived:

$$\frac{dS}{dt} = [-\frac{1}{2}\frac{dS}{dC}(e^R)^2]^a . \tag{3.16}$$

To eliminate S from the *dS/dC* term of the evolution equation (3.16), the chain rule is applied:

$$\frac{dC}{dS} = \frac{dC}{dt}\frac{dt}{dS}. \tag{3.17}$$

From (3.16) and (3.17), the damage evolution rate, *dS/dt*, is represented by Equation (3.18):

$$\frac{dS}{dt} = [-\frac{1}{2}\frac{dC}{dt}(e^R)^2]^{a/(1+a)}. \tag{3.18}$$

Thus, S can be obtained:

$$S = \int_0^t [-\frac{1}{2}\frac{dC}{dt}(e^R)^2]^{a/(1+a)} dt. \tag{3.19}$$

Because both the function C and e^R are dependent upon time t, a numerical approximation can be used with the measured data to obtain S as a function of time.

Therefore, the damage parameter can be approximated to Equation (3.20):

$$S \cong \sum_{i=1}^{n} [-\frac{(e^R)^2}{2}(C_i - C_{i-1})]^{a/(1+a)}(t_i - t_{i-1})^{1/(1+a)}, \tag{3.20}$$

where the $(C_i - C_{i-1})$ term is the pseudo stiffness change at each time increment; *i* is each data point; and a is the material property 1/n, where n is the slope of the LVE response function plotted as a function of time in a logarithmic scale.

The S values are plotted with the pseudo stiffness values, C, to obtain the damage characteristic curve. This relationship is then fitted to some analytical form. In this study, the simple form presented in Equation (3.21) is used:

$$C = e^{-aS^b}. \tag{3.21}$$

3.3 VECD-FEP++ Analysis for Pavements

First of all, it must be noted that all the simulations are carried out by one of the NCSU research group members. Although VECD-FEP++ is used as a tool to simulate the damage evolution in asphalt pavements, it is prudent to present its theoretical aspects to provide the necessary background for the results presented herein. The following theoretical aspects related to this research are cited from the FHWA project report.

3.3.1 Introduction

Implementation of the viscoelastic continuum damage (VECD) model into the VECD-FEP++ requires introducing a framework that permits the use of a finite element method (FEM) in modeling the damage in asphalt pavements. The framework should be capable of scaling to two- or three-dimensional analysis as required, which is usually done by employing strain/stress invariant forms in the material model. The framework is based on Schapery's work on viscoelastic continuum damage (Schapery 1981, 1984, 1990; Hinterhoelzl and Schapery 2004). A single parameter damage model developed by the Principle Investigator and his associates was integrated into the framework for the purpose of modeling damage evolution.

The model assumes that a material is isotropic when undamaged and growth of damage under loading lead to local transverse isotropy, i.e., the material has a local axis of symmetry oriented along the maximum principal stress direction. The current framework is formulated for an axisymmetric case but can easily be extended to three dimensions.

3.3.2 Constitutive model

Starting with Schapery's work potential theory for an elastic material and making use of VE fracture mechanics and the correspondence principle for VE materials (Schapery 1981, 1990), a pseudo strain energy density function, W^R, can be written in terms of the pseudo strains in the local axis as

$$W^R = \frac{1}{2}\left[A_{11}e_V^2 + A_{22}e_d^2 + 2A_{12}e_d e_V + A_{44}\left(\left(g_{13}^R\right)^2 + \left(g_{23}^R\right)^2\right) + A_{66}\left(\left(g_{12}^R\right)^2 + e_S^2\right)\right], \quad (3.22)$$

where $e_V^S = e_{11}^R + e_{22}^R + e_{33}^R;\ e_d^R = e_{33}^R - e_V^S/3;\ e_S^R = e_{22}^R - e_{11}^R$ and e_{11}^R, e_{22}^R, e_{33}^R, g_{12}^R, g_{13}^R and g_{23}^R are the pseudo strains along the local axis.

When the local axis is also a principal axis, the shear strains are zero and Equation (3.22) becomes

$$W^R = \frac{1}{2}\left[A_{11}(e_V^R)^2 + A_{22}(e_d^R)^2 + 2A_{12}e_d^R e_V^R + A_{66}(e_S^R)^2 \right]. \quad (3.23)$$

In this case, e_{11}^R, e_{22}^R and e_{33}^R are the principal pseudo strains (which lie in the local axis) with the axis of isotropy oriented along direction 3. These directions are found from the pseudo strains along the global axis using standard tensor transformation. The LVE pseudo strains along the global axis, $e_{kl}^R(t)$, are calculated from strains along the global axis, e_{kl}, using the convolution integral:

$$e_{kl}^R(t) = \frac{1}{E_R}\int_0^t E(t-\tau)\frac{\partial e_{kl}}{\partial \tau}d\tau\ , \quad (3.24)$$

where E_R is a reference modulus having the same dimensions as the modulus and usually taken as 1, and $E(t)$ is the relaxation modulus for uniaxial loading. This same equation is

presented in Chapter 2 and is repeated here because the form in Equation (3.24) is more general.

The calculation of the convolution integral can be computationally very expensive. In practice, the pseudo strains are calculated using a state variable approach to reduce the computational expense. When the relaxation modulus of the material, $E(t)$, is represented using the Prony series of the form shown in Equation (3.25), an approximation can be obtained to the convolution integral in Equation (3.24):

$$E(t) = E_{\infty} + \sum_{i=1}^{M} E_i \exp\left(-\frac{t}{r_i}\right), \tag{3.25}$$

where E_8 is the relaxation modulus at $t = 8$, and E_i are the Prony coefficients corresponding to the relaxation times r_i. The pseudo strains along the global axis can be calculated from

$$\begin{aligned} e_{kl}^{R}(t_{n+1}) &= \frac{1}{E_R}\left(E_{\infty} e_{kl}(t_{n+1}) + \sum_{i=1}^{M} E_i e_{kl}^{i}(t_{n+1})\right) \\ e_{kl}^{i}(t_{n+1}) &= e^{-\Delta t_{n+1}/r_i} e_{kl}^{i}(t_n) + e^{-\Delta t_{n+1}/(2r_i)} \Delta e_{kl}(t_{n+1}) \end{aligned} \tag{3.26}$$

where $e_{kl}^{i}(t_{n+1})$ (i = 1..M) are the internal state variables that record the history of the material up to time t_{n+1}, $De_{kl}(t_{n+1}) = e_{kl}(t_{n+1}) - e_{kl}(t_n)$ and $Dt = t_{n+1} - t_n$.

The factors A_{11}, A_{22}, A_{12} and A_{66} are stiffness terms that can be related to a damage function $C(S)$ based on the work of Ha and Schapery (1998) as

$$\begin{aligned} A_{11} &= \frac{1}{9}\left[C(S) + E_R \cdot \frac{2(1+n)}{(1-2n)}\right] \\ A_{22} &= C(S) + E_R \cdot \frac{(1-2n)}{2(1+n)} \\ A_{12} &= \frac{1}{3}\left[C(S) - E_R\right] \\ A_{44} &= A_{66} = \frac{E_R}{2(1+n)} \end{aligned} \tag{3.27}$$

In Equation (3.27), n is the Poisson's Ratio of the material; $C(S)$ is a stiffness function that depends on damage in the material; and S is a damage parameter used to track the growth of damage in the specimen.

The principal stresses along the local axis can be found from Equation (3.23) using

$$s_{ii} = \frac{\partial W^R}{\partial e_{ii}^R} \quad (i = 1, 2, 3), \tag{3.28}$$

which gives:

$$\begin{aligned} s_{11} &= (A_{11} - \frac{1}{3}A_{12})e_V^R + (A_{12} - \frac{1}{3}A_{22})e_d^R - A_{66}e_S^R \\ s_{22} &= (A_{11} - \frac{1}{3}A_{12})e_V^R + (A_{12} - \frac{1}{3}A_{22})e_d^R + A_{66}e_S^R \\ s_{33} &= (A_{11} + \frac{2}{3}A_{12})e_V^R + (A_{12} + \frac{2}{3}A_{22})e_d^R. \end{aligned} \tag{3.29}$$

The stresses along the global axis are then obtained by standard stress transformation, when the orientation of the local axis with respect to the global axis is known.

3.3.3 Damage model

The growth of the damage parameter, S, is modeled by extending the ideas found in VE fracture mechanics to microcracking, as proposed by Schapery (1984):

$$\frac{dS}{dt} = \left(-\frac{\partial W^R}{\partial S} \right)^a, \tag{3.30}$$

where W^R is the pseudo strain energy density function, shown in Equation (3.22), and a is a material-dependent parameter. From Equation (3.23), the quantity $\partial W^R / \partial S$ can be calculated as a function of pseudo strains in the local axis as

$$\frac{\partial W^R}{\partial S} = \frac{1}{2}\frac{\partial C}{\partial S}\left(\frac{1}{9}\left(e_V^R\right)^2 + \frac{2}{3}e_d^R e_V^R + \left(e_d^R\right)^2\right), \tag{3.31}$$

where $C(S)$ is the damage function that is assumed to be of the form shown in (3.32) based on experimental data,

$$C(S) = \exp\left(-aS^b\right). \tag{3.32}$$

It must be noted that when the damage parameter is zero and no damage evolution occurs, the above equations simplify to the case of linear viscoelasticity. Thus, the same framework can be used for modeling LVE materials.

3.3.4 Finite element implementation

The finite element solution of the problem requires the material tangent stiffness matrix, which is used to assemble the global tangent stiffness matrix used for the solution of the nonlinear system of equations using the Newton-Raphson method. The material tangent stiffness matrix, $[C]$ (not to be confused with the damage function, $C(S)$), is given by

$$[C] = \frac{\partial\{s\}}{\partial\{e\}} = \frac{\partial\{s\}}{\partial\{e^R\}}\frac{\partial\{e^R\}}{\partial\{e\}}, \tag{3.33}$$

where $\{s\} = \{s_{rr}, s_{qq}, s_{zz}, s_{rz}\}$and $\{e\} = \{e_{rr}, e_{qq}, e_{zz}, e_{rz}\}$are the stresses and strains for the axisymmetric problem and $[C]$ is the material tangent stiffness matrix oriented along the global axis. Because the stresses along the global axis are obtained by the transformation of the stresses in the local axis, it is easier to construct the material tangent stiffness matrix along the local axis and then transform it to the tangent stiffness along the global axis. The tangent stiffness matrix in the local axis, $[C_L]$, is given by

$$[C_L]=\frac{\partial\{s_L\}}{\partial\{e_L^R\}}=\begin{bmatrix}\left(A_{11}-\frac{2}{3}A_{12}+\frac{1}{9}A_{22}+A_{66}\right) & \left(A_{11}-\frac{2}{3}A_{12}+\frac{1}{9}A_{22}-A_{66}\right) & \left(A_{11}+\frac{1}{3}A_{12}-\frac{2}{9}A_{22}\right) & 0 & 0 & 0\\ \left(A_{11}-\frac{2}{3}A_{12}+\frac{1}{9}A_{22}-A_{66}\right) & \left(A_{11}-\frac{2}{3}A_{12}+\frac{1}{9}A_{22}+A_{66}\right) & \left(A_{11}+\frac{1}{3}A_{12}-\frac{2}{9}A_{22}\right) & 0 & 0 & 0\\ \left(A_{11}+\frac{1}{3}A_{12}-\frac{2}{9}A_{22}\right) & \left(A_{11}+\frac{1}{3}A_{12}-\frac{2}{9}A_{22}\right) & \left(A_{11}+\frac{4}{3}A_{12}+\frac{4}{9}A_{22}\right) & 0 & 0 & 0\\ 0 & 0 & 0 & A_{66} & 0 & 0\\ 0 & 0 & 0 & 0 & A_{44} & 0\\ 0 & 0 & 0 & 0 & 0 & A_{44}\end{bmatrix} \quad (3.34)$$

where $\{s_L\}= \{s_{11}, s_{22}, s_{33}, s_{12}, s_{13}, s_{23}\}$ is the stress vector along the local axis and $\{e_L\}= \{e_{11}, e_{22}, e_{33}, e_{12}, e_{13}, e_{23}\}$ is the pseudo strain vector along the local axis. The pseudo shear strains are zero along the local axis but the stiffness values corresponding to them are non-zero. The matrix $[C]$ can be obtained by transforming $[C_L]$, as shown in Equation (3.35):

$$[C]=[T_R]^{-1}[C_L][T_R], \quad (3.35)$$

where $[T_R]$ is the rotation and permutation matrix that changes the order of the vector components (axis 3 along the local axis is always oriented along the maximum principal pseudo strain direction) and transforms a vector from the local axis to the global axis.

As seen from Equations (3.30) and (3.31), the damage growth involves a nonlinear differential equation that can be expensive to solve in a large FEM problem. Hence, a semi-implicit method is used for predicting the damage parameter in the next time-step, S^{n+1}, using the damage parameter in the current time-step, S^n, and the pseudo strain vector in the local axis, $\left\{e_L^R\right\}^{n+1}$, for the next time-step, as:

$$S^{n+1}=S^n+\dot{S}\left(\left\{e_L^R\right\}^{n+1},S^n\right)\Delta t\,. \quad (3.36)$$

This method should give results similar to an exact nonlinear analysis when the time-steps are made small enough.

Chapter 4

Experimental Program

This chapter provides a description of the mixtures selected for testing, the procedure for the fabrication and preparation of specimens, and the testing program for the SPTs, |E*| and flow number tests, as well as characterization tests for the tensile VECD model.

A list of the laboratory experimental programs is presented in Table 4.1. The experiments conducted are presented as the darkened cells. The tests of mixes in Task 1 were conducted using both lime-modified and unmodified mixtures. The test results of the mixes in Task 3, such as Control 5.6% and Lsub 5.3% were used in Task 4.

Table 4.1 Test Factorial

Task	Mix ID	Experiment Program Type						
		Mix Design	Dynamic Modulus Test	Constant Crosshead Rate Test	TRLPD Test	VECD FEP++ Simulation	TSR Test	APA Test
1	S9.5AF							
	S12.5BF							
	I19.0BF							
	B25.0BF							
	S9.5CC							
2	Control							
	Lsub							
	Leco							
	Lmod							
3	Control 5.6%AC							
	Control Moisture							
	Lsub 5.3%AC							
	Lsub Moisture							
4	Control 5.1%AC							
	Control 5.6%AC							
	Control 6.1%AC							
	Control 6.6%AC							
	Lsub 4.8%AC							
	Lsub 5.3%AC							
	Lsub 5.8%AC							
	Lsub 6.3%AC							
	Control Field mix							
	Lsub Field mix							

4.1 Materials

Materials used for the work presented here are representative of mixtures typically used in North Carolina. Mixture types cover both the fine and coarse range of various sizes of Superpave mixtures. Specific details of the materials used in this study are given where appropriate.

4.2 Sample Preparation

4.2.1 Specimen fabrication for performance tests

Asphalt mixtures were mixed and compacted at temperatures in accordance with the requirements for each binder. All mixtures were aged at 135°C for four hours (i.e., short-term oven aging) before compaction. The mixtures were compacted into gyratory plugs of 150 mm in diameter by 178 mm in height. Then, they were cut and cored to cylindrical specimens with dimensions of 100 mm in diameter and 150 mm in height for the |E*| test and TRLPD test, and 75mm in diameter and 150 mm or 140 mm in height for the constant crosshead test. Both ends of the cored specimens were cut to ensure a more consistent air void distribution along the length of the test specimens. The mass of HMA that was added to make the gyratory plugs was adjusted so that the air void content in the final test specimens would fall within 4% ± 0.5%.

For each of the mixtures tested, two or three replicate mixtures were also tested. If errors were made or densities were not met during either fabrication or testing, then the specimen was discarded and an additional specimen was manufactured and tested.

4.2.2 Target air voids

The air voids for all mixtures were 4% ± 0.5%. In order to achieve this density, the target air void for the gyratory plug had to be higher than that of the cut and cored specimens. The requirements for the different target air voids change because of density variations throughout the height and diameter of the compacted specimen. The center of the gyratory plug is the most dense, with the least dense areas on the outer surfaces. The difference

between the target for the gyratory plug and the cut and cored specimen typically increases as the nominal maximum size aggregate increases. Details on these issues can be found elsewhere (Chehab 2002, Daniel 2001).

Air voids were measured using the Corelok® vacuum sealing device. Specifications provided in ASTM D6752-03 were followed in taking these measurements and making these calculations. Appropriate adjustments were made to the density of the water when measurements were made at temperatures other than 25°C.

After obtaining specimens of the appropriate dimensions, air void measurements were taken via the Corelok® method, and specimens were stored until testing. During storage, specimens were sealed in bags and placed in an unlit cabinet to reduce the effects of aging. Also, no test specimens were stored for longer than two weeks before testing.

4.3 Testing Setup and Program

This section provides information on testing equipment, measurement instrumentation, and data acquisition systems.

4.3.1 Testing systems

Two different closed-loop servo-hydraulic testing machines were utilized in this study. Testing in Task 1 was conducted using a closed-loop servo-hydraulic machine, manufactured by MTS. The machine is a MTS 810 loading frame equipped with either a 25 kN or 8.9kN load cell, depending on the nature of the test. This machine is capable of applying loads up to

20 kips, from 0.01 Hz to 25 Hz. A temperature chamber, cooled by liquid nitrogen, was used to control the test temperatures.

A servo-hydraulic universal testing machine, UTM-25, was used in testing for Task 2. It is manufactured by Industrial Process Controls in Australia. It has a loading capacity of 25 kN, and it is capable of applying loads over a wide range of frequencies, from 0.01 Hz to 25 Hz. The UTM is fully computer-controlled.

The temperature control system of the UTM is refrigeration-based and has a heating element to achieve high temperatures. The temperature control systems in both the MTS and UTM can achieve the required testing temperatures ranging from -10°C to 55°C, which are the lowest and highest temperatures, respectively, of interest in this research. An asphalt concrete dummy specimen with a temperature probe placed in the middle of the specimen was placed inside the chamber and triaxial cell in order to monitor the actual temperature of the specimen during testing.

The data acquisition system for both the MTS and UTM is also fully computer-controlled and is capable of measuring and recording data from several channels simultaneously. Six channels were used in the |E*| test and the constant crosshead test: four for vertical LVDTs, one for the load cell, one for the actuator, and another channel was added for confining pressure especially for the TRLPD test. Data acquisition programs were prepared using LabView software for data collection and analysis.

Vertical deformations were measured using LVDTs. Four loose-core, CD type LVDTs measured deformations at 90° radial intervals. Targets were glued to the specimen face, and the LVDTs were mounted to the targets to measure the deformation in the middle of the

specimen (100 mm in height). For consistency in measurements, a gluing device was used to maintain consistent spacing between the LVDT targets. The tested specimens are shown in Figure 4.1 with the LVDTs mounted.

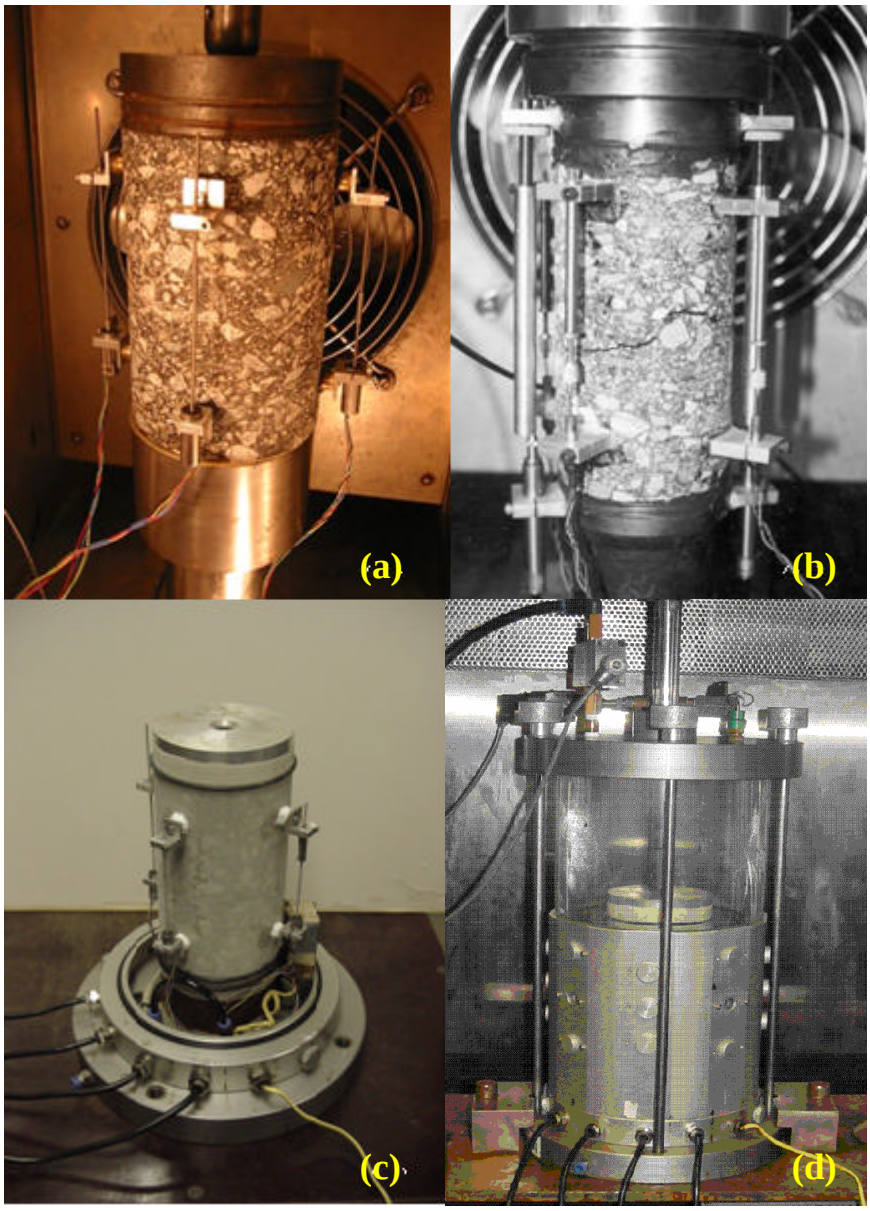

Figure 4.1 LVDT mounting and spacing for: (a) dynamic modulus test; (b) monotonic constant crosshead rate test; and (c) and (d) TRLPD test

In this study, both tensile and compressive testing protocols have been utilized. For tensile testing, steel end plates were glued to the specimen with DEVCON® steel putty. Extreme care was taken to completely clean both the end plates and the specimen ends before each application. It was observed early in the testing that failure to do so could result in the premature failure of the specimen. To ensure specimens were properly aligned, a special gluing jig was employed that ensured the end plates were parallel and, thus, minimized any eccentricity that might occur during the test. For the compression tests, the criteria for test specimen geometry presented in NCHRP Report 465 (Witczak et al. 2000) were followed. Two 0.3048 mm thick rubber membranes, 100 mm in diameter and separated by a thin layer of lubricant, were used to avoid the end effect caused by friction between the end plate and the surface of the specimen (Kim et al. 2005).

4.3.2 Testing program

Performance-based tests are tests that measure material properties that can be used in a fundamental response model to predict mixture responses to various loadings and environmental conditions. In this study, three different performance-based test protocols were employed to extract the material behavior: |E*| tests, TRLPD tests and constant crosshead rate tension tests. In the following sections, details of these test protocols, as they relate to the work at hand, are given.

4.3.2.1 Dynamic modulus testing

To facilitate the presentation of results it is important to understand the principle of time-temperature superposition (or time-temperature equivalence). Simply stated, the same

modulus value of a material can be obtained both at low test temperatures and long times (slow frequencies) or at high test temperatures but short times (fast frequencies). More generally, the behavior of a material at high temperatures is the same as that under long loading times or slow loading rates/frequencies, and the material behavior at low temperatures is the same as that under short loading times or fast loading rates/frequencies. Materials that exhibit this type of behavior are called *thermorheologically simple* (TRS). The time-temperature superposition of a material can be checked by performing E* tests at varying temperatures and frequencies, as is done in the AASHTO TP 62 protocol.

Asphalt concrete in the LVE range is known to be TRS material and, thus, the effects of time and temperature can be combined into a joint parameter, i.e., reduced time/frequency, through the time-temperature shift factor (a_T) using Equation (4.1):

$$f_R = f \times a_T \,. \tag{4.1}$$

Figure 4.2 shows typical data for this scenario. As expected, the |E*| increases as the loading frequency increases and the temperature decreases. This behavior allows for the horizontal shifting of the data to form a single mastercurve and accounts for the constitutive behavior of asphalt concrete over a wide range of reduced frequencies. The simplifying feature afforded by time-temperature superposition is that all of these curves can be superposed to form a single continuous curve by means of horizontal translations only. Figure 4.3 presents such mastercurves for the replicate tests shown in Figure 4.2. The amount of shifting is dependent on the temperature chosen as the reference and, therefore, varies according to temperature, as shown in Figure 4.4.

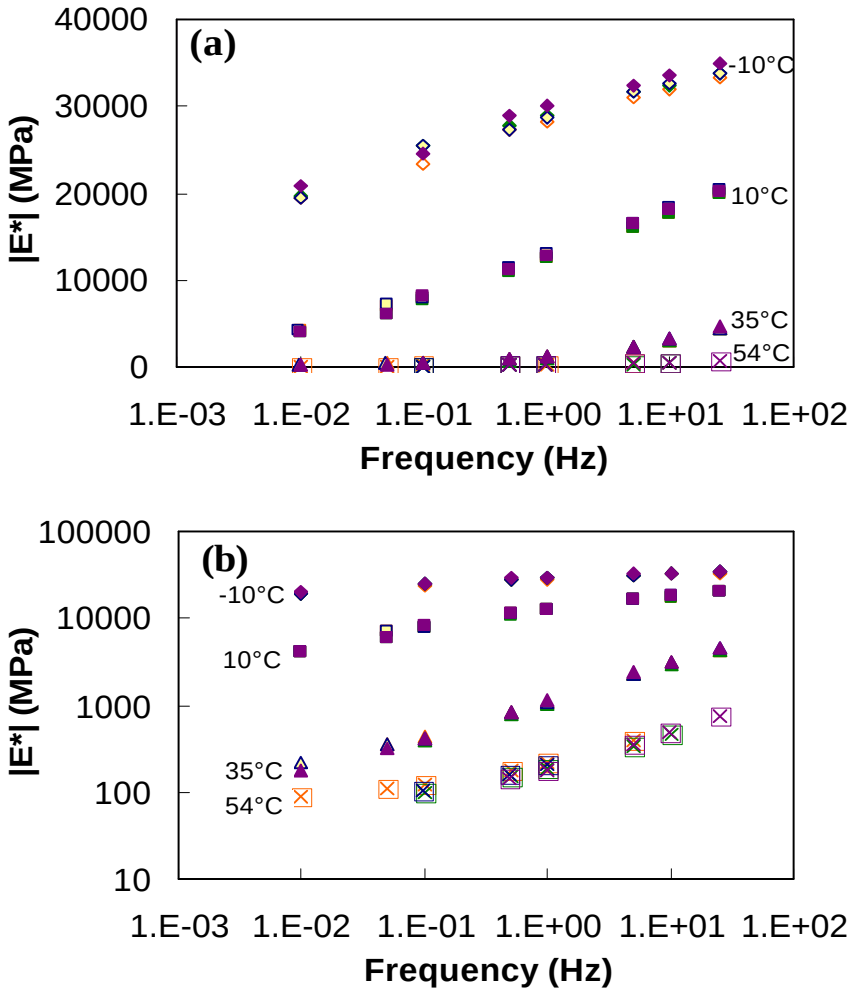

Figure 4.2 Typical unshifted dynamic modulus in: (a) semi-log space; and (b) log-log space

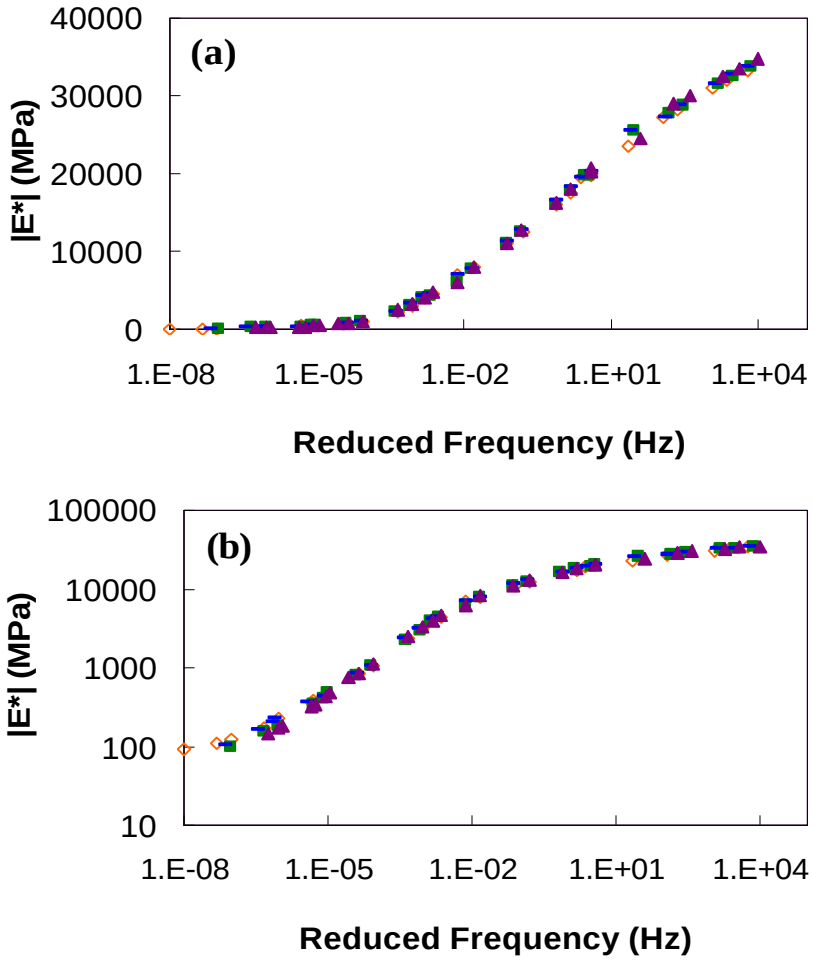

Figure 4.3 Typical dynamic modulus mastercurve in: (a) semi-log space; and (b) log-log space

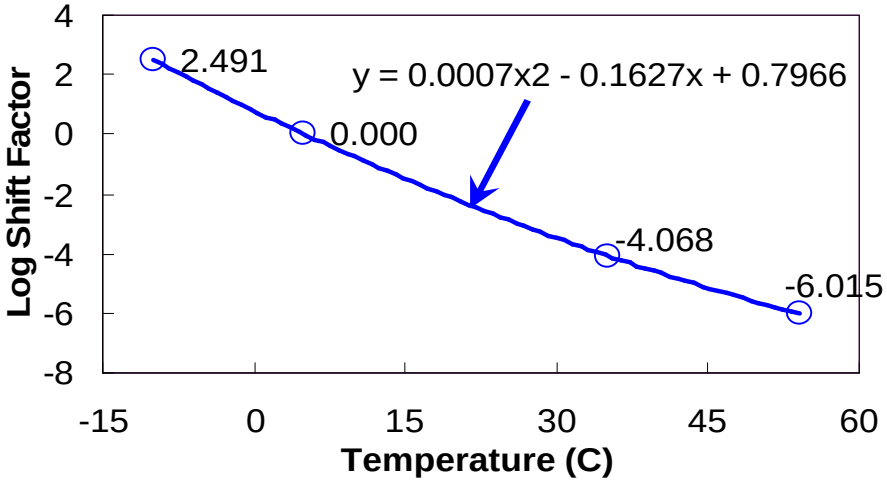

Figure 4.4 Log shift factor function for a typical mixture

Figure 4.4 presents these factors at each temperature along with the fitting curve. It is observed that temperatures below the reference temperature (log $a_T > 0$) are shifted to the right in the frequency domain, whereas temperatures higher than the reference temperature (log $a_T < 0$) are shifted to the left in the same domain. The mastercurve is fitted to a sigmoidal functional form, Equation (4.2), and the relationship between the shift factor and temperature is fitted to a second order polynomial function (4.3). The sigmoidal coefficients and the time-temperature shift factors can be optimized by the Solver function in EXCEL.

$$\log|E^*| = a + \frac{b}{1+\frac{1}{e^{d+g*\log(f_R)}}}. \quad (4.2)$$

$$\log(a_T) = a_1 T^2 + a_2 T + a_3. \quad (4.3)$$

Using the coefficients obtained from (4.2) and (4.3), it is then possible to predict the stiffness at any frequency and temperature combination.

In this study, the |E*| test was performed in load-controlled mode in axial compression, generally following the protocol given in AASHTO TP62-03 (2003). Tests were completed for all mixtures in this study at –10°, 10°, 35° and 54.4°C and at frequencies of 25, 10, 5, 1, 0.5, 0.1, 0.05 and 0.01 Hz. These frequencies approximate the full range of loading rates that pavements experience, from highway speeds down to very slow traffic speeds. Load levels were determined by a trial and error process so that the resulting strain amplitudes were between 50 and 70 microstrains. Based on the work of other researchers (Chehab et al. 2002, Kaloush 2001), it was felt that these criteria ensured accurate VE characterization.

4.3.2.2 TRLPD tests

For realistic and accurate relationships between laboratory performance and actual performance in the field, it is important to conduct laboratory tests under the same stress and environmental conditions found in the field, such as climatic conditions (temperature), traffic level (number of load repetitions and rate of loading), and stress levels (triaxial state of stress). These factors must be considered for any performance test in order to simulate pavement conditions in the field (Kaloush 2001).

TRLPD tests, or Flow Number tests, in which these factors can be included, were conducted to assess the rutting potential of asphalt concrete mixtures following the protocol presented in NCHRP Report 465 (Witczak et al. 2000). According to this test protocol, an effective pavement temperature covers the temperature range of approximately 25° to 60°C. The deviator stress level range is from 10 to 30 psi for the unconfined tests and 70 to 140 psi for the confined tests. The confining stress ranges between 5 and 30 psi.

In this test procedure, the specimen is subjected to a deviatoric, haversine stress pulse for 0.1 second and then allowed to rest for 0.9 second. For the mixtures presented here, only a single confining stress (138 kPa), temperature (54.4°C) and deviatoric stress level (827 kPa) were examined. It is noted that this test protocol is one of the proposed SPTs to ensure the satisfactory performance of Superpave mixtures for rutting. Figure 4.1 (c) and Figure 4.1 (d) show the TRLPD test setup in the UTM-25.

Figure 4.5 shows the typical relationship between the total cumulative plastic strain and the number of load cycles in normal and log-log scales, respectively. In Figure 4.6, three zones – primary, secondary, and tertiary – are defined along the cumulative permanent strain curve. In the primary zone, permanent deformations accumulate rapidly. In the secondary

zone, the incremental permanent deformations decrease and reach a constant value. Finally, the incremental permanent deformations again increase, and permanent deformations accumulate rapidly in the tertiary zone. The cycle number at which tertiary flow starts is referred to as the flow number. It is important to note that good rutting performance mixtures stay in the secondary zone and do not show any tertiary flow in normal loading conditions under standard axle loads (Kaloush et al. 2002).

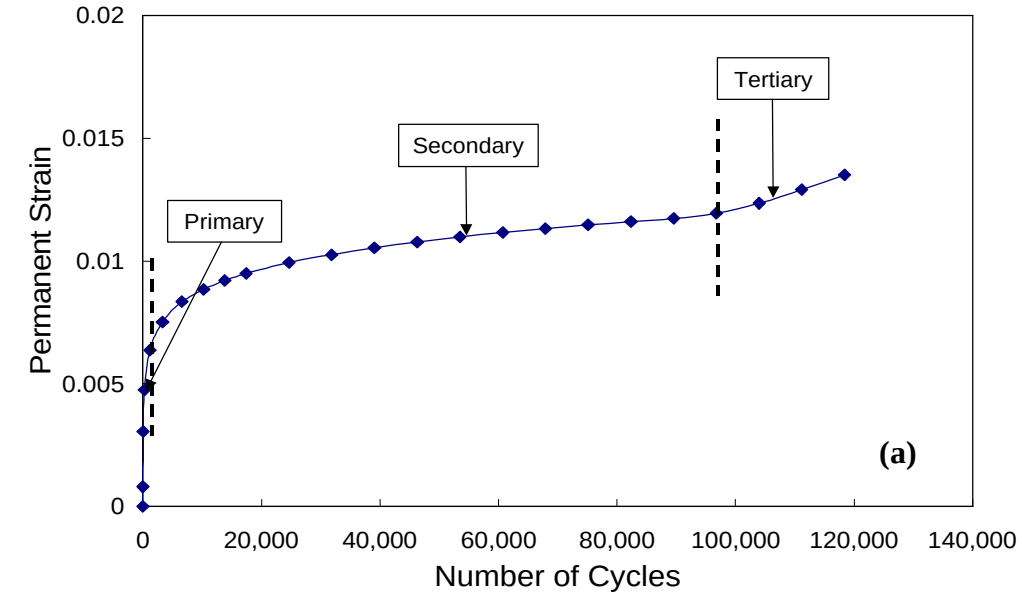

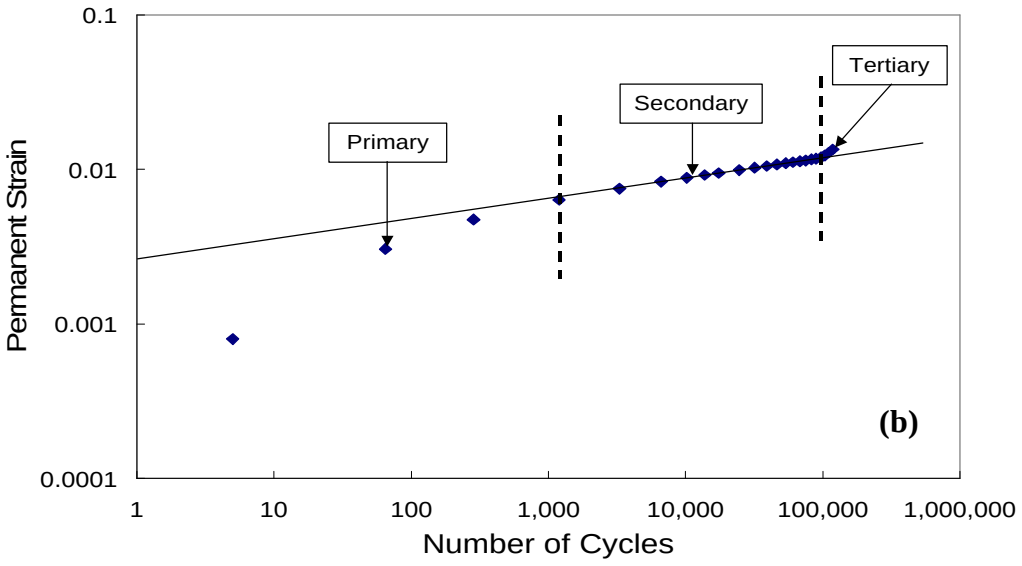

Figure 4.5 Typical relationship between total cumulative plastic strain and number of load cycles: (a) plotting on arithmetic scale; (b) plotting on log-log scale with regression constants a, b

The linear portion in the middle of the curve in Figure 4.5 (b) represents the permanent strain response of a mix. This portion can be expressed by the following classical power model:

$$e_p = aN^b, \tag{4.4}$$

where *a* and *b* are regression constants. The intercept *a* represents the permanent strain at N = 1. The slope *b* represents the rate of change in log (ε_p) as a function of the change in log (N). An alternative form of the mathematical model used to characterize the plastic strain per load repetition (ε_{pn}) relationship can be expressed by:

$$\frac{\partial e_p}{\partial N} = \frac{\partial (aN^b)}{\partial N} = e_{pn}; \tag{4.5}$$

then

$$e_{pn} = abN^{(b-1)}. \tag{4.6}$$

The resilient strain (ε_r) is assumed to be independent of the load repetition value (N). As a result, the ratio of plastic to resilient strain components of the material can be defined by:

$$\frac{e_{pn}}{e_r} = (\frac{ab}{e_r})N^{b-1}. \tag{4.7}$$

Letting $m = \frac{ab}{e_r}$ and $a = 1 - b$ gives

$$\frac{e_{pn}}{e_r} = mN^{-a}, \tag{4.8}$$

where, ε_{pn} is the permanent strain due to a single load application, i.e., at the N^{th} application. The coefficient μ is the permanent deformation parameter representing the constant of

proportionality between permanent strain and elastic strain. The exponent α is a permanent deformation parameter indicating the rate of decrease in incremental permanent deformation as the number of load applications increases.

4.3.2.3 Constant crosshead rate tension tests

In Chapter 3, normalized secant pseudo stiffness C and damage parameter S are defined in terms of structural material integrity and the amount of damage in the material, respectively. Daniel and Kim (2002) state, "A single characteristic curve can be found that describes the reduction in material integrity as damage grows in the specimen, regardless of the applied loading conditions (cyclic vs. monotonic, amplitude/rate, frequency) and temperature." Simply stated, a single damage characteristic curve can be obtained from either a monotonic tension test or cyclic loading test, as long as the same damage parameter is used. However, these factors are only applicable when the viscoplastic flow is at a minimum, such as in cases of a low temperature or high loading rate, because not only viscoelastic continuum damage, but also viscoplastic damage, occurs in these scenarios. Thus, it is necessary to add viscoplasticity to the entire model, but such an alteration is out of the scope of this study. Details about adding viscoplasticity to the existing VECD model to transform it to the VEPCD model can be found elsewhere (Chehab 2002).

Constant crosshead rate tests were performed with the application of a constant rate of deformation over the complete loading train. Because each component in the loading train (machine ram, load cell, etc.) deforms slightly, the on-specimen displacement rate or strain rate is not constant (Chehab et al. 2003). Tests were completed at two temperatures (5° and

40°C) and at multiple rates. The test rates and temperatures and the purpose of each are summarized in Table 4.2.

Table 4.2 General Controlled Crosshead Testing Matrix for VEPCD Characterization in Tension

Test ID	Temperature (°C)	Strain Rate (e/s)	Purpose
DT-1-(Mix Type)	5	0.000055	VECD Characterization
DT-2-(Mix Type)		0.000030	
DT-3-(Mix Type)		0.000021	
DT-VP1-(Mix Type)	40	0.010000	VP Characterization
DT-VP2-(Mix Type)		0.003000	
DT-VP3-(Mix Type)		0.001000	
DT-VP4-(Mix Type)		0.000300	

4.3.2.4 VECD-FEP++ for fatigue damage simulation

Finite element simulations were performed for the fatigue damage simulations of pavements. The field response for passing a moving load on the pavement was predicted to investigate the effect of lime modification on fatigue performance. Because the purpose of these simulations was to rank the fatigue resistance of the various lime-modified mixtures, all the simulations were performed on an assumed pavement structure. Also, the modulus used for the subgrade and base were likewise assumed from the unpublished project. In these simulations, the pavement is assumed to be LVE without any damage. The data common to all simulations performed are described in the following.

- **Load Details**

  Wheel load = 16.6 kip (73.84 kN)

  Uniform tire pressure = 120 psi (827.37 kPa)

Radius = 16.855 cm

Number of load cycles = 10,000,000

Loading period in a cycle = 0.1 sec

Rest period in a cycle = 0.9 sec

- **Pavement Details**

  Asphalt concrete pavement temperature = 19 °C

  Pavement thickness = 10 cm

- **Base Details**

  Crushed Aggregate Base (CAB) thickness = 20.3 cm

  Aggregate base modulus = 75 ksi (517107 kPa)

- **Subgrade Details**

  Infinite element with subgrade modulus = 10.9 ksi (75056 kPa)

The details of the pavement structure are shown in Figure 4.6.

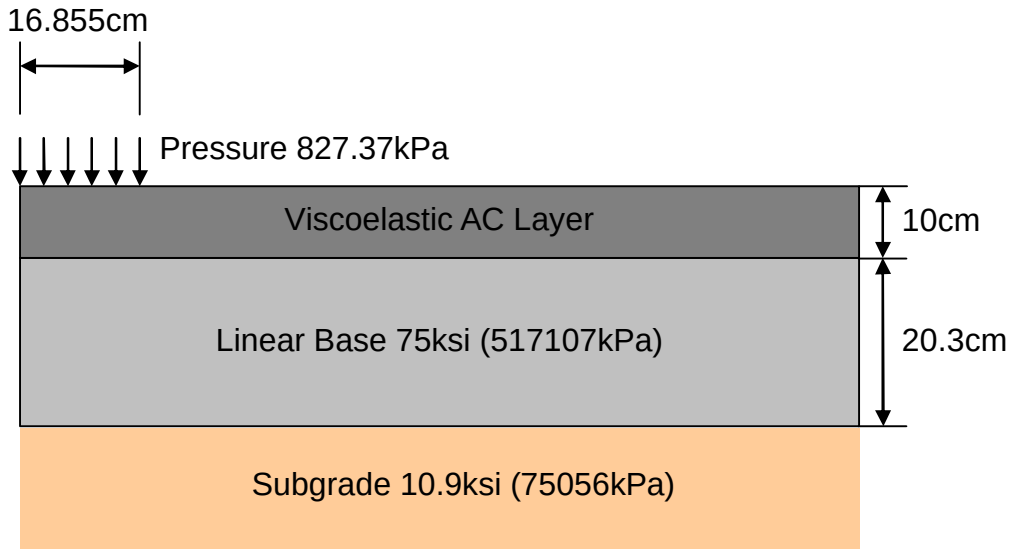

Figure 4.6 Structure of pavement used for the damage simulation

The damage simulation is performed with uniform loading by running the simulation up to 10,000,000 cycles with appropriate cycle jumps. In this case, a smaller cycle jump was

used to capture the rapid variation of C in the early cycles and a larger cycle jump was used to capture the relatively slower variation at a larger number of cycles.

Ranking of the pavements was done by two means. The first method is a visual observation of the contour plots of the extent of the pavement region. The other method examined the two parameters, the Average *C* and the percentage of crack (% Crack) area. Those parameters are defined as the averaged value of C in the pavement region and the number of nodes below C equal to 0.25 out of the total number of nodes (217) within the extent of the pavement region (0.5m in width) after 10,000,000 cycles, respectively. Therefore, the % Crack area can be considered as the area of macrocrack based on simulation results, and the Average C represents the overall status of the damage propagation in the pavement. These contour plots and parameters after 50,000, 100,000, 500,000, 1,000,000, 2,500,000, 5,000,000, 7,500,000, and 10,000,000 cycles were compared to investigate the fatigue resistance of the mixes.

Chapter 5

Determining the Effects of Hydrated Lime on the Dynamic Modulus of Typical North Carolina Mixtures

5.1 Introduction

The dynamic modulus (|E*|) is an important property for asphalt concrete because it represents the fundamental relationship between stresses and strains in the material. Although this value has been known to some researchers (Shook 1969, Kallas 1970, Yeager 1975) since the 1960s, its use by state highway agencies has not been widespread. However, the work completed under the NCHRP 1-37a project towards developing a national mechanistic-empirical design procedure has increased both the awareness and interest in this fundamental material property. Mechanistic-empirical analysis procedures require the modulus of each layer material to determine the stresses and strains (i.e., responses) in pavement structures and, thus, to predict the performance of asphalt concrete pavements. It is prudent then to examine whether the addition of lime has any significant effect on this material property. It has been shown that hydrated lime does increase the stiffness of asphalt concrete mixtures. However, the majority of this research has been confined either to examining engineering

properties, such as the resilient modulus (McCann 2003), or to nonlinear regions of the material behavior (Mohammad 2006, McCann 2003, Mohammad et al. 2000, Kim et al. 2003).

5.2 Experimental Design

The experimental design for this study involves the selection of test materials and the determination of the appropriate asphalt content. Various typical mixture types used by the NCDOT were selected, and the volumetric mix design was performed. These same mixtures were then modified with hydrated lime, and the optimal asphalt content was re-evaluated. These two types of mixtures (lime-modified and unmodified) were then tested for the |E*| to evaluate the effect of the hydrated lime.

5.2.1 Mixture selection

The NCDOT has categorized Superpave mixtures used in North Carolina based on layer location, aggregate gradation, and traffic volume. Table 5.1 presents 12 mixtures designated by the NCDOT based on this categorization method.

Table 5.1 Guidelines for Superpave Mixes in North Carolina

Mix Type	Loading Range (Million ESALs)	% Asphalt Binder	Asphalt Binder Grade	Density (lbs/SY/in)
Surface				
S[a]9.5[b]A[c]	Less than 0.3	6.5	PG 64-22	112
S9.5B	Less than 3	6.5	PG 64-22	112
S9.5C	3 to 10	6.5	PG 70-22	112
S12.5B	Less than 3	5.5	PG 64-22	112
S12.5C	3 to 30	5.5	PG 70-22	112
S12.5D	Over 30	5.5	PG 76-22	112
Intermediate				
I19.0B	Less than 3	4.7	PG 64-22	114
I19.0C	3 to 30	4.7	PG 64-22	114
I19.0D	Over 30	4.7	PG 70-22	114
Base				
B25.0B	Less than 3	4.3	PG 64-22	114
B25.0C	3 or Greater	4.3	PG 64-22	114
B37.5C	3 or Greater	4.3	PG 64-22	114

Note: [a]S is surface mix; I is intermediate mix; and B is base mix.

[b]Superpave mix designation (Nominal Maximum Aggregate Size)

[c]Traffic volume indicator

For the study presented here, one mixture from each of the S9.5A, S9.5C, S12.5C, I19.0B, and B25.0B mixture types has been evaluated. For each case, two mix designs, lime-modified and unmodified, were created for a total of 10 different mixture types. These mixes are the most frequently used Superpave mixes in North Carolina, according to the NCDOT Pavement Management Unit. This selection includes three mixtures for the surface layer (S),

one for the intermediate layer (I), and one for the base layer (B). Aggregate gradations of the mixes are presented in Figure 5.1, and details are given in Table 5.2.

Table 5.2 Aggregate Gradations of Selected Mixes for Dynamic Modulus Study

% Stock Pile	Mix Types				
	S9.5AF	S9.5CC	S12.5CF	I19.0BF	B25.0BF
#5			20.0		36.0
#67			41.4	22	
#78	17.0	55.0	12.0	38.0	30.0
Dry screenings	0.0	33.0	1.0	28.0	22.0
Washed screenings	83.0	10.0	0.5		12.0
Sand/Baghouse fines		2.0		12.0	
Sum	100.0	100.0	100.0	100.0	100.0
Sieves (mm)	% Passing Blend				
37.5	100	100	100.0	100	100
25.0	100	100	99.2	100	98
19.0	100	100	95.3	99	82
12.5	100	100	77.6	88	66
9.5	99	97	59.2	76	63
4.75	86	62	45.1	52	42
2.36	63	40	32.5	38	30
1.18	44	34	19.9	2	23
0.600	32	25	12.2	21	16
0.300	21	14	6.3	13	10
0.150	12	8	6.3	6	6
0.075	5.2	5.6	6.3	3.8	4

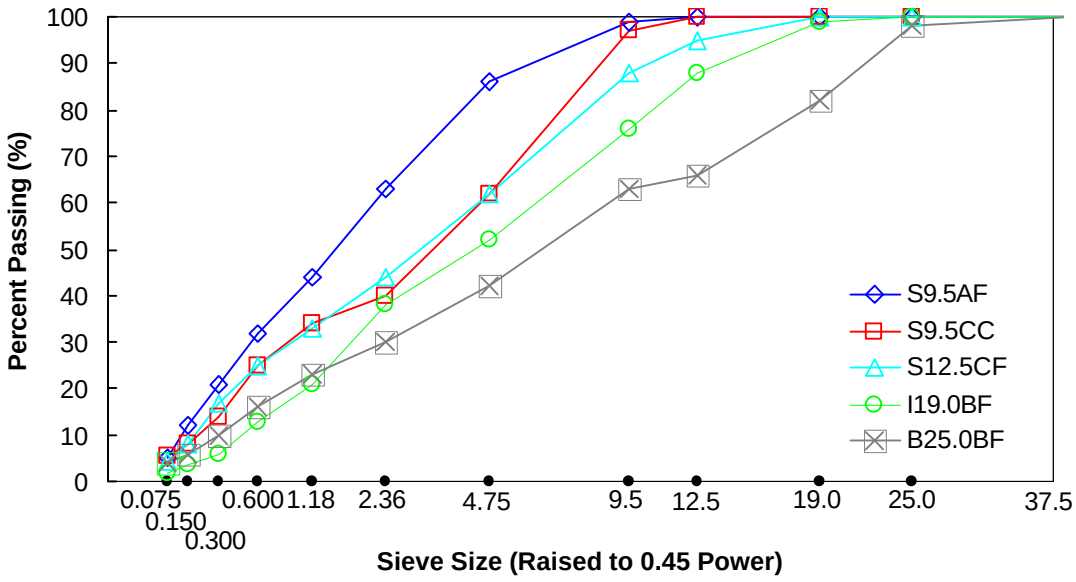

Figure 5.1 Gradation chart for selected mixtures

In addition to the mix types shown in Table 5.2, factors that are important, but not explicitly shown in Table 5.2, are aggregate type and specification. These factors are presented in Table 5.3 for each of the mixtures. For this study, only granite aggregates are considered because they constitute approximately 70% of all pavement construction in North Carolina.

Table 5.3 Specifications of Selected Mixes for Dynamic Modulus Study

Mix Design	Fine, S9.5A	Fine, S12.5C	Fine, I19.0B	Fine, B25.0B	Coarse, S9.5C
Aggregate Type	Granite				
Aggregate Source	Pineville/ Charlotte	Concord/ Cabarrus	Garner	Garner	Holly Springs
Aggregate Specific Gravity	2.932	2.757	2.633	2.639	2.652
Binder Grade	PG 64-22	PG 70-22	PG 64-22	PG 64-22	PG 70-22
Binder Source	Citgo Wilmington				
Anti-strip Additive %	0.5% of Binder	0.5% of Binder	0.5% of Binder	0.25% of Binder	0.5% of Binder
Anti-Strip Supplier	Arr-Maz (Ad-Here 6500 LOF)				
Chemical Lime %	1% of mix				
Lime SG	2.300				
Nini/Ndes/Nmax	6/50/75	8/100/160	7/75/115	7/75/115	8/100/160

5.2.2 Mix designs with hydrated lime

The NCDOT does not currently require the use of hydrated lime in asphalt concrete mixtures. So, for this study, lime-modified mix designs were developed based on the standard NCDOT mixtures shown in Table 5.3. These mix designs were performed at NCSU following the standard Superpave procedure. As shown in Table 2.1, several proven and effective methods for adding hydrated lime to asphalt are available. Multiple methods exist because states have developed different approaches to meet their specific requirements.

It is necessary then to decide the most appropriate means of introducing lime into the mixtures for this study. For economic reasons, the dry method with a lime content of 1% by weight of mixture was chosen. Two different methods can be used for adding this amount of

lime to the mixture: 1) the substitution of mineral filler from the unmodified mixture and 2) the simple addition of the lime. The second method was chosen as an appropriate first step in understanding the effects of lime on volumetric mix design.

The mix design specimens were compacted in the aforementioned Superpave Gyratory Compactor with a 150 mm diameter mold and a target mixture weight of 4,500 g. Results from the mix design process for both unmodified and modified mixtures are shown in Table 5.4. Fine and coarse mixtures are denoted with the final letter of the mixture identification.

From Table 5.4 it is seen that the optimal asphalt content for all of the mixtures modified with hydrated lime decreased between 0.35% to 0.90%% (saving an average of approximately 12% of the untreated optimal asphalt content). Care should be taken in utilizing hydrated lime in existing mix designs without first reassessing the asphalt content. Because hydrated lime acts as an extender in asphalt concrete, failure to readjust the asphalt content could lead to excessively rich mixtures or very poor mixtures. Rich mixtures may be more prone to permanent deformation failures or vice versa. Conversely, it is possible that the benefits of hydrated lime could offset the higher than optimal asphalt content.

Table 5.4 Mix Design Results for Dynamic Modulus Study

Mix type		Design Asphalt Content		G_{mm}	VMA		VFA	
		Opt. AC (%)	? AC (%)		(%)	Min.	(%)	Min.-Max.
Fine, S9.5A	Unmod.	5.90	0.35	2.659	17.9	15	79.0	70-80
	Lime	5.55		2.620	18.5		80.0	
Fine, S12.5C	Unmod.	4.70	0.60	2.591	14.1	14	71.0	65-75
	Lime	4.10		2.592	13.2		70.0	
Fine, I19.0B	Unmod.	4.30	0.60	2.492	13.1	13	69.3	65-78
	Lime	3.70		2.495	12.0		69.0	
Fine, B25.0B	Unmod.	3.90	0.40	2.506	12.5	12	67.5	65-78
	Lime	3.50		2.488	12.4		68.0	
Coarse, S9.5C	Unmod.	4.90	0.90	2.492	14.2	15	72.0	65-76
	Lime	4.00		2.497	13.0		66.0	

It should be noted from Table 5.4 that some of the VMA values for the lime-modified mixtures and one of the unmodified mixtures are lower than the minimum criteria. Under normal design situations such mixtures would be rejected. However, the aim of this project is to determine the effects of lime addition on the optimal asphalt content; therefore, the VMA violation does not adversely affect the conclusions. It is of interest to note that the lime modification method utilized in this study causes a reduction in the VMA for all mixtures.

5.2.3 Dynamic modulus tests

Complex modulus (E*) testing is performed in uniaxial compression. The E* test is performed in a stress-controlled manner and is designed to measure the VE response of asphalt concrete.

5.3 Test Results

In this section, the results for all five mixtures are presented in a graphical format plotted with the axial compression data. Two replicates for each mix were tested for unmodified and lime-modified mixes, and the dynamic moduli were plotted against reduced frequencies after shifting the data in Figure 5.2 through Figure 5.6. The reference temperature that was used as the basis for shifting the data is 10°C.

Data are presented in both semi-log and log-log scales. Both scales are presented to show both the high temperature (log-log) and low temperature (semi-log) behaviors. In Figure 5.2 through Figure 5.6, the filled symbols are used to present the |E*| values of the lime-modified mixes, and the unfilled symbols are used for the unmodified mixes. The amount of asphalt reduction is noted for each mixture on the respective plot. It is important to note these values because both the lime and the asphalt content reduction have a stiffening effect.

In general, the lime-modified mixtures do show higher stiffness at a higher reduced frequency and lower stiffness at a lower reduced frequency. However, this difference could be related to specimen variability, as can be seen in the spread of the replicate mastercurves.

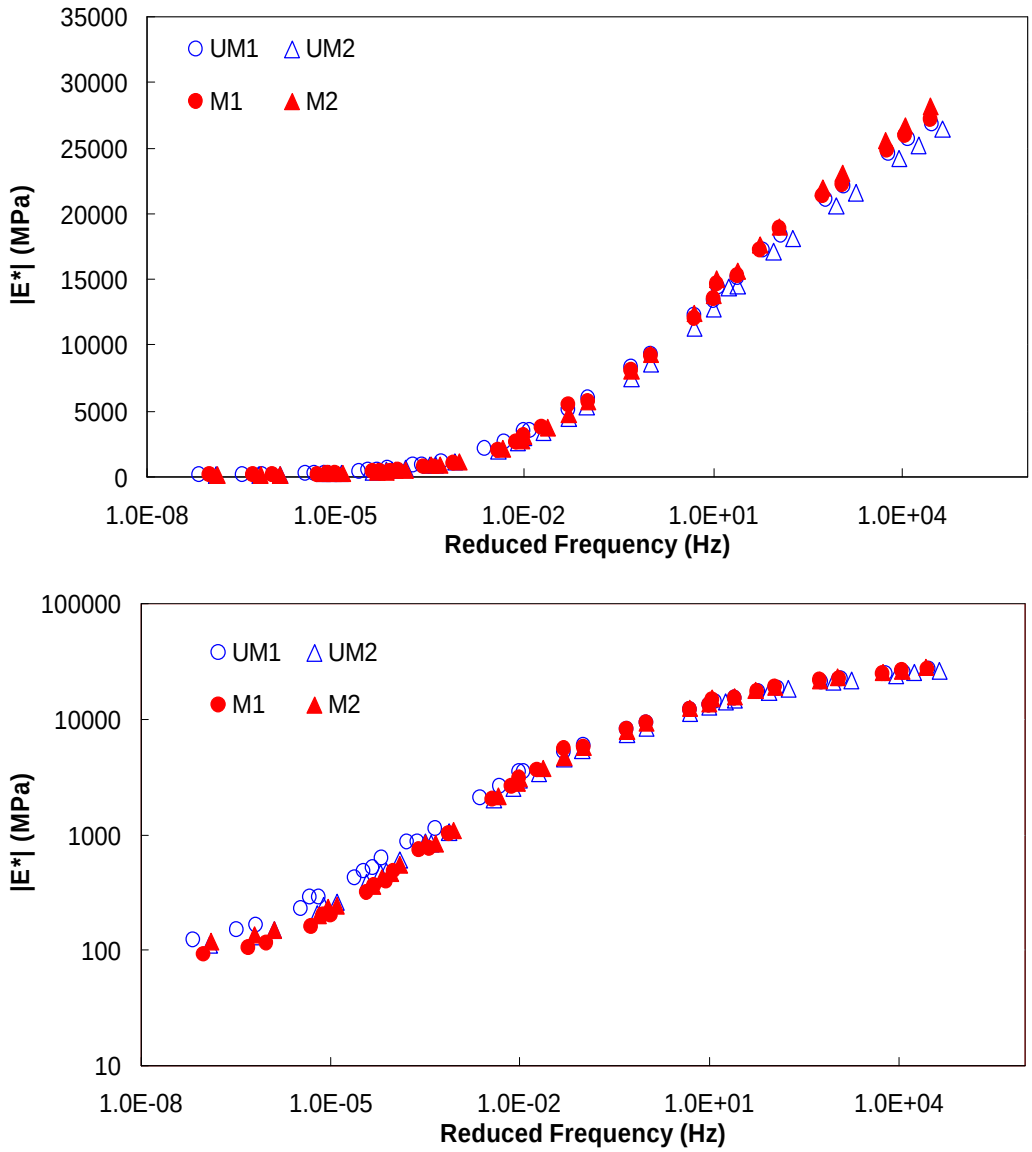

Figure 5.2 |E*| comparison between unmodified and lime-modified mixtures (S9.5AF)

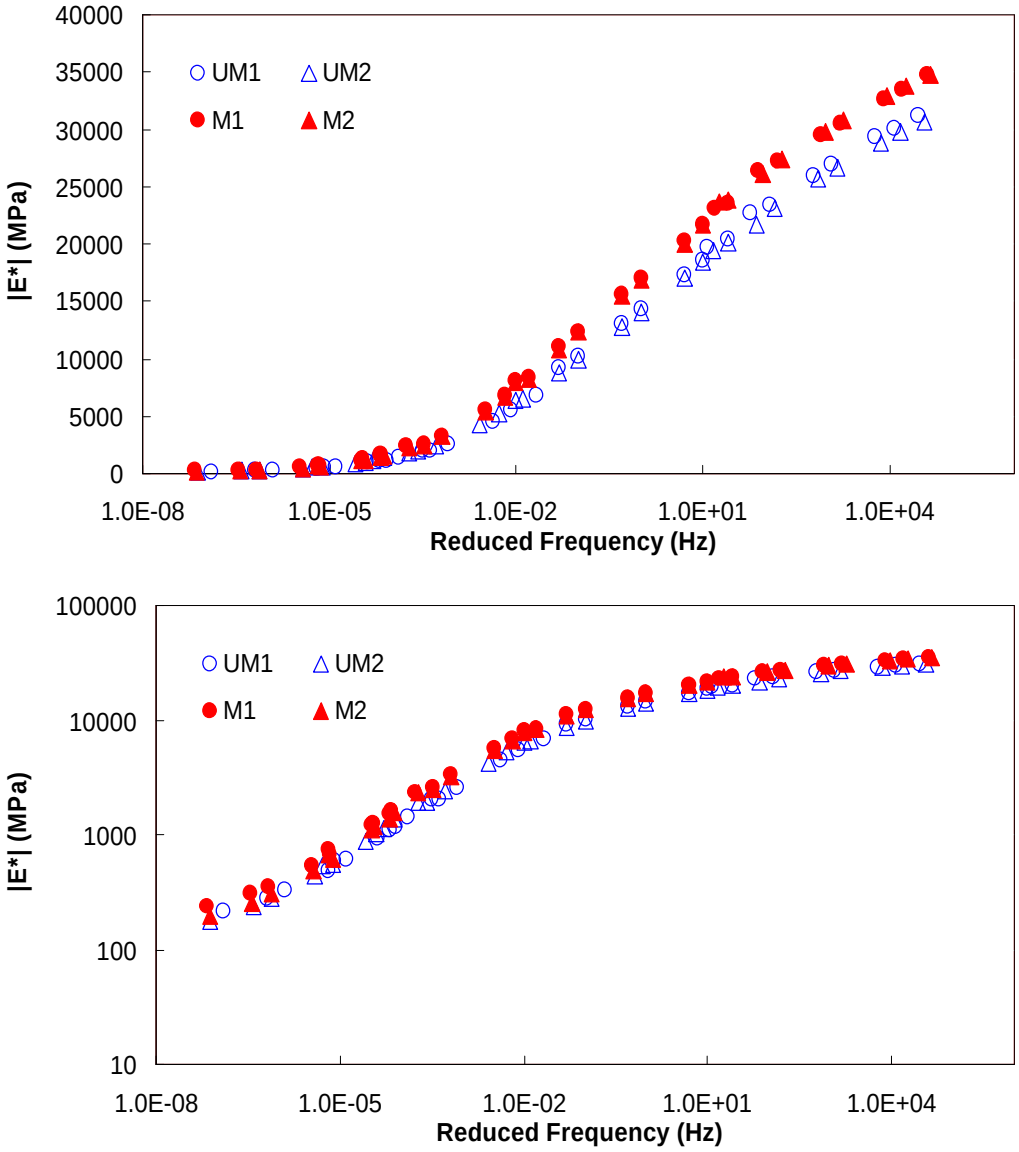

Figure 5.3 |E*| comparison between unmodified and lime-modified mixtures (S12.5CF)

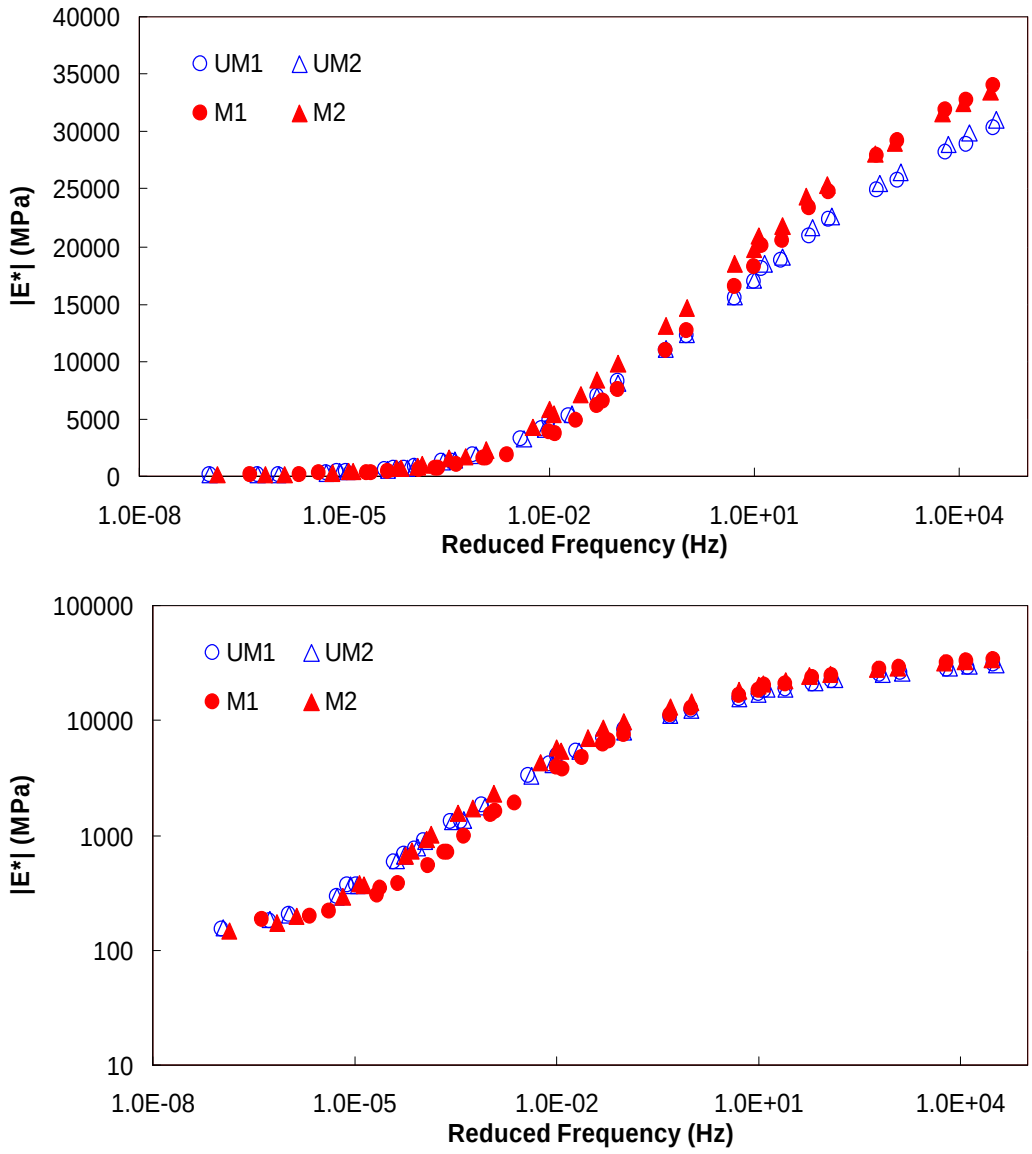

Figure 5.4 |E*| comparison between unmodified and lime-modified mixtures (I19.0BF)

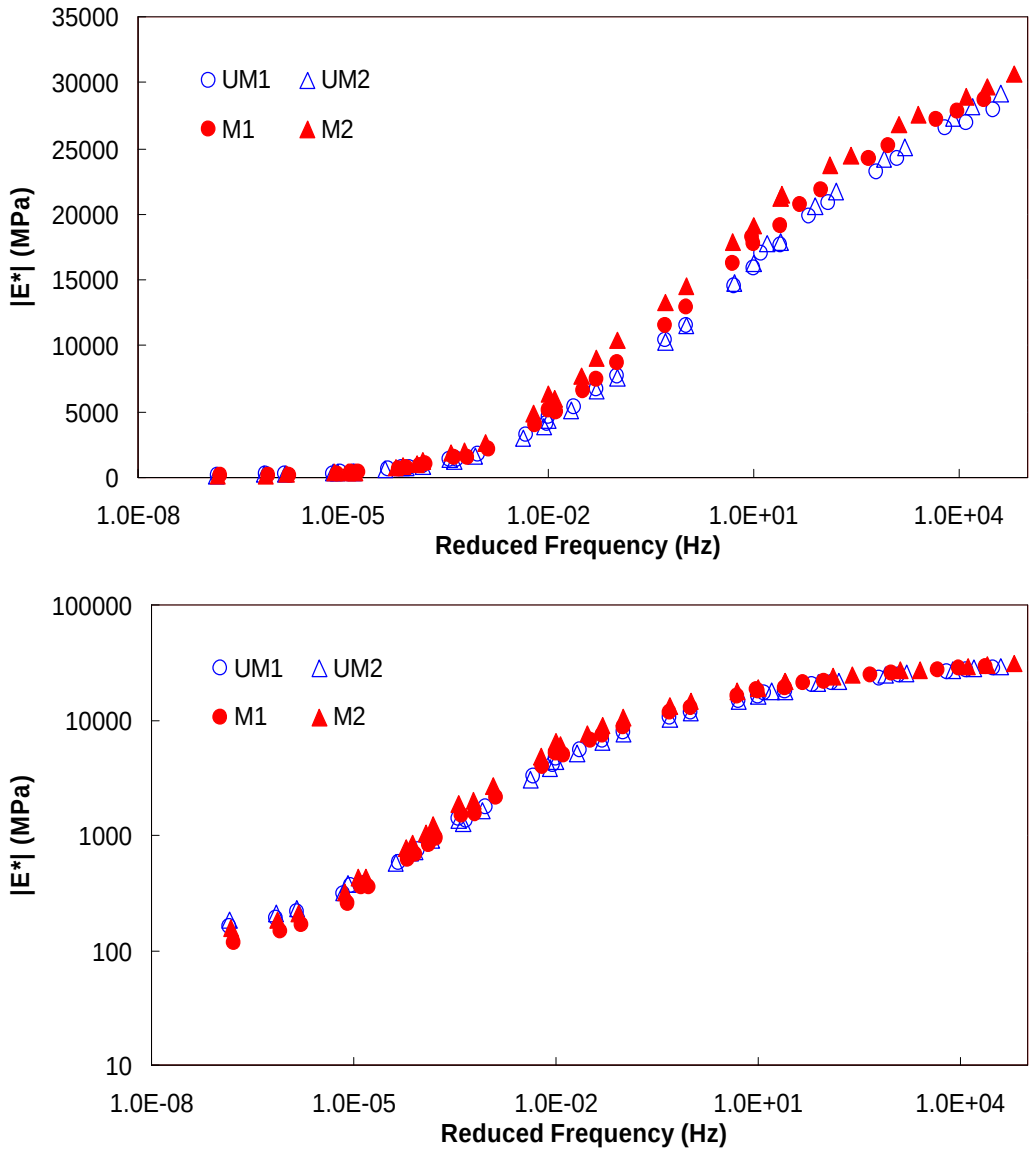

Figure 5.5 |E*| comparison between unmodified and lime-modified mixtures (B25.0BF)

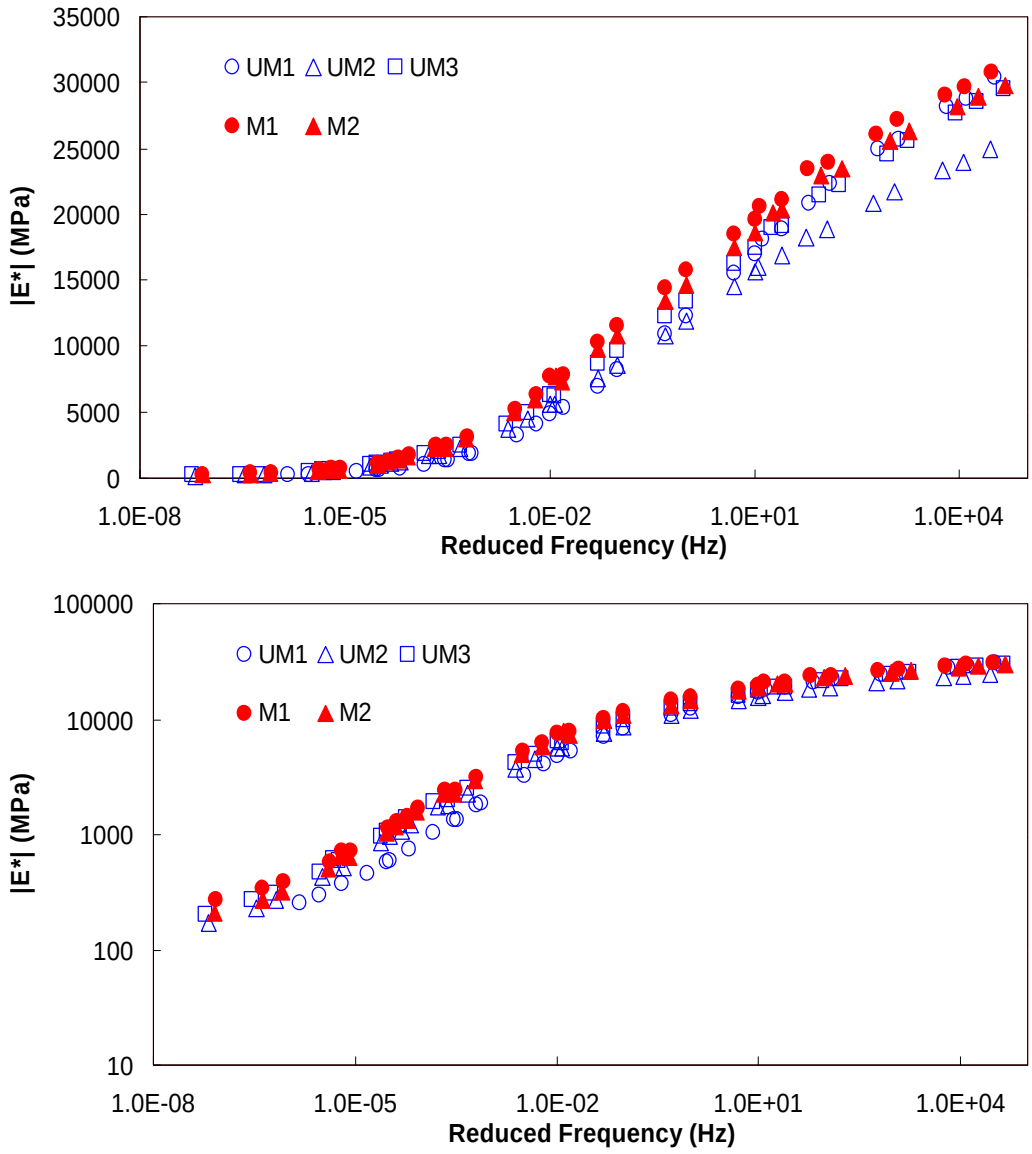

Figure 5.6 |E*| comparison between unmodified and lime-modified mixtures (S9.5CC)

Further, results from |E*| testing are summarized for all of the mixes with the line-of-equality plots shown in Figure 5.7. The data are presented in both semi-log and log-log space to examine both the low temperature (semi-log) and high temperature (log-log) results. From Figure 5.7, it is observed that the lime-modified mixtures tend to be stiffer at the highest modulus conditions (i.e., under the lowest test temperature conditions), but show little

difference at the low modulus (high temperature) conditions. It is noted that these results conflict with those presented elsewhere (Witczak et al. 2004) where it is shown that hydrated lime increases the stiffness by a constant factor under all conditions.

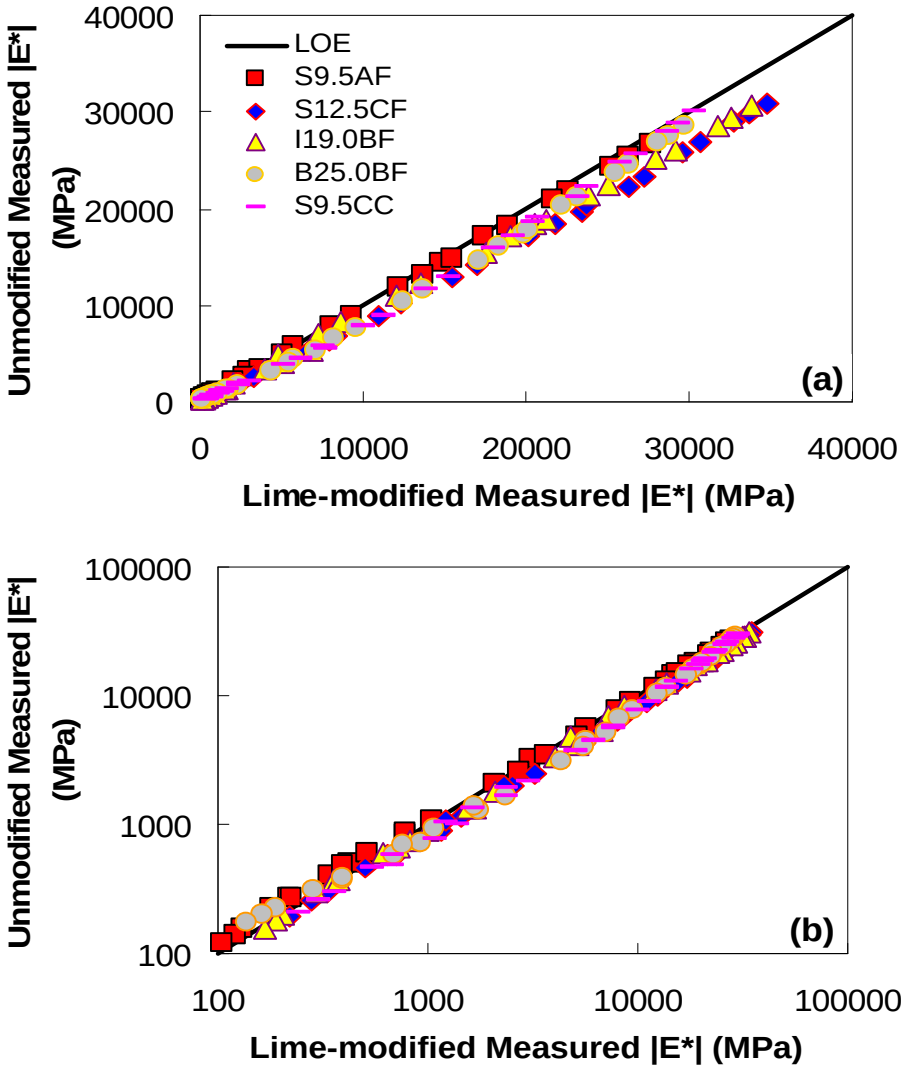

Figure 5.7 Comparison of the |E*| of lime-modified and unmodified measured data in: (a) semi-log; and (b) log-log space

The plots shown in Figure 5.7 are only partially useful for examining the effects of lime on the |E*| because they do not show the variability in the results. To resolve this issue, a statistical analysis of all the mixtures was performed.

5.4 Statistical Analysis

Multiple equivariance t-tests, at the significance level of $a = 0.05$, were conducted to examine the statistical significance of the results. The F-test was used to verify the equivariance assumption used in this analysis. The hypothesis test was constructed with the following parameters:

Ho: $\mu 1 - \mu 2 = 0$; and

H1: $\mu 1 - \mu 2 > 0$,

where $\mu 1$ is the mean |E*| at a given reduced frequency for the unmodified mixture, and $\mu 2$ is the mean |E*| at the same reduced frequency for the lime-modified mixtures. Because each test did not have the same reduced frequency, comparisons were made by using interpolated data at specific reduced frequencies (24000 Hz, 1400 Hz, 2 Hz, 0.03 Hz, 0.0001 Hz, 0.00001 Hz, 0.00000013 Hz). These reduced frequencies cover the range of material behavior when the mastercurve is constructed at a reference temperature of 10°C. Explicitly, 24000 Hz to 1400 Hz represents -10°C; 2 Hz to 0.03 Hz represents 10°C; 0.0001 Hz represents 35°C; and 0.00001 Hz to 0.00000013 Hz represents 54.4°C. Results from the statistical analysis are summarized in Table 5.5 and Figure 5.8. For convenience, the conditions where lime-modified mixtures exhibit higher |E*| values are denoted with darkened cells.

Table 5.5 Statistical Analysis of the Impact of Lime on the Dynamic Modulus

Mix ID	Reduced Frequency (Hz)						
	2.4E+4	1.4E+3	2.0E+0	3.0E-2	1.0E-4	1.0E-5	1.3E-7
S9.5AF	0.084	0.108	0.240	0.439	0.101	0.127	0.224
S12.5CF	0.005	0.002	0.002	0.053	0.021	0.052	0.198
I19.0BF	0.007	0.007	0.133	0.446	0.271	0.109	0.153
B25.0BF	0.118	0.085	0.050	0.097	0.243	0.315	0.112
S9.5CC	0.204	0.129	0.017	0.018	0.107	0.132	0.150
P-value < 0.05	40.0 %	40.0 %	60.0 %	20.0 %	20.0 %	0.0 %	0.0 %

Although in general the null hypothesis was not statistically rejected, a visual comparison of the data at higher reduced frequencies shows a consistent rejection of the null hypothesis. This observation suggests that lime modification has some stiffening effects, especially at intermediate and low temperatures. It is also interesting to note that no clear trend exists that supports the results of previous studies showing that the effect of lime modification depends highly on the physico-chemical composition of the mixture.

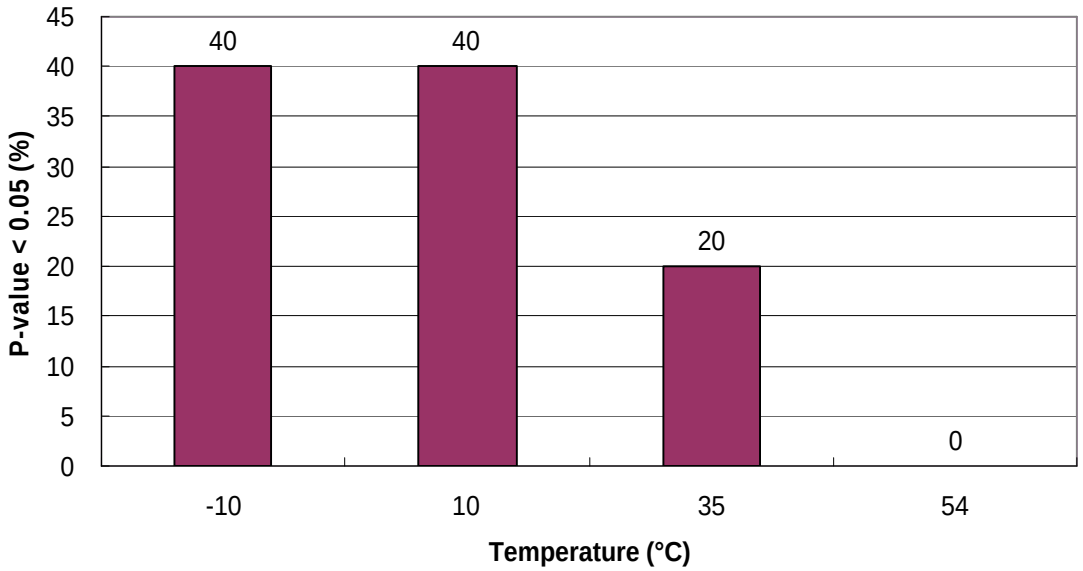

Figure 5.8 Rate of rejected null hypothesis with temperature change

5.5 Summary and Conclusions

New mix designs for five Superpave mixtures commonly used in North Carolina have been developed with lime modification. Characterization of these mixtures was performed using the newly developed |E*| test protocol. This study of the effects of lime on various mixtures reveals the following conclusions.

- An additional 1% lime by weight of mixture reduces the optimal asphalt content by 0.35 to 0.9%.
- Lime modification of HMA increases the |E*|, especially at high frequencies and lower temperatures.

Chapter 6

Effects of the Lime Introduction Method on the Performance of the Mixtures

6.1 Introduction

The results from Task 1 show the importance of hydrated lime as a stiffening agent in asphalt concrete, even at the low strain levels applied in the |E*| tests. Furthermore, the properties of hydrated lime that allow it to act as an extender of the asphalt binder make it attractive as a cost-savings tool. At the outset of this project, work from the NCHRP 9-19 project and other work (Pellinen 2001, Kallas 1970) suggested that the |E*| would be an excellent indicator of both the rutting and fatigue cracking propensity of asphalt concrete mixtures. However, more recent studies now suggest that these preliminary findings do not hold for a wider range of mixtures (Mohammad et al. 2006, Bhasin et al. 2004, Zhou et al. 2003). Additionally, work from other researchers (Witczak et al. 2004) indicates that hydrated lime results in a large increase in the |E*|, even at high temperatures. In that research, however, lime was introduced by substituting the hydrated lime for a portion of the mineral filler in a standard mixture. That is, that research suggests that lime modification can be performed in different

ways to serve different purposes. For example, the addition of lime can be used to reduce costs or to improve performance.

The primary objective of the work presented here is to evaluate the differences in performance among lime-modified asphalt mixes with different mix designs. To evaluate the mixture performances, the following tests are conducted: the SPTs recommended by NCHRP 465; the |E*| and flow number tests; characterization tests for the tensile VECD model; and the cyclic fatigue simulation of VECD-FEP++ on the pavement.

6.2 Experimental Design

The experimental program for this portion of the work involves the development of three different lime-modified mix designs – Leco, Lmod and Lsub – and one unmodified mix design, Control. The HMA mixture used is a Superpave 9.5 mm surface mix (S9.5C in Table 5.1). Granite aggregate from the Pineville/Charlotte quarry, Reclaimed Asphalt Pavement (RAP) and PG58-28 binder obtained from the Citgo refinery in Salisbury, North Carolina, were used to produce all the mixtures. It should be noted that the presence of RAP in the mixture changes the true PG of the asphalt binder in the mixture. According to the NCDOT, the true PG for this mixture is PG 64-22. The aggregate gradation of each mixture is shown in Figure 6.1.

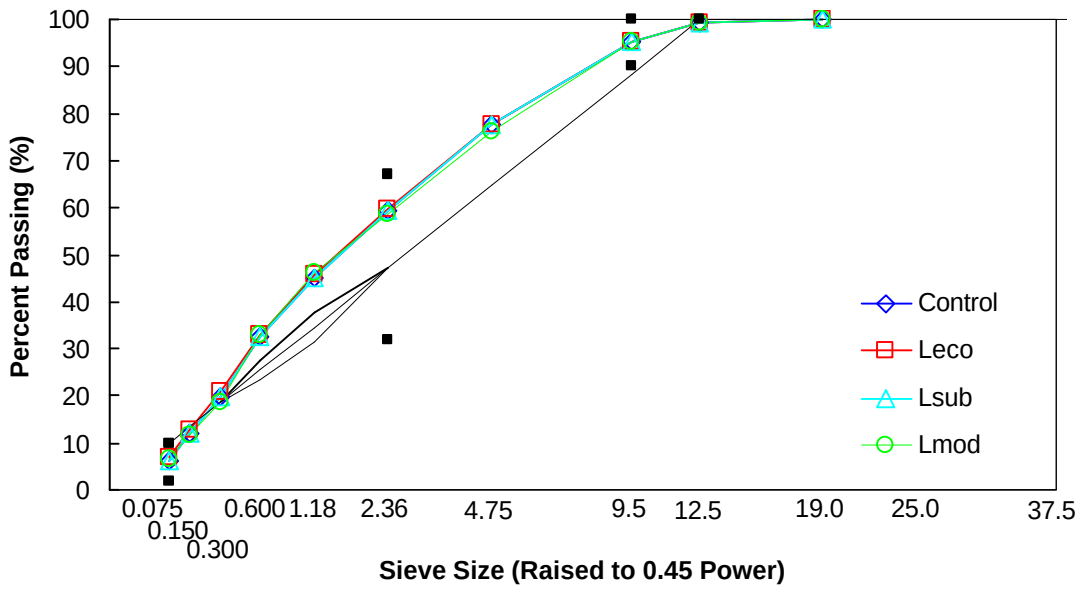

Figure 6.1 Gradation chart for the lime-modified mixtures

For each of the mixtures, a Superpave volumetric mix design was performed to obtain the optimal asphalt content. For the modified mix designs, two dry methods and one wet method were performed. Differences in the aggregate structure designs center primarily on the proportioning of the lime. For the first method, termed Leco in this study, 1% hydrated lime by total aggregate weight was added without any modification to the aggregate structure. This mix design follows the same methodology used in the first phase of this study. The second method, Lsub, also uses a dry introduction technique and follows the same method used in the Witczak study (Witczak et al. 2004); that is, hydrated lime is substituted for a portion of the baghouse fines (1% by aggregate weight). The final modified mix design, Lmod, introduces the hydrated lime to wet aggregate at a moisture content of 2-3% over saturated-surface-dry (SSD) conditions. For this design, 1% by aggregate weight hydrated lime is first added to the original unmodified mixture, and then the proportions of the various

stockpiles in this original mix design, particularly the sand stockpile, are slightly altered. The alterations were performed to ensure that the blended gradation was the same as that of the original mix design and that the optimal asphalt content remained the same.

Results from the volumetric mix design are summarized in Table 6.1 and Table 6.2. From these tables it is observed that the SuperPave volumetric criteria are met for all the mixtures. It is also seen that, as expected, the Leco mixture shows the most drastic reduction in optimal asphalt content, followed next by the Lsub mixture. Finally, it is seen from Table 6.2 that, in general, the coarse aggregate gradation does not change across the mixture types.

Table 6.1 Mix Design Results of the Lime Introduction Methods

Mix Type	Design Asphalt Content (%)		% Gmm @ Nini, Nmax		VMA		VFA	
Fine RS9.5C	Binder Grade	Opt. AC (%)	90.5% max.	98% max.	(%)	Min.	(%)	Min.-Max.
Control	PG58-28	5.60	89.4	97.0	16.2	15	75.0	65-80
Leco		5.15	89.4	96.8	15.8		74.0	
Lsub		5.30	89.5	96.1	15.7		74.0	
Lmod		5.60	89.8	96.1	15.9		75.8	

* Aggregate Source: Pineville/Charlotte, NC
* Binder Source: Citgo; Salisbury, NC

Table 6.2 Gradation Information for the Lime Modification Methods

% Stock Pile	Mix Types			
	Control	Leco	Lsub	Lmod
78-M Stone	20.0	19.8	20.0	22.5
Washed screenings	41.4	41.0	41.4	32.5
Asphalt sand	12.0	11.9	12.0	17.5
Lime	0.0	1.0	1.0	1.0
Baghouse fines	1.5	1.5	0.5	1.4
RAP	25.1	24.9	25.1	25.1
Sum	100.0	100.0	100.0	100.0
Sieves (mm)	% Passing Blend			
19.0	100.0	100.0	100.0	100.0
12.5	99.2	99.2	99.2	99.2
9.5	95.3	95.4	95.3	95.1
4.75	77.6	77.8	77.6	76.2
2.36	59.2	59.6	59.2	58.7
1.18	45.1	45.7	45.1	46.0
0.600	32.5	33.1	32.5	32.8
0.300	19.9	20.7	19.9	18.8
0.150	12.2	13.0	12.2	11.6
0.075	6.3	7.1	6.3	6.5

6.3 Performance Tests and Analysis of Results

The |E*| test was performed in accordance with the AASHTO TP62-03 protocol. Specimens of 150 mm diameter and 178 mm height were fabricated using the ServoPac Superpave Gyratory Compactor (SGC). These specimens were cut and cored to produce 100 mm diameter, 150 mm height specimens. Three replicates were tested for each mix. |E*| mastercurves were developed and compared to assess the stiffening effects of the different lime modification approaches.

The fatigue cracking resistance of the four mixes was evaluated using the newly developed viscoelastoplastic continuum damage (VEPCD) model. The major advantage of this model is that the fatigue cracking behavior of an asphalt mix under widely varying

conditions can be determined using a relatively simple test protocol. The required test protocol for the development of the VEPCD model includes:

a. Temperature-frequency sweep dynamic modulus tests
b. Monotonic constant crosshead rate tests in uniaxial tension at 5°C
c. Monotonic constant crosshead rate tests in uniaxial tension at 40°C

Monotonic constant crosshead rate tests were conducted in tension using 75 mm diameter, 150 mm tall specimens cut and cored from the 150 mm diameter, 178 mm tall SGC specimens. Several different rates were used. The stress-strain data from the 5°C testing were used in developing the VECD model. The data from the 40°C testing were used to determine the viscoplastic model. These two models were integrated to determine the VEPCD model, from which the fatigue behavior of the asphalt mix under varying conditions can be predicted. This method has been successfully used in evaluating the fatigue resistance of four FHWA ALF mixes, including three different polymer-modified mixtures. However, the VECD model, not the VEPCD model, was used to assess the fatigue resistance in this study. The rutting characteristics of the mixtures were evaluated using TRLPD tests at 55°C. These tests were conducted using the same geometry as the SGC specimens for the |E*| test. A 120 psi deviatoric stress with a 0.1 sec. haversine loading and a 0.9 sec. rest period was applied to the specimen under a constant confining pressure of 20 psi. The permanent-to-resilient strain ratio was determined as a function of the number of loading cycles and the temperature. This relationship is used in the NCHRP 1-37A Mechanistic-Empirical Pavement Design Guide (MEPDG). More than two replicates were tested for each temperature.

In order to gain further insight into the cause of rejection, the Bonferroni multiple pairwise comparison method using Least Significant Difference (LSD) was employed after each performance test to make individual mixture comparisons.

Finally, the field responses, obtained from the cyclic fatigue simulation of VECD-FEP++ on the pavement, were predicted to evaluate the effects of the various lime modification methods on fatigue performance.

6.3.1 Dynamic modulus tests and statistical analysis

Results from the |E*| tests are shown in the form of mastercurves of both the |E*| (Figure 6.2) and phase angle (Figure 6.3). By themselves, these figures indicate that no significant effect from the lime addition methods can be detected in the |E*| testing. However, for completeness, a statistical analysis similar to that discussed in Chapter 5 of this study has been completed.

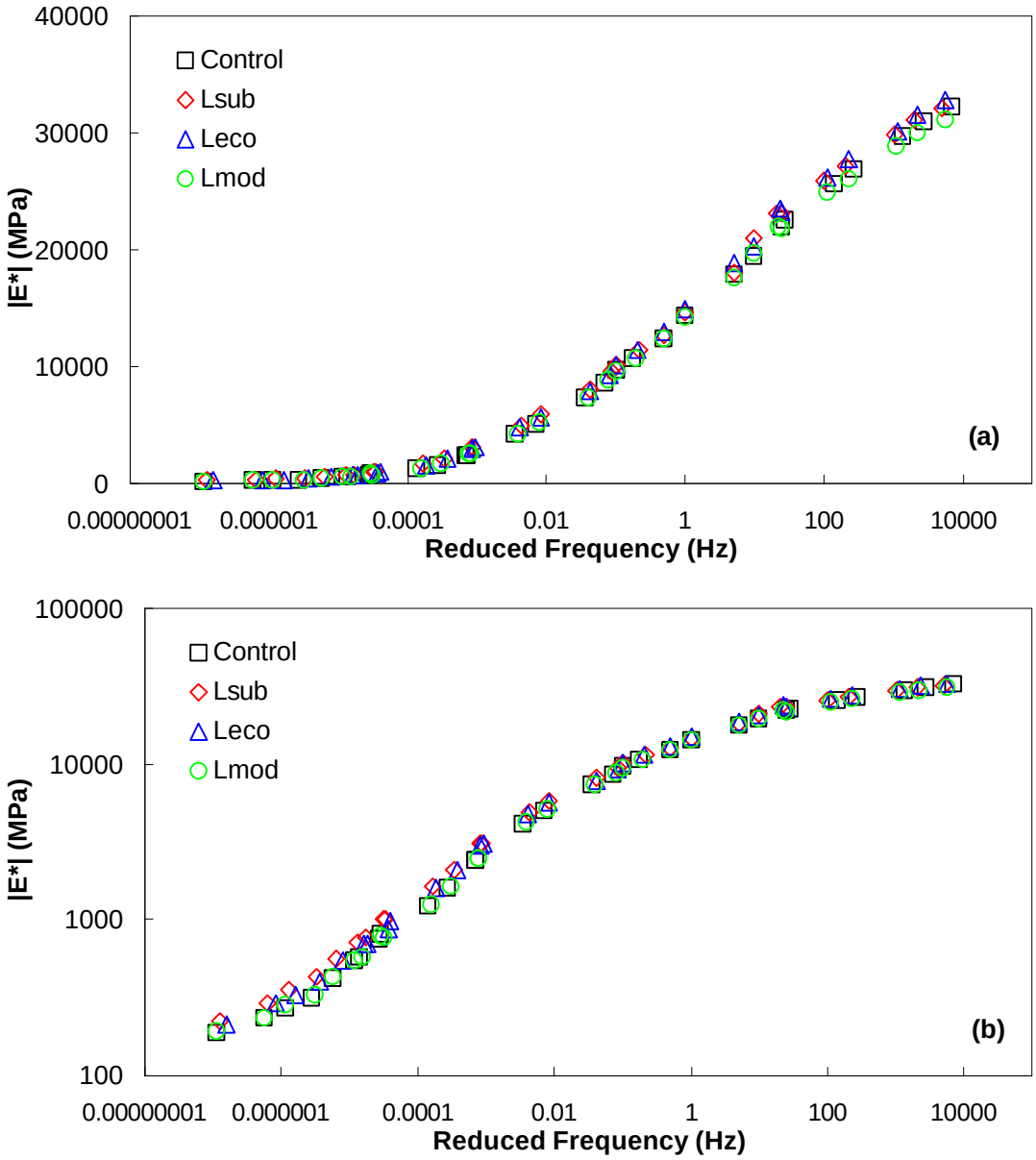

Figure 6.2 Effects of the lime introduction method on the |E*| in: (a) semi-log and (b) log-log space

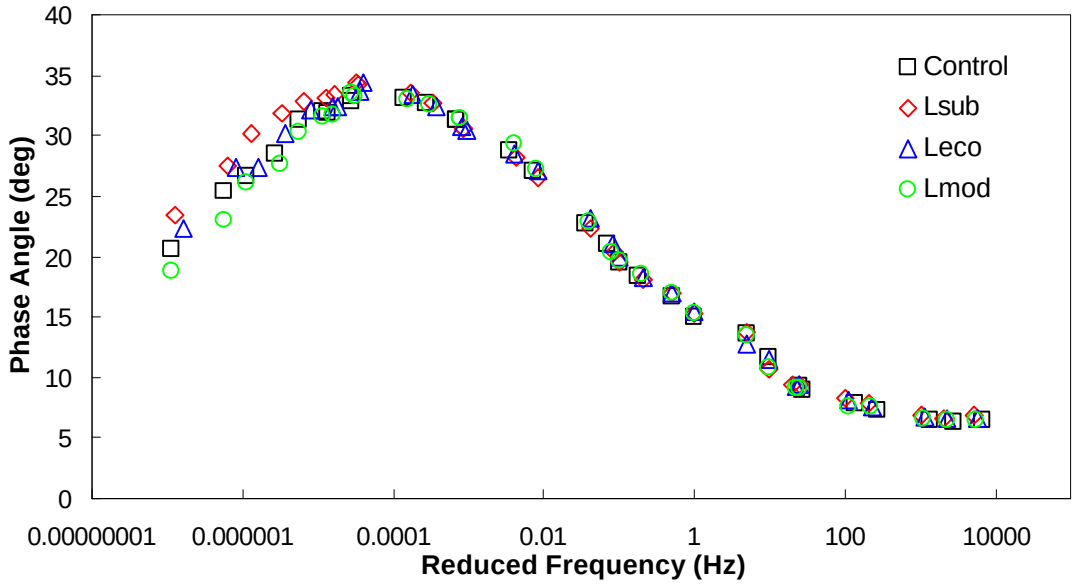

Figure 6.3 Effects of the lime introduction method on the phase angle

The first step in such an analysis involves a single factor analysis of variance (ANOVA) under the null hypothesis that the |E*| value for each mixture is equivalent. This analysis is performed with the significance level a = 0.05 at the same reduced frequencies (24000 Hz, 1400 Hz, 2 Hz, 0.03 Hz, 0.0001 Hz, 0.00001 Hz, 0.00000013 Hz) used in Chapter 5. The results of this analysis are presented in Table 6.3. It is observed from this table that the null hypothesis is rejected at the lowest reduced frequencies, i.e., conditions marked with darkened cells.

To gain further insight into the cause of rejection, the Bonferroni multiple pairwise comparison method using LSD is again used to make individual mixture comparisons. The significance level, a = 0.05, is again used for the analysis, and the results are summarized in Table 6.3. The specimen that produced the highest value of dynamic moudulus (|E*|) at a given frequency was ranked “A”. From this point, the E* value for each of the other specimens was compared to this value to determine if they were significantly lower. If the

specimen with the second highest value of E* is found to be significantly less it will be ranked “B”, if not, it also would be ranked “A”. The process is continued for the third and forth specimens for each of the frequencies to produce the results shown in Table 6.3 and all subsequent tables. In Table 6.3, one can see cases where there is no significant difference between any of the E* values, thus the A-A-A-A values. If each of the specimens had E* values significantly less than the E* of the specimens more stiff than it, the ranking would be A-B-C-D. An A, A-B, B, C ranking means that the E* value of the specimen is not significantly different from that of the first or third specimens but the third is less stiff than the first. It is seen from this analysis that, in general, at conditions rejected by ANOVA, the Lsub, Leco, and to a lesser extent the Lmod mixtures show a consistently higher modulus than the Control mixture. It is somewhat surprising to see these differences in the modulus, particularly considering that the results from the previous study consistently indicate no statistical difference in the data at the lowest reduced frequency. However, a closer examination of the data in both studies shows that the variability in this second project is less than that observed in the first. So, it is possible that the higher data quality makes comparisons at low reduced frequencies clearer.

Table 6.3 Statistical Analysis of the Effects of the Lime Introduction Method on the Dynamic Modulus

		Least Significant Difference Ranking			
Reduced Frequency (Hz)	p-value	Control	Lmod	Leco	Lsub
2.40E+04	0.3182	A	A	A	A
1.40E+03	0.2315	A	A	A	A
2.00E+00	0.2330	A	A	A	A
3.00E-02	0.0053	B	B	A-B	A
1.00E-04	0.0027	B	B	A-B	A
1.00E-05	0.0000	C	C	B	A
1.30E-07	0.0092	B	A	A	A

Regardless of the outcome of the statistical analysis, it is clear from Figure 6.2 that the inclusion of lime does not increase the stiffness of the material by a great amount. Further, it is interesting to note that the small visual increase in stiffness agrees with the observations drawn regarding the S9.5AF mixture, shown in Table 5.5. This mixture contains aggregate from the same source as the S9.5CF mixture used as the basis for the Control, Lmod, Leco and Lsub mixtures. It is unclear from these limited results if similar results regarding the effects of lime on the |E*| would hold for other types of mixtures using this same aggregate source; however, the results do support the claim that the specific physico-chemical properties of the constituent materials strongly affect the impact of lime on the material behavior.

6.3.2 TRLPD test results

For the mixtures in this study, the TRLPD tests were carried out until 10,000 cycles without observing tertiary flow. Such results indicate that each of the mixtures should exhibit

adequate rutting performance. Even though none of the mixtures exhibited tertiary flow, differences in material performance may be assessed by examining the permanent strain growth over the 10,000 test cycles. Such strain growth is presented in the plot shown in Figure 6.4. It is noted that the ordinate is presented in time; it should be recalled that a single cycle in the TRLPD test requires one second including the rest period. In this case, cycles and time may be used interchangeably.

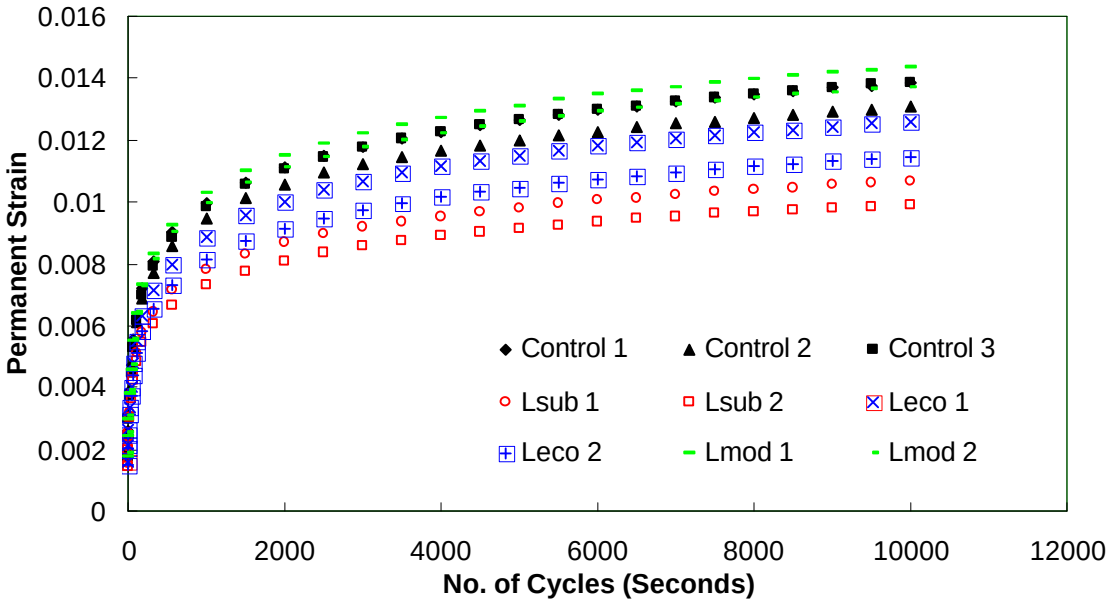

Figure 6.4 Effects of the lime introduction method on the permanent strain accumulation in TRLPD tests

The most critical observation from Figure 6.4 is the superior performance of the Lsub mixture relative to the other mixtures, and the inferior performance of the Control mixture. Statistical analysis was used to compare the differences of the mixtures.

ANOVA was performed under the null hypothesis that the permanent strain value for each mixture is equivalent. This analysis was performed with the significance level, a = 0.05, at various cycles (10, 50, 100, 200, 500, 1000, 2000, 3000, 5000, 7000, 10000) covering the

range of the permanent deformation and providing assessment of early, middle and late stage behavior.

The results of this analysis are presented in Table 6.4. It is observed from this table that the null hypothesis is rejected at all cycles; i.e., conditions marked with darkened cells. The same Bonferroni multiple pairwise comparison method using LSD was used to make individual mixture comparisons. Again, a significance level, a = 0.05, was used for the analysis; the results are summarized in Table 6.4. It is seen from this analysis that, in general, the Lsub and Leco mixtures show a consistently lower permanent strain than the Control and Lmod mixtures. However, from the 500 cycles of repetitive loading, the Lsub mixture shows a better rutting resistance than the Leco mixture. This result shows a similar ranking of the |E*| statistical analysis at lower reduced frequencies.

Table 6.4 Statistical Analysis of the Effects of the Lime Introduction Method on the Permanent Deformation Resistance

Cycles	p-value	Least Significant Difference Ranking			
		Control	Lsub	Leco	Lmod
1E+01	0.0051	B	A	A	B
5E+01	0.0028	B	A	A	B
1E+02	0.0028	B	A	A	B
2E+02	0.0027	B	A	A	B
5E+02	0.0036	B	A	A-B	B-C
1E+03	0.0041	B	A	A-B	B-C
2E+03	0.0046	B	A	A-B	B
3E+03	0.0050	B	A	A-B	B
5E+03	0.0056	B	A	A-B	B
7E+03	0.0060	B	A	A-B	B
1E+04	0.0064	B	A	A-B	B

Further, an examination of Table 6.4 shows that asphalt content alone does not explain the change in performance, because the Leco mixture does not exhibit the best performance although it contains the lowest asphalt content.

Also, it is noted that the Lmod mixture does not seem to exhibit any effects of lime in its performance. Roberts et al. (1996) state that mixtures designed with high amounts of natural sands and uncrushed gravels exhibit low stability and are prone to excessive rutting due to their rounded shape, smooth texture, and sometimes clay and organic dust on their surfaces. Even though the amount of natural sands utilized in the Lmod mixture, 17.5% by weight of total aggregate, is within the range (10 to 25 %), it is nonetheless higher than those of other mixtures (12%); therefore, this amount of natural sands may help cancel out the effect of lime. Overall, it is noted that the effects of lime modification range from negligible (Lmod) to large (Lsub).

6.3.3 Constant crosshead rate monotonic results

The damage characteristic curves, or C vs. S curves, which represent the fundamental resistance of a mixture to damage, are shown in Figure 6.5 for the mixtures examined in this study. These curves are obtained from constant crosshead rate tests performed at 5°C and at the rates noted in Table 4.2. Although the differences in Figure 6.5 seem small, the observed differences, particularly at high damage levels, are evident in the materials. Normally, little variation exists among the replicates, and the curves determined from tests at various rates collapse very well. To lend further credence to this observation, a statistical analysis, similar to that performed for the comparison of the dynamic moduli of these mixtures, was performed.

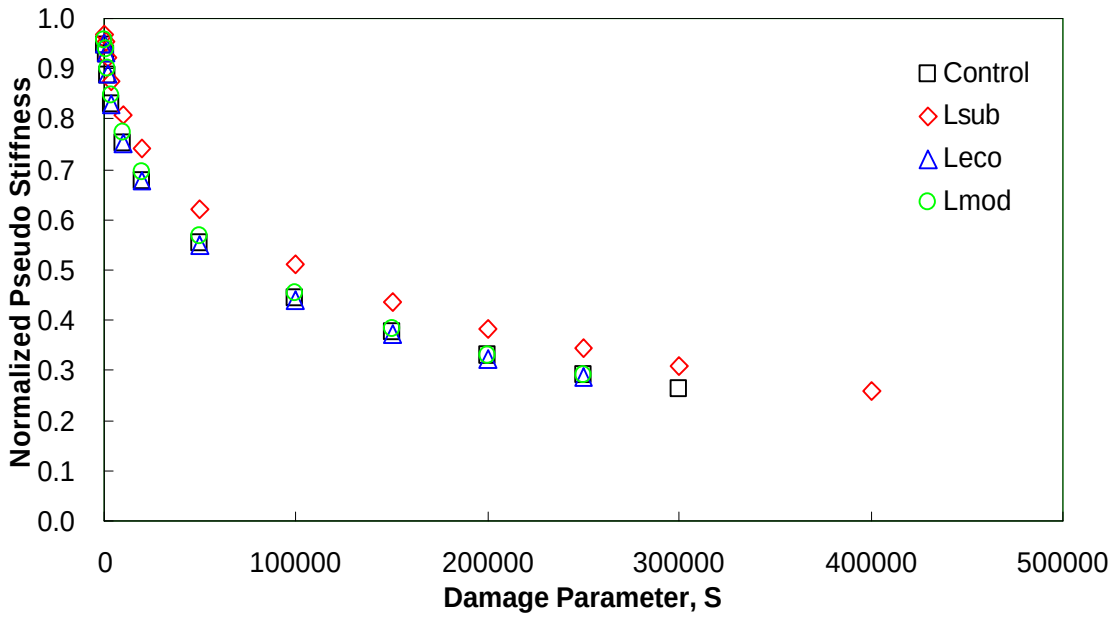

Figure 6.5 Damage characteristic relationships for Control, Lsub, Leco, and Lmod mixtures

ANOVA was carried out under the null hypothesis that the damage characteristic curve for each mixture is equivalent; this analysis is similar to the process of comparing the effects of the various methods of lime introduction on fatigue characteristics. This analysis was performed with the significance level, a = 0.05, at the same damage parameter, S (250, 500, 1500, 4000, 10000, 20000, 50000, 100000, 150000, 200000, 250000), which covers the range of the damage characteristic curves and provides assessment of early, middle and late stage behavior. From Table 6.5 it is observed that ANOVA suggests that the damage characteristic curves are statistically not the same for the overall range of S values. The same Bonferroni multiple pairwise comparison method using LSD (a = 0.05) was used to make individual mixture comparisons, and the results are summarized in Table 6.5. It is observed from this analysis that the Lsub mixture shows consistently higher pseudo stiffness than the other mixtures. Also, the Lsub mixture is the most favorable in terms of fatigue resistance, showing good agreement in the ranking of the |E*| statistical analysis at lower reduced frequencies and rutting resistance.

Table 6.5 Statistical Analysis of the Effects of the Lime Introduction Method on Fatigue Resistance

Refined S	p-value	Least Significant Difference Ranking			
		Control	Lsub	Leco	Lmod
2.50E+02	0.000029	B	A	B	B
5.00E+02	0.000025	B	A	B	B
1.50E+03	0.000020	B	A	B	B
4.00E+03	0.000016	B	A	B	B
1.00E+04	0.000012	B	A	B	B
2.00E+04	0.000010	B	A	B	B
5.00E+04	0.000007	B	A	B	B
1.00E+05	0.000006	B	A	B	B
1.50E+05	0.000006	B	A	B	B
2.00E+05	0.000007	B	A	B	B
2.50E+05	0.000009	B	A	B	B

Generally, care must be taken in examining such damage characteristic curves to evaluate various mixtures' resistance to fatigue damage, because the damage characteristic curves present only a material's resistance to damage. The fatigue performance of asphalt concrete, however, is known to be affected by the mixture's ability to resist both damage and deformation. The statistical analysis of the |E*| of these mixtures presented in Table 6.3 shows that the resistance to deformation is found under the same conditions as those where fatigue is generally considered to occur, i.e., intermediate to low temperatures and/or high to intermediate frequencies. Therefore, under such conditions, the damage characteristic curve ranking should relate directly to the respective fatigue performance of the mixtures.

By examining Table 6.5 for material performance, it is first observed that the Lsub mixture exhibits the most favorable characteristics. Along similar lines, the asphalt content does not appear to be a major factor. Although experience shows that mixtures with a higher

asphalt content perform better in terms of fatigue resistance, in the case of Leco, which has an asphalt content 0.45% less than that of the Control and Lsub mixtures, and an asphalt content 0.3% less than that of the Control mixture, the fatigue rankings are higher. Observing that the differences between the Lsub mixture and the Control mixture lie in the properties of the filler portion of the mixture, it seems clear that lime has a highly beneficial effect with regard to the fatigue life of asphalt mixtures. The differences in asphalt content make this point particularly strong. The degree to which lime is beneficial is expected to depend highly on the exact physico-chemical composition of the respective mixture (Little et al. 2005). Further, the inclusion of lime modification does not necessarily exhibit a consistent improvement across mixtures with different aggregate and binder sources. It would appear from these results that, for the physical conditions of these mixtures, hydrated lime offers a significant improvement over the baghouse fines normally used. The improvement is likely due to the unique chemical characteristics of hydrated lime when it is dispersed in the asphalt binder (Petersen et al. 1987a, b) and also due, in particular, to its ability to withstand microcrack damage growth (Little et al. 2005). These effects vary depending on the exact composition of the filler portion, which is a likely reason that the behavior of the other two modified mixtures, Control and Lsub, lies between the two extremes. Continuing along this same path, the observation that the Leco mixture performs worse than the Lsub mixture seems to suggest that the filler microstructure formed in the binder of the Leco mixture is poorer, due to a higher concentration of baghouse fines, than that formed in the Lsub mixture, even though both mixtures have the same amount of lime. Conversely, the differences observed between the Leco and Lsub mixtures could be related to the reduced asphalt content

in the Leco mixture. However, it is judged more likely that these observations, when combined with the results obtained from the TRLPD tests (i.e., that a lower asphalt content results in more permanent strain growth), are primarily related to the effects of the lime and not the asphalt content.

While the fatigue performance is known to be affected by a material's resistance to damage and deformation, the damage characteristic curves present only a material's resistance to damage. The VECD-FEP++ simulation is implemented with regard to the material's resistance to damage and deformation. Even though the limitation of continuum damage to fracture properties still remains, at this time no clear link between them is evident. The trends of the fatigue performance of the mixtures can be captured using the VECD-FEP++.

6.4 VECD-FEP++ Simulation Results

The field responses for the cyclic fatigue simulation on the pavement were predicted to evaluate the effect of the various lime modification methods on fatigue performance. Because the purpose of these simulations is to rank the different lime-modified mixtures for fatigue resistance, each simulation was performed assuming a simple pavement structure. The ranking was produced based on different lime modification methods for the Control, Lsub, Leco, and Lmod mixes.

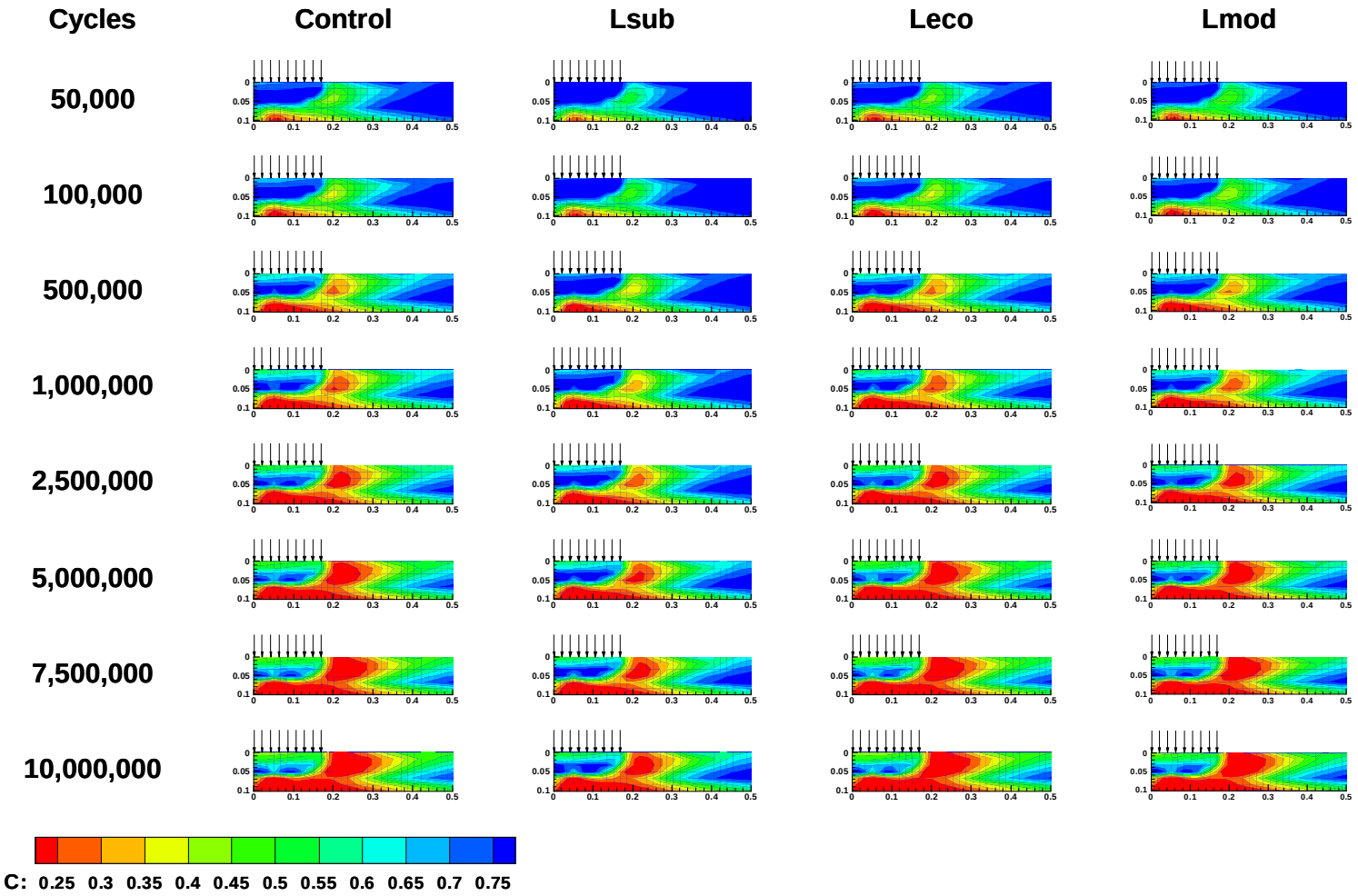

Figure 6.6 Comparison of the Damage Contour Plots at Various Load Cycles for the Different Lime Addition Methods

Regarding the contour plots shown in Figure 6.6, it should be noted that if the C value decreases below 0.25, the area where the material has reduced in integrity, i.e., the localization of the damage, starts to spread over the pavement section that is indicated in red in the figure. It is clearly observed that as the number of cycles increases, all the mixtures tend to spread damage throughout the pavement. Another interesting observation is that the damage tends to concentrate at the bottom of the layer and the right edge of the upper layer where the load is applied.

The localization of the damage appears to develop first at the bottom of the pavement under the load. Then, once the number of cycles increases to 500,000 the damage appears to begin at the middle of the layer at the right edge of the load. The first development of damage may be considered the lower damaged zone and the late stages of damage as the upper damaged zone. In general, a bottom-up crack is caused by the tensile strain due to radial stress at the lower surface of the layer, and a top-down crack is caused by the shear stress of the traffic load at the upper side of the layer. The lower and upper damage zones appear to be bottom-up and top-down cracking, respectively. However, the VECD model does not account for the asphalt concrete's post-peak behavior and fracture properties; therefore, it is difficult to make a direct link between the damaged zone and cracking. Until the number of cycles was applied up to 2,500,000, the localization of damage at the right edge of the load could not be found in the Lsub mix other than one instance at the bottom of the pavement, whereas the top-down cracking could be observed from 500,000 cycles in the other mixes. By observing the localization of the damage at the lower side of the layer, it may be stated that the Lsub mix shows better resistance against damage growth than the other mixes over

the entire range of load cycles. The Control, Leco, and Lmod mixes show similar damage propagation through the cycles. Until 2,500,000 cycles, slightly less damage propagation was observed in the Lmod mix compared to the Control and Leco mixes. This observation may be due to the higher asphalt content and the small effect of lime in the Lmod mix. The damage localization in the Leco mix was propagated through the full depth at the final stage of the load cycle. Because no clear trend was observed among the Control mix, Leco mix, and Lmod mix, it was decided to examine the % Crack area and the Average C of those mixes at the same cycles that were used for the comparison of the contour plots.

Since the % Crack area examined for the different mixes is the number of nodes below C equal to 0.25 out of the total number of nodes within the extent of the pavement region (0.5 m in width), the % Crack area can also be considered as the area of the damage localization, based on the simulation results. Also, the Average C value can represent the overall status of the damage propagation in the pavement, because the Average C value is the averaged value of C in the pavement region at each examined cycle. It can be explained that the higher the value of the % Crack area, the larger the area in which the damage localization occurs, whereas the lower the Average C value, the more the pavement damage. Therefore, these parameters can be used to examine the fatigue performance of the pavement.

The results of both the % Crack area and the Average C are plotted in Figure 6.6 and Figure 6.7. As a function of the load cycles, the overall trend of the fatigue performance of each mix is evaluated in Figure 6.6, whereas discrete trends of the fatigue performance of each mix at each cycle are compared in Figure 6.7. The number after each mix type in the legend of Figure 6.6 indicates the volumetric optimal asphalt content. For example, C5.6 is

the Control mix at the optimal asphalt content of 5.6%, and Ls5.3 is the Lsub mix at the optimal asphalt content of 5.3%.

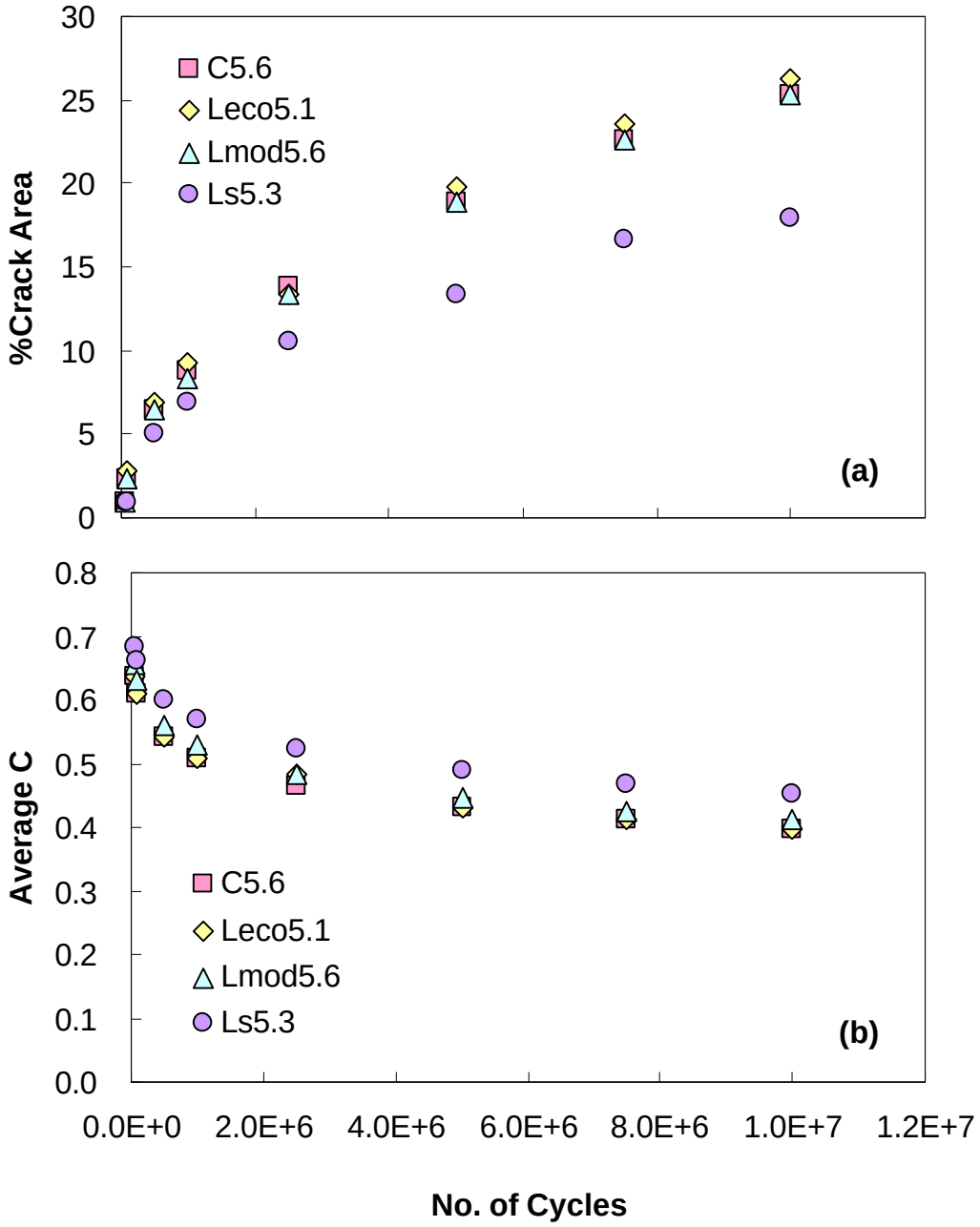

Figure 6.7 Overall comparison of the fatigue performance based on: (a) % Crack area: and (b) Average C

In both plots seen in Figures 6.7 (a) and (b), it can be clearly observed that the Lsub mix shows the most favorable fatigue performance from the early stages of the load cycles among the mixes. The Leco mix shows a higher value than the other mixes in the % Crack area plot, whereas the Control and Leco mixes show a lower average C in the Average C plot. However, clear observations regarding the ranking of mixes can be made by examining Figure 6.8. In this graph, the Lsub mix shows the same results as from visual observations in the damage contour plots and the overall comparison plots of the parameters; that is, the data points are lower in the % Crack area plots and higher in the Average C plots. Even though each mix other than the Lsub mix shows a slightly different ranking in each plot (for example, the Lmod mix has a slightly higher value than the Leco mix, and the Leco mix has an adverse result in the % Crack area plot), the differences are minimal among the Control, Leco, and Lmod mixes; thus, it is difficult to determine if these small differences are realistic. A comparison of the damage characteristic curves for the Lsub mix with those of the other mixes clearly shows that the Lsub mix offers the most favorable damage characteristics, whereas the damage characteristics of the other mixes are about the same. This observation is also supported by the statistical analysis results shown in Table 6.5.

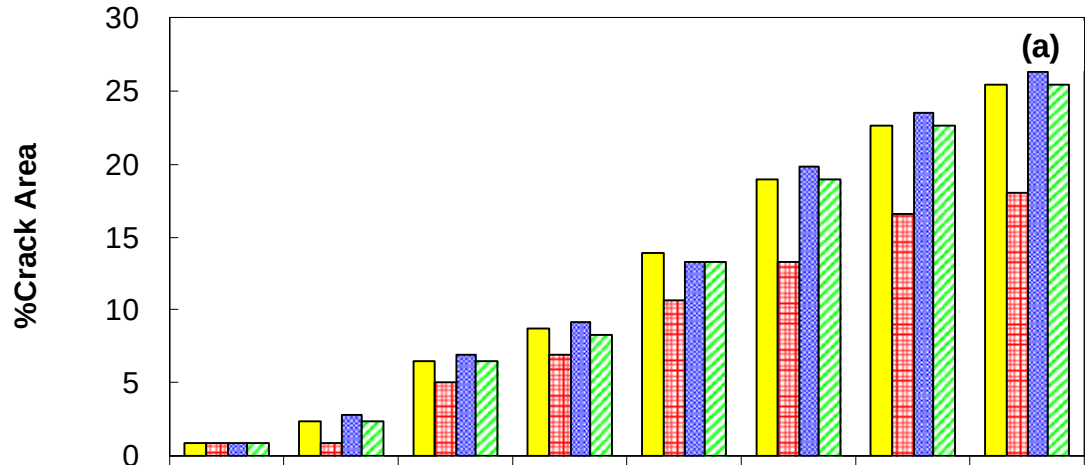

	5.E+04	1.E+05	5.E+05	1.E+06	3.E+06	5.E+06	8.E+06	1.E+07
C5.6	0.92	2.30	6.45	8.76	13.82	18.89	22.58	25.35
Ls5.3	0.92	0.92	5.07	6.91	10.60	13.36	16.59	17.97
Leco5.1	0.92	2.76	6.91	9.22	13.36	19.82	23.50	26.27
Lmod5.6	0.92	2.30	6.45	8.29	13.36	18.89	22.58	25.35

No. of Cycles

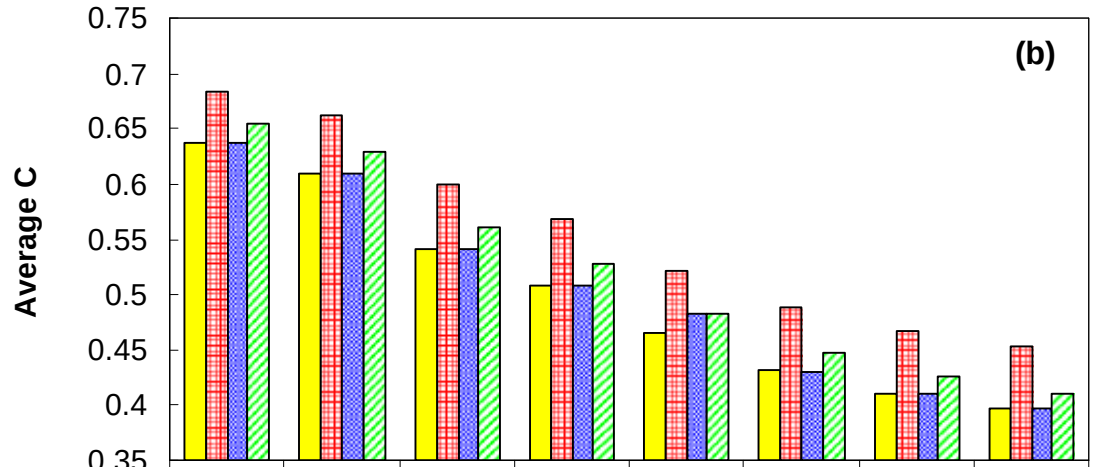

	5.E+04	1.E+05	5.E+05	1.E+06	3.E+06	5.E+06	8.E+06	1.E+07
C5.6	0.64	0.61	0.54	0.51	0.47	0.43	0.41	0.40
Ls5.3	0.68	0.66	0.60	0.57	0.52	0.49	0.47	0.45
Leco5.1	0.64	0.61	0.54	0.51	0.48	0.43	0.41	0.40
Lmod5.6	0.66	0.63	0.56	0.53	0.48	0.45	0.43	0.41

No. of Cycles

Figure 6.8 Discrete comparison of fatigue performance based on (a) % Crack area and (b) Average C at various cycle stages

Based on the observations of the damage contour plots and parameters, the ranking of the lime modification methods can be determined. The ranking obtained by these observations is given below.

Table 6.6 Ranking of Various Lime Introduction Methods

Ranking	Damage contour	% Crack area	Average C
Contol	3	2	3
Lsub	1	1	1
Leco	3	3	3
Lmod	2	2	2

The rankings shown in Table 6.6 indicate that the Lsub mix is the most favorable mixture with respect to fatigue performance. However, it should be noted that because VECD-FEP++ is implemented with the VECD model, which is related to the E* and damage characteristics of the materials, the VECD-FEP++ results can be determined by these properties. If similar |E*| behaviors for the various materials are observed, then the simulation results can be determined based on the results of the damage characteristic curves. Under such conditions, i.e., similar results of the |E*| for all four mixes, then the damage contour and simulation parameters (% Crack area and Average C) appear to parallel the results of the damage characteristic curves.

6.5 Summary and Conclusions

Task 2 is presented in this chapter to study multiple techniques for introducing lime into asphalt concrete mixtures. A single mix type is examined and three different lime introduction techniques are evaluated. For each of the methods the optimum volumetric asphalt content is found and the performance is assessed via |E*| tests, TRLPD tests, characterization tests for the VECD model; and the field responses are obtained by the cyclic fatigue simulation of VECD-FEP++ on the pavement.

Through this investigation it is found that different introduction techniques show varying levels of performance enhancement, from negligible to major. Such findings support the need for laboratory performance assessment and careful consideration of the technique used to introduce hydrated lime into asphalt concrete mixtures. Of the mixtures studied herein, the substitution of existing mineral filler with hydrated lime (Lsub) results in the most favorable performance characteristics. The specific observations leading to this conclusion are:

- Increased |E*| in the high reduced frequency range (high temperature or low frequency);
- Accumulation of less permanent strain in the TRLPD tests;
- Increased resistance to tensile damage growth from the VECD characterization; and
- The most favorable fatigue performance based on the ranking study via VECD-FEP++ simulation.

Chapter 7

Evaluation of the Effects of Hydrated Lime on Moisture Damage

7.1 Introduction

Moisture damage can occur when the bond between asphalt cement and aggregate breaks down due to the presence of moisture on the interface of the asphalt-aggregate system, thus causing the binder to separate from the aggregate surface. This failure causes loss of strength, stiffness and durability in an asphalt mixture. Usually moisture damage is considered as a premature failure, and often occurs within a few years after construction.

Loss of adhesion and moisture damage occur together. While loss of adhesion causes a serious moisture damage problem, a different type of moisture damage may also occur more slowly. In such a case, stripping may not be obvious, but the integrity of the mix performance, which relates to the resistance to fatigue cracking and rutting, is gradually diminished by moisture. The former case is directly related to the physico-chemical properties of the material (i.e., internal factors) and the latter relates to external factors, such as heat, heavy rains, F-T cycles, and traffic-induced premature stripping, that affect the in-place properties

of HMA pavements. Most research has focused on the first type of failure, and less attention has been given to the second case.

When lime is added to HMA, it reacts with the aggregates, strengthening the bond between the bitumen and the aggregate. At the same time that it treats the aggregate, lime also reacts with the asphalt itself to form insoluble salts that no longer attract water (Petersen et al. 1987). However, out of the many various test procedures – such as the boiling test, tensile strength ratio (TSR) test, Lottman test, and modified Lottman test that have been developed to evaluate HMA moisture susceptibility in the laboratory – none has been found to accurately predict the magnitude of moisture damage in different asphalt mixtures in the field. Due to several disadvantages related to the empirical nature of these test methods, the conditioning procedures in these tests generally do not adequately simulate the actual field conditions. These tests are used to screen mixes and to prevent premature failure. Therefore, it is necessary to examine moisture sensitivity using pavement performance-based tests incorporated into a rational conditioning procedure to better represent the field performance of mixes by considering both internal factors and external factors.

The primary objective of the work presented in this Chapter 7 is to evaluate the effects of lime modification on performance properties with regard to moisture damage by comparing the results from both a dry (nonmoisture-conditioned) state and a moisture-conditioned state. First, the test procedure is determined. Then, a comparison study is conducted to compare the results of the performance properties against the moisture damage of the lime-modified mixtures and the unmodified mixture, as per the determined test procedure.

7.2 Experimental Program

The experimental program for this task involves the evaluation of the effects of lime modification on moisture damage that is induced by multiple F-T cycling conditions. Based on the performance properties discussed in Task 2, a lime substitution mixture (Lsub) is selected as the most favorable lime-modified mixture among four different lime introduction methods. In order to evaluate the performance properties of the Lsub mixture and the unmodified (Control) mixture at the optimal volumetric asphalt content, the same SPTs discussed in Chapter 6, such as the |E*| test, TRLPD test, and constant crosshead strain rate test, were performed. In addition, the performance of the pavement in the field was simulated using VECD-FEP++ as a tool.

7.2.1 Sample preparation

The air voids for the test specimens were 4% ± 0.5%. F-T conditioning was conducted in accordance with AASHTO T-283 for three multiple cycles. Due to the constraint of material availability, the TRLPD test was conducted on the same specimens that were used for the |E*| test. That is, after allowing the specimen to restabilize after the |E*| test, the TRLPD test was performed. Because the |E*| test is nondestructive, the TRLPD test could be performed on the same sample. However, experience has shown that at higher temperatures some creeping may occur, even though it is known that the |E*| is the response of material behavior within the LVE range.

7.2.2 Moisture conditioning process

The purpose of the moisture conditioning process is to introduce a certain amount of moisture damage in the specimen prior to fatigue testing (Quing and Harvey 2007). They performed a sensitivity test with various combinations of parameters to determine a moisture conditioning process. Three primary parameters were determined for the preconditioning process: moisture content (or saturation level), conditioning temperature, and conditioning duration. Of these three parameters, the conditioning temperature has the most significant effect on the moisture resistance of asphalt mixes; it is followed, in order of the effect on moisture resistance, by the conditioning duration and then the moisture content (Quing and Harvey 2007).

Provided that the multiple cycles of F-T conditioning, according to the AASHTO T-283, are incorporated into the moisture preconditioning process with its determined parameters, a more realistic and worst-case field condition regarding the moisture damage of asphalt mixtures may be obtained. Because the testing methods are different from those in AASHTO T-283, it was necessary to adjust the conditioning procedures related to saturation level and postconditioning temperature.

It is generally believed that the higher the air voids, the higher the permeability and, thus, the more water can penetrate an asphalt pavement. That is, the permeability of asphalt mixtures is proportional to air void content when the property and structure of the aggregate is similar (Saleh et al. 1992). In this study, all the mixtures consisted of the same aggregate and had lower air voids (4%) than those used for TSR testing (7%). It took three times longer than the maximum 10 minutes specified in the AASHTO T-283 to obtain a certain level of

saturation for premoisture conditioning. Next, the saturated specimens (preconditioned specimens) were subjected to three multiple F-T cycles consisting of freezing at 0°F for 24 hours followed by thawing at 140°F for 24 hours. The conditioned specimens were then subjected to stabilization for 2 hours at 77°F in a water bath, not for purposes of the AASHTO T-283 TSR test, but rather to minimize the possibility of creep by the weight of the specimens. In order to minimize the effects of saturation, all the conditioned specimens were dried to a certain level of saturation by a core dryer instrument. Because the setup for the constant crosshead strain rate test takes 18 hours, the specimens were wrapped with parafilm to avoid moisture evaporation until the setup was complete. The test saturation level (postconditioning) was determined based on the testing setup time. At the time of testing, the samples retained a saturation level of about 33% to 38%. The saturation levels for preconditioning and postconditioning are shown in Table 7.1. Note: *Preconditioning* refers to the level of moisture saturation of specimens before the F-T cycling conditioning, and *postconditioning* refers to the level of saturation of the F-T-conditioned specimen prior to testing.

Table 7.1 The Level of Saturation for the Moisture Conditioning Process

		Saturation Level (%)			
Test Type	Mix	Control		Lsub	
	Stage	Preconditioning	Postconditioning	Preconditioning	Postconditioning
Dynamic modulus test	1	56.0	33.3	56.7	38.4
	2	60.2	34.8	57.6	38.0
	3	58.3	37.3	54.2	37.9
	Avg.	58.2	35.1	56.2	38.1
DT test	1	59.1	33.7	59.5	37.1
	2	58.3	35.7	60.1	36.6
	3	58.6	35.6	60.3	38.0
	Avg.	58.7	35.0	60.0	37.2

7.3 Results of Performance Tests and Statistical Analysis

7.3.1 Dynamic modulus test

In this section, three replicates were tested for unmodified (Control) and lime-modified (Lsub) mixes using the moisture conditioning process that includes three F-T cycles; the results are plotted against reduced frequency after shifting the data. The reference temperature that was used as the basis for shifting the data is 10°C. Figure 7.1 and Figure 7.2 represent the |E*| mastercurves and phase angle of the three replicates, respectively.

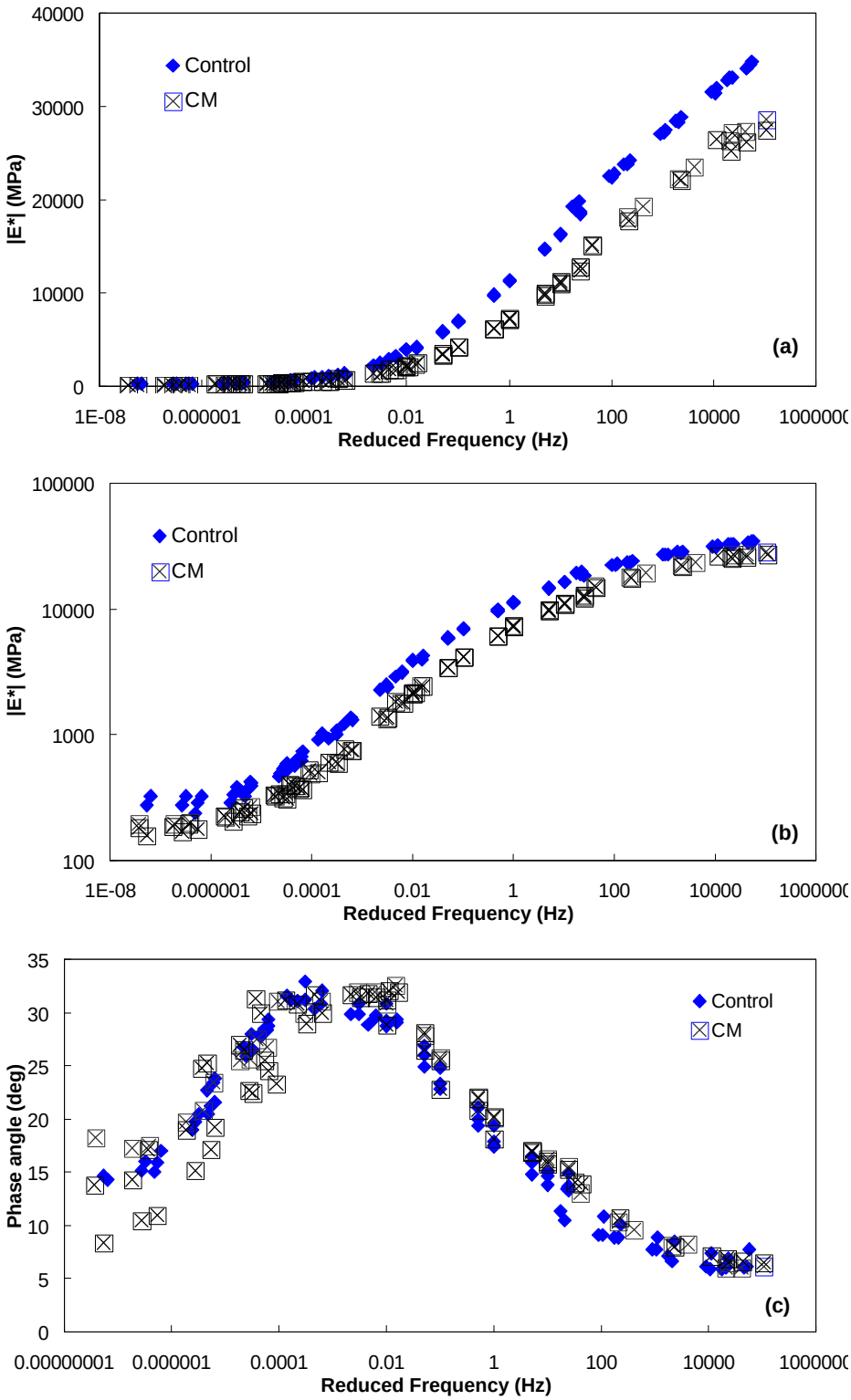

Figure 7.1 Dynamic modulus mastercurves for the Control mixture with conditioning in: (a) semi-log space; (b) log-log space; and (c) the phase angle

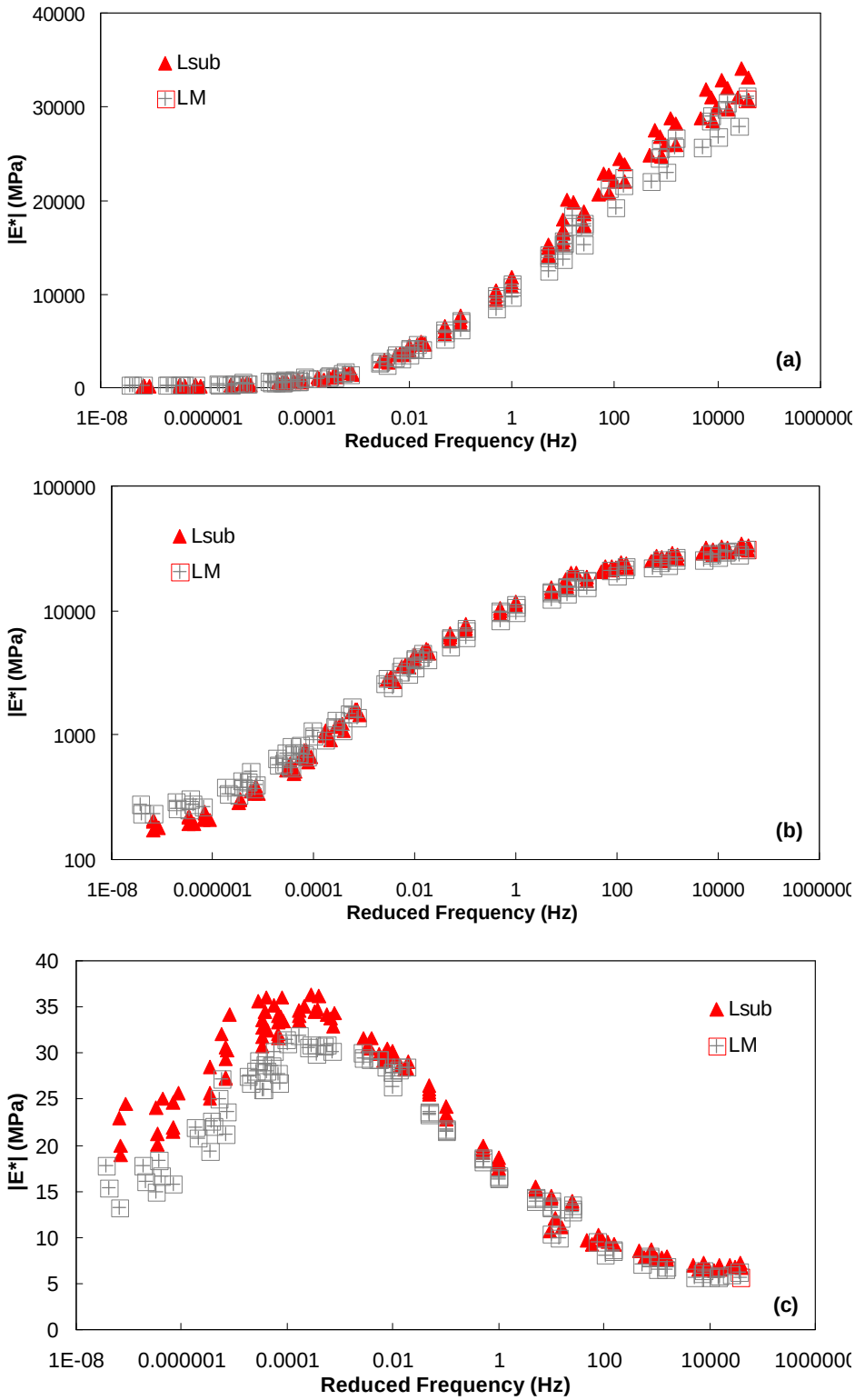

Figure 7.2 Dynamic modulus mastercurves for the Lsub mixture with conditioning in: (a) semi-log space; (b) log-log space; and (c) the phase angle

Data are presented in both semi-log and log-log scales. Both scales are presented to show both the low temperature (semi-log) and high temperature (log-log) behaviors. In both Figure 7.1 and 7.2, filled symbols are used to present the dynamic moduli values of the unconditioned mixes, and x and cross symbols are used for the moisture-conditioned mixes.

In the Control mix, depicted in Figure 7.1, the unconditioned mix shows higher stiffness than the moisture-conditioned mix, and shows similar phase angle behavior at overall reduced frequencies, as can be seen by observing the mastercurves. Based on other studies on the effects of moisture damage on stiffness reduction, the reduction of stiffness by moisture conditioning can be expected. This effect of moisture conditioning is due to the disintegration of bonding in the aggregate and binder system by the intrusion of moisture with severe changes in temperature via F-T cycling.

In the case of the lime-modified mix, which is shown in Figure 7.2, the unconditioned mix shows higher stiffness at higher reduced frequencies and lower stiffness at lower reduced frequencies than the moisture-conditioned mix. In the intermediate frequencies, the two mixes are about the same. It can be seen that the phase angle is higher at overall reduced frequencies, which indicates that the lime-modified moisture-conditioned specimen shows more elastic behavior at overall reduced frequencies. Based on these results, it is interesting to note that the effect of lime modification is magnified in the presence of moisture, which is ordinarily considered to be a damaged state. However, this result could be related to specimen variability, as can be seen in the spread in the replicate mastercurves. Therefore, it was decided to perform statistical analysis of all the mixtures to resolve this issue.

T-tests at the significance level of a = 0.05 were conducted to assess the statistical significance of the results of the two groups. A hypothesis test was constructed with the following parameters:

Ho: μ1 – μ2 = 0 and

H1: μ1 – μ2 ? 0,

where μ1 is the mean |E*| at a given reduced frequency for the unconditioned mixture, and μ2 is the mean |E*| at the same reduced frequency for the moisture-conditioned mixtures. Because each test did not have the same reduced frequency, comparisons were made by using interpolated data at specific reduced frequencies (24000 Hz, 1400 Hz, 2 Hz, 0.03 Hz, 0.0001 Hz, and 0.00001 Hz). Results from the statistical analysis are summarized in Table 7.2. For convenience, the conditions where the p-value is lower than 0.05 are denoted with darkened cells for both the unmodified and lime-modified mixes; these low p-values indicate that the dynamic moduli of the unconditioned mixtures exhibit higher values than those of moisture-conditioned mixtures.

The amount of modulus reduction by moisture conditioning and unconditioning in the lime-modified mixes is presented in Table 7.2.

Table 7.2 Results of Statistical Analysis and Dynamic Modulus Ratio (DMR) with the Moisture Damage at Various Reduced Frequencies

Reduced Frequency (Hz)	Control		Lsub	
	p-value	DMR (%)	p-value	DMR (%)
24000	0.000499	81.25	0.255871	92.65
1400	0.003037	76.36	0.129778	92.54
2	0.000001	66.46	0.139443	94.36
0.03	0.000004	59.04	0.238689	97.28
0.0001	0.000023	56.43	0.081158	119.87
0.00001	0.000589	66.94	0.012056	131.17

The null hypothesis for the Control mixture was consistently rejected over all given reduced frequencies. The dynamic modulus ratio (DMR), which is the ratio of the |E*| for the conditioning and for the unconditioning at a given reduced frequency, decreases as the reduced frequency decreases. In other words, the moisture damage increases significantly as the temperature becomes higher.

Although the statistical analysis for the Lsub mixtures shows that the mixtures do not differ significantly in terms of the moisture conditioning process except at the lowest reduced frequency (0.00001 Hz), the DMR presents the opposite result from the Control mixture. That is, as the reduced frequency increases, the |E*| of the conditioned specimens increases. In other words, the effect of lime modification on the |E*| appears to make the mixtures less susceptible to moisture damage as the temperature increases. The |E*| test seems to increase the likelihood of sample-to-sample variation at high testing temperatures and lower loading frequencies. Indeed, the moisture-conditioned samples may experience a larger variability from the conditioning process itself. Thus, even though the DMR is higher than 100% at the lowest reduced frequency, it is difficult to say that the effect of lime modification causes a higher increase in the stiffness of the moisture-damaged mixture than that of the undamaged mixture. Therefore, an assessment of these mixtures' behavioral trends is needed to explain these results. Based on the trend observed in the DMR plot in Figure 7.3, the Control mixture shows a decreasing trend of the DMR as a function of reduced frequency, whereas the lime-modified mixture shows the opposite. Because water is itself a highly polar material, it will react with the polar molecules in the asphalt binder, resulting in softening. Even the aggregate's affinity for water aids the bonding failure between the aggregate and the asphalt

binder. This adverse effect of water damage may cause the reduction of the DMR. However, the addition of lime strengthens the bond between the asphalt binder and the aggregate system by its reaction with the highly polar molecules in the asphalt binder so that the system no longer attracts water (Petersen et al. 1987). Indeed, the reaction in the asphalt binder reduces the sensitivity of the asphalt binder at a low temperature, thus improving the low temperature flow properties (Petersen et al. 1987, Hoffman et al. 1998, Little et al. 2005). These studies may support the trends seen in the DMR plots in Figure 7.3. In other words, the reduced sensitivity of the asphalt binder at the lower temperatures and the increasing stiffness at high temperatures caused by the lime modification can also hold for the DMR trend for the Lsub mixture, and the Control mixture's continuous drop in DMR at overall frequencies can be explained by the moisture damage.

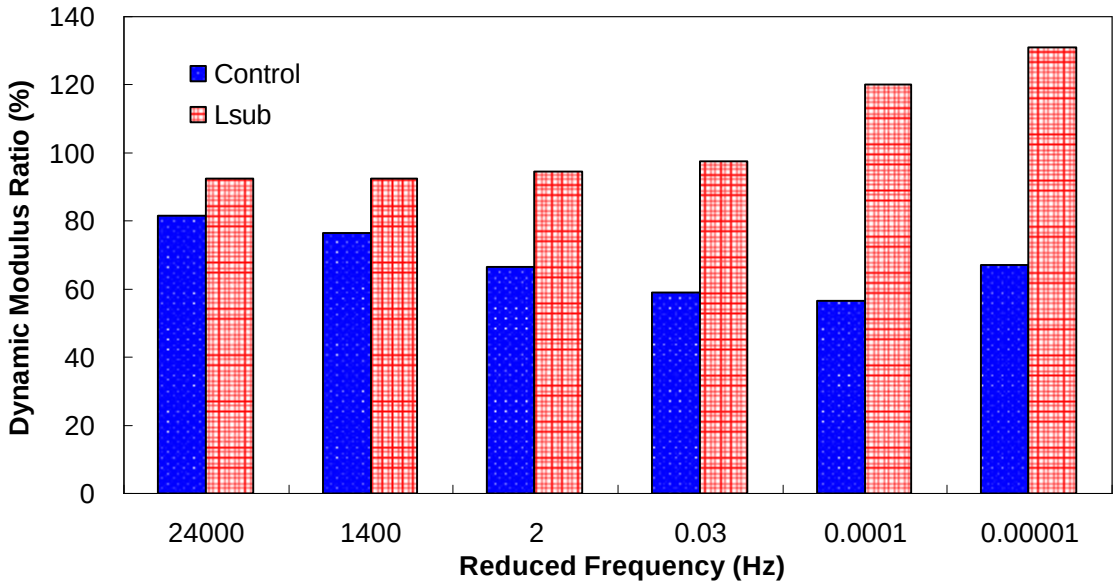

Figure 7.3 Dynamic modulus ratio (DMR) as a function of reduced frequency

7.3.2 TRLPD test results

For the mixtures in this study, the TRLPD tests were carried out in the same manner as described in Chapter 6. None of the mixtures exhibited tertiary flow. However, differences in material performance related to moisture damage can be captured by examining the permanent strain growth over the 10,000 test cycles. Such permanent strain growth is presented in the plots shown in Figure 7.4 using an arithmetic scale and in Figure 7.5 using the log scale. It should be noted that due to the lack of available materials, the TRLPD tests were conducted on the same specimens as used for the |E*| tests. Even though the specimens were allowed to restabilize, a certain level of densification occurred. This outcome may affect the initial stage of permanent deformation because of the sensitivity of this initial phase to the effects of air voids; that is, this initial phase is the phase during which the rate of accumulated permanent deformation stabilizes and becomes constant. Regardless of such predensification, the effect of the lime modification on the rutting performance of the Lsub mixture versus the moisture damage relative to the inferior performance of the Control mixture is obvious, as seen in Figure 7.4. The permanent strain in the initial phase can be seen in Figure 7.5. The initial permanent strain shows a much higher increase in the Control mixture than the Lsub mixture.

This observation is consistent with that from the DMR, which shows an overall decrease in stiffness for the moisture-damaged Control mixture and an increase in stiffness as a function of reduced frequency.

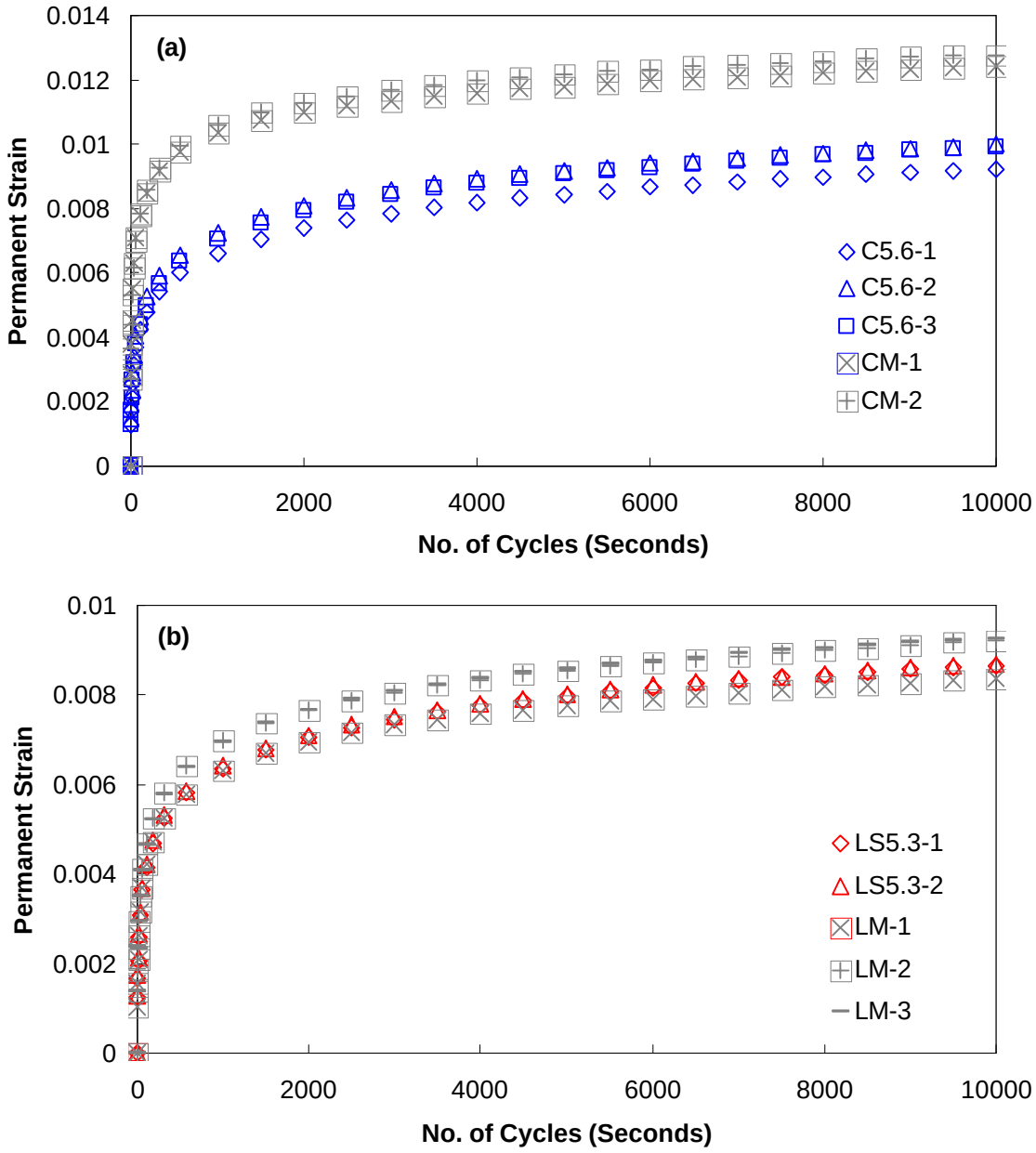

Figure 7.4 Permanent strain results with and without moisture conditioning for: (a) Control mixture; and (b) Lsub mixture in arithmetic scale

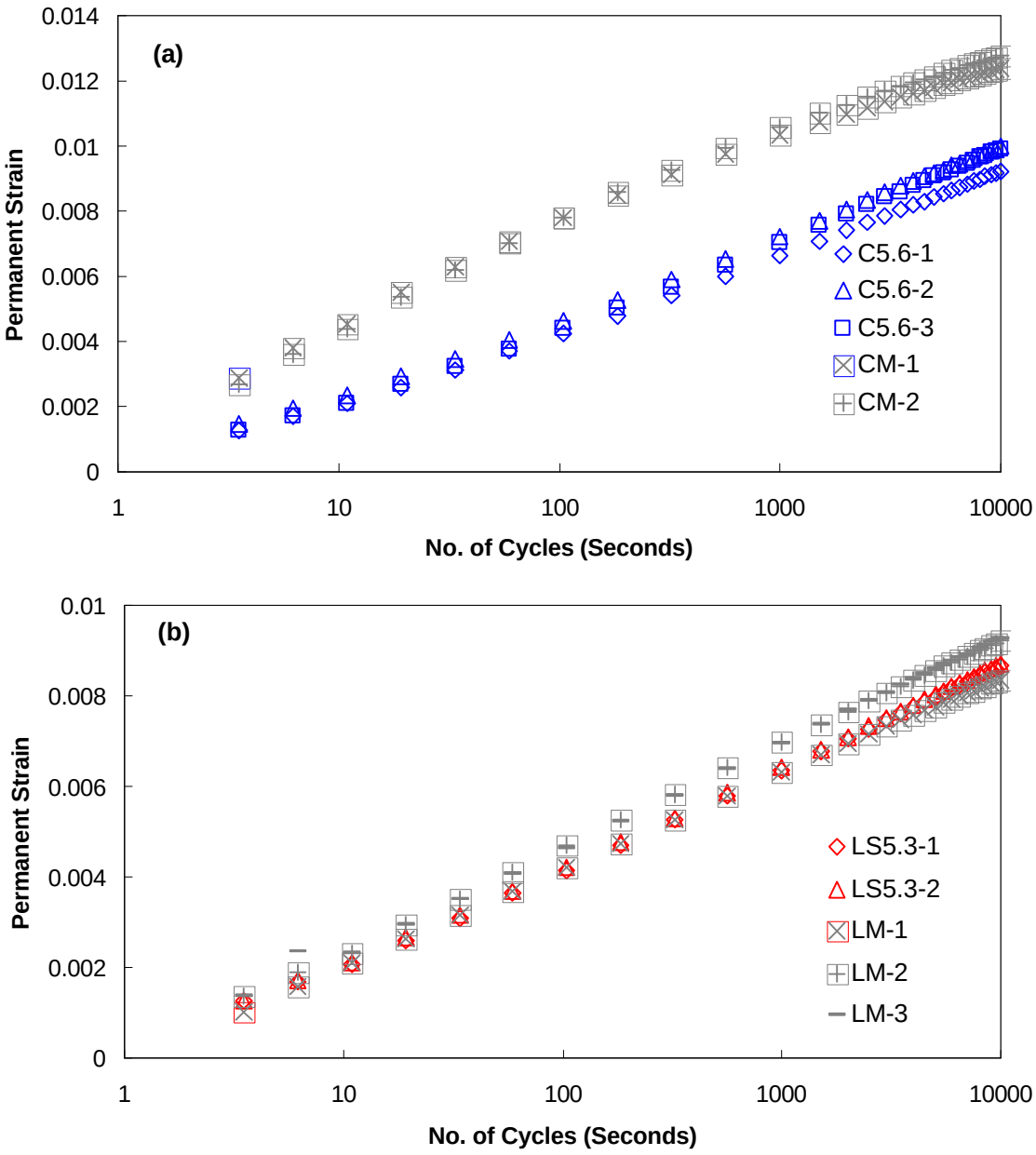

Figure 7.5 Permanent strain results with and without moisture conditioning for: (a) Control mixture; and (b) Lsub mixture in log scale

Also, statistical analysis was used to compare the differences of the moisture conditioning effects on the permanent deformation of the lime-modified mixtures. T-tests were conducted to assess the statistical significance of the results of the two groups. The t-

tests use the significance level of a = 0.05 at cycles (11, 59, 104, 184, 568, 1000, 2000, 3000, 5000, 7000, 10000) that cover the range of the permanent deformation and provide assessment of early, middle and late stage behavior. The results of this analysis are summarized in Table 7.3. The rejected conditions are marked with darkened cells. It is observed from this table that the null hypothesis for the Control mixture is rejected at all cycles, whereas that for the Lsub mixture is not rejected at any cycle. This finding indicates that the permanent deformation results of the conditioned Control mixture are statistically significantly different from those of the unconditioned control mixture. The reverse is true in the case of the Lsub mixture that shows no statistical difference between conditioning and unconditioning. These results suggest that moisture damage has less impact on the rutting performance of the lime-modified mixtures than on that of the Control mixture. The permanent strain ratio (PSR) of moisture-conditioned to unconditioned is summarized in Table 7.3 and also plotted in Figure 7.6.

Based on the PSR at the initial stage, the permanent deformation of the conditioned Control mixture is about 1.5 to 2.0 times higher than the unconditioned Control mixture, whereas the permanent deformation is 1.1 times higher in the Lsub mixture. The lower the PSR value, the better the rutting resistance to moisture damage.

Table 7.3 Statistical Analysis and Permanent Strain Ratio (PSR) with Moisture Damage at Various Numbers of Load Cycles

No. of Cycles	Control		Lsub	
	p-value	PSR	p-value	PSR
11	0.0002	2.0	0.0955	1.1
59	0.0001	1.8	0.0929	1.1
104	0.0001	1.8	0.0971	1.1
184	0.0001	1.7	0.1090	1.1
568	0.0003	1.6	0.1306	1.1
1000	0.0004	1.5	0.1453	1.1
2000	0.0007	1.4	0.1641	1.1
3000	0.0009	1.4	0.1860	1.0
5000	0.0012	1.3	0.2214	1.0
7000	0.0015	1.3	0.2480	1.0
10000	0.0002	1.3	0.2668	1.0

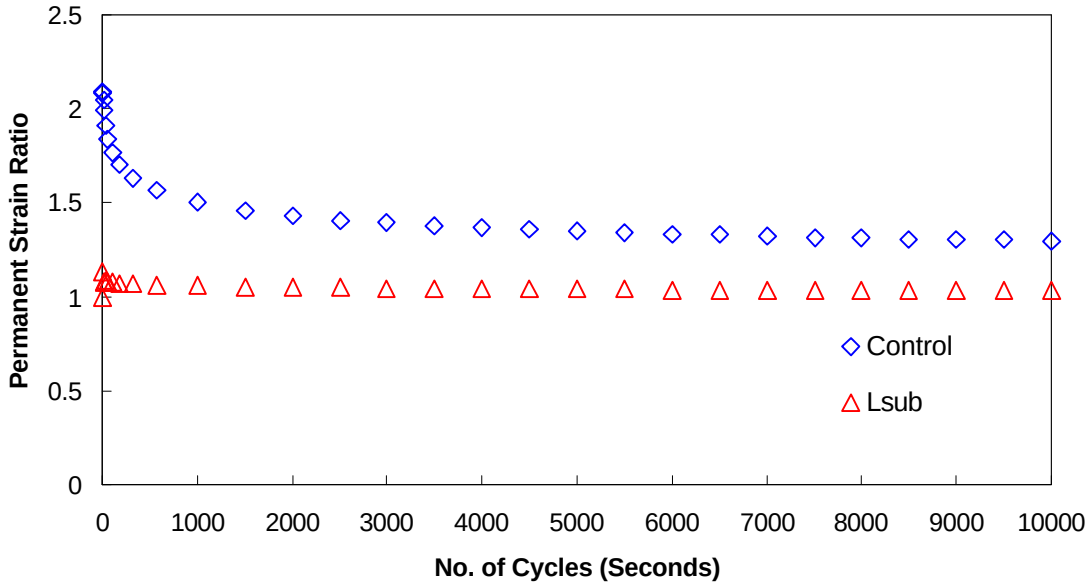

Figure 7.6 Permanent strain ratio between conditioning and unconditioning for the Control mixture and the Lsub mixture

It is interesting to note that while the Control mixture shows a relatively drastic decrease from 2.0 to 1.4 in PSR until the accumulated permanent strain rate becomes stabilized at around 2000 to 3000 cycles, the Lsub mixture shows quite a small decrease from

1.1 to 1.0 in PSR as a function of the number of cycles. These results support previous research with respect to the effect of lime on rutting resistance (Petersen et al. 1987, Little et al. 2005).

7.3.3 Constant monotonic crosshead strain rate tests and analysis

The same conditions for the crosshead strain rate and temperature as discussed in Chapter 6 were used to examine the viscoelastic damage characteristics of moisture damage on the lime-modified and unmodified mixtures. The damage characteristic curves for the tested mixtures are plotted together in Figure 7.7. Figure 7.7 (a) clearly shows the moisture conditioning effect on the damage characteristic curve of the Control mixture; this curve is positioned lower than that of the nonmoisture-damaged plot. From Figure 7.7 (b), no moisture damage is evident from the damage characteristic curve of the Lsub mixture. Instead, the damage characteristic curve is positioned slightly higher than that of the unconditioned mixture. However, to lend further credence to this conclusion, a statistical analysis similar to that performed for the comparison of the |E*| and permanent deformation of these mixtures was performed.

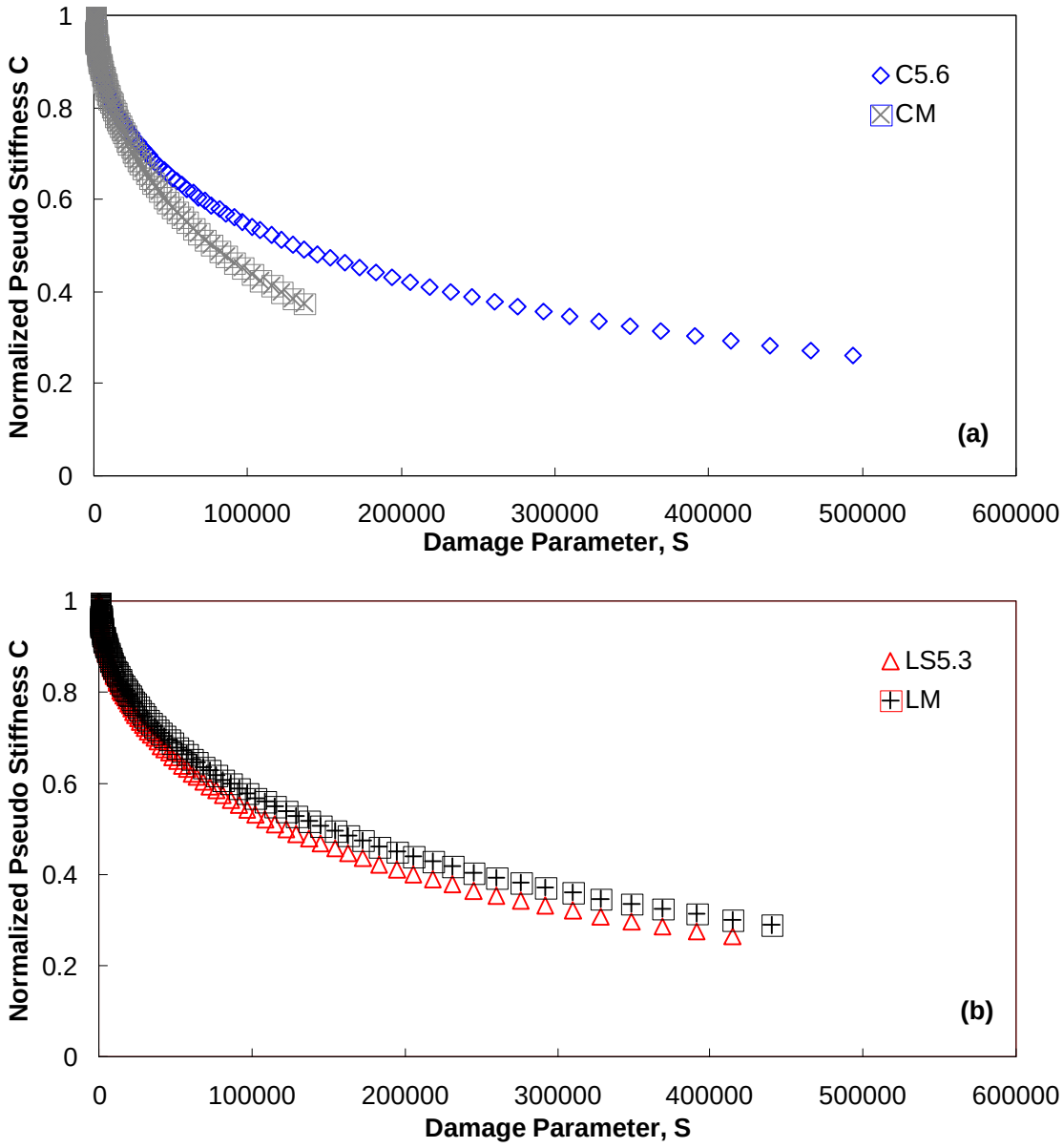

Figure 7.7 Effect of the moisture damage on the damage characteristic curves for the (a) Control mixture; and (b) Lsub mixture

The t-test results are summarized in Table 7.4. It is observed from this analysis that both moisture-damaged Control and Lsub mixtures show no significant difference from the nonmoisture-damaged mixture at the early damage stage. However, damage characteristic

curves start to deviate at 50,000 and 100,000, which are the S values of the Control and Lsub mixtures, respectively. The analysis suggests that the damage characteristic curves are statistically not the same for those ranges of S values where the null hypothesis is rejected. The Control mixture consistently shows lower pseudo stiffness than the nonmoisture-damaged mixture after a certain amount of damage develops, whereas the moisture-damaged Lsub mixture shows the higher pseudo stiffness after these conditions. These results suggest that moisture damage has less of an impact on the lime-modified mixture than on the Control mixture.

Table 7.4 Statistical Analysis and Damage Characteristic Ratio (DCR) with the Moisture Damage at Various Damage Levels

Damage Parameter, S	Control	Lsub
	p-value	p-value
250	0.238	0.274
500	0.273	0.255
1,500	0.361	0.220
4,000	0.494	0.183
10,000	0.319	0.145
20,000	0.168	0.113
50,000	0.043	0.071
100,000	0.012	0.043
150,000	0.005	0.030
200,000		0.023
250,000		0.018
300,000		0.015
400,000		0.011

In other words, the Control mixture is easier to damage by moisture than the Lsub mixture, which indicates that the effect of lime modification on fatigue performance is less susceptible to moisture damage. Based on other research (Petersen et al. 1987, Lesueur et al. 1999, Little et al. 2005), it is accepted that the dispersion of the tiny hydrated lime particles

can intercept the microcracks and make the mixture stiffer and tougher, thus reducing the possibility of the fatigue failure in the pavement. These studies also hold for the trends of the Lsub mixture. Care must be taken when examining the trends of the moisture-damaged mixtures because it is difficult to link the fracture properties to the continuum damage and the variability of the moisture conditioning process. From experience, little replicate variation exists normally, and tests at different rates collapse very well. However, the damage characteristic curves of the Lsub mixture have a larger variability than those of the Control mixture. Thus, the moisture-damaged characteristic curve for the Lsub mixture is the byproduct of averaging a larger amount of variability. Also, disregarding the effects of moisture on the fracture properties may affect the damage characteristic results.

7.3.4 VECD-FEP++ simulation results

The field response for the cyclic fatigue simulation is predicted to evaluate the effect of lime modification on fatigue resistance to moisture damage. The simulations were performed under the same conditions as presented in Chapter 6.

The damage contours of the moisture-damaged and nonmoisture-damaged mixtures are compared and depicted in Figure 7.8. Similar to the discussion of the simulation results found in Chapter 6, it is clearly observed that as the number of cycles increases, all the mixtures tend to spread damage over the pavement. Again, the damage zone develops from the bottom to the middle of the layer. The area of the lower damage zone in the moisture-damaged Control mix is larger than that of the nonmoisture-damaged one at overall load cycles, whereas the lower damage zone of the Lsub mixture shows the opposite. Indeed, the lower

damage zone of the Control mix develops first in the moisture-damaged condition, whereas the Lsub mixture's damage zone develops first in the nonmoisture-damaged condition.

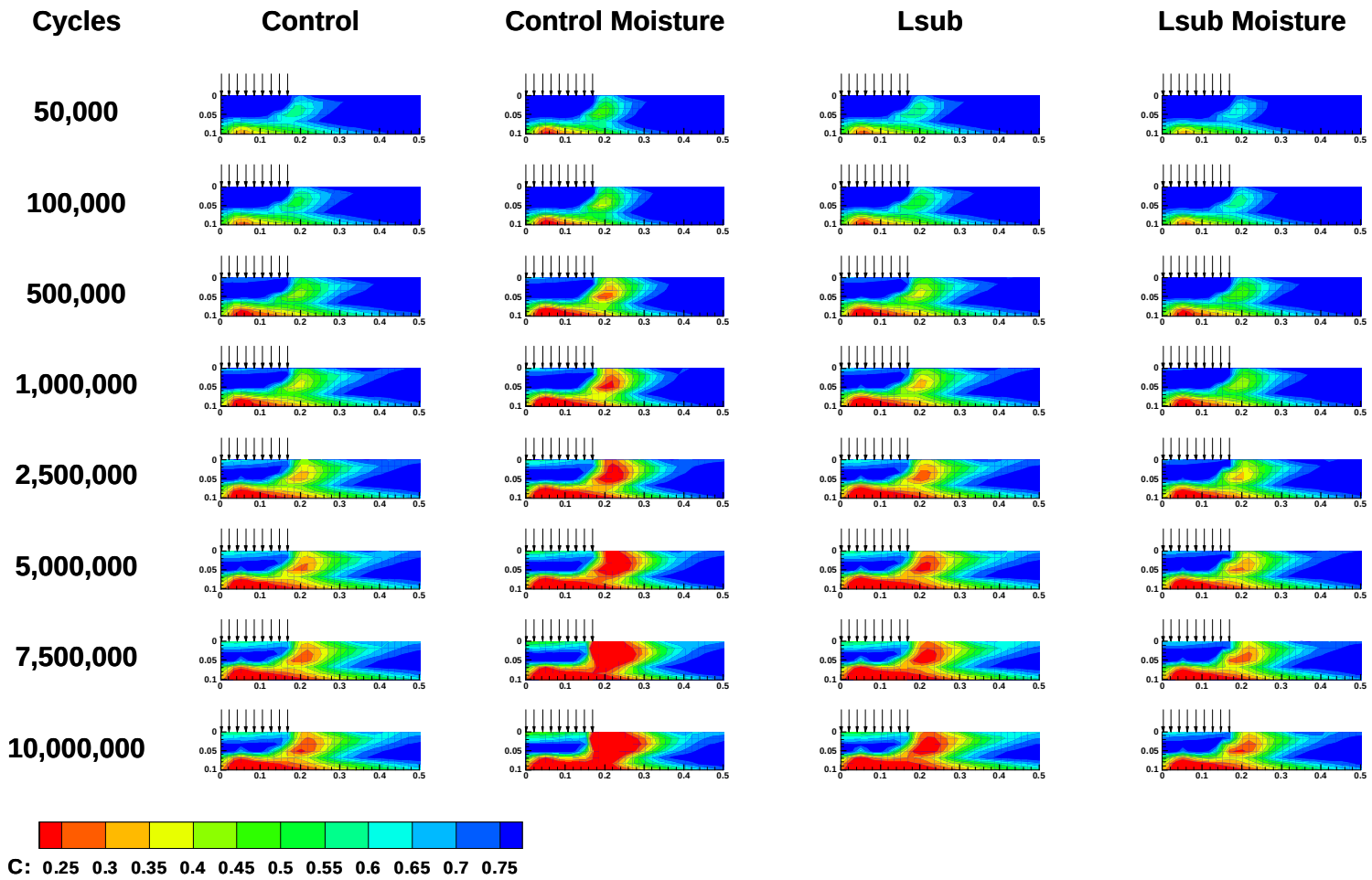

Figure 7.8 Comparison of the damage contour plots at various load cycles with and without moisture damage

When the number of cycles is applied up to the final stage of the load cycle to 10,000,000, the upper damage zone begins to develop in the nonmoisture-damaged Control mixture, whereas the moisture-damaged mixture reaches the upper damage zone at the 1,000,000 cycle. The upper damage zone in the moisture-damaged control mixture is fully developed through the depth of the layer at 7,500,000 cycles. Even at the final stage of the load cycle, the nonmoisture-damaged control mixture still is not fully damaged through the layer. Based on these observations, it is evident that severe moisture damage affects the fatigue performance of the Control mixture.

On the other hand, the upper damage zone in the nonmoisture-damaged Lsub mixture develops at the final stage of the load cycle, whereas the upper damage zone in the moisture-damaged mixture develops at 5,000,000 cycles. In order to evaluate the effects of moisture damage on performance more closely, it was again decided to examine the % Crack area and the Average C of those mixtures at the same cycles that were used for the contour plots. At the same time, the ratio of each % Crack area and Average C was examined to quantify the effect of moisture damage on lime-modified and unmodified mixtures. These results for the Control and Lsub mixtures are presented in Figure 7.9 and Figure 7.10, respectively. As described in Chapter 6, the % Crack area and Average C can be considered as the areas of damage localization and the overall status of the damage propagation in the pavement, respectively.

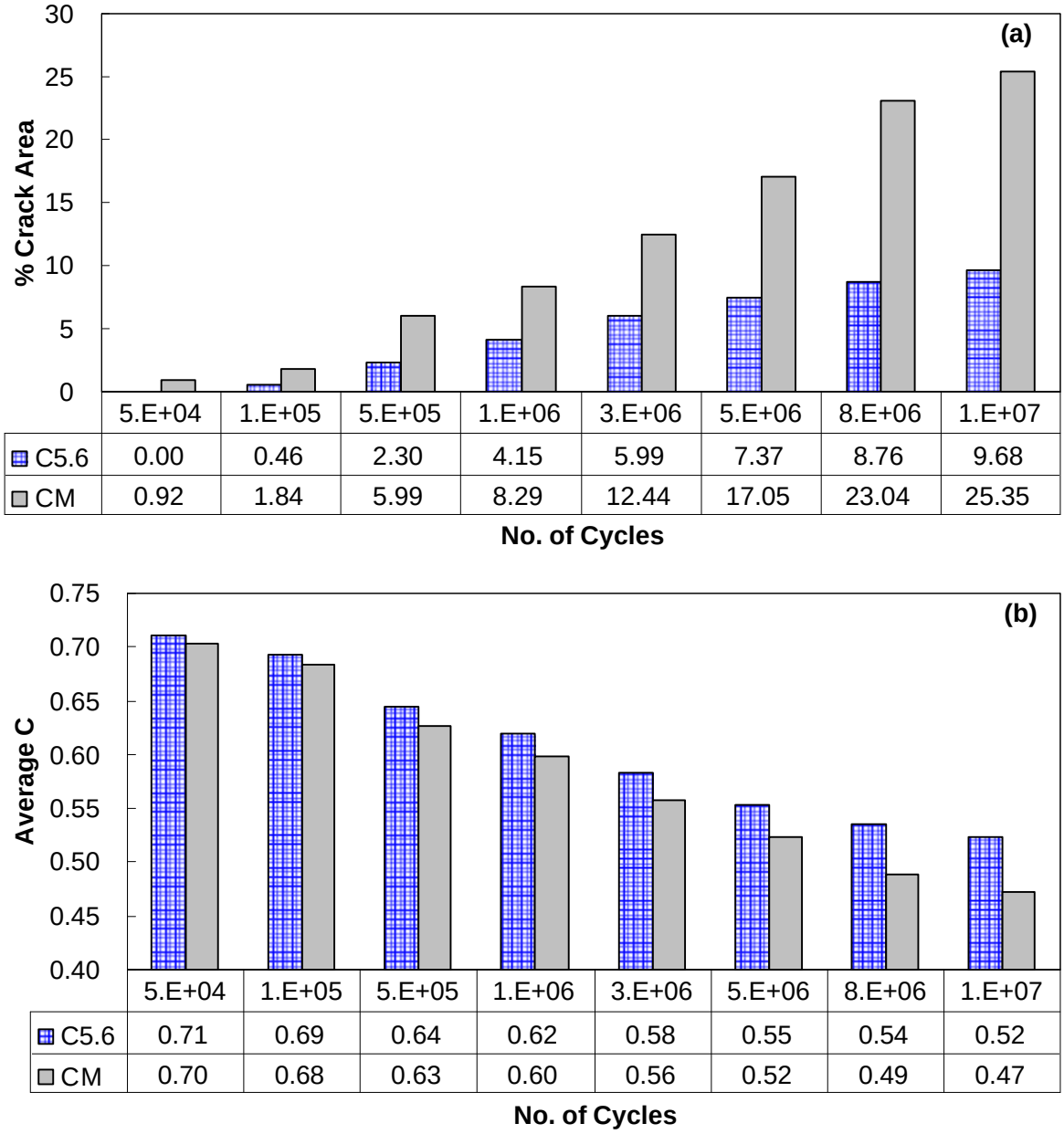

Figure 7.9 Discrete comparison of fatigue performance of the Control mixture with and without moisture damage based on: (a) % Crack area; and (b) Average C at various cycle stages

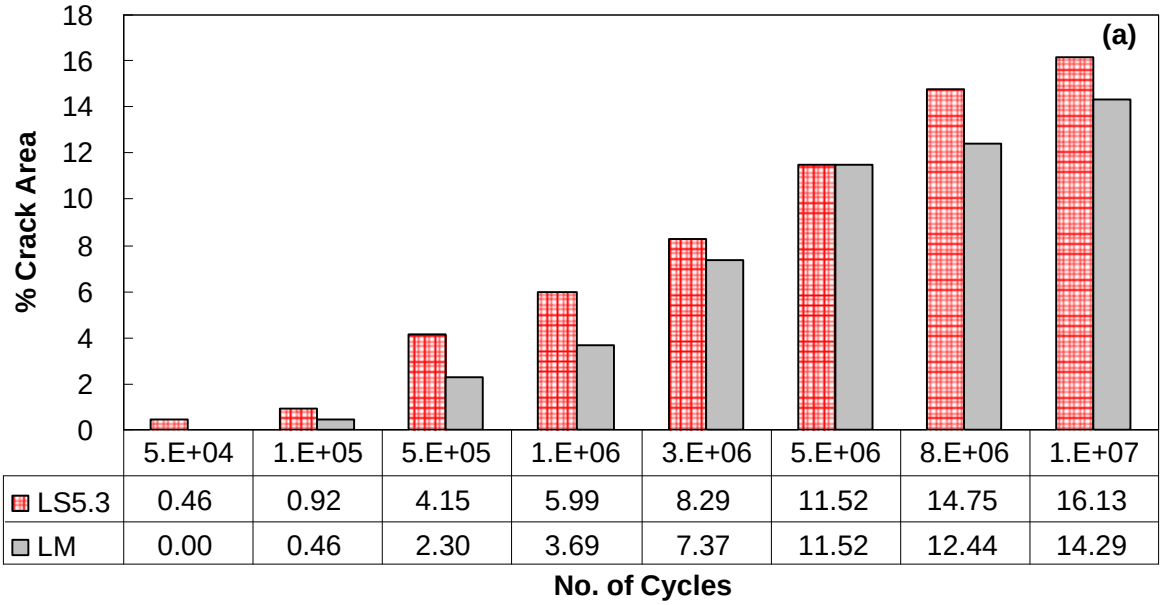

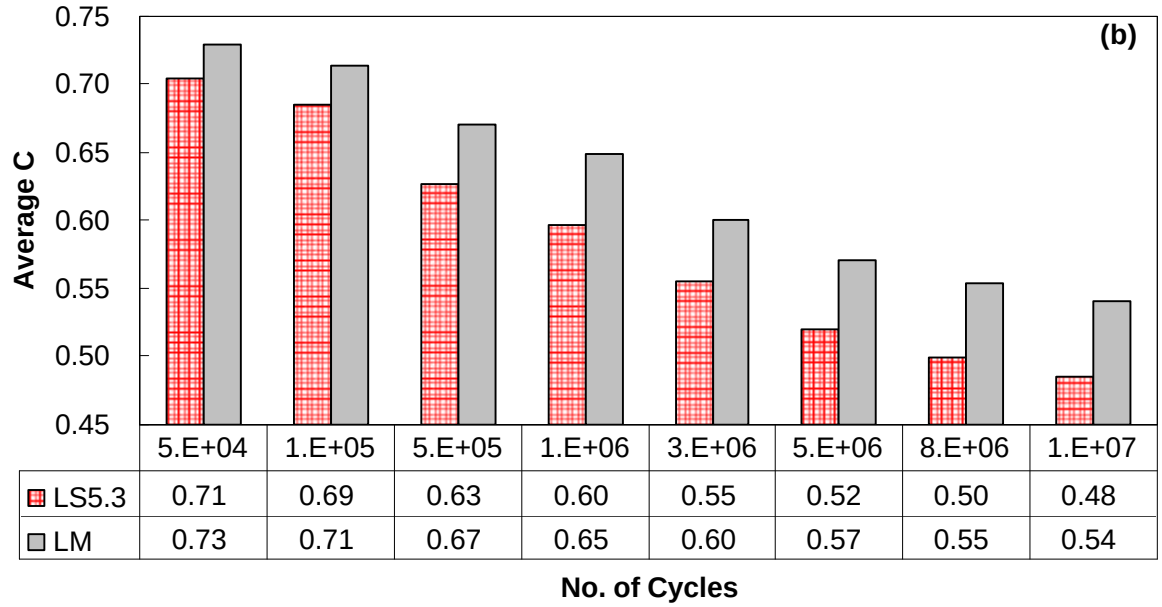

Figure 7.10 Discrete comparison of fatigue performance of the Lsub mixture with and without moisture damage based on: (a) % Crack area; and (b) Average C at various cycle stages

In both Figure 7.9 and 7.10, clear trends are seen in the increase of the % Crack area and decrease in the Average C, both as a function of load cycles. The magnitude of change in the % Crack area and the Average C caused by moisture damage can also indicate the fatigue

performance of the mixture against the effects of moisture damage. In Figure 7.9, it can be clearly observed that moisture damage has an effect on the fatigue performance for the overall stages of the load cycles. That is, as the number of load cycles increases, the deterioration rate of the material integrity in the pavement due to moisture damage shows a greater increase in the Control mixture than the Lsub mixture. This observation is consistent with the results of previous damage characteristics comparisons.

7.4 Summary and Conclusions

A laboratory study has been conducted to evaluate the effect of lime modification on performance properties' resistance to moisture damage by comparing the results both at a dry (nonmoisture) state and at the moisture-conditioned state in HMA mixtures. This evaluation uses |E*| tests, TRLPD tests, and characterization tests for the VECD model that combine multiple F-T conditioning cycles. The field responses are obtained by the cyclic fatigue simulation of VECD-FEP++ on the pavement. Based on the laboratory experiments and analyses, the following conclusions may be drawn:

- The effect of lime modification on the |E*| makes a mixture less susceptible to moisture damage as the temperature increases; this observation is also supported by the increasing trend of the Lsub mixture and the decreasing trend of the Control mixture in the DMR at overall frequencies.
- Moisture damage has less impact on the rutting performance of the Lsub mixture than that of the Control mixture, based on less permanent strain accumulation, as found from TRLPD testing.

- The effect of lime modification on fatigue performance makes a mixture less susceptible to moisture damage based on the VECD characterization results.
- The results of the VECD-FEP++ simulations suggest that the effects of lime modification on fatigue performance make a mixture less susceptible to moisture damage.

Chapter 8

Performance-based Evaluation of Lime-modified Hot Mix Asphalt Mixtures

8.1 Introduction

The primary objective of this study is to evaluate the performance of the lime-modified mixture at the asphalt contents that exhibit the most favorable characteristics, as identified in Task 2; the identified lime-modified mixture is the Lsub mixture. For comparison, the unmodified mixture is also evaluated. The asphalt contents examined vary from -0.5% to +1.0% of the volumetric optimum of the Superpave mix design. To evaluate the mixture performance, the same performance tests were conducted as were performed in Task 2. Further, performance-based mix design methodology with the favorable lime introduction method and without lime modification is suggested.

8.2 Experimental Program

The volumetric mix design results for both lime-modified and unmodified mixtures are presented in Table 6.1, and the aggregate gradation information is given in Table 6.2. Based on the mix design results of Chapter 6, test samples were fabricated in the same manner outlined in Chapters 6 and 7 at four different asphalt contents and maintaining the same aggregate structure. The volumetric optimum asphalt contents of the Lsub and the Control mixtures are 5.3% and 5.6% by the weight of the total mixture, respectively. For the Lsub mixture, the asphalt contents examined are 4.8%, 5.3%. 5.8%, and 6.3% and asphalt contents of 5.1%, 5.6%, 6.1%, and 6.6% were examined for the Control mixture. For convenience, these mixtures with different asphalt contents are referred to as the name of the mixture followed by the asphalt content. For example, the lime-modified mixture with 4.8% asphalt content is Lsub4.8, and the unmodified mixture with 6.6% asphalt content is C6.6. For the experimental side, the same approach described in previous chapters 6 and 7 for the test methods and statistical analyses are employed to evaluate the performance of the Lsub and the Control mixtures.

8.3 Results of Performance Tests and Statistical Analysis

8.3.1 Dynamic modulus test results

The dynamic modulus tests results are presented in the form of mastercurves for the Lsub and the Control mixtures in Figure 8.1 and Figure 8.2, respectively. From Figure 8.1 and Figure 8.2, it seems that the dynamic moduli of the mixtures are affected by the asphalt

content. A general trend for the dynamic modulus curves as a function of asphalt content is that the dynamic modulus is lower over the range of reduced frequencies as the asphalt content increases. The Lsub4.8 mix shows a consistently higher dynamic modulus at each reduced frequency and is followed, in order, by Lsub5.3, Lsub5.8, and Lsub6.3, as seen in Figure 8.1 (a). In the log-log scale plot, in the relatively lower reduced frequency region, the ranking of the mixtures by asphalt content is less clear with the exception of the Lsub4.8 mix, which remains the stiffest. The observation on the phase angle is that the Lsub4.8 curve has the lowest |E*| values at reduced frequencies greater than 0.0001Hz, indicating that the lowest asphalt content mix is more elastic. This finding is consistent with the dynamic modulus results. The more asphalt content present, the more plastic the material and, consequently, the greater the phase angle. However, the phase angles of all the mixtures begin to decrease with the unclear order of the ranking after showing the peak region of the phase angle, as the reduced frequency continuously decreases. Because the material behavior begins to be governed by the interlocking of the aggregate from the lower reduced frequency region or higher temperature region where the flow begins, the possibility exists of having a larger sample-to-sample variability, as seen also in Chapters 5, 6 and 7.

Similar results for the Control mixture can be seen in Figure 8.2. The Control mixture seems to show relatively clearer ranking by asphalt content than the Lsub mixture. The C5.1 mix shows consistently higher dynamic moduli at the overall reduced frequencies, followed by C5.6, C6.1, and C6.6, as shown in Figure 8.2 (a). In the log-log scale plot, at the relatively lower reduced frequency region (higher temperature), the dynamic modulus mastercurve of the C5.6 mix seems to be no different than the C5.1 mix. The phase angle plot presents no

big difference among mixtures with different asphalt contents at the very high reduced frequency region (around -10°C of the test temperature). However, the phase angle mastercurves start to deviate with the ranking in the order of the asphalt content as the reduced frequency decreases (around 10°C of the test temperature). The C5.1, the mixture with the lowest asphalt content, shows the lowest values among the mixtures. This finding is consistent with the dynamic modulus result of the Lsub and Control mixtures. Similar to the Lsub mixture, the phase angles of all the mixtures decrease with the reverse order of the ranking after showing the peak region of the phase angle, as the reduced frequency decreases. It is interesting to note that the change in slope in the phase angle vs. reduced frequency curve occurs at lower reduced frequencies as the asphalt content decreases. The change in slope indicates that the binder becomes so soft that below this reduced frequency the aggregate overtakes the rheological behavior. This transition occurs at higher reduced frequencies according to the asphalt content in the system; that is, the more asphalt, the higher the reduced frequencies (i.e., the lower temperature) as the transition occurs.

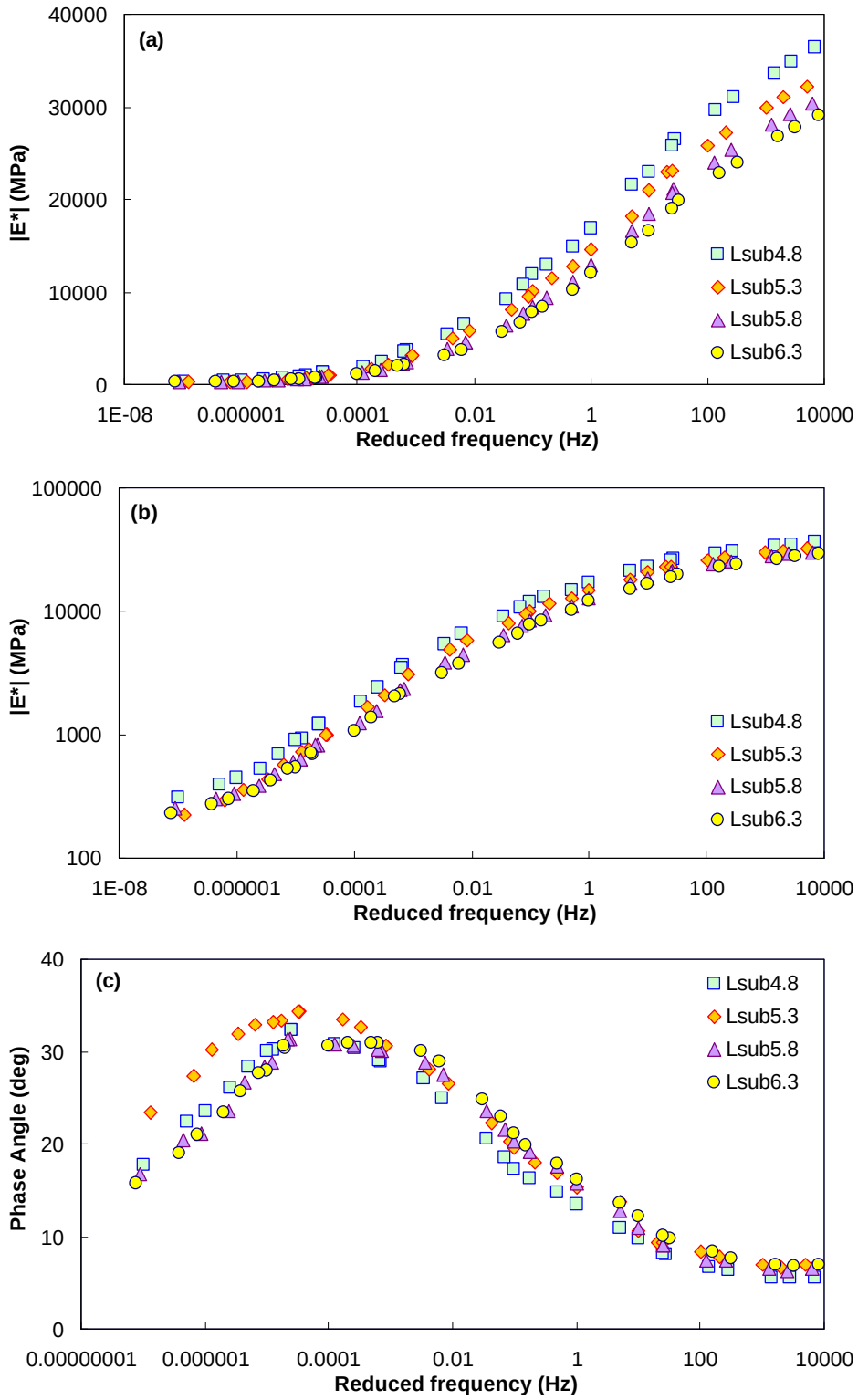

Figure 8.1 Effect of asphalt content: (a) |E*| in semi-log space; (b) |E*| in log-log space; (c) phase angle (lime-modified mixture)

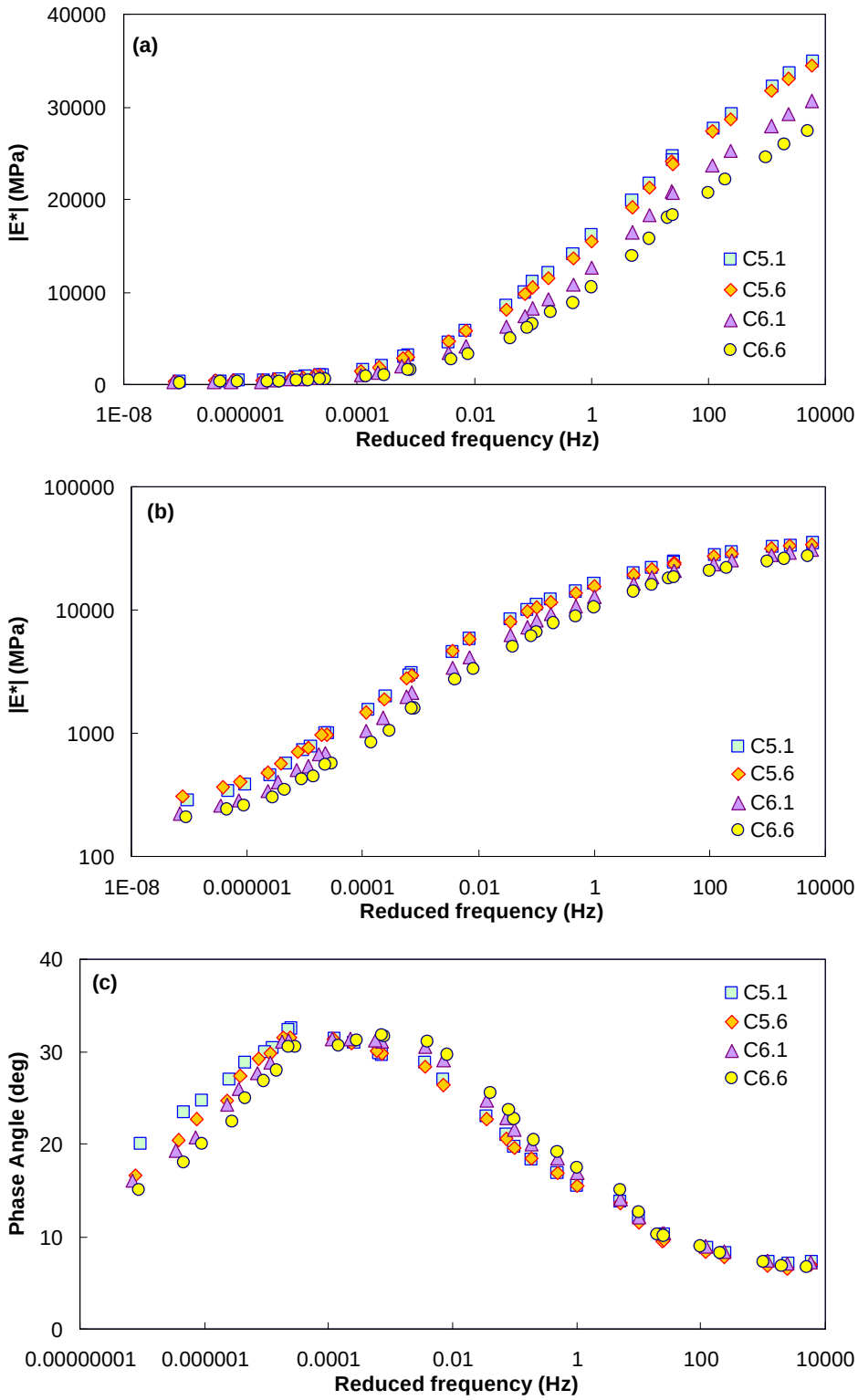

Figure 8.2 Effect of asphalt content: (a) |E*| in semi-log space; (b) |E*| in log-log space; (c) phase angle (unmodified mixture)

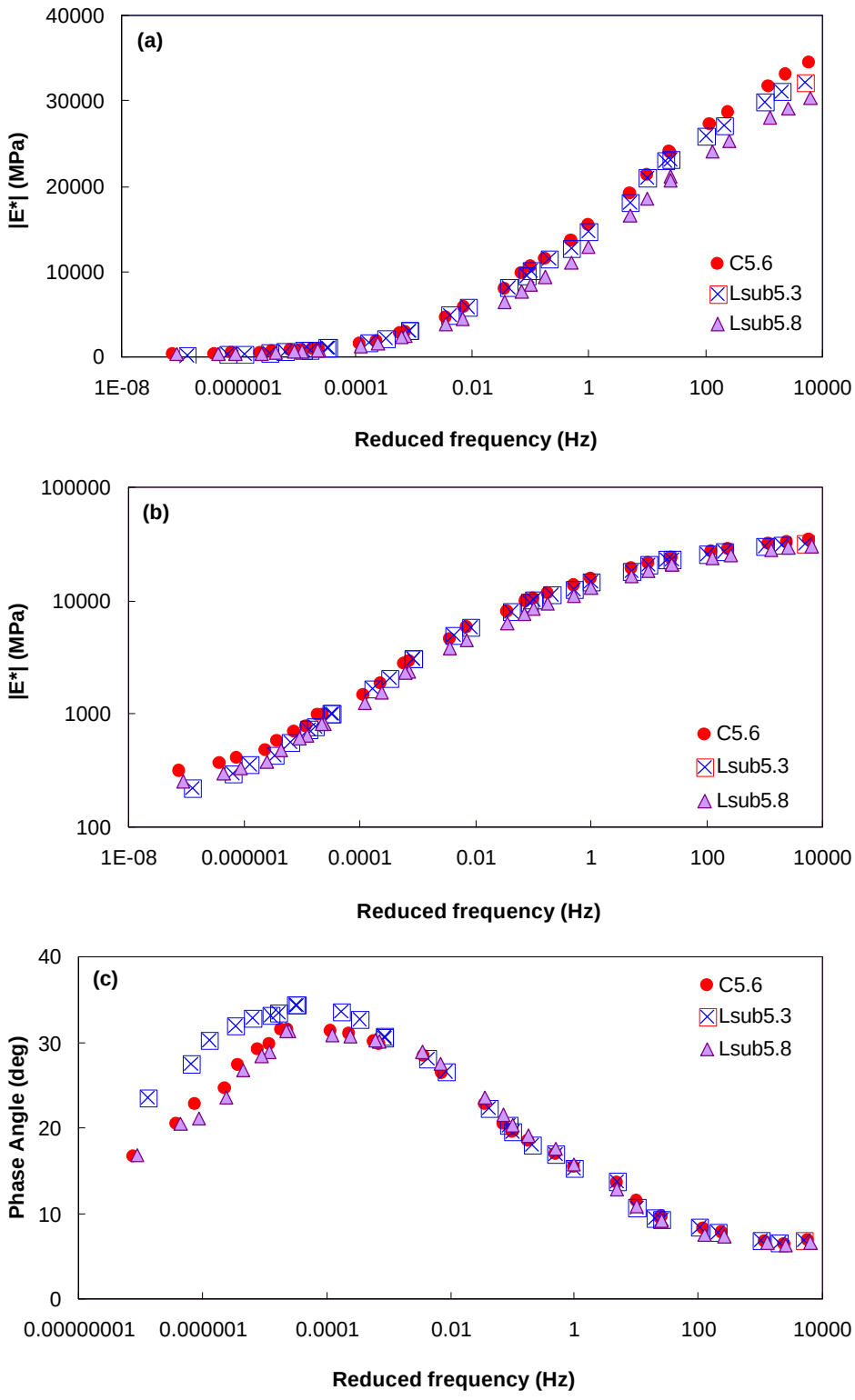

Figure 8.3 Comparison between Control and Lsub mixtures: (a) |E*| in semi-log space; (b) |E*| in log-log space; (c) phase angle

Because the asphalt contents used in the Control and Lsub mixtures are different, the effects of the lime modification on the dynamic modulus and phase angle should be observed between the optimum asphalt content (5.6%) of the Control mixture and the Lsub mixtures at 5.3% (the optimum) and 5.8%, as seen in Figure 8.3. In general, the lime modification reduces the dynamic modulus slightly and does not have any significant effect on the phase angle. Although lime modification is known to increase the stiffness of the HMA mixture, the manner by which the lime is added to the HMA mixture does affect the stiffness change. The lime substitution method used in this study does not significantly affect the dynamic modulus and phase angle.

8.3.2 TRLPD test Results and Statistical Analysis

TRLPD tests were conducted under the same conditions as described in Chapters 6 and 7. The results indicate that the mixtures exhibit adequate rutting performance without tertiary flow even at the higher asphalt contents. Such strain growths for the Lsub mixture and the Control mixture with different asphalt contents are presented in the plots shown in Figure 8.4 and Figure 8.5, respectively.

The overall observation made from Figure 8.4 and Figure 8.5 is that the permanent strain growth increases as the asphalt content increases. The amount of change in the permanent strain growth is gradually increased as the asphalt content increases and then becomes larger at 6.3% of the highest asphalt content for the Lsub mixture. This same phenomenon can also be observed in the result of the Control mixture. The results indicate that too much asphalt content causes a dramatic increase in rutting. The rutting resistance

rankings of the Lsub mixture and the Control mixture with varying asphalt contents are in line with the ranking from the dynamic modulus test results, because the rutting performance is directly related to the stiffness of the mixture. The permanent strain growths for each mixture at the early stage are also depicted in Figure 8.4 (b) and Figure 8.5 (b) in log-log scale. The Control mixture shows larger sample-to-sample variability at the early stage than the Lsub mixture. Because the permanent strain growth at the early stage is dependent primarily on the air voids of the samples, it can be clearly seen after the specimens are stabilized that the differences in the early stage are realistic. Therefore, statistical analysis is needed with regard to the differences at the overall test cycles, including the early stage, to examine the effects of asphalt content on the rutting performance of the mixtures.

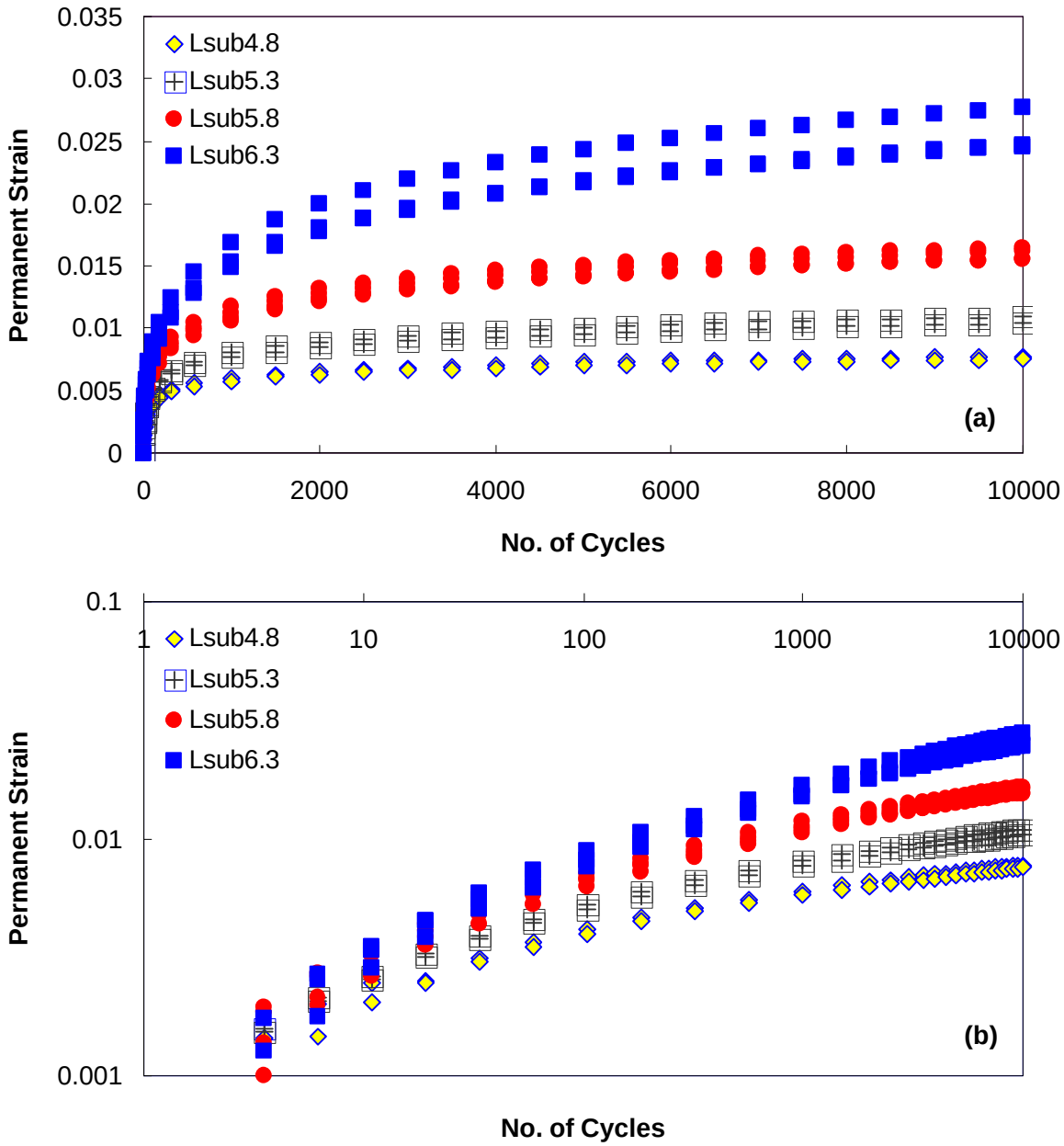

Figure 8.4 Effect of asphalt content on permanent strain accumulation with the lime-modified mixture: (a) arithmetic scale; (b) log-log scale

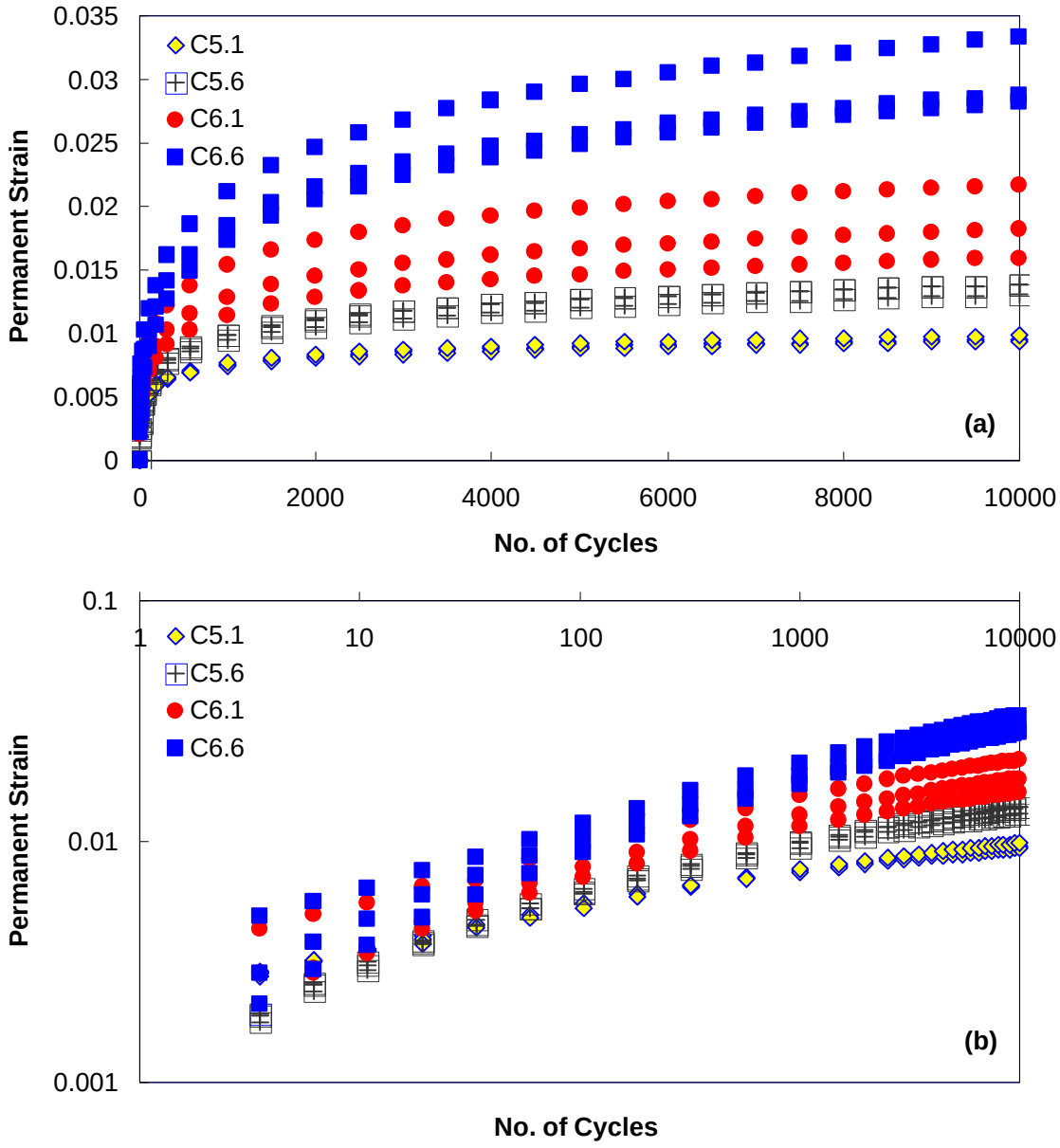

Figure 8.5 Effect of asphalt contents on permanent strain accumulation with the unmodified mixture: (a) arithmetic scale; (b) log-log scale

The ANOVA test was performed under the null hypothesis that the permanent strain value for each mixture is equivalent. From these results, the same Bonferroni multiple pairwise comparison method using LSD was used to make individual mixture comparisons.

These analyses were performed with the significance level, a= 0.05, at various cycles (11, 59, 104, 184, 568, 1,000, 2,000, 3,000, 5,000, 7,000, 10,000), covering the range of the permanent deformation and providing assessment of early, middle and late stage behavior. The results of this analysis are presented in Tables 8.1 and 8.2, for the Lsub and the Control mixture, respectively. It is observed from Table 8.1 and Table 8.2 that the null hypothesis is rejected at all cycles other than the first cycle, as can be seen in the conditions marked with dark colored squares. Again, based on the results from the Bonferroni multiple pairwise comparison, it is seen that, in general, the mixture with the lower asphalt content shows consistently a better ranking of rutting performance as is evident in the dynamic modulus. However, no significant difference is observed between the Lsub mixtures with 4.8% and 5.3% asphalt content over the whole range other than the earliest cycle. Similarly, the same observation can be found in the Control mixture. However, the Control mixture with 6.1% asphalt content shows no significant difference with the 5.6%, even though 5.1% is significantly different than 6.1%.

Table 8.1 Statistical Analysis of the Effect of Asphalt Content on the Permanent Deformation Resistance of the Lime-Modified Mixture

No. of Cycles	p-value	Least Significant Differences Ranking			
		Lsub4.8	Lsub5.3	Lsub5.8	Lsub6.3
11	0.054156	A	A	A	A
59	0.000183	A	A	B-C	B-C
104	0.000067	A	A	B	C
184	0.000022	A	A	B	C
568	0.000005	A	A	B	C
1,000	0.000003	A	A	B	C
2,000	0.000002	A	A	B	C
3,000	0.000001	A	A	B	C
5,000	0.000001	A	A	B	C
7,000	0.000001	A	A	B	C
10,000	0.000001	A	A	B	C

Table 8.2 Statistical Analysis of the Effect of Asphalt Content on the Permanent Deformation Resistance of the Unmodified Mixture

No. of Cycles	p-value	Least Significant Differences Ranking			
		C5.1	C5.6	C6.1	C6.6
11	0.137582	A	A	A	A
59	0.003621	A	A	A-B	B
104	0.001178	A	A-B	B	B-C
184	0.000356	A	A-B	B	B-C
568	0.000082	A	A-B	B	C
1,000	0.000046	A	A-B	B	C
2,000	0.000022	A	A-B	B	C
3,000	0.000017	A	A-B	B	C
5,000	0.000013	A	A-B	B	C
7,000	0.000011	A	A-B	B	C
10,000	0.000009	A	A-B	B	C

Because one of the objectives in this study is to evaluate the effects of lime modification on the rutting performance with varying asphalt contents, it was decided to plot

the results of both mixtures in one graph so as to rank the rutting performance in a visual way. The permanent strain growth curve presented in Figure 8.6 is the average of the replicates of each mixture. The critical observation regarding this plot is the definitive ranking in the decreasing order of the asphalt contents, even though the plot does not show a particularly clear trend at the earliest stage. Because the amount of change in the permanent strain growth becomes larger as the asphalt content increases in both the lime-modified and unmodified mixtures, evaluating the effects of the lime itself on the rutting performance is difficult to evaluate by visual observation.

In order to assess the effects of lime, it was decided simply to interpolate and extrapolate from the results of the Control mixture with varying asphalt contents. In other words, it was interpolated from the permanent strains of 5.1% and 5.6% asphalt contents to generate the permanent strain of 5.3% asphalt content; thus, a comparison with the Lsub5.3 mixture could be made to examine if the effects were due not to the asphalt content, but to the lime. It is noted that several assumptions must be made in order to interpolate and extrapolate. On assumption is that the permanent strain growth follows a linear increase within two consecutive asphalt contents and, secondly, that the average value of the replicates can represent the permanent strain growth at the asphalt content; that is, there is no significant sample-to-sample variation to cause the possibility of limiting the linear strain growth. Again, it should be noted that the potential for error from extrapolation may be larger because of the difference of the increasing rate in permanent strain growth as a function of the asphalt content. Using interpolation and extrapolation, the relative permanent strain growth ratio (RPSR) was calculated. The RPSR is the ratio of the difference of the permanent

strain between the Lsub mixture and the generated data to that of the Lsub mixture at the same asphalt content. The results are depicted in Figure 8.7. Because larger variability exists in the lower number of cycles before stabilization, the ratio was evaluated from the 1,000 number of cycles, which is the linear stage in permanent strain growth. If the RPSR (%) shows a negative value, then there is an effect of lime on the permanent strain reduction. From Figure 8.7, an effect of lime on the rutting performance can be seen. This result is in agreement with other studies (Petersen et al. 1987; Little et al. 1996, 2001, 2005; Sebaaly et al. 2007). However, it must be noted that as the asphalt content increases, the ratio increases, which means that the effect of lime decreases. It appears that because the amount of lime was fixed while the asphalt content was changed, the effect of the lime became diluted as the asphalt content increase; that is, as the lime-to-asphalt ratio decreases, the effect of lime on rutting performance also decreases.

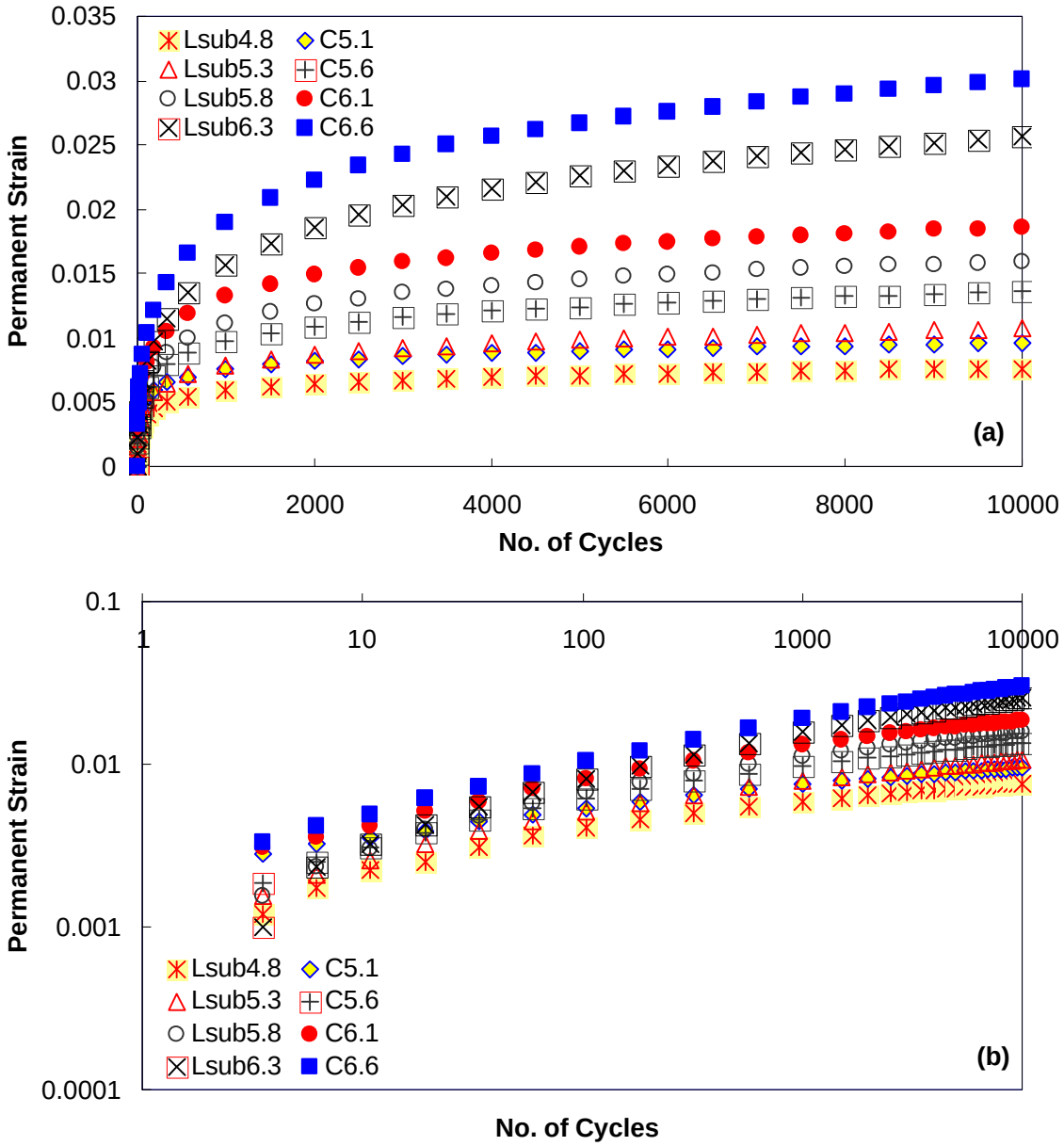

Figure 8.6 Effect of asphalt content on permanent strain accumulation in (a) arithmetic scale; (b) log-log scale

Along a similar line, as seen in Table 6.3, again it appears that the asphalt content alone does not explain the change in performance, because the Leco mixture does not exhibit the best performance although it contains the lowest asphalt content.

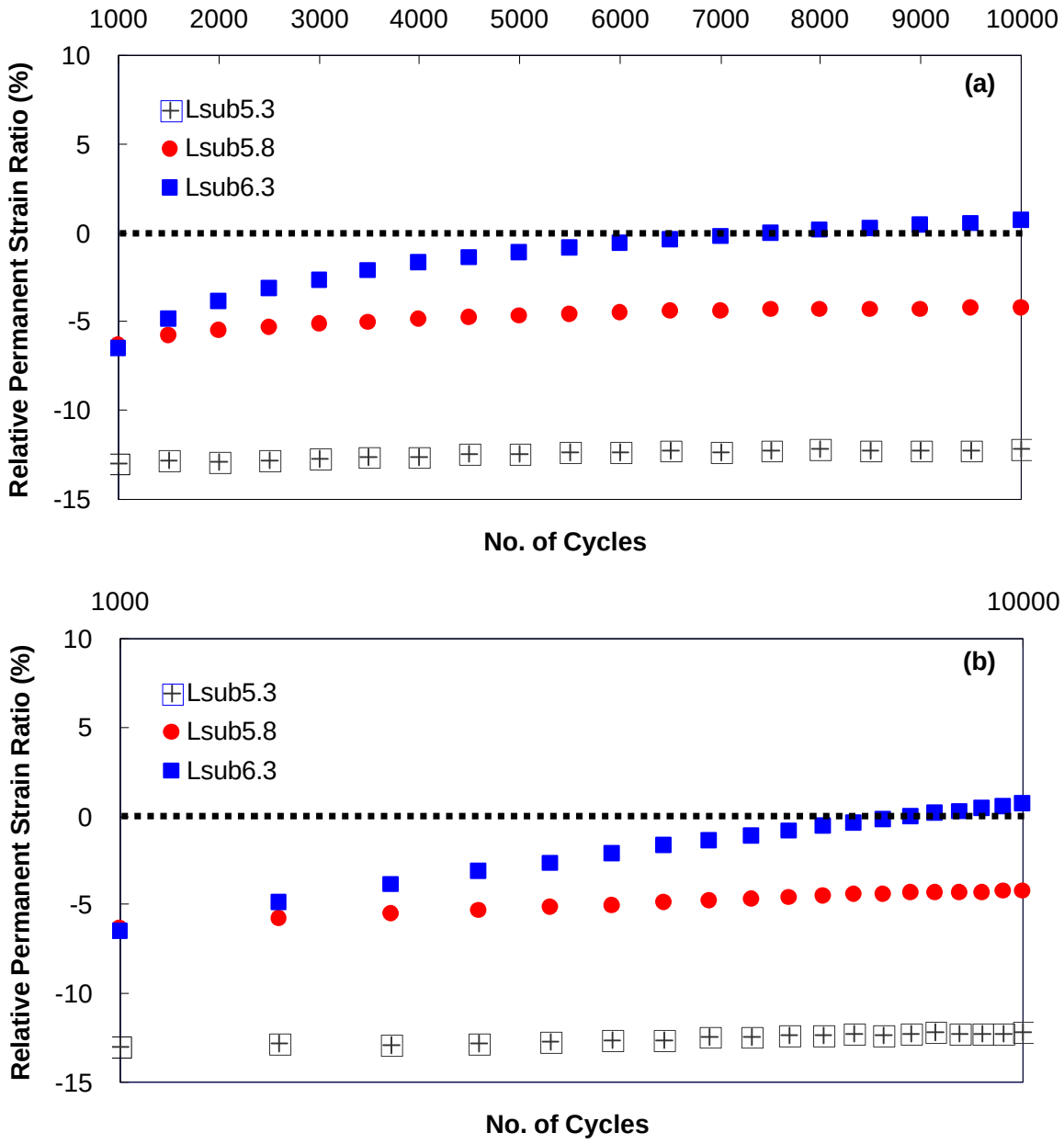

Figure 8.7 The relative permanent strain ratio regarding the effect of lime on permanent strain accumulation in (a) arithmetic scale; (b) log-log scale

8.3.3 Constant Crosshead Rate Monotonic Test Results

The damage characteristic curve obtained from constant crosshead rate tests performed with varying asphalt contents at 5°C and at the same rates found in Chapters 6 and 7 is presented in Figure 8.8 and Figure 8.9. This damage characteristic curve indicates that for the same amount of damage, the higher stiffness allows better fatigue resistance. Similar to the test results discussed in Chapter 6, and although the differences in Figure 8.8 and Figure 8.9 seem small, a difference in fatigue resistance is evident because little replicate variation exists and the tests at different rates collapse very well. From these plots it is seen that the damage characteristic curves for the different asphalt contents are ranked in that as the asphalt content increases, the damage characteristic curve is in a lower position. Normally, experience would suggest that the more asphalt that is present in the mix, the higher the fatigue resistance. However, at the highest asphalt content, the lower stiffness allows an inferior fatigue resistance for the same damage. Similar results can be found in the Control mixture with varying asphalt content. However, Figure 8.9 presents that the damage characteristic curve at the volumetric optimum asphalt content (5.6%) shows a higher stiffness than the lowest asphalt content mixture (5.1%). It is important here to recognize the data for the beginning of the damage characteristic relationship because the stiffness of the mixture lessens faster as the unit increasing of the damage. In Figure 8.8 (b) and Figure 8.9 (b), the data for the beginning stage of the damage characteristic relationship are presented in the semi-log scale to examine the differences of the stiffness of the mixture with varying asphalt contents. Based on the visual observation of the plots, again it can be found that a

clear difference is evident in the Lsub mixture; that is, as the asphalt content increases, the damage characteristic curve is in a lower position. Even though the difference between 5.1% and 5.6% of the asphalt content of the Control mixture does not appear to be much, other curves show a clear ranking similar to that of the Lsub mixture.

To evaluate the effects of asphalt content and lime modification on fatigue performance, the same statistical method (i.e., the Bonferroni multiple pairwise comparison with a significance level of a = 0.05) was conducted at various damage parameters, S (5,000, 1,000, 20,000, 50,000, 100,000, 150,000, 200,000, 250,000, 300,000, 400,000, or 500,000). It is observed from Table 8.3 that the null hypothesis is rejected over all the damage parameter S values in the case of the Lsub mixture, while it is not rejected until the damage parameter S values reach 20,000 in the Control mixture. In other words, there is significant difference among the Lsub mixtures with varying asphalt contents for the overall damage parameter S, whereas there is no significant difference among the Control mixtures with varying asphalt contents to 20,000 of damage parameter S.

As described in Chapters 6 and 7, the fatigue resistance is the material's ability to resist both damage and deformation. The damage characteristic relationship exhibited that the resistance to damage decreases as the asphalt content increases, while the dynamic modulus, which is the resistance to deformation, showed that it changes with respect to the asphalt content. Therefore, under such conditions, the damage characteristic curve ranking alone cannot explain the respective fatigue performance of the mixtures. The VECD-FEP++ simulation is implemented with regard to the material's resistance to damage and

deformation. Trends in fatigue performance of the various mixture can be captured with VECD-FEP++, as with the moisture damage study.

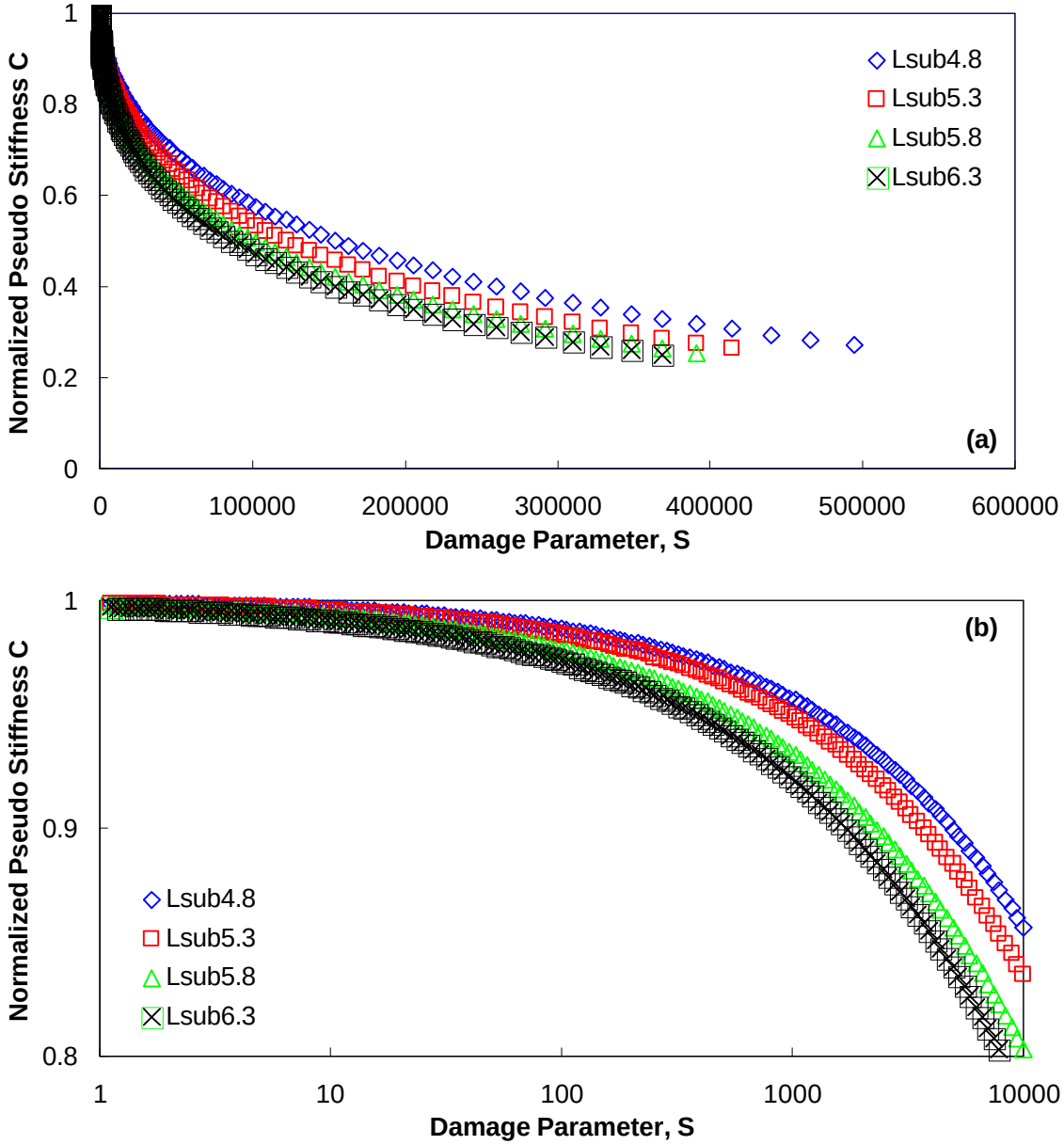

Figure 8.8 Effect of asphalt content on the fatigue resistance of the lime-modified mixture in (a) arithmetic scale; (b) semi-log scale at early stage of damage

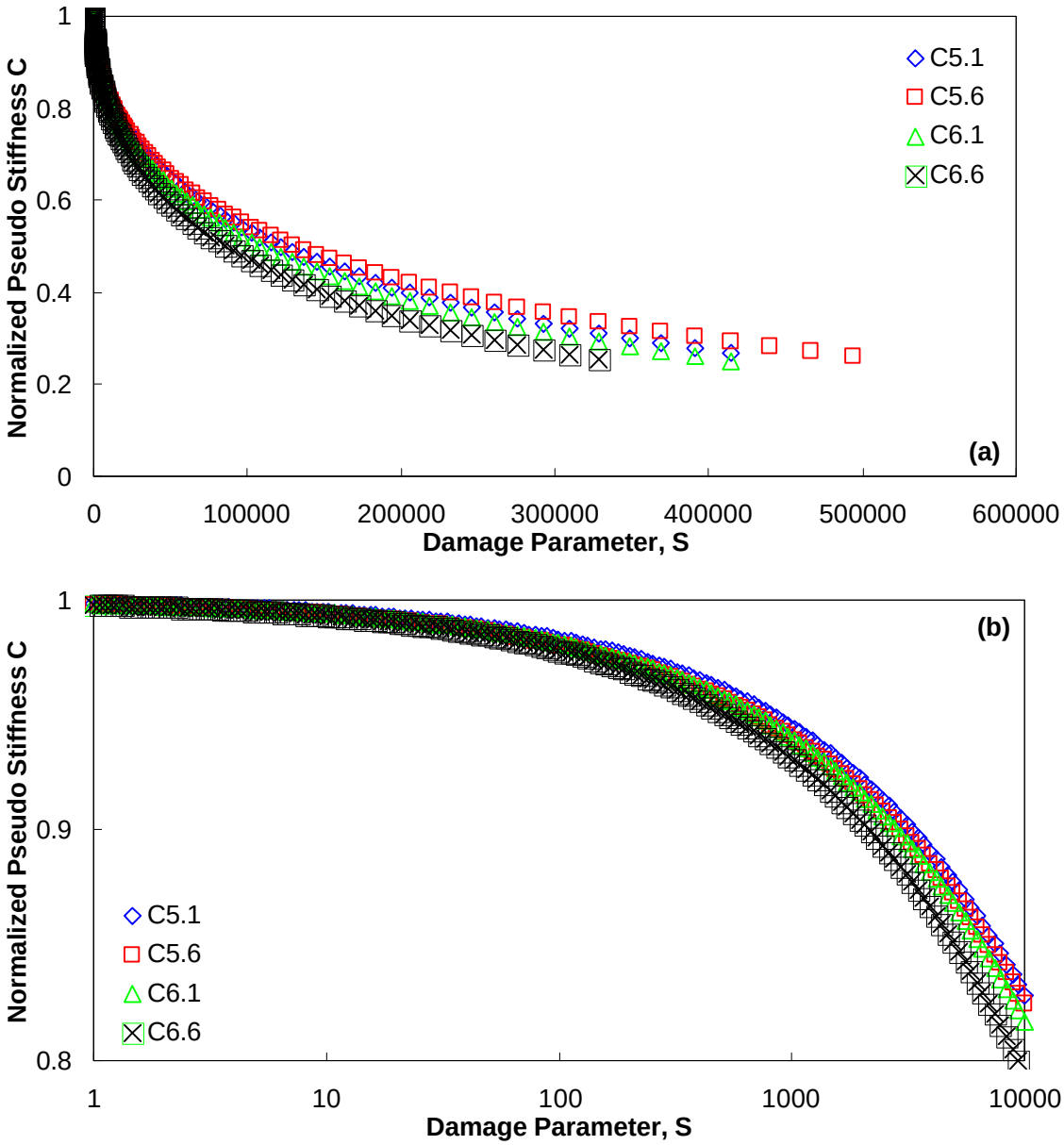

Figure 8.9 Effect of asphalt content on the fatigue resistance of the unmodified mixture in (a) arithmetic scale; (b) semi-log scale at early stage of damage

Table 8.3 Statistical Analysis of the Effects of Asphalt Content on the Resistance to Damage for the Lime-modified Mixture with Varying Asphalt Contents

Refined S	p-value	Least Significant Differences Ranking			
		Lsub4.8	Lsub5.3	Lsub5.8	Lsub6.3
2.50E+02	0.011657	A	A	A-B	B
5.00E+02	0.010685	A	A	A-B	B
1.50E+03	0.009112	A	A	A-B	B
4.00E+03	0.007642	A	A	A-B	B
1.00E+04	0.006193	A	A-B	B	B-C
2.00E+04	0.005054	A	A-B	B	B-C
5.00E+04	0.003563	A	A-B	B	B-C
1.00E+05	0.002582	A	A-B	B	B-C
1.50E+05	0.002168	A	A-B	B	B-C
2.00E+05	0.002006	A	A-B	B	B
2.50E+05	0.002006	A	A-B	B	B
3.00E+05	0.002138	A	A-B	B	B
4.00E+05	0.002805	A	A-B	B	B
5.00E+05	0.004166	A	A-B	B	B

Table 8.4 Statistical Analysis of the Effects of Asphalt Content on the Resistance to Damage for the Unmodified Mixture with Varying Asphalt Contents

Refined S	p-value	Least Significant Differences Ranking			
		C5.1	C5.6	C6.1	C6.6
2.50E+02	0.227481	A	A	A	A
5.00E+02	0.212414	A	A	A	A
1.50E+03	0.180985	A	A	A	A
4.00E+03	0.144171	A	A	A	A
1.00E+04	0.103531	A	A	A	A
2.00E+04	0.071649	A	A	A	A
5.00E+04	0.034781	A	A	A-B	B
1.00E+05	0.015652	A	A	A-B	B
1.50E+05	0.008647	A	A	A-B	B
2.00E+05	0.005343	A	A	A-B	B
2.50E+05	0.003559	A	A	A-B	B
3.00E+05	0.002508	A-B	A	B	B-C
4.00E+05	0.001412	A-B	A	B	B-C

8.4 VECD-FEP++ Simulation Results

The damage contours of the lime-modified and unmodified mixtures with varying asphalt contents are depicted in Figure 8.10 and Figure 8.11. Similar to the simulation results found in Chapters 6 and 7, it is clearly observed that as the number of cycles increases, all the mixtures tend to spread damage over the pavement. Again, the damage zone develops from the bottom to the middle of the layer. From the visual observation of the plot of the damage contour for the Lsub mixture at the last load cycle, the largest damaged zone develops at 5.3% volumetric optimum asphalt content, followed by Lsub4.8, Lsub5.8, and C6.3, in order. The observation from Figure 8.11 for the Control mixture at the last load cycle is that the lowest asphalt content exhibits the largest damaged zone, followed by C6.6, C6.1, and C5.6. The observation of the Lsub mixture at the final stage is that the upper damaged zone becomes larger as the asphalt content increases, while the lower damaged zone becomes smaller. This finding is true also for the Control mixture, other than C5.1, which shows the largest upper damaged zone.

In order to evaluate the effects of asphalt content with lime on the fatigue performance more closely, it was again decided to examine the percentage of crack area (% Crack area) and the Average C of each mixture with varying asphalt contents at the same cycles that were used for the contour plots. The results for the Control and Lsub mixtures are presented in Figure 8.12 and Figure 8.13, respectively.

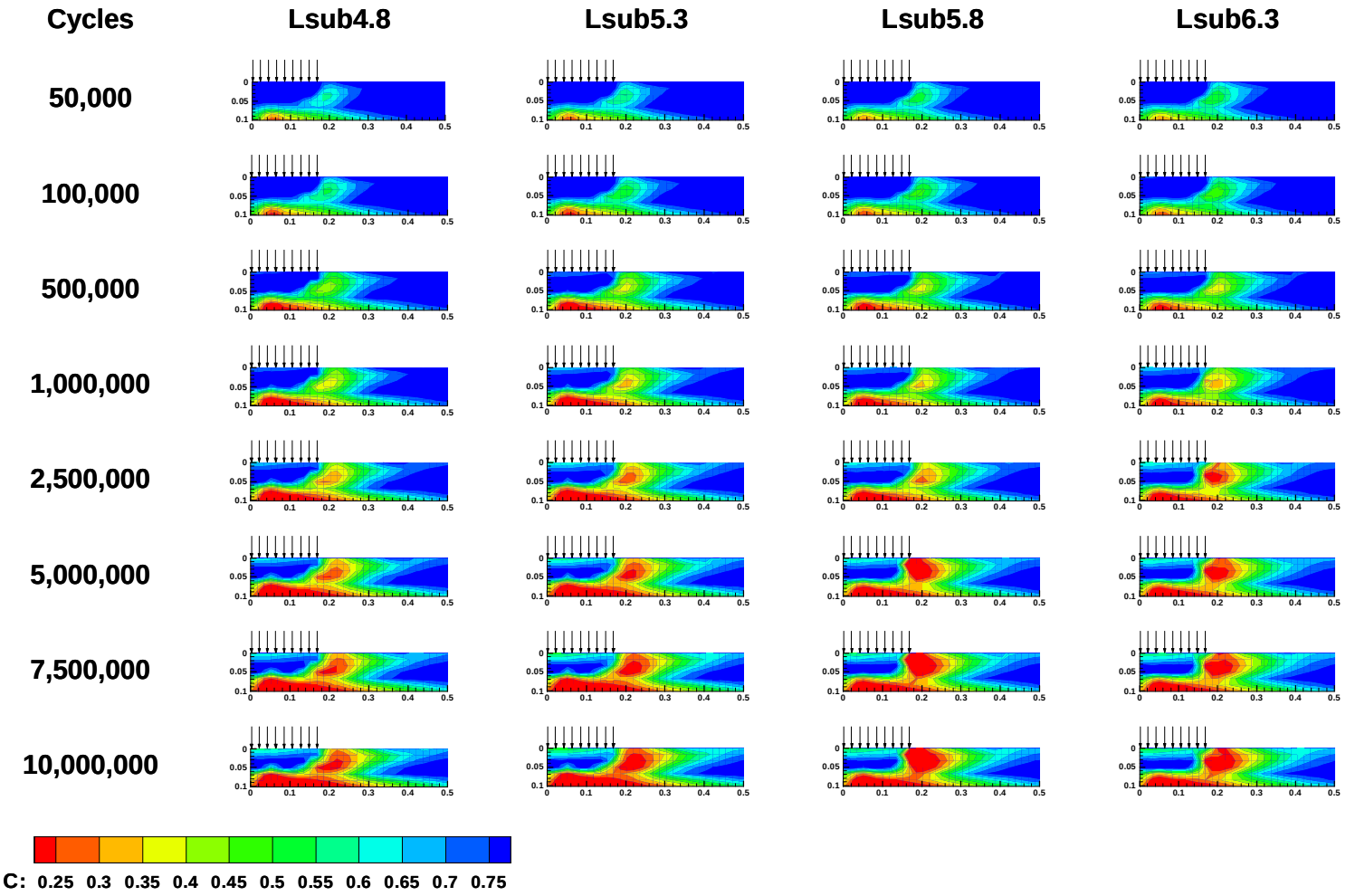

Figure 8.10 Comparison of the damage contour plots at various load cycles for the lime-modified mixtures

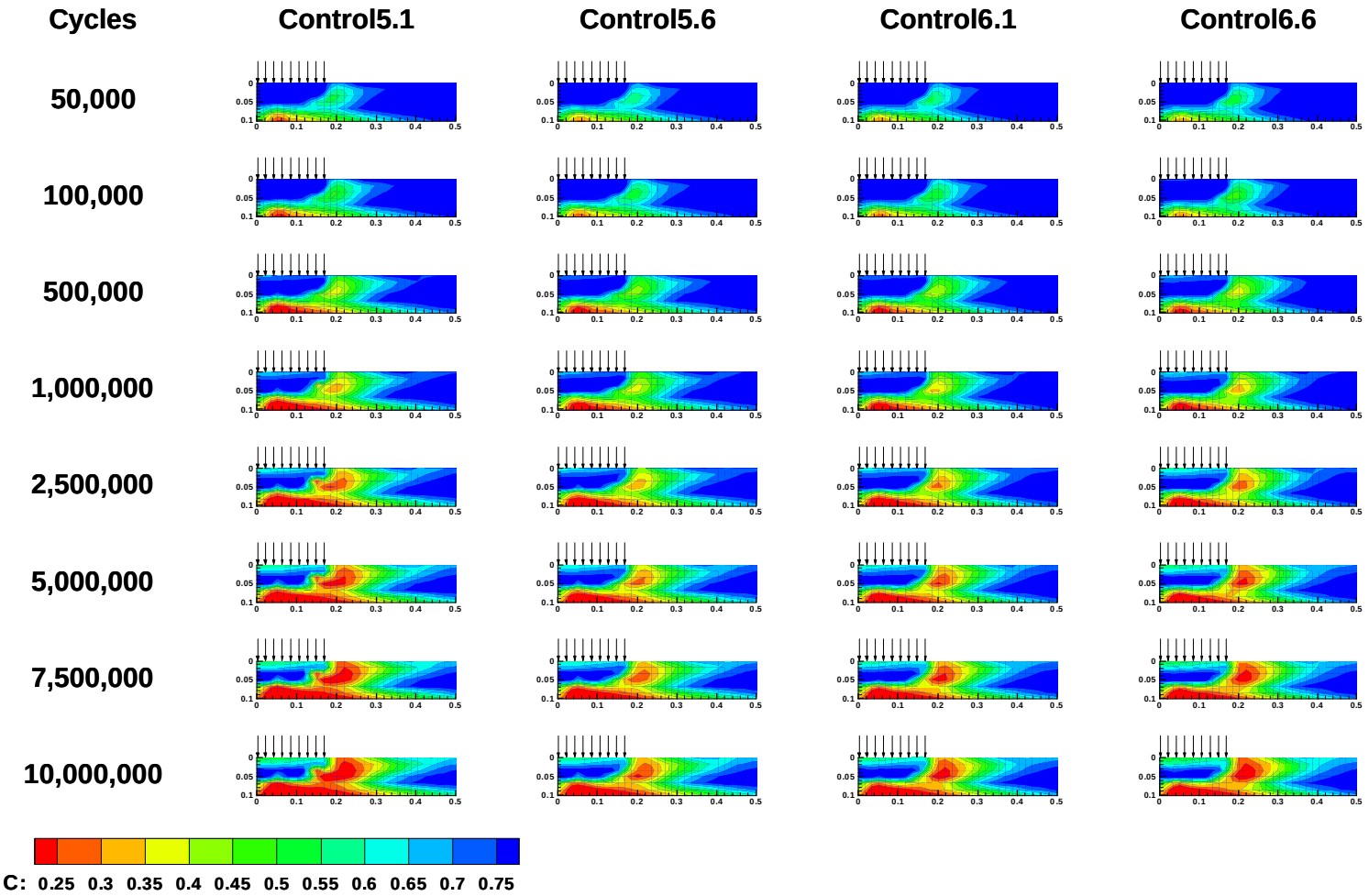

Figure 8.11 Comparison of the damage contour plots at various load cycles for the unmodified mixtures

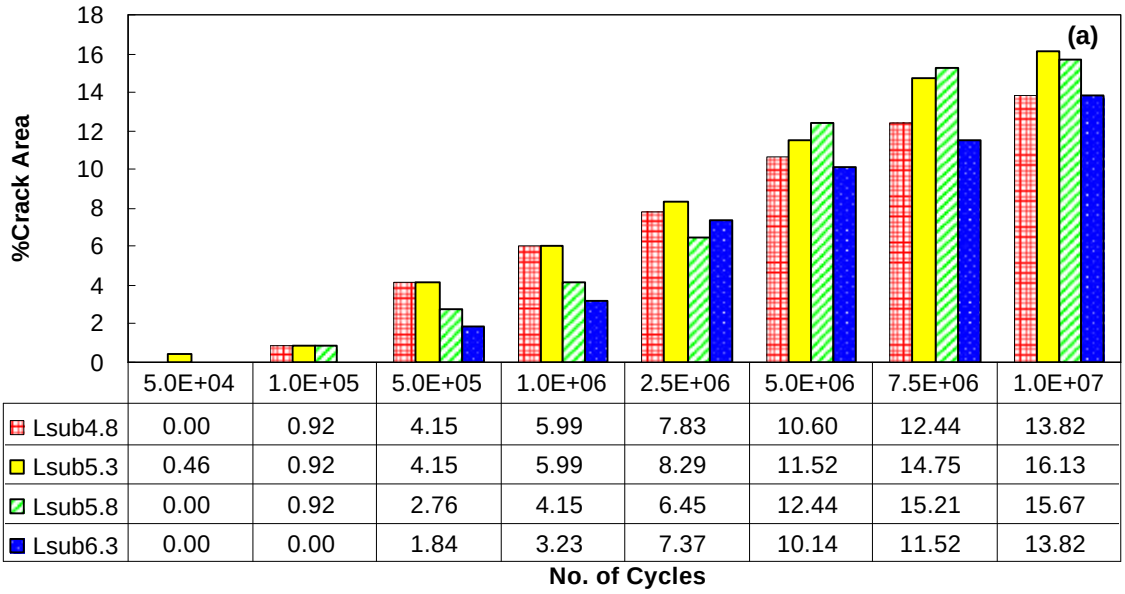

	5.0E+04	1.0E+05	5.0E+05	1.0E+06	2.5E+06	5.0E+06	7.5E+06	1.0E+07
Lsub4.8	0.00	0.92	4.15	5.99	7.83	10.60	12.44	13.82
Lsub5.3	0.46	0.92	4.15	5.99	8.29	11.52	14.75	16.13
Lsub5.8	0.00	0.92	2.76	4.15	6.45	12.44	15.21	15.67
Lsub6.3	0.00	0.00	1.84	3.23	7.37	10.14	11.52	13.82

No. of Cycles

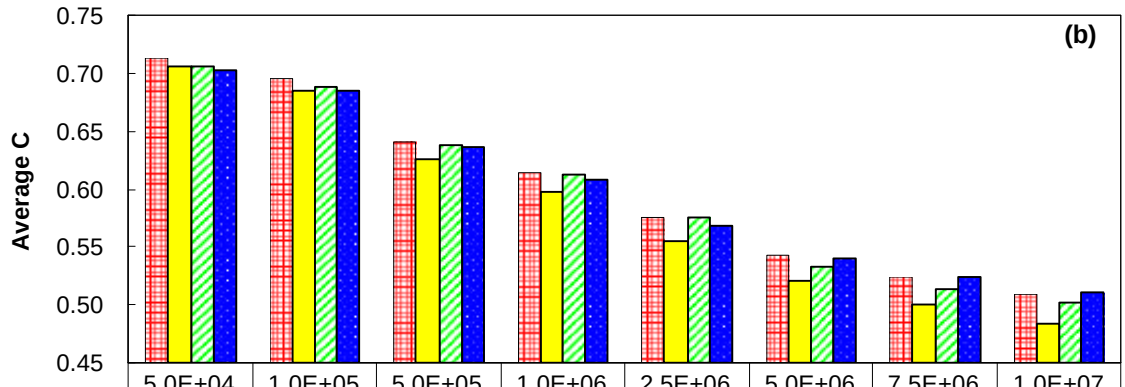

	5.0E+04	1.0E+05	5.0E+05	1.0E+06	2.5E+06	5.0E+06	7.5E+06	1.0E+07
Lsub4.8	0.71	0.69	0.64	0.61	0.58	0.54	0.52	0.51
Lsub5.3	0.71	0.69	0.63	0.60	0.55	0.52	0.50	0.48
Lsub5.8	0.71	0.69	0.64	0.61	0.58	0.53	0.51	0.50
Lsub6.3	0.70	0.68	0.64	0.61	0.57	0.54	0.52	0.51

No. of Cycles

Figure 8.12 Discrete comparison of fatigue performance of the lime-modified mixtures with varying asphalt contents based on: (a) % Crack area; and (b) Average C at various cycle stages

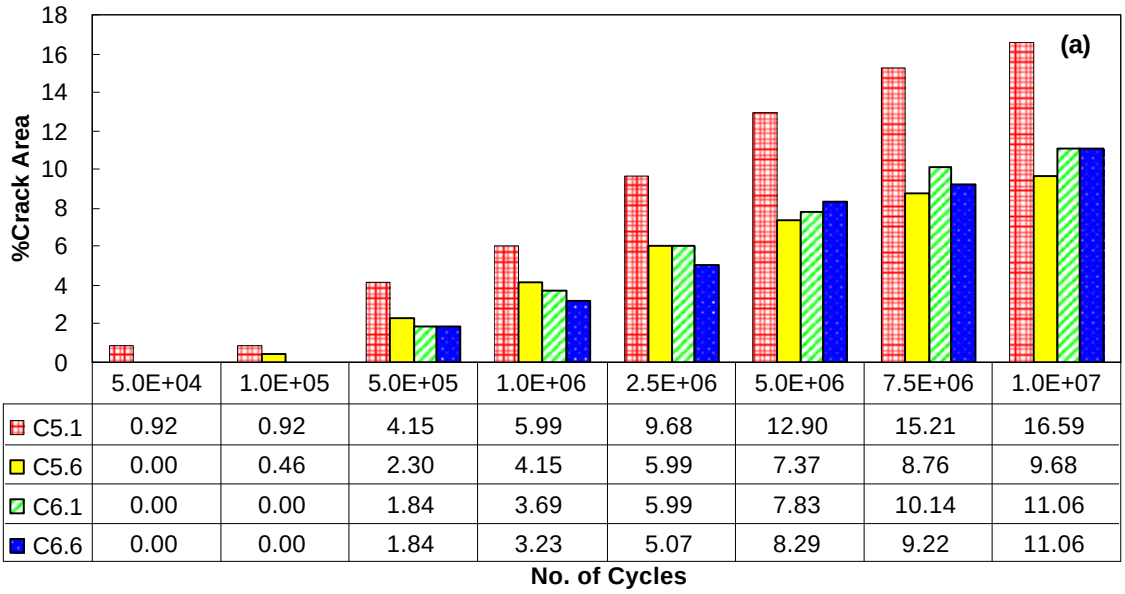

	5.0E+04	1.0E+05	5.0E+05	1.0E+06	2.5E+06	5.0E+06	7.5E+06	1.0E+07
C5.1	0.92	0.92	4.15	5.99	9.68	12.90	15.21	16.59
C5.6	0.00	0.46	2.30	4.15	5.99	7.37	8.76	9.68
C6.1	0.00	0.00	1.84	3.69	5.99	7.83	10.14	11.06
C6.6	0.00	0.00	1.84	3.23	5.07	8.29	9.22	11.06

No. of Cycles

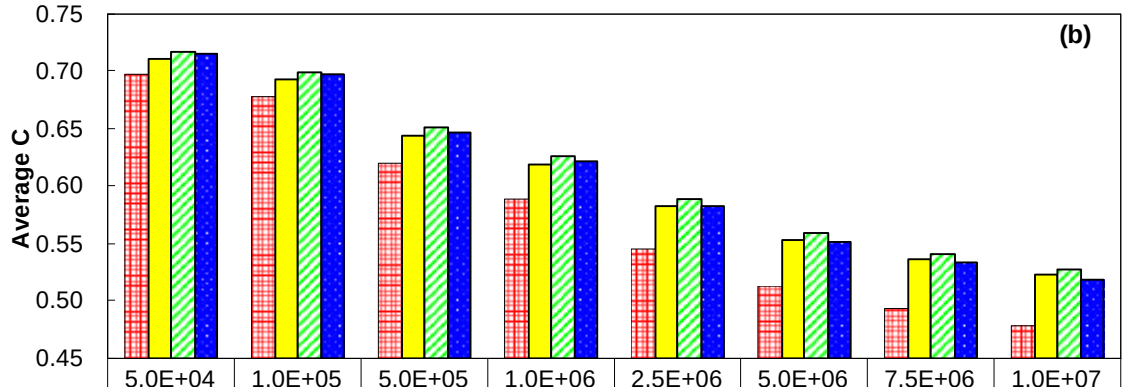

	5.0E+04	1.0E+05	5.0E+05	1.0E+06	2.5E+06	5.0E+06	7.5E+06	1.0E+07
C5.1	0.70	0.68	0.62	0.59	0.55	0.51	0.49	0.48
C5.6	0.71	0.69	0.64	0.62	0.58	0.55	0.54	0.52
C6.1	0.72	0.70	0.65	0.63	0.59	0.56	0.54	0.53
C6.6	0.72	0.70	0.65	0.62	0.58	0.55	0.53	0.52

No. of Cycles

Figure 8.13 Discrete comparison of fatigue performance of the unmodified mixtures with varying asphalt contents based on: (a) % Crack area; and (b) Average C at various cycle stages

In both Figure 8.12 and 8.13, clear trends are seen in the increase of the % Crack area and decrease in the Average C as a function of load cycles. The amount of change in the % Crack area and the Average C can also indicate the effect of asphalt content with lime on the

fatigue performance of the mixture. In Figure 8.12 and Figure 8.13, it can be clearly observed that the fatigue performance ranking with respect to the effect of asphalt content exists until 1,000,000 and 2,500,000 of the load cycles for the Lsub and Control mixtures, respectively. It is interesting to see the difference in the Average C of each mixture at the lowest asphalt content. The Average C of the Lsub4.8 mixture with the lowest asphalt content for the overall number of load cycles shows continuously higher values among mixtures with varying asphalt contents, whereas that of the C5.1 mixture shows continuously lower values than the others. From observations made from Figure 8.6, regarding rutting performance, it appears that the effect of lime is diluted as the asphalt content increases. Because rutting performance is directly related to the stiffness of the material, at the lower asphalt content the stiffening effect of lime is magnified. Along similar lines, other research (Petersen et al. 1987; Lesueur et al. 1999; Little et al. 2005) shows that the hydrated lime particles can make the mixture stiffer and tougher, thus reducing the possibility of fatigue failure in the pavement. Indeed, it is general knowledge that as the asphalt content increases, the material becomes more resistant to fracture or more resistant to crack propagation (Mamlouk et al. 2004). However, even though the effect of lime on the toughness of the mixture can magnify the fatigue resistance, it is difficult to explain the trend of the Average C at the other asphalt contents with increased load cycles. As the VECD theory considers mostly the continuum damage, not the fracture properties, the fatigue resistance of mixtures affected by the increased asphalt content would be understated. In other words, because the fracture toughness, which increases according to the effect of higher asphalt content, is not considered in the continuum damage relationship for evaluating fatigue resistance, the trend shown in Figure 8.12 and

Figure 8.13 may be understating the fatigue performance of the mixture. Thus, taking the fracture properties into account, at the higher asphalt content the Average C may have have the potential not to decrease and the % Crack area may not increase as much, whereas at the lower asphalt content, the opposite may occur. According to the trend of the % Crack area shown in Figure 8.12 (a) and Figure 8.13 (a), the fatigue performance ranking with respect to the effect of asphalt content is evident until 1,000,000 and 2,500,000 of the load cycles for the Lsub and Control mixtures, respectively. After those cycles, the trend becomes unclear. It appears that the fracture processing becomes a factor around those ranges in a cycle. Because the Average C value is more complicated and does not exhibit clear fatigue performance trends of the mixtures, it was decided to use the % Crack area parameter to evaluate the effect of asphalt contents within lime. Figure 8.14 shows the overall trends of the % Crack area of mixtures with varying asphalt contents in semi-log scale. It can be observed from Figure 8.14 that as the asphalt content increases, the slope of the % Crack area growth curve decreases according to the various rates. The growth rate of the Lsub mixture at varying asphalt contents is different from that of the Control mixture. If the rate is higher, despite the small number of loading cycles, the mixture is subjected to a relatively large % Crack area or vice versa.

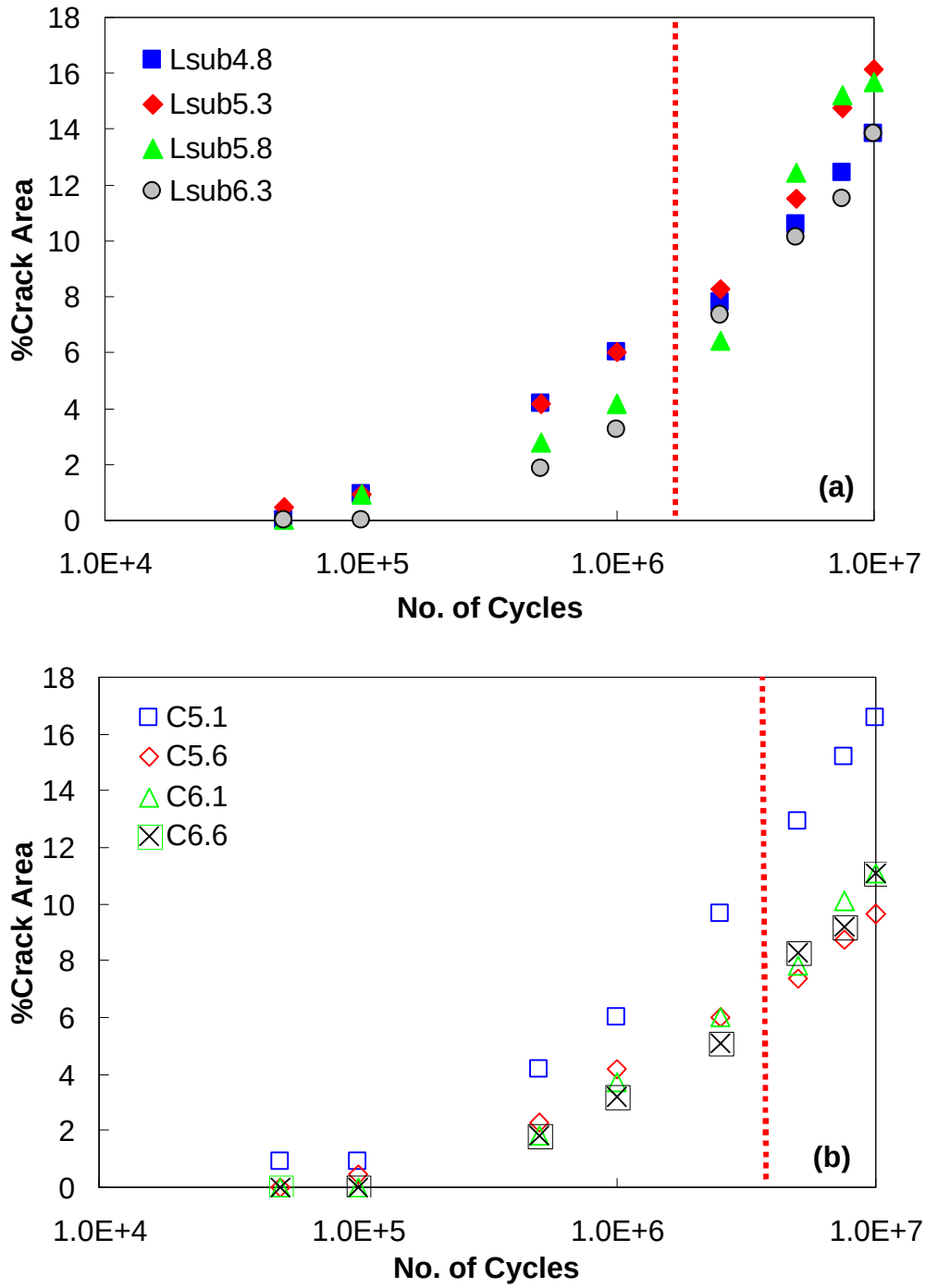

Figure 8.14 The overall trends of the % Crack area of mixtures with varying asphalt contents in semi-log scale for the (a) lime-modified mixture; (b) unmodified mixture

Because the ranking of the % Crack area gets confused after fracture processing, it was decided to compare the growth of the % Crack area of each asphalt content within the range of cycles that is presented on the left-hand side of the red dashed line in Figure 8.14. The changes in % Crack area at each cycle, examined as a function of asphalt content, are presented in Figure 8.15. This figures shows, generally speaking, a relatively large reduction in % Crack area above certain asphalt contents, which are 5.8% and 5.6% for the Lsub and Control mixtures, respectively. In other words, below those asphalt contents, the % Crack area increases drastically, even with the small decrease in asphalt content. Therefore, those asphalt contents that result in a relatively large change in % Crack area below those asphalt contents are the minimum asphalt contents for the fatigue performance side. The relationship observed from Figure 8.15 is that the effect of the asphalt content on the % Crack area growth rate is based on the decreasing trend as a function of asphalt content as well as the effect of lime on that is based on the relatively lower % Crack area of the Lsub mixture than the Control mixture. This result is consistent with the previous discussion on fatigue resistance with respect to asphalt content and lime modification.

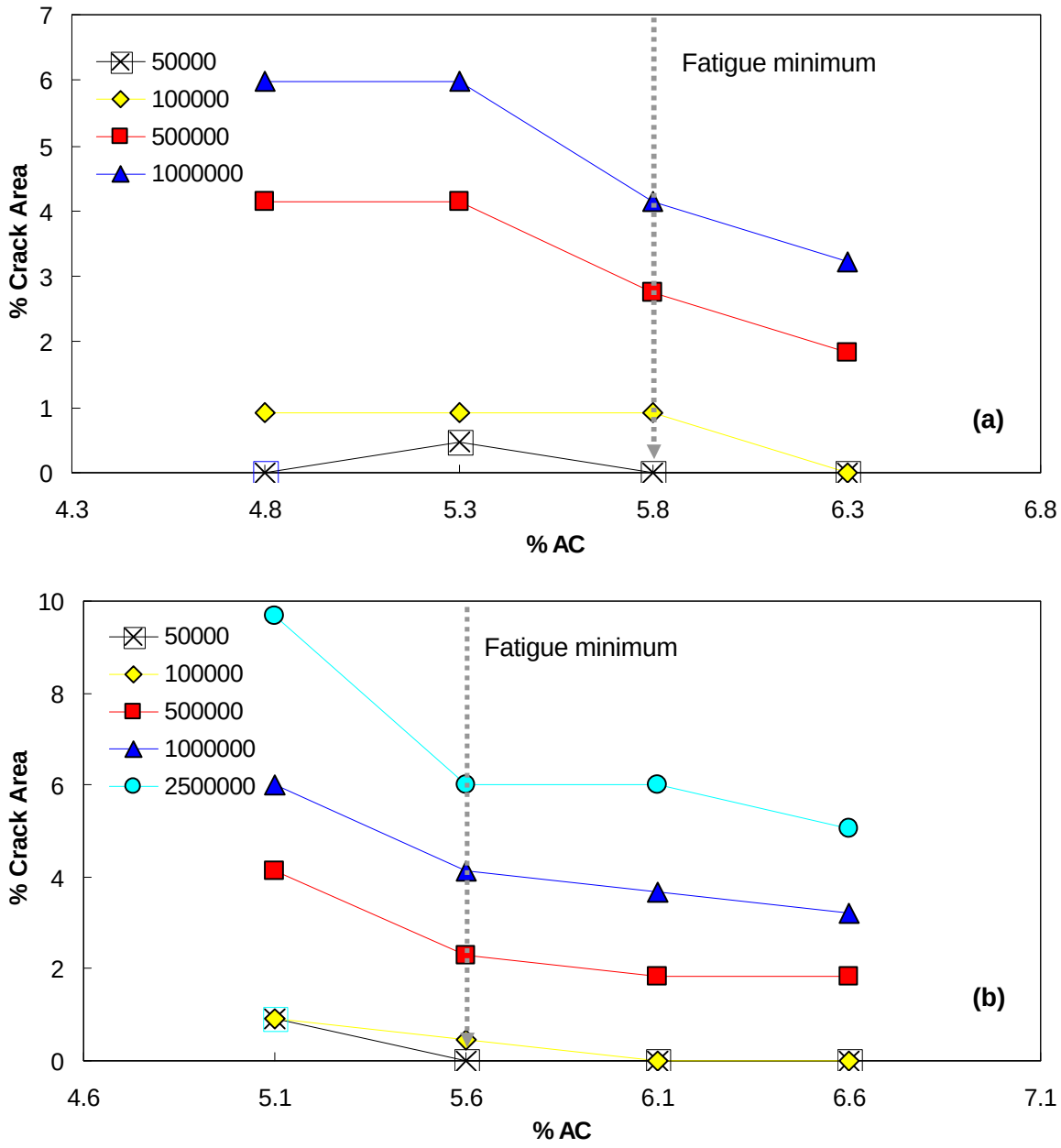

Figure 8.15 The changes in % Crack area at each cycle as a function of asphalt content: (a) lime-modified mixture; (b) unmodified mixture

8.5 Determining optimum asphalt content based on performance

It is important that a mix designer does not concentrate on optimizing only one property of a mix at the expense of the others. A successful rut-resistant mix is fairly easy to produce by using a hard-grade binder, reducing the binder content and adding extra filler. Such a mix, however, may be likely to fail through fatigue and would probably be prone to rapid oxidation hardening. Therefore, in the new mix design procedure, a balance should be obtained between the property of rutting and fatigue as well as the volumetric mix design. The question, therefore, is how to determine the optimum asphalt content that can satisfy both rutting and fatigue performance.

Satisfying both rutting and fatigue performance criteria is the main issue for a performance-based mix design. It cannot be simply considered that the intersection point of the rutting and fatigue plot as a function of asphalt content is the performance-based optimum. In general, fatigue resistance increases as a function of asphalt content while rutting resistance decreases. In order to have both performance plots intersect with a common parameter for mixture characteristics, criteria such as the pavement structure of a surrogate rutting or fatigue model and more detailed analysis on the threshold value of fatigue resistance need to be incorporated. Further, determining the optimum asphalt content depends on environmental factors, such as traffic and temperature or climate, as well as the type of overlay and surface course. For example, if the project includes a surface course that is in a high temperature area, rutting resistance becomes more critical than fatigue. Therefore, adjusting the optimum asphalt content toward a dry mixture is more favorable than a rich

mixture. In order to determine the optimum asphalt content for lime-modified mixtures based on rutting and fatigue performance tests, both performance parameters described previously should be set up as a function of asphalt content. Figure 8.16 depicts the concept of the suggested performance-related mix design criteria in this study.

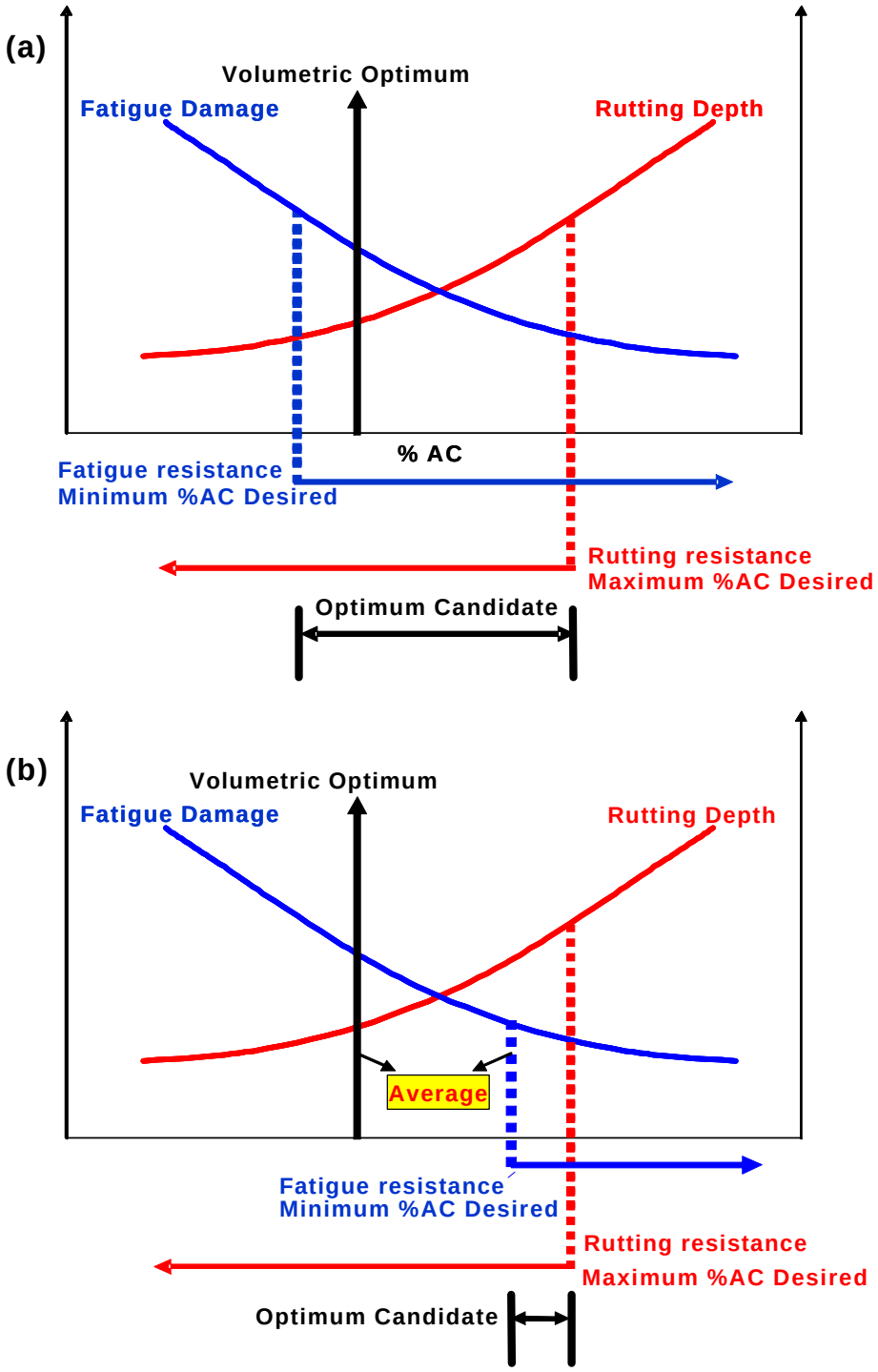

Figure 8.16 Concept of the performance related mix design methodology in case of (a) volumetric optimum within the optimum candidate range; (b) volumetric optimum below the optimum candidate range; (continued)

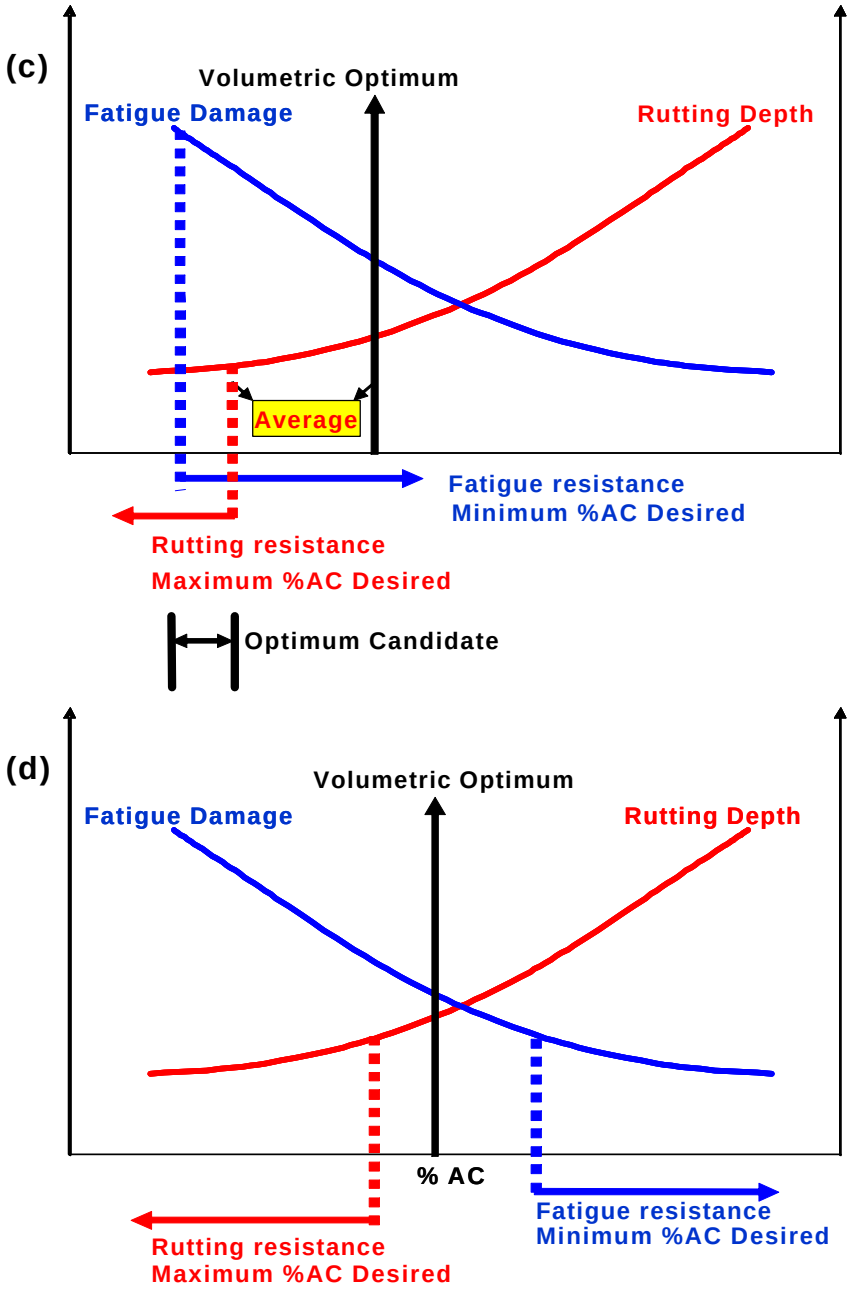

Figure 8.16 Concept of the performance related mix design methodology in case of (c) volumetric optimum above the optimum candidate range; and (d) no optimum candidate range

Also it should be noted that the volumetric mix design had been developed with the objectives; the resistance to permanent deformation; fatigue resistance; resistance to low

temperature cracking; resistance to moisture induced damage; durability; skid resistance; and workability. Of those objectives, resistance to low temperature cracking and moisture damage is prone to selection of proper binder grade and physical-chemical aggregate and binder property respectively, and performance related resistance such as rutting and fatigue resistance can be secured better by conducting the performance based mix design. However, durability which is minimizing asphalt cement hardening or aging during production and in service with adequate film thickness around the aggregate particles can be more subjected to volumetric mix design. Therefore, it is important to secure the balance between the performance optimum and volumetric optimum. From the observation on Figure 8.16(a), if the volumetric optimum asphalt content is determined within the range of candidate optimum asphalt content for the performance, the volumetric optimum could be the balanced optimum asphalt content. In the case of Figure 8.16(b), if the volumetric optimum is below the range, the average of the volumetric and fatigue minimum can be suggested to determine the balanced optimum asphalt content because the volumetric optimum asphalt content satisfies the rutting performance while the fatigue performance is not.. Then the volumetric properties such as VMA and VFA at the final balanced asphalt content should be checked whether it satisfy the volumetric criteria. . In the case of Figure 8.16(c), if the volumetric optimum is below the range, the average of the volumetric and rutting maximum can be suggested to determine the balanced optimum asphalt content because the volumetric optimum asphalt content satisfies the fatigue performance while the rutting performance is not.. Then the volumetric properties such as VMA and VFA at the final balanced asphalt content should be checked whether it satisfy the volumetric criteria. If there is no optimum candidate range in

the case of Figure 8.16(d), since the volumetric optimum asphalt content can not be satisfied with any performance, it is suggested to redo the mix design.

8.5.1 Rutting performance indicator

The permanent deformation response of mixtures under cyclic loading can be obtained from the triaxial repetitive permanent deformation test. Figure 8.16 shows the relationship of the Lsub mixture between the total cumulative plastic strain and the number of load cycles using the regression line in log-log scales. The secondary linear portion in the middle of the curve, as seen in Figure 8.17, is used to represent the permanent strain response of a mix. This portion can be expressed by the following classical power mode:

$$e_p = aN^b,$$

where *a* and *b* are regression constants. The intercept *a* represents the permanent strain at N = 1. The slope *b* represents the rate of change in log (ε_p) as a function of the change in log (N). If the slope of the secondary linear portion, which is expressed by regression constant b, is steeper, then despite the small number of loading cycles, the mixture is subjected to a relatively large accumulative deformation, or vice versa. Consequently, rutting resistance can be created with a smaller regression constant b.

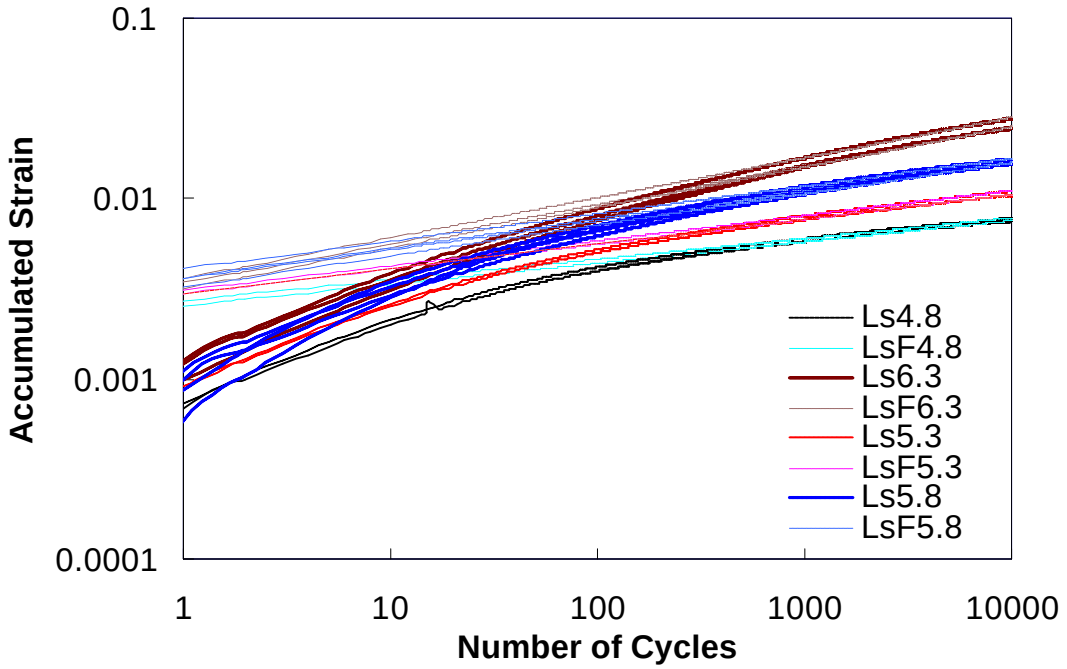

Figure 8.17 Relationship between the total cumulative plastic strain and the number of load cycles using a regression line in log-log scale

Rutting indicator *b* as a function of asphalt content is plotted, and then the regression analysis is conducted to obtain the relationship. An S-shape trend is found in Figure 8.18 between *b* and the asphalt content. This S-shape trend is more evident in the Control mixture. Based on the S-shape curve for the Control mixture, it could appear that the 6.1% asphalt content is better than the volumetric optimum of 5.6% because it provides more asphalt to the mixture which, in turn, reduces fatigue cracking and yields basically the same *b* value. However, drawing conclusions solely from the *b* vs. asphalt content relationship is misleading because the intercept *a* also has an effect on permanent strain. The effects of the combined *a* and *b* values on permanent strain growth can be seen in Figure 8.5, where the permanent strain growth of the 6.1% mixture is significantly greater than that of the 5.6% mixture, even though their *b* values are about the same. One valid conclusion that can be

drawn from the S-shape trend shown in Figure 8.18 is that above a certain asphalt content, the slope of the permanent strain growth curve increases in an unstable manner.

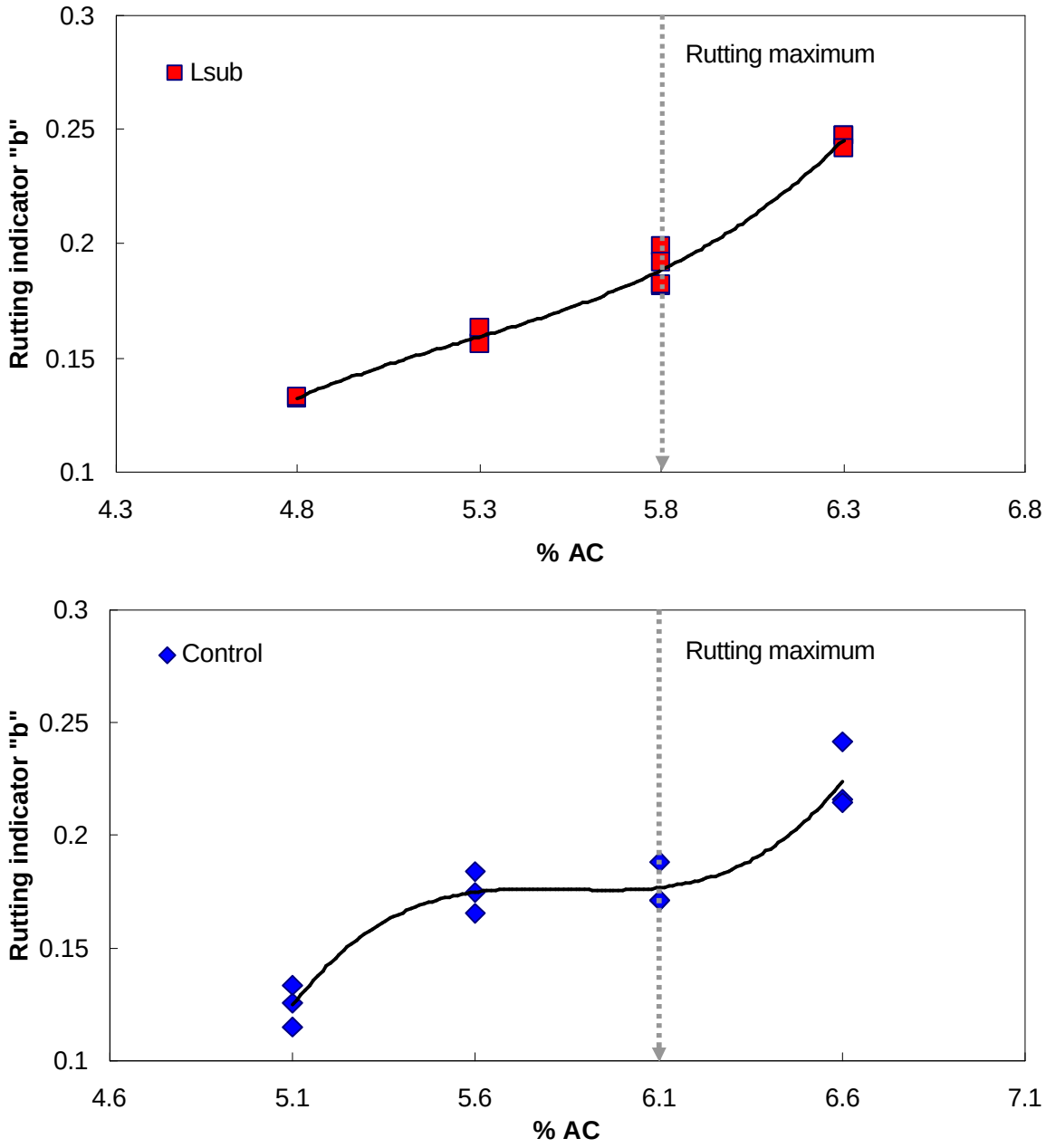

Figure 8.18 Rutting indicator *b* as a function of asphalt content for: (a) lime-modified mixture; and (b) unmodified mixture

For the Control mixture, this value is about 6.1%, whereas this point is about 5.8% in the Lsub mixture. Therefore, it can be suggested to use those asphalt contents as the maximum rutting criteria.

8.5.2 Fatigue performance indicator

The damage characteristic curve obtained from constant crosshead rate tests at 5°C indicates that for the same damage, a higher stiffness (meaning a curve that is positioned high in the plot) lends better fatigue resistance to the damage. The initial S values are plotted with the pseudo stiffness values, C, to obtain the damage characteristic curve. This relationship is then fit to some analytical form, which can be expressed by the exponential function, $C = e^{aS^b}$. If the slope of that function is steep, for a small amount of damage the mixture is prone to a comparatively large reduction in stiffness, or vice versa. Therefore, fatigue resistance to the damage is created with a gradual change in a high slope fitting the coefficient of *b*. However, having one parameter from the C vs. S curve serve as an indicator for the fatigue resistance may not be adequate or proper, because fatigue resistance of the material is affected by deformation and damage. Even the trend of the C vs. S fitting coefficient as a function of asphalt content results in the opposite trend using simulation results. Therefore, in order to assess the material's fatigue resistance correctly, both the E* and the C vs. S curve should be evaluated together. The FEP++ simulation is implemented with the resistance to deformation (e.g., the dynamic modulus), damage (e.g., the C vs. S curve), and the effect of the boundary condition (e.g., thickness, sublayer support, etc.). Therefore, it is recommended to use the FEP++ simulation methodology presented in Section

8.5.1 for the fatigue cracking evaluation. Thus, potential fatigue minimum criteria for the Lsub and Control mixtures as a function of asphalt content are plotted in Figure 8.19 (a) and (b), respectively with the maximum asphalt content for rutting performance from Figure 8.18. Then, the candidate performance optimum asphalt content range can be obtained from the fatigue minimum criteria and the rutting maximum criteria. From the observation on Figure 8.19 (a), the minimum fatigue criteria and maximum rutting criteria are the same in Lsub mixture, while Control mixture shows the range of 5.6% and 6.1% for the candidate performance optimum asphalt content.

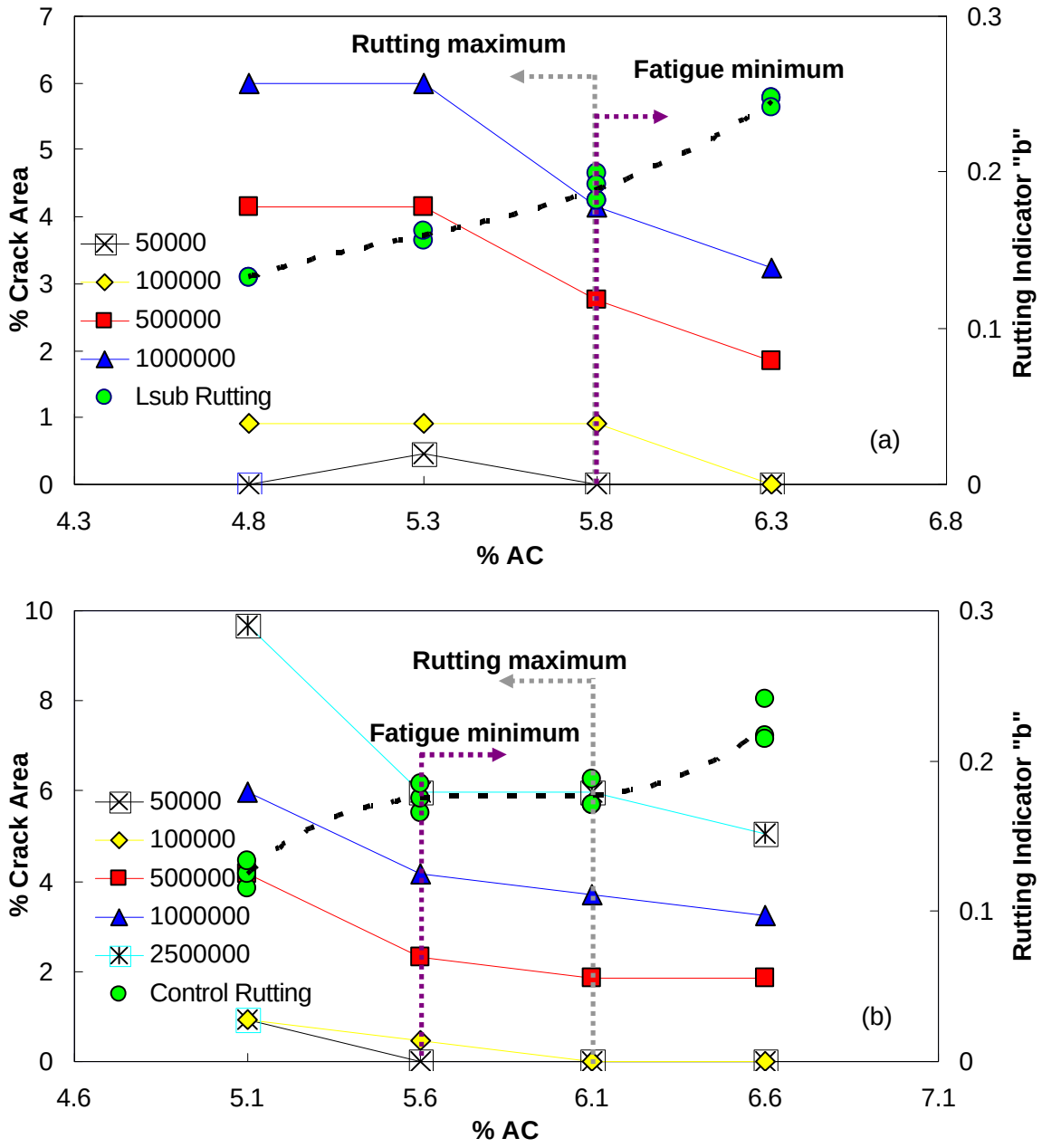

Figure 8.19 Potential fatigue minimum criteria and rutting maximum criteria as a function of asphalt content for (a) lime-modified mixture; and (b) unmodified mixture

However, those potential fatigue minimum criteria are developed based on the % Crack area growth rate trend from FEP++ simulation with a thin pavement boundary condition. Therefore, it is necessary to evaluate the trend of the fatigue crack growth rate in parallel to

the parameter from the FEP++ simulation results using a different structure, such as thick pavement. In this way, a common trend can be obtained that can be evaluated if it follows the trend of the simulation results generally, regardless of the boundary conditions of the pavement structure. Then, the fatigue indicator can be set as the fatigue indicator for the general case. However, this concept is beyond the scope of this study; in this study, the performance-based mix design methodology is suggested for the scope of a simple thin pavement using lime-modified or unmodified mixtures as the surface layer. Because the rutting indicator *b* as a function of asphalt content shows that the tertiary behavior for both mixtures as well as the fatigue indicator is limited within the thin pavement, the range from the rutting indicator *b* can set the criterion for the performance-based mix design methodology.

8.5.3 Optimal asphalt content based on performance tests

For the Lsub mixture, one volumetric optimal , one maximum for rutting performance, and one minimum for fatigue performance of asphalt contents suggested for the performance based mix design, which are 5.3% as a volumetric optimum, and 5.8% for the fatigue and the rutting resistance obtained from Figure 8.19 (a), respectively. However, it is important to secure the balance between the performance optimum and volumetric optimum. Average asphalt content of volumetric and performance optimum is taken to determine the balanced performance optimum, which is the case of Figure 8.16(b), because rutting resistance can be secured unless the average is out of the maximum value. Therefore, the balanced optimum asphalt content is 5.5%, the rounded up value. These results are summarized in Figure 8.20.

Then the volumetric properties at this asphalt content should be checked whether it meets the volumetric criteria. The volumetric properties at the balanced optimum asphalt content for the Lsub and Control mixture are summarized in Table 8.5 and also depicted in Figure 8.21. From the evaluation of the volumetric properties of the Lsub mixture such as air voids, VMA, and VFA, they all meet the volumetric criteria.

Along similar line with the Lsub mixture, the performance optimum asphalt content for the Control mixture could be simply decided. Based on the observation on the Figure 8.18 (b) which is supported by the simulation results, the fatigue minimum 5.6% can be the lower range of the candidate optimum asphalt content, while the rutting maximum 6.1% can be the upper range of the candidate optimum asphalt content. Therefore, within the stable range of the rutting and fatigue, 5.6% to 6.1%, the performance optimum asphalt content can be suggested at 5.6% satisfying both rutting and fatigue performance. At the same time, the volumetric optimum asphalt content, 5.6% is satisfied, which is the case of Figure 8.16(a). Then it doesn't need to check the volumetric properties.

In view of the results so far achieved, 5.5% and 5.6% are suggested as the balanced optimal asphalt contents of the lime-modified and unmodified mixture based on performance, respectively. These results are not conclusive; however, with further study and evaluation, they can nonetheless be suggested for the mix design methodology.

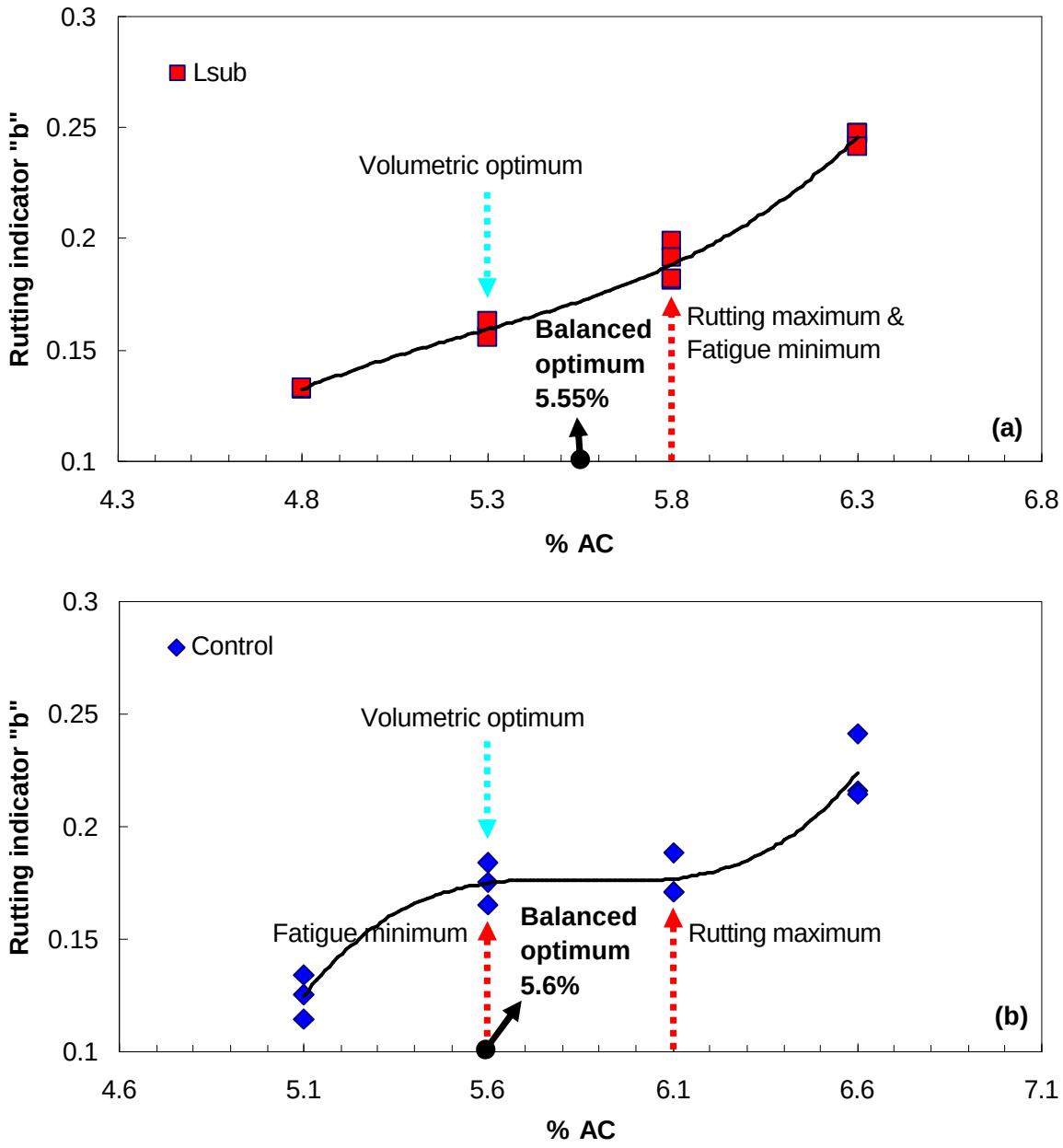

Figure 8.20 Balanced optimal asphalt contents for (a) lime-modified mixture; and (b) unmodified mixture

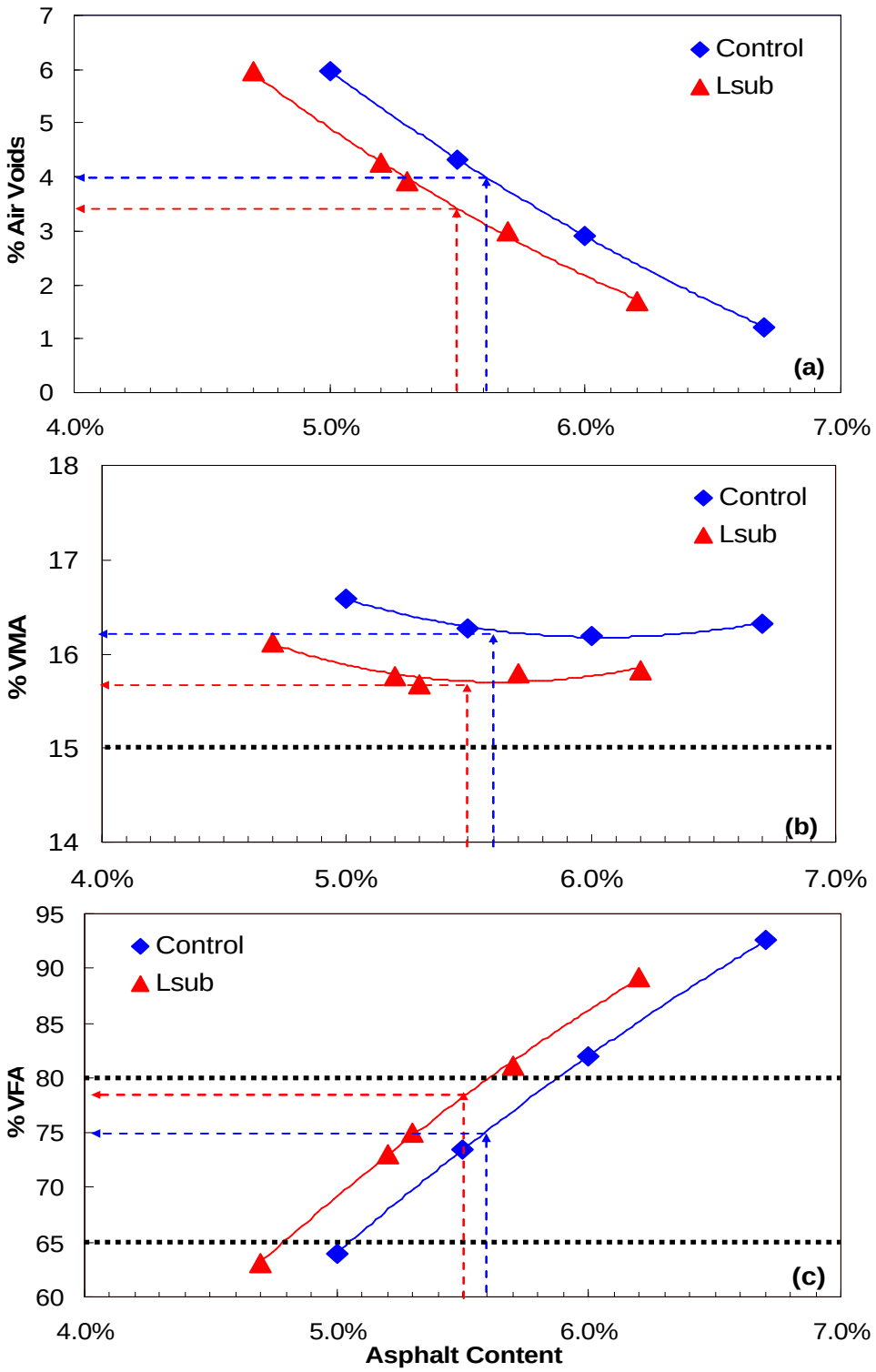

Figure 8.21 Volumetric propeties of the Lsub and Control mixture

Table 8.5 Results of the Volumetric Properties of the Lsub Mixture

Volumetric Property	Criteria	Result
% Air Voids	4%+-0.5%	3.5%
% VMA	Minimum 15%	15.7%
% VFA	Within 65-80%	78%

8.6 Summary and Conclusions

This study evaluates the performance of the most favorable characteristic lime–modified mixtures using the substitution method at different asphalt contents, varying from -0.5% to +1.0% according to the volumetric optimum of the Superpave mix design using performance tests. Simultaneously, the performance of unmodified mixtures is evaluated using the same criteria as used for the lime-modified mixtures in order to compare the performance of the mixtures in terms of the effects of lime. The final objective is to determine the optimal asphalt content for a performance-based mix design using the lime-modified and unmodified mixtures. Through this investigation, it was found that simple performance tests, such as the dynamic modulus test and the TRLPD test represent the mechanical properties of the material as a function of asphalt content. The lower asphalt content results in the higher modulus and lower deformation, indicating that elasticity is involved. However, too much asphalt causes a dramatic increase in permanent deformation. Tthe VECD characterization test results, however, show a reverse trend from the results of the dynamic modulus test and the TRLPD test as a function of asphalt content. Thus, the VECD-FEP++ simulation was implemented with regard to the material's resistance to damage and deformation. Fatigue performance trends of the mixtures could be captured using VECD-FEP++ as was done with the moisture damage study. Along similar lines with the study on the effect of asphalt content on the performance of the mixtures, the effect of lime on the performance of the mixtures was evaluated by comparing the results of the permanent strain and the VECD-FEP++ simulation to the results of the performance of the unmodified

mixture. The effect of lime was evaluated by the permanent strain reduction and % Crack area growth rate in terms of fatigue resistance. At the end of this study, the optimal asphalt content of the mixture based on the performance tests was determined. From this study, the following conclusions are drawn:

As the asphalt content increases,

- the dynamic modulus decreases over all frequencies;
- the permanent strain growth increases; and
- resistance to tensile damage growth increases.

As lime is added to the mixture,

- the permanent strain growth rate decreases; and
- tensile damage growth rate decreases.

Through the performance indicator, 5.4% and 5.6%, which are the average asphalt contents from the volumetric and performance optimums, could be suggested as the optimal asphalt contents of the lime-modified mixtures and unmodified mixtures, respectively, based on performance. However, these optimal asphalt contents are not conclusive but can be suggested for the balanced mix design methodology. Further study is needed to evaluate the performance of these optimal asphalt contents.

Chapter 9

Verification Test with Field-Produced Mixture

9.1 Field Construction

The final goal of one of the research projects involved in this proposal is the construction of a field test section using the lime-modified mix based on the optimal asphalt content so as to assess the effects of the lime introduction method. A field test section of 1,500 feet was constructed using both the lime-modified mixture and unmodified mixture based on the results obtained thus far. Those mixtures resurfaced an existing asphalt layer built about 1992. It is noted that the performance mix design for the field test section was determined using results from Chapter 8. The optimal asphalt content was adjusted by reducing the asphalt content so that it was drier to minimize rutting, because rutting should be the critical factor of the project. In summary, based on three given asphalt contents for Lub mixture (volumetric optimum 5.3%, fatigue minimum 5.8%, and rutting maximum 5.8%), and the Control mixture (volumetric 5.6%, fatigue minimum 5.6%, and rutting maxixmum 6.1%) the optimal asphalt contents for the field test section were 5.55 % and 5.6%, which were for the Lusb and

the Control mixture, respectively. Thus the optimal asphalt content for the Lsub mixture adjusted to the drier side of 5.5% of the Lsub mixture to account for rutting and 5.6% of the Control mixture.

After the test section had been constructed with the optimal asphalt contents for Lime modified and Control mixture, the volumetric and physical properties of those field-produced mixtures were checked in the field laboratory for compliance with quality requirements specified by the agency. Table 9.1 shows the volumetric properties and component material analysis results of the field-produced mixtures from the laboratory compaction and asphalt ignition oven test, respectively. Table 9.1 indicates that the aggregate gradation of each field mixture is close to the laboratory target. The Lsub-2 sample comes much closer to the mix design criteria. However, the control sample shows a little bit higher asphalt content and a smaller amount of passing #200 fines than the laboratory target.

Table 9.1 Field Gradation Information for Lime Modification Study

Volumetric Properties	Mix Types				
	Control	Control Lab	Lsub-1	Lsub-2	Lsub Lab
Gmb @ Ndes	2.474	2.543	2.504	2.490	2.542
Gmm	2.593	2.646	2.622	2.612	2.640
VTM @Ndes	4.6	3.9	4.5	4.7	3.7
VMA @Ndes	18.8	16.3	17.1	17.5	15.9
VFA @Ndes	76	74.8	74	77	77
%Gmm @Nini	89.1	89.4	88.7	88.7	89.5
Sieves (mm)	%Passing Blend				
25	100	100	100	100	100
19	100	100	100	100	100
12.5	99	99	98	99	99
9.5	94	95	93	94	95
4.75	74	78	71	76	78
2.36	56	59	53	59	59
0.075	5	6.4	5.4	6.8	6.3
% Binder	5.9	5.6	5.5	5.5	5.4
P0.075/Pbe	0.8	1.3	1.1	1.4	1.3

9.2 Field Conditions of the Production Process

The lime substitution method selected for its superior performance could not be reproduced in the plant. The method is to replace 1% baghouse fines with 1% lime. This method can be produced through the laboratory mix design process because the substation of 1% baghouse fines can be adjusted manually. However, in the plant, each aggregate stockpile in a cold bin apportioned by job mix formula is dumped into the drum mixer and, subsequently, the baghouse fines are collected and reintroduced from the storage bin or dust silo after metering to satisfy the job mix formula portion. The dust silo is always filled with a certain amount of baghouse fines because of continuous processing. Therefore, to produce

the lime substitute mix, the dust silo must be emptied to collect and reintroduce only a specific amount of lime and baghouse fines into the drum mix as well as to ensure enough space to store the excess dust that will not be returned to the mix.

However, when the mixture was produced, moisture and clogging problems occurred because of humid weather conditions the day before, which caused the empty silo to be condensed with moisture. The clogging slowed production and, consequently, the first sample within the first 200 tons of production did not come close to the mix design target. However, the second sample, produced during the next 300 tons when the plant was able to operate consistently, came much closer to the mix design target.

9.3 Moisture Sensitivity Testing and Results

Indirect tensile (IDT) strength testing was performed by the NCDOT Materials and Tests Unit and the field laboratory of the contractor in accordance with AASHTO T-283. Test pills of Lsub and the unmodified mix were made with component materials and loose mixtures pulled out of field. Those specimens were 150 mm in diameter and a height of 95 mm with 7±1 % air void levels. The freeze/thaw cycle, which is optional in T-283, was not used in this project. Eight specimens were tested for unconditioned and conditioned states, respectively. For the conditioned states, four specimens were saturated and then conditioned in a water bath at 140^{o} F (60^{O}C) for 12 and 24 hours, respectively. After conditioning, the indirect tensile strengths for the conditioned and unconditioned samples were measured at 77^{o} F. The indirect tensile strength (ITS) for each specimen was computed as follows:

$S_t = 2*P/\pi tD$,

where S_t = tensile strength (psi); P = maximum load (lb); t = specimen height (in.); and D= specimen diameter (in.).

The maximum load, P, was obtained using a Geotest loading frame, which is equipped with a chart recorder, as shown in Figure 9.1. From the measured tensile strengths a tensile strength ratio (TSR) was calculated, as follows:

$TSR = S_{tm}/S_{td} *100$,

where S_{tm} = average tensile strength of the moisture-conditioned subset (fully conditioned) (psi); S_{td} = average tensile strength of the unconditioned subset (psi).

Figure 9.1 Loading frame used for measuring indirect tensile strength

Table 9.2 Comparison of Indirect Tensile Strength Test Results for Lime-modified and Unmodified Mixtures

Testing Lab.	Mix Type	Air Voids (%)		Temperature (°C)		Tensile Strength (psi)		Avg. Saturation Level (%)	TSR(%)
		UC[a]	C[b]	UC	C	UC	C		
NCDOT Lab	Contorl 1	6.7	6.7	73.4	73.4	1336.0	1143.9	71.5	85.6
	Control 2	6.8	6.8	73.5	74.6	1299.9	1110.0	74.1	85.4
	Lsub 1	6.7	6.7	73.0	75.0	1295.3	1123.9	71.9	86.8
	Lsub 2	6.7	6.7	73.8	76.8	1286.4	1004.4	73.2	78.1
	Control Field 1	7.0	7.0	77.5	76.0	1191.6	1048.3	73.4	88.0
	Lsub Field 1	7.0	7.0	77.0	76.0	1086.1	1004.2	76.9	92.5
	Lsub Field 2	6.8	7.0	77.0	77.0	1098.0	931.8	75.4	84.9
Field Lab	Control Field 1	7.0	7.0	77.0	76.3	1168.2	1048.7	76.5	89.8
	Lsub Field 1	7.1	7.1	77.5	76.3	1091.2	1080.0	76.7	99.0
	Lsub Field 2	7.0	7.0	77.3	78.4	1128.0	1099.0	76.8	97.4

Note: UC[a]: Unconditioned specimen
C[b]: Conditioned specimen

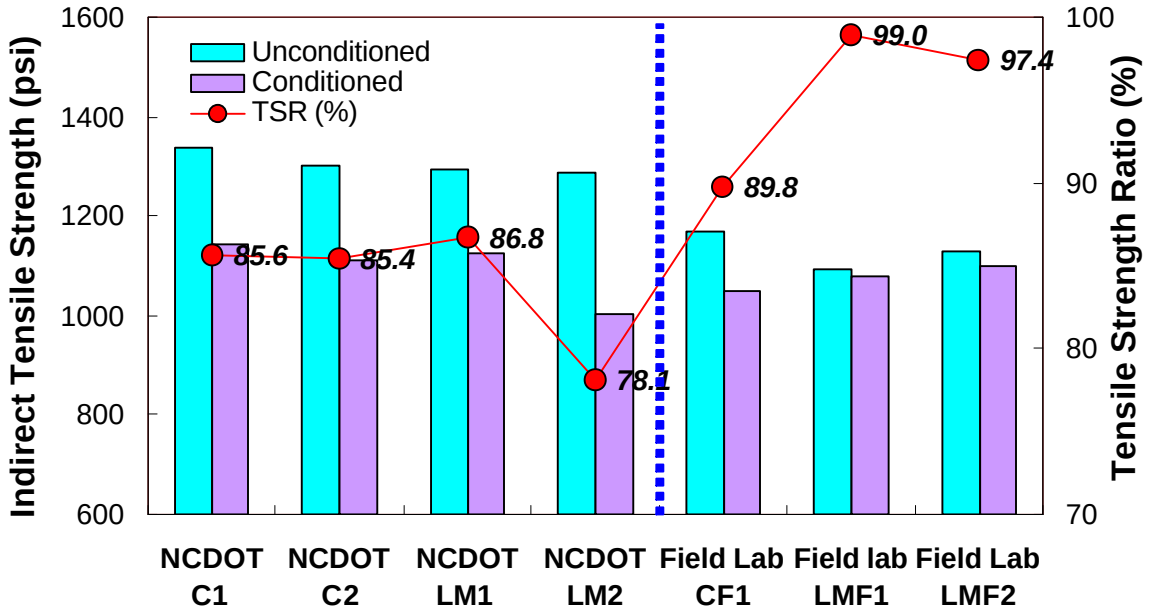

Note: C: Unmodified lab mix specimen set; LM: Lime-modified lab mix specimen set
CF: Unmodifed field mix set; LMF: Lime modified field mix set
NCDOT: Tested by Dot M&T; Field: Tested by field laboratory

Figure 9.2 Comparison of loss in tensile strength values for lime-modified and unmodified mixtures (TSR tests for NCSU Lab mix and Field mix were done by DOT and Field lab, respectively.)

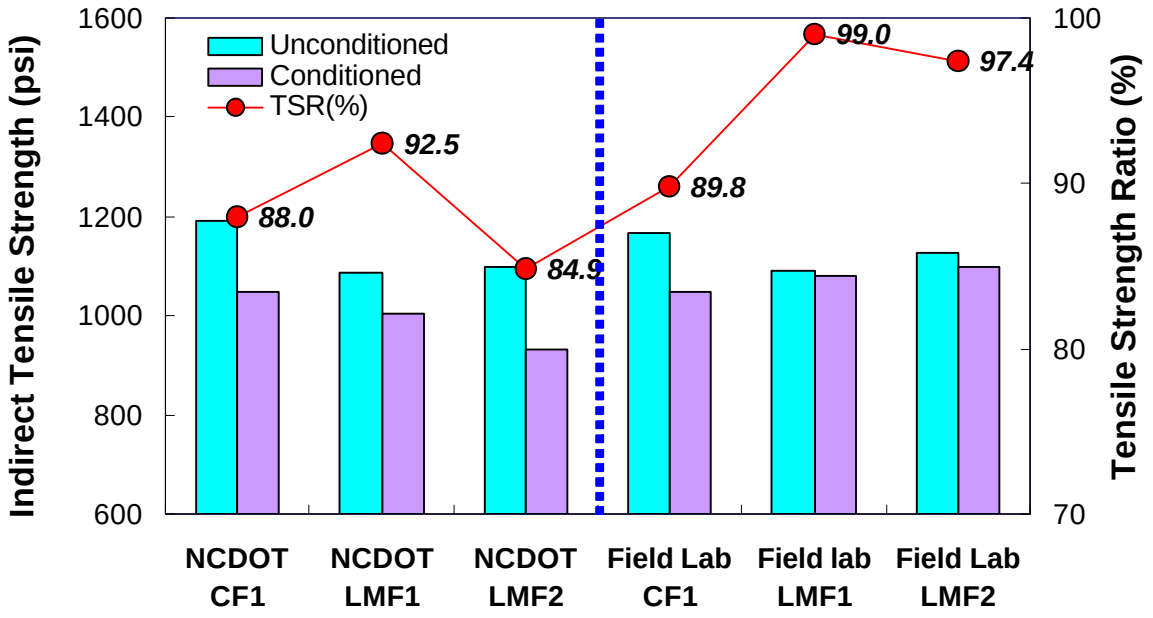

Figure 9.3 Comparison of loss in tensile strength values for lime-modified and unmodified mixtures (TSR tests for Field mixes were done by DOT and field Lab.)

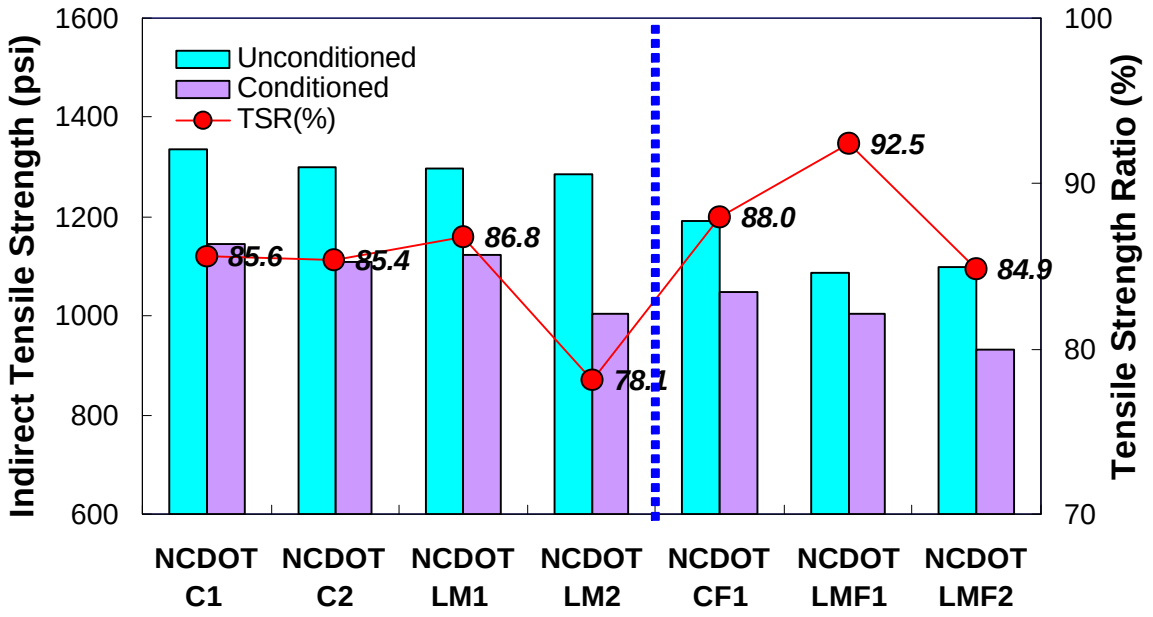

Figure 9.4 Comparison of loss in tensile strength values for lime-modified and unmodified mixtures (TSR tests for NCSU Lab mix and Field mix were done by DOT.)

The observation on two set of field lime-modified mixes in Table 9.1 in terms of volumetric properties indicates that the first sample having a smaller amount of passing #200 fines (Field LM1) than the second sample (Field LM2) shows a coarser gradation which cause thicker film thickness. Therefore, it shows higher TSR value (99.0%) than that (97.4%) of the second sample in Table 9.2. Also, the smaller amount of passing #200 of the Control field mix resulted in a higher TSR value (89.8%) than the TSR value (average 85.5%) of the control lab mix. It is noted that the conditioned indirect tensile strength test was conducted at higher temperatures (2-3°F difference) than the unconditioned test for the lime-modified mix made of component materials. This higher temperature may have a possibility of causing the difference between the TSR values of NCDOT LM mix. Further study is needed using another subset of the lime-modified mix. However, the higher TSR test result of the lime-modified mixes other than the NCDOT LM2 indicates an effect of lime modification on the moisture sensitivity.

9.4 Asphalt Pavement Analyzer (APA) Rut Test and Results

Asphalt pavement analyzer rut testing was performed by the NCDOT Materials and Tests Unit. Test pills of the Lsub and unmodified mixes were made using component materials. Those specimens were 150 mm in diameter and a height of 75 mm with 4±1 % air void levels.

Samples were placed under repetitive loads of a wheel-tracking device, known as an Asphalt Pavement Analyzer (APA), to assess the rutting susceptibility of the mixtures. The APA is the new generation of the Georgia Loaded Wheel Tester (GLWT). The APA has

additional features that include a water storage tank, and it is capable of testing both gyratory and beam specimens. Three beam or six gyratory samples can be tested simultaneously. Figure 9.5 shows the inside of an APA chamber.

The APA basically consists of three parallel steel wheels, rolling on a pressurized rubber tube, which applies loading to beam or cylindrical specimens in a linear track. The test specimens, loading tubes and wheels are all contained in a thermostatically controlled environmental chamber. The depth of rutting in the test specimens was measured after the application of 8000 loading cycles. Test parameters of 8000 cycles with a 534 N (120 lbs) wheel load and 827 kPa (120 psi) hose pressure were used. Typically, test temperatures for the APA range from 40.6°C to 64°C (105°F to 147°F). For this study, APA tests were carried out at 64°C, and the higher binder performance grade was used in the mix.

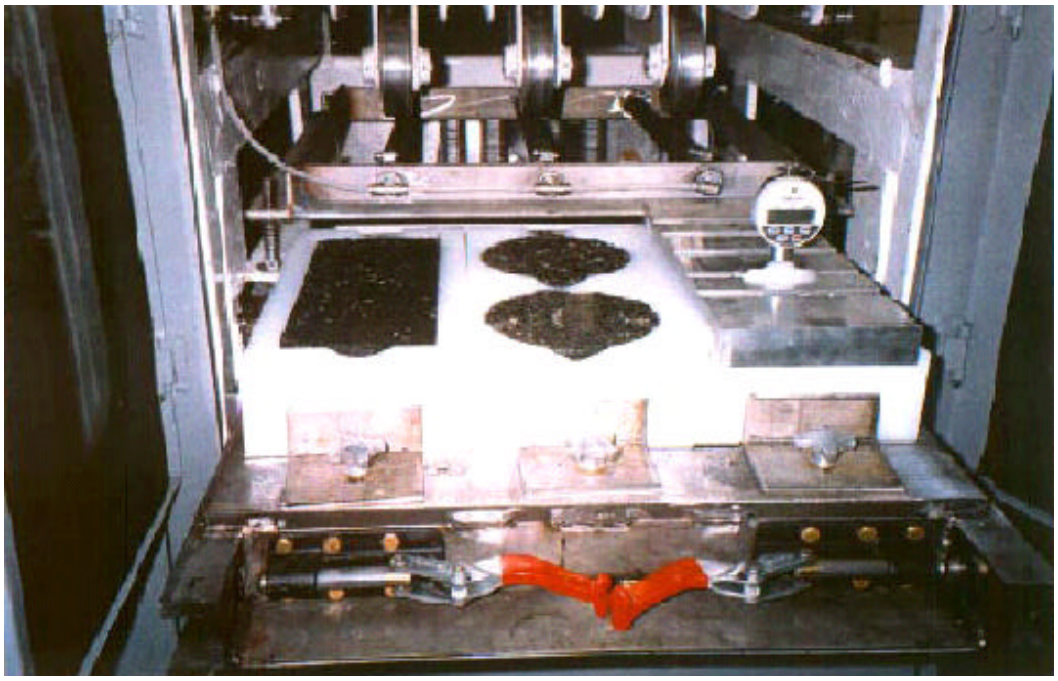

Figure 9.5 Asphalt Pavement Analyzer

The findings of a previous study conducted by Choubane et al. (2000) suggest that average values within the ranges of 8 to 9 mm (0.31 to 0.35 in.) may be used as performance limiting criteria at 8,000 cycles for gyratory samples.

Table 9.3 Comparison of APA Test Results

Mixture ID		Temperature (°F)	% Air voids	Rut depth at 8000 strokes (in mm)
Control	1	147.2 (64°C)	4.23	4.11
	2		4.18	5.00
	3		4.22	4.86
	average		4.21	4.66
Lime-modified	1	150.8 (66°C)	4.27	4.04
	2		4.27	4.63
	3		4.30	5.33
	average		4.28	4.67

The test results indicate that both the control and lime-modified mixes show similar average rut depths, which were 4.66 mm for the control mix and 4.67 mm for the lime-modified mix, respectively. In a previous study conducted by Choubane, Page and Musseleman for assessing the rutting potential of asphalt mixes in Florida, the APA can be used to evaluate the ranking of mixes in terms of the respective rut performance or to check pass/fail for the rutting resistance of a given mix (2000). When compared to the rut criteria for gyratory samples, average rut depths of the lime-modified and control mixes stayed below the average value within the range of 8 to 9 mm. In other words, both mixes showed good performance in rutting resistance.

However, it is noted that the APA tests for the lime-modified mixtures were conducted at higher temperatures (3.6°F difference) than the Control mix. This difference may cause an increase in the rut depth of the lime-modified mix. Moreover, there could be adverse effects

from the increased asphalt content for the rutting resistance of the lime-modified mix compared to the TRLPD test results. That is, the lime-modified specimens evaluated in the APA test were fabricated using the optimal asphalt content based on the performance mix design.

9.5 Summary and Conclusions

- APA results passing NCDOT minimum criteria
- Difference of averaged rut depth results very small
- Difference in averaged TSR values are various.
- TSR and APA test are not sensitive enough to capture the difference in performance.

Chapter 10

Conclusions and Recommendations

Conclusions and recommendations drawn from the results discussed in this dissertation are presented in this chapter.

Conclusions

Four separate studies were conducted:

- ✓ Evaluation of the effect of lime on the optimal asphalt content (%);
- ✓ Selection of the best lime addition method;
- ✓ Investigation into the effects of lime modification on moisture susceptibility; and
- ✓ Investigation into the effects of lime on the performance of mixture at varying asphalt contents.

Through this investigation, it is observed that simple performance tests, such as the dynamic modulus test and the TRLPD test, represent the mechanical properties, and the VECD-FEP++ can capture the changes in fatigue resistance of the various mixtures.

(1) The effects of lime on various mixtures with volumetric optimal asphalt contents were evaluated by comparing the dynamic modulus test results. The findings are:

- An additional 1% lime by weight of mixture reduces the optima; asphalt content by 0.35 to 0.9%.
- Lime modification of HMA increases the dynamic modulus, especially at high frequencies and lower temperatures.

(2) The multiple techniques for introducing lime into asphalt concrete mixtures with volumetric optimal asphalt contents were assessed via performance tests. The substitution of existing mineral filler with hydrated lime (Lsub), the most favorable performance characteristics, led to:

- An increased dynamic modulus in the high reduced frequency range (high temperature or low frequency);
- Accumulation of less permanent strain in the TRLPD tests;
- Increased resistance to tensile damage growth from the VECD characterization; and,
- The most favorable fatigue performance based on the ranking study via VECD-FEP++ simulation.

(3) The effects of lime modification on performance resistance to moisture damage in HMA mixtures were examined, and the following conclusions may be drawn:

- The effect of lime modification on the dynamic modulus makes a mixture less susceptible to moisture damage as the temperature increases;

- Moisture damage has less impact on the rutting performance of the Lsub mixture than that of the Control mixture, based on less permanent strain accumulation, as found from TRLPD testing.
- The effect of lime modification on fatigue performance makes a mixture less susceptible to moisture damage based on the VECD characterization results.
- The results of the VECD-FEP++ simulations suggest that the effect of lime modification on fatigue performance makes a mixture less susceptible to moisture damage.

(4) In parallel, the performances of the lime-modified mixtures and unmodified mixtures at different asphalt contents varying from -0.5% to +1.0% by the volumetric optimum of the Superpave mix design were evaluated and compared using performance tests. Finally, the optimal asphalt content of mixtures based on the performance tests was suggested. From this study the following conclusions are drawn:

As the asphalt content increases,

- the dynamic modulus decreases over all frequencies;
- the permanent strain growth increases; and
- resistance to tensile damage growth increases.

As lime is added to the mixture,

- the permanent strain growth rate decreases; and
- tensile damage growth rate decreases.

Through the performance indicator,

- the average asphalt contents from the volumetric and performance optimums are suggested as the balanced optimal asphalt content.

Recommendations

From the findings of this research, the following recommendations are made:

(1) More samples are needed to evaluate the damage characterization using the moisture conditioning procedure in order to build confidence in the test results, because the moisture conditioning process, even including multiple F-T cycles, has the potential to cause a large sample-to-sample variability.

(2) More varied types of pavement structures are needed for the VECD-FEP++ simulation in order to draw general comparisons that are not limited by a specific case; the pavement structure used in this study was assumed as a simple thin pavement.

(3) A more advanced VECD model that can account not only for the continuum damage characteristics but also for fracture properties may provide a more accurate assessment of the performance of a given mixture.

(4) Due to the impracticality of the lime modification method that substitutes 1% baghouse fines with 1% hydrated lime in the mix, another lime modification method should be suggested. The candidate lime modification will be the Lmod mixture, which was evaluated in Chapter 6.

(5) It is necessary to continue monitoring the field section because the TSR and APA tests are not sensitive enough to capture the differences in performance.

References

1. D.N. Little and J.C. Petersen. “Unique Effects of Hydrated Lime Filler on the Performance-Related Properties of Asphalt Cements: Physical and Chemical Interactions Revisited.” *Journal of Materials in Civil Engineering*. ASCE. March/April 2005. pp. 207-218. (2005).
2. J.C. Petersen, H. Plancher and P.M. Harnsberger. “Lime Treatment of Asphalt.” *Final Report Prepared for the National lime Association*, Western Research Institute, Laramie, Wyoming. (1987a).
3. J.C. Petersen, H. Plancher and P.M. Harnsberger. “Lime Treatment of Asphalt to Reduce Age Hardening and Improve Flow Properties.” *Asphalt Paving Technology*. AAPT, Vol. 56. pp 632-653. (1987b).
4. H. Plancher and J.C. Petersen. “Reduction of Oxidative hardening of Asphalts by Treatment with Hydrated Lime – a Mechanistic Study.” *Asphalt Paving Technology*, AAPT, Vol. 45. pp 1-24. (1976).
5. R. Collins. “Status Report on the Use of Hydrated lime in Asphaltic Concrete Mixtures in Georgia.” *Georgia DOT, Materials and Research*. Georgia. (1988).
6. P.E. Sebaaly, E. Hitti and D. Weitzel. “Effectiveness of Lime in Hot-Mix Asphalt Pavements.” *Transportation Research Record 1832*. Transportation Research Board, National Research Council, Washington, D.C. pp 34-41. (2003).

7. P.E. Sebaaly, P. Tohme, E. Hitti, K. Stansbury and J. Epps. “Asphalt Concrete Anti-Stripping Techniques: Final Report” *South Dakota Department of Transportation*. Study SD99-10. (2003).

8. D. H. Tunnicliff and R.E. Root. “Anti-Stripping Additives in Asphalt Concrete: State of the Art”. *Asphalt Paving Technology,* AAPT, Vol. 51. pp 265-289. (1982).

9. B.H. Welch and M.L. Wiley. “Investigation of Hydrated Lime-Asphalt and Aggregate Interactions.” *State Study No. 923,* Utah Department of Transportation, UDOTMR-76-9. (1977).

10. D.A. Anderson and W.H. Goetz. “Mechanical Behavior and Reinforcement of Mineral Filler-Asphalt Mixtures.” *Asphalt Paving Technology,* AAPT, Vol. 42. pp 37-66. (1973).

11. R.N. Traxler. “The Evaluation of Mineral Powders as Fillers for Asphalt.” *Asphalt Paving Technology*. AAPT. Vol. 8. p 60. (1937).

12. W.B. Warden, S.B. Hudson and H.C. Howell. “Evaluation of Mineral Fillers in Terms of Practical pavement Performance.” *Asphalt Paving Technology*. AAPT, Vol. 28. p 316. (1959).

13. A.A. Tayebali, M.B. Kulkarni and H.F. Waller. “Delamination and Shoving of Asphalt Concrete Layers Containing Baghouse Files.” *Department of Civil Engineering North Carolina State University, Technical Report* (2000).

14. J. Craus, I. Ishai and A. Sides. “Some Physico-Chemical Aspects of the Effect and the Rold of the Filler in Bituminous Paving Mixtures.” *Asphalt Paving Technology,* AAPT, Vol. 47. pp 558-588. (1978).

15. L. N. Mohammad, C.D. Abadie, C. Dranda, Z. Wu, and Z. Zhongie. "Permanent Deformation Analysis of Hot-Mix Asphalt Mixtures Using Simple Performance Tests and 2002 Mechanistic-Empirical Pavement Design Software." Transportation Research Board Annual Meeting CD ROM. Transportation Research Board, National Research Council, Washington, D.C. (2006).
16. J.W. Button and J.A. Epps. "Evaluation of Methods of Mixing Lime and Asphalt Paving Mixtures." *Texas Hot Asphalt Pavement Association*. (1983).
17. M. Stroup-Gardiner and J.A. Epps. "Four Variables Affectig the Performance of Lime in Asphalt-Aggregate Mixtures." *Transportation Research Record 1115*. Transportation Research Board, National Research Council, Washington, D.C. pp 12-22. (1987).
18. T. Kennedy, J.A. Epps, N. Turningham, C.W. Smoot, F.M. Young, J.W. Button and C.D. Zeigler. "Evaluation of Methods for Field Applications of lime to Asphalt Concrete Mixtures." *Asphalt Paving Technology*, AAPT, Vol. 52. pp 508-535. (1983).
19. G. Chehab. "Characterization of Asphalt Concrete in Tension Using a Viscoelastoplastic Model." Ph.D. Dissertation, North Carolina State University, Raleigh, NC. (2002).
20. J.S. Daniel. "Development of a Simplified Fatigue Test and Analysis Procedure Using a Viscoelastic, Continuum Damage Model and its Implementation to WesTrack Mixtures." Ph.D. Dissertation, North Carolina State University, Raleigh, NC. (2001).
21. M.W. Witczak, K. Kaloush, T. Pellinen, M. El-Basyouny, and H. Von Quintus. Simple Performance Test for Superpave Mix Design. NCHRP Report 465. National Research Council, Transportation Research Board. Washington, D.C. (2000)

22. Y.R. Kim, M.N. Guddati, B.S. Underwood, T.Y. Yun, V. Subramanian and A. Homayoun Heidari. “Characterization of ALF Mixtures Using the Viscoelastoplastic Continuum Damage Model: Final Report.” Federal Highway Administration. (2005).

23. American Association of State Highway and Transportation Officials, “TP-62 Standard Method of Test for Determining Dynamic Modulus of Hot-Mix Asphalt Concrete Mixtures.” Washington D.C. (2003).

24. G. Chehab, Y.R. Kim, R.A. Schapery, M. Witczack, R. Bonaquist. “Time-Temperature Superposition Principle for Asphalt Concrete Mixtures with Growing Damage in Tension State.” *Asphalt Paving Technology*, AAPT, Vol. 71, pp: 559-593. (2002).

25. K. Kaloush. “Simple Performance Test for Permanent Deformation of Asphalt Mixtures.“ Ph.D. Dissertation, Arizona State University, Tempe, AZ. (2001).

26. G. Chehab, Y.R. Kim, R.A. Schapery, M. Witczack, R. Bonaquist. “Characterization of Asphalt Concrete in Uniaxial Tension Using a Viscoelastoplastic Model.” *Asphalt Paving Technology*, AAPT, Vol. 72, pp: 315-355. (2003).

27. J.F. Shook, B.F. Kallas, and B.F. McLeod. “Factors Influencing Dynamic Modulus of Asphalt Concrete,” *Asphalt Paving Technology*, AAPT, Vol. 38. (1969)

28. B.F. Kallas. “Dynamic Modulus of Asphalt Concrete in Tension and Tension-Compression,” *Asphalt Paving Technology*, AAPT, Vol. 39. (1970).

29. A.O. Bohn, P. Ullidtz, and R. Stubstad. “The Dynamic Modulus of Asphalt Concrete Surfaces,” Dansk Vejtidsskrift, Vol. 47. (1970)

30. R. Cragg and P.S. Pell. “The Dynamic Stiffness of Bituminous Road Materials,” *Asphalt Paving Technology*, AAPT, Vol. 40. (1971)

31. L.L. Yeager and L.E. Wood. “Recommended Procedure for Determining the Dynamic Modulus of Asphalt Mixtures,” *Transportation Research Record 549*, Transportation Research Board, National Research Council, Washington, D.C. (1975)

32. K.S. Majidzadeh, Khedr, and M. El-Mojarrush. “Evaluation of Permanent Deformation in Asphalt Concrete Pavements,” *Transportation Research Record 715*, Transportation Research Board, National Research Council, Washington, D.C. (1979)

33. G. F. Akhter and M.W. Witczak. “Sensitivity of Flexible Pavement Performance to Bituminous Mix Properties,” *Transportation Research Record 1034*, Transportation Research Board, National Research Council, Washington, D.C. (1985)

34. J.S. Miller, J. Uzan, and M.W. Witczak. “Modification of the Asphalt Institute Bituminous Mix Modulus Predictive Equation,” *Transportation Research Record 911*, Transportation Research Board, National Research Council, Washington, D.C. (1983)

35. M. McCann and P.E. Sebaaly. “Evaluation of moisture Sensitivity and Performance of Lime in Hot-Mix Asphalt: Resilient Modulus, Tensile Strength and Simple Shear Tests.” *Transportation Research Record 1832.* Transportation Research Board, National Research Council, Washington, D.C. pp 9-16. (2003).

36. L. Mohammad, C. Abadie, R. Gokmen, and A. Puppala. “Mechanistic Evaluation of Hydrated Lime in Hot-Mix Asphalt Mixtures.” *Transportation Research Record 1723*, Transportation Research Board, National Research Council, Washington, D.C., pp 26-36. (2000).

37. Y.R. Kim, D.N. Little and I. Song. “Mechanistic Evaluation of Mineral Fillers on Fatigue Resistance and Fundamental Material Characteristics.” *Proc., 82nd*

Transportation Research Board Meeting, Transportation Research Board, Washington, D.C. (2003)

38. M.W. Witczak and J. Bari, "Development of a Mastercurve(E*) Database for Lime Modified Asphalt Mixtures," Report of National Lime Association. (2004)
39. T.K. Pellinen. Investigation of the Use of Dynamic Modulus as an Indicator of Hot-Mix Asphalt Performance. Ph.D. Dissertation, Department of Civil and Environmental Engineering, Arizona State University. (2001)
40. A. Bhasin, J.W. Button, A. Chowdhury. "Evaluation of Simple Performance Tests on Hot-Mix Asphalt Mixtures from South Central United States." *Transportation Research Record 1891*. Transportation Research Board, National Research Council, Washington, D.C. pp 174-181. (2004).
41. F. Zhou and T. Scullion. "Preliminary Field Validation of Simple Performance Tests for Permanent Deformation: Case Study." *Transportation Research Record 1832*. Transportation Research Board, National Research Council, Washington, D.C. pp 209-216. (2003).
42. Y.R. Kim, and D.N. Little. "One-Dimensional Constitutive Modeling of Asphalt Concrete." *ASCE Journal of Engineering Mechanics*, Vol. 116, No. 4, pp. 751-772. (1990).
43. H.J. Lee. "Uniaxial Constitutive Modeling of Asphalt Concrete Using Viscoelasticity and Continuum Damage Theory." Ph.D. Dissertation, North Carolina State University, Raleigh, NC. (1996).

44. H.J. Lee and Y.R. Kim,?"A Uniaxial Viscoelastic Constitutive Model for Asphalt Concrete under Cyclic Loading." ASCE *Journal of Engineering Mechanics*, Vol. 124, No. 1, pp. 32-40. (1998).

45. H.J. Lee and Y.R. Kim. "A Viscoelastic Continuum Damage Model of Asphalt Concrete with Healing." ASCE *Journal of Engineering Mechanics*, Vol. 124, No. 11, pp. 1224-1232. (1998).

46. J.S. Daniel and Y. R. Kim. "Development of a Simplified Fatigue Test and Analysis Procedure Using a Viscoelastic Continuum Damage Model." *Asphalt Paving Technology*, AAPT, Vol. 71, pp: 619-650. (2002).

47. S.W. Park, Y.R. Kim, and R.A. Schapery. "A Viscoelastic Continuum Damage Model and Its Application to Uniaxial Behavior of Asphalt Concrete." *Mechanics of Materials*, Vol. 24, No. 4, pp. 241-255. (1996).

48. B.S. Underwood. Y.R. Kim and M.N. Guddati. "Characterization and Performance Prediction of ALF Mixtures Using a Viscoelastoplastic Continuum Damage Model." *Asphalt Paving Technology*, AAPT, Vol. 75. (2006).

49. R.A. Schapery. "On Viscoelastic Deformation and Failure Behavior of Composite Materials with Distributed Flaws." *Advances in Aerospace Structures and Materials*, AD-01, ASME, New York, pp. 5-20. (1981).

50. R.A. Schapery. "A Theory of Mechanical Behavior of Elastic Media with Growing Damage and Other Changes in Structure." *J. Mech. Phys. Solids*, 38, pp.215-253. (1990).

51. R. A. Schapery. “Nonlinear Viscoelastic and Viscoplastic Constitutive Equations with Growing Damage.” *Int. Journal of Fracture*, Vol. 97, 33-66. (1999).

52. J. Uzan. "Asphalt Concrete Characterization for Pavement Performance Prediction.” *Asphalt Paving Technology*, AAPT, Volume 65, pp 573-607. (1996).

53. A.A. Tayebali, W.K. Fischer, Y.X, Huang, M.B. Kulkarni. “Effect of Percentage Baghouse Fines on the Amount and Type of Anti-Stripping Agent Required to Control Moisture Sensitivity.” FHWA/NC/2003-04, Final Report. (2003).

54. Jian-Shiuh Chen and Chun-Hsiang Peng. “Analyses of Tensile Failure Properties of Asphalt-Mineral Filler Mastics,” ASCE, Journal of Materials in Civil Engineering. (1998).

55. Badru M. Kiggundu, Freddy L. Roberts “Stripping in HMA mixtures: State-Of-The-ART and Critical Review of Test Methods.” NCAT Report 88-02. (1988).

56. Shin-Che Huang; Raymond E. Robertson; Jan F. Branthaver; and J. Claine Petersen. “Impact of Lime Modification of Asphalt and Freeze–Thaw Cycling on the Asphalt–Aggregate Interaction and Moisture Resistance to Moisture Damage.” ASCE, Journal of Materials in Civil Engineering. (2005).

57. Shin-Che Huang, Raymond E. Robertson, and Jan F. Branthaver. “Physico-Chemical Characterization of Asphalt-Aggregate Interactions under the Influence of Freeze-Thaw Cycles.” TRB. (2003).

58. Arno W. Hefer, Dallas N. Little, Robert L. Lytton. “A Synthesis of Theories and Mechanisms of Bitumen-Aggregate Adhesion Including Recent Advance in

Quantifying the Effects of Water," Submitted Association of Asphalt Paving Technologists. (2005).

59. Dallas N. Little, Jon A. Epps. "The Benefits of Hydrated Lime in Hot Mix Asphalt." NLA report. (2001).
60. Dallas N. Little. "Hydrated Lime as a Multi-Functional Modifier for Asphalt Mixtures." prepared for the Lhoist Group-European Seminar. (1996).
61. Raymond E. Robertson. "Chemical Properties of Asphalt and Their Relationship to Pavement Performance." SHRP-A/UWP-91-510 Report. (1991).
62. R.P. Lottman. "The Moisture Mechanism that Causes Asphalt Stripping in Asphalt Pavement Mixtures." University of Idaho, Moscow. Final Report Research Project R-47. (1971).
63. K.Majidzadeh and F.N. Brovold. "Effect of Water on Bitumen-Aggregate Mixtures." University of Florida, Gainesville, Report CE-1. (1966).
64. Prithvi S. Kandhal. "Moisture susceptibility of HMA Mixes: Identification of Problem and Recommended Solution." NCAT Report No. 92-1. (1992).
65. Dallas N. Little. "Stabilization of pavement subgrades and base courses with lime." NLA. (1995).
66. Lesuerr, D., and Little, D. N. "Effect of hydrated lime on rheology, fracture and aging of bitumen." Transportation Research Record, 1661, Transportation Research Board, Washington, D.C., 93-105. (1999).
67. F.N. Finn, K. Nair and J.Hilliard. "Minimizing cracking of asphalt concrete pavement." Proceedings Association of Asphalt paving technologists, (1976).

68. Choubane, Bouzid, Gale C. Page, and James A. Musselman. “Suitability of Asphalt Pavement Analyzer for Predicting Pavement Rutting”, TRR 1723, Transportation Research Board, National Academy of Engineering, Washington, D.C. (2000).

69. Vijay. V. Kadayam.. “Development of Asphalt Pavement Analyzer (APA) Design Criteria for Surface Mixtures.” Thesis of Master degree at North Carolina State University. (2006).

70. A.L. Companion. “Chemical Bonding” 2nd Edition, New York: McGraw-Hill Book Co. (1979).

71. H-J Butt, K. Graf, and M. Kappl. “Physics and Chemistry of Interfaces, Weinheim. (2003).

72. R.J. Good. “Intermolecular and Interatomic Forces” Treatsie on adhesion and adhesives. (1966).

73. E.W. Mertens and J.R. Wright, “Cationic Emulsions: How they Differ from Conventional Emulsions in Theory and Practice.” Highway Research Board Proceedings, 38, 386-397. (1959).

74. A.R. Tarrar and V.P. Wagh. “The Effect of the Physical and Chemical Characteristics of the Aggregate on Bonding.” Report SHRP-A/ UIR-91-507, (1992).

75. Y.W. Jeon and C.W. Curtis. “A Literature Review of The Adsorption of Asphalt Functionalities on Aggregate Surfaces.” Report SHRP-A/IR-90-014. (1990).

76. J. Schultz and M. Nardin, “Theories and Mechanisms of Adhesion.” Handbook of Adhesive Technology, (1994).

77. H.H. Yoon and A.R. Tarrar. “Effect of Aggregate Properties on Stripping.” Transportation Research Record, 1171, 37-43. (1988).

78. M.E. Labib, Asphalt-Aggregate Interactions and Mechanisms for Water Stripping, American Chemical Society, Fuel, 37, 1472-1481, (1992).

79. R.E. Robertson. “Chemical Properties of Asphalts and Their Effects on Pavement Performance.” Transportation Research Circular No. 499. Washington, D.C., Transportation Board. (2000).

80. J.C. Petersen, H. Plancher, E.K. Ensley, G. Miyake, and R.L. Venable. “Chemistry of Asphalt-Aggregate Interaction Relationship with Moisture Damage Prediction Test,” Transportation Research Record, 843, 95 (1982).

81. Jamieson, J.S. Moulthrop, and D.R. Jones, “SHRP Results on Binder-Aggregate Adhesion and Resistance to Stripping,” Asphalt Yearbook 1995, 17-21. (1995).

82. P. Hubbard, “Adhesion of Asphalt to Aggregate in the Presence of Water.” Highway Research Board, 8, Part 1. (1938).

83. Hubbard, P. “Adhesion in Bituminous Road Materials: A Survey of Present Knowledge.” Journal of the Institute of Petroleum, Vol. 44, No. 420, pp.423-432. (1958).

84. Hicks, R.G. “Moisture Damage in Asphalt Concrete.” NCHRP Synthesis of Highway Practice, Vol.175, Transportation Research Board. (1991).

85. Rice, J.M. “Relationship of Aggregate Characteristics to the Effect of Water on Bituminous Paving Mixtures.” ASTM STP 240, American Society for Testing and Materials. (1958).

86. Western Research Institute (WRI), “Impact of Freeze-Thaw Cycles on Asphalt-Aggregate Interactions,” In Fundamental Properties of Asphalts and Modified Asphalts, Draft Final Report, FHWA Contract No. DTFH61-99C-00022, Volume 1, 57-116 Wyoming: WRI (2003).

87. S. Logaraj, “Chemistry of Asphalt-Aggregate Interaction –Influence of Additives,” Presented at the Moisture Damage Symposium, Laramie, Wyoming (2002).

88. D.N. Little and J.R. Jones, “Chemical and Mechanical Mechanisms of Moisture Damage in Hot Mix Asphalt Pavements,” National Seminar in Moisture Sensitivity, San Diego, CA (2003).

89. Brown, E.R., JL. McRae, and A. Crawley. “Effect of Aggregates on Performance of Bituminous Concrete.” ASTM STP 1016, (1989).

90. Kandhal, P.S. “Evaluation of Baghouse Fines in Bituminous Paving Mixtures.” Proceedings of Association of Asphalt Paving Technologists, Vol. 50. (1981).

91. Anderson, D.A. “Guidelines on the Use of Baghouse Fines.” National Asphalt Paving Associaiton, Inforamtion Series 101. (1987).

92. Freddy L. Roberts, Prithvi S, Kandhal, E. Ray Brown, Dah-Yinn Lee, Thomas W. Kennedy. “Hot mix asphalt materials, mixture design, and construction.” Second Edition. (1996).

93. L. Quing and J. Harvey. “Inclusion of Moisture Effect in Fatigue Test for Asphalt Pavement.” TRB 2007 Annual meeting CD-ROM (2007).